CZECH TECHNICAL UNIVERSITY IN PRAGUE

Faculty of Nuclear Sciences and Physical Engineering

Department of Physics

PhD. thesis

# Coherence effects in hadron-nucleus and heavy ion collisions at high energies

**Jan Čepila**

Supervisor: RNDr. Ján Nemčík, CSc.

Prague, 2013

ČESKÉ VYSOKÉ UČENÍ TECHNICKÉ v PRAZE

Fakulta jaderná a fyzikálně inženýrská

Katedra fyziky

Disertační práce

# Koherenční jevy v hadron-jaderných a těžko -iontových srážkách při vysokých energiích

**Jan Čepila**

Vedoucí práce: RNDr. Ján Nemčík, CSc.

Praha, 2013

*Title:*
Coherence effects in hadron-nucleus and heavy ion collisions at high energies

*Supervisor:*
RNDr. Ján Nemčík, CSc.
Department of Physics, Faculty of Nuclear Physics and Physical Engineering, Czech Technical University in Prague & Institute of Experimental Physics SAS, Košice

*Abstract:*
In this work, production of dileptons and direct photons in proton-nucleus and nucleus-nucleus collisions is studied within the color dipole approach formulated in the rest frame of the target. Coherence effects associated with quark shadowing are treated using Glauber-Gribov theory of multiple scattering. At energies corresponding to LHC experiments, higher Fock components containing gluons become important. This leads to gluon shadowing included as a leading twist correction to coherence effects. Besides effects of quantum coherence, complementary mechanism causing a suppression of the nucleus-to-nucleon production rate at large Feynman $x_F$ and/or $x_T = 2p_T/\sqrt{s}$ is introduced. It is formulated as a restriction coming from the energy conservation near the kinematic limit in multiple initial state interactions(ISI) inside the nucleus. Consequently, a correlation between nuclear target and the projectile parton distribution leads to a breakdown of the QCD factorization. As a manifestation of net ISI effects a strong nuclear suppression in production of large-$x_F$ dileptons is predicted in a good agreement with data from E772 and E866 experiments, where no coherence effects are possible. Further predictions for expected suppression of dileptons with large Feynman $x_F$ can be verified by the planned low energy experiment E906. The onset of ISI effects at large $p_T$ was also confirmed by RHIC data on direct photon production in d+Au and Au+Au collisions. The expected suppression of large-$p_T$ photons produced in p+Pb and Pb+Pb collisions at different rapidities and centralities can be verified in the future by experiments at LHC.

*Titul:*
Koherenční jevy v hadron-jaderných a těžko-iontových srážkách při vysokých energiích

*Vedoucí práce:*
RNDr. Ján Nemčík, CSc.
Katedra fyziky, Fakulta jaderná a fyzikálně inženýrská, České vysoké učení technické v Praze
& Ústav experimentálnej fyziky SAV, Košice

*Abstrakt:*
V této práci je studována produkce dileptonů a přímých fotonů v proton-jaderných a jádro-jaderných srážkách v rámci přiblížení barevného dipólu, který je formulován v klidové soustavě terče. Koherenční jevy spojené s kvarkovým stíněním jsou řešeny použitím Glauber-Gribovovy teorie vícenásobných rozptylů. Při energiích dosažitelných na LHC experimentech se začnou projevovat i vyšší Fockovské komponenty obsahující gluony, což vede na korekci ke koherenčním jevům ve formě gluonového stínění. Kromě efektů kvantové koherence je zde zaveden mechanismus způsobující potlačení poměru jaderného a nukleonového účinného průřezu při velkých Feynmanovských $x_F$ a/nebo $x_T = 2p_T/\sqrt{s}$. Tento mechanismus je formulován jako omezení plynoucí ze zachování energie poblíž kinematické hranice při vícenásobných interakcích počátečního stavu(ISI) uvnitř jádra. Důsledkem toho je korelace mezi jaderným terčem a distribucí nalétavajícího partonu, která vede na narušení QCD faktorizace. Efekty ISI předpovídají silné jaderné potlačení dileptonů s velkým $x_F$, což je v souladu s daty z experimentů E772 a E866, kde se koherenční jevy nemohou projevit. Další předpověď očekávaného potlačení dileptonů s velkým $x_F$ může být ověřena na plánovaném nízko-energetickém experimentu E906. Projev ISI efektů při velkých $p_T$ byl také potvrzen daty pro produkci přímých fotonů v d+Au a Au+Au srážkách na urychlovači RHIC. Očekávané potlačení fotonů s velkým $p_T$ produkovaných v p+Pb a Pb+Pb srážkách při různých rapiditách a centralitách může být ověřeno v budoucnu experimenty na urychlovači LHC.

**Acknowledgement**
I would like to thank my supervisor Ján Nemčík for his guidance and advices through all my studies. Our discussions significantly contributed to shape my insight to the field of particle physics.
I would like to acknowledge the Head of the Department of Physics Igor Jex and the Head of the Experimental Nuclear Physics specialization Vojtěch Petráček from the Faculty of Nuclear Sciences and Physical Engineering at the Czech Technical University in Prague. I am indebted to them for their continuous support.
Many thanks belong also to my colleagues Michal Křelina, Miroslav Myška, Michal Petráň, Libor Škoda, Michal Šumbera and many others who greatly contributed to my understanding of physics and who helped me with many formulations in the text of this thesis.
Last but not least, I would like to thank my parents, my dearest partner and the family who gave me the support on my way to the finishing of this thesis...

**Declaration**
This thesis is the result of my own work, except where explicit reference is made to the work of others, and has not been submitted for another qualification to this or any other university.

Jan Čepila

# Contents

# Chapter 1

# Introduction

This thesis is focused on the study of coherence effects in proton-nucleus and nucleus-nucleus collisions. The fundamental theory for the description of strongly interacting systems is the quantum chromodynamics(QCD)[1]. The usage of nuclei instead of hadrons in high energy scattering experiments provides unique possibility to investigate the space-time development of systems described by the QCD. In proton collisions, the products of scattering processes can be observed in a detector located within a macroscopic distance from the interaction point. In contrast, a nuclear medium can serve as a detector itself located directly at a place where the interaction occurs. As a consequence, one can use nuclear targets to study coherence effects in QCD, which are not accessible in proton-proton scattering. Moreover, it is advantageous to use hard real or virtual photon emission to study coherence effects, since photons are not subject to any final state interaction.
In the QCD parton model, a hard photon is produced via the annihilation of a quark from an incident proton with an antiquark from the target proton. The produced photon is either real or virtual. The latter one decays into a dilepton. In contrast to the deep inelastic scattering that probe only valence quarks, photon emission processes provide information on both valence and sea quarks, since there is no valence antiquark in the hadron. One has to measure high energy collisions that allow for high momentum transfer processes to reveal the sea quark component of the interacting proton. As the energy of the collision rises, the target quark carrying the Bjorken momentum fraction $x$ of the proton looks like consisting of a quark and a gluon with the same total momentum fraction. In addition, gluons can split to quark-antiquark pairs. As one goes to lower $x \ll 0.1$, the partonic content of the proton is dominated by gluons. The calculation of the cross-section for these processes in the infinite momentum frame was first published by S. Drell and T. Yan[2]. Nevertheless, it faces many difficulties e.g. the need to use the K-factor and the problem of collinear divergences[3]. On the contrary, the color dipole approach formulated by B. Kopeliovich and S. Brodsky[4, 5] treats the photon or lepton production in proton-proton collisions in the rest frame of one of the colliding protons. In this approach, the quark from the incident proton fluctuates into a coherent state of a quark and a virtual photon. The lifetime of this fluctuation is

controlled by uncertainty principle. The color interaction with a target proton leads to a disruption of coherence and, therefore, the photon is released and, eventually, decays into a lepton pair. Although the description in the color dipole approach is different from the description in the infinite momentum frame, these two approaches are not in contradiction. It is a direct consequence of the fact that the partonic description is not Lorentz invariant in contrast to the cross-section, which is Lorentz invariant. The only part of the dipole model, that does not come from the theory, is the dipole cross-section of the interaction between the fluctuation and the target nucleon. This cross-section cannot be reliably predicted because of poorly known perturbative QCD corrections and non-perturbative effects. However, it can be extracted from data for the deep inelastic scattering. There are several parametrizations on the market[6, 7, 8].

One may ask, how the scattering looks like on nuclear target at high energies. Note that not only partonic interpretation of the scattering process is frame dependent. Also a partonic structure of the nucleus depends on the reference frame. In the infinite momentum frame, the nucleus is strongly contracted in the longitudinal direction. The clouds of low $x$ gluons from different nucleons can extend over the whole nucleus and through them nucleons can communicate with each other. However, in the nuclear rest frame, nucleons are well separated from each other by a distance of approximately 2 fm. At high energies, nuclear scattering is governed by coherence effects. It is advantageous to use the target rest frame for the understanding of these effects. The fluctuation of the incident low $x$ parton arise long before entering the nucleus. The lifetime of the fluctuation called the coherence length can be derived using uncertainty principle and is inversely proportional to $x$[9]. In the case of coherence length greater than the nuclear radius, the fluctuation undergoes multiple scatterings on different nucleons inside the nucleus. The long lifetime of the fluctuation, therefore, leads to coherence effects. This is the analogy of the overlap of gluon clouds in the infinite momentum frame.

One of the most commonly known manifestation of the coherent interaction of nucleons inside the nucleus is the nuclear shadowing. It was first observed in the deep inelastic scattering by the EM Collaboration[10] and in the dilepton production by the E772 experiment[11] as a suppression of the cross-section on nuclear target with respect to the proton target. The mechanism behind the nuclear shadowing is most easily understood in the target rest frame. The fluctuation arises long before entering the nucleus. Due to large interaction cross-section, it interacts with the nucleons at the surface of the nucleus, which casts shadow on the inner nucleons. This applies to fluctuations with sufficient transverse separations. Small fluctuations are not shadowed, and so, they can propagate through the whole nucleus. In the limit of maximal coherence length, the shadowing can be calculated using Glauber-Gribov eikonalization[12, 13].

Note that the effect of multiple scattering on the bremsstrahlung is well known from the quantum electrodynamics as the Landau-Pomeranchuk-Migdal effect(LPM)[14]. The LPM effect leads to a reduction of the cross-section due to destructive interferences in multiple scattering inside an amorphous medium. An electron incident on a target with many scatter-

ing centers will radiate bremsstrahlung after the first scattering. Any successive scattering does not lead to the bremsstrahlung, since the electron needs a long time to recreate it's electromagnetic field. If the coherence length is long enough, the electron can travel macroscopic distance without any bremsstrahlung. Therefore, the overall cross-section is lower than the sum of cross-sections for corresponding number of independent scatterings. On the contrary, if the coherence length is short, each successive scattering leads to the bremsstrahlung and coherence effects vanish. This limit is called Bethe-Heitler regime[15].
The nuclear shadowing is also expected for gluons. In the rest frame of the target, it corresponds to shadowing of more complex fluctuations containing one or more gluons. Therefore, this effects is a leading twist correction to the quark shadowing. It can be calculated within the light-cone dipole approach using Green functions technique[16].
Besides coherence effects responsible for the nuclear shadowing at small $x$, one should include another mechanism valid at any energy, which was proposed at [17, 18] and applied for the description of various processes in proton-nucleus and nucleus-nucleus collisions. It can be interpreted as a restriction coming from the energy conservation near kinematic limit in multiple initial state interactions inside the nucleus. This leads to additional suppression in particle production off nuclei. As a result, nuclear modified quark distribution functions of the incident proton correlates with the target in contrast to the QCD factorization[19].
The influence of coherence effects on the nuclear modification factor for dilepton and direct photon production is examined in this work in the color dipole approach at energies from the fixed target E772 up to collider LHC experiments. In the second chapter, more detailed outlook on observed nuclear effects is presented within kinematical regions where they are expected to dominate. In the third chapter, the color dipole approach to direct photon and dilepton production on proton target is presented including all the ingredients needed for calculations. The fourth chapter contains a formulation of the coherence length and the proper derivation of the cross-sections needed for the calculations of coherence effects in the limit of long and short coherence length for proton-nucleus collisions. Also a formula for the leading twist correction to coherence effects in the form of gluon shadowing is derived in this chapter. The fifth chapter contains a study of nuclear effects not connected with quantum coherence - ISI effects and izospin corrections. Previously derived cross-sections for proton-nucleus collisions are further extended to heavy-ion collisions in the sixth chapter. The summary is presented in the last chapter.
Note: Throughout the work, system of natural units $\hbar = c = 1$ is used. Therefore, energy, momentum and mass units are always referred as $GeV$ omitting the speed of light.

# Chapter 2

# Nuclear effects

It is known for a long time that the cross-section of the particle production in proton-nucleus collisions is not equal to $A$ times the cross-section of the particle production in proton-proton collisions, where $A$ is the mass number of a nucleus. The ratio of these two cross-sections is called the nuclear modification factor $R$ and the deviation of this quantity from unity is a measure of nuclear effects. Several kinds of nuclear effects can be recognized(see fig. 2.1) that influence the distribution of the modification factor, but the overall integral of the distribution has to be unity to preserve the parton distribution sum rules.

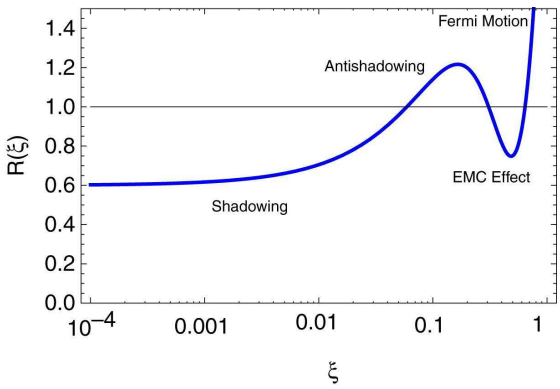


Figure 2.1: A sketch of the nuclear modification factor dependence on the light-front momenta $\xi = x_2$. The four main regions can be recognized with different physical explanations named in the plot. The figure is taken from [20].

Each effect dominates in different kinematic region characterized by the Bjorken variable in the target. If a particle is produced with the mass $M$, the transverse momentum $p_T$ and the pseudorapidity $\eta$ in a hard reaction, the corresponding values of the Feynman variable $x_F$ and Bjorken variables $x_1$ and $x_2$ with respect to the beam and the target are[21]

$$x_1 = \frac{\sqrt{M^2 + p_T^2}}{\sqrt{s}} e^{\eta} \qquad x_2 = \frac{\sqrt{M^2 + p_T^2}}{\sqrt{s}} e^{-\eta} \qquad x_F = x_1 - x_2 \tag{2.1}$$

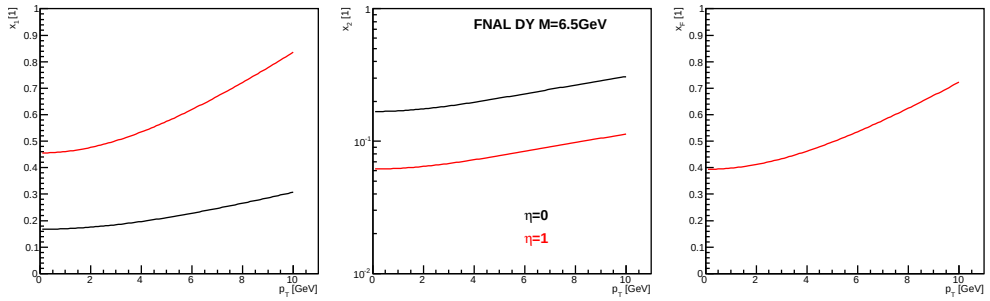


Figure 2.2: Transverse momentum dependence of Bjorken $x_1$ and $x_2$ and Feynman variable $x_F$ for energies accessible at FNAL experiments $\sqrt{s} = 36GeV$ for various rapidities.

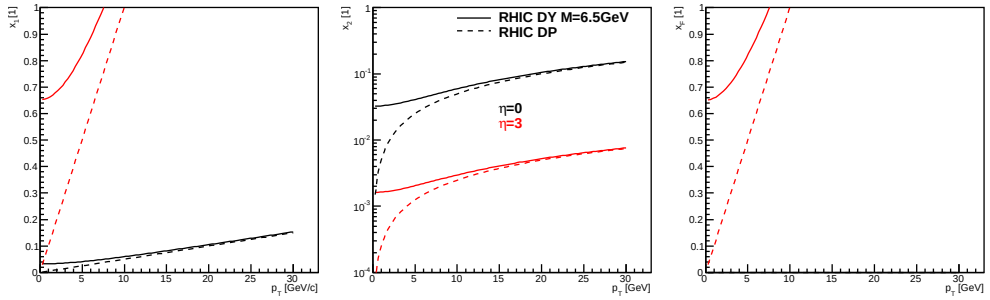


Figure 2.3: Transverse momentum dependence of Bjorken $x_1$ and $x_2$ and Feynman variable $x_F$ for energies accessible at RHIC experiments $\sqrt{s} = 200GeV$ for various rapidities.

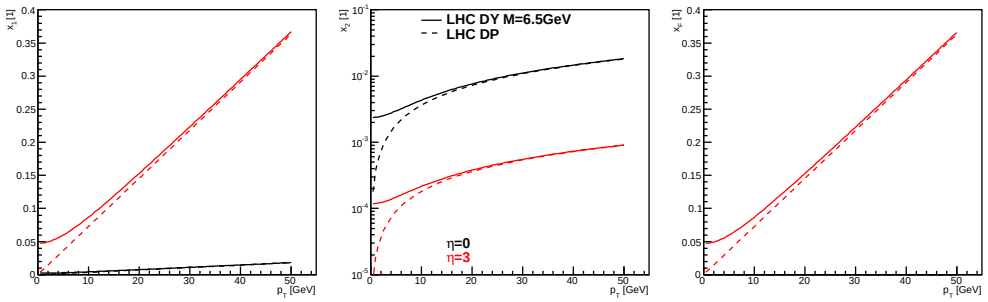


Figure 2.4: Transverse momentum dependence of Bjorken $x_1$ and $x_2$ and Feynman variable $x_F$ for energies accessible at LHC experiments $\sqrt{s} = 2760GeV$ for various rapidities.

In the region $x_2 \sim 1$, there is a rapid enhancement called a Fermi effect, which is connected to the enhancement of a particle production near the kinematical threshold. In the limit $x_2 \to 1$, the quasi-free Fermi motion of nucleons inside nucleus can add to the sub-threshold total energy available for particle production leading to the enhanced production of studied particles[22, 23]. This effect has a non-negligible contribution at SPS energies and lower, and thus, it is not taken into consideration in this work.

In the region $x_2 \sim 0.5$, there is a suppression of the production rate first observed by the European Muon Collaboration[24]. There is no common agreement on the source of this effect, yet several explanations exist[25, 26] - nuclear binding force, pion exchange or a change in the nucleon radius. There is no evidence that this effect is of the coherent origin. Therefore, this effect is not included into calculations presented here.
In the region $x_2 \sim 0.1$, there is a slight enhancement called Cronin effect or anti-shadowing, which was first observed in high-$p_T$ hadron production[27] and is related to the effect of nuclear broadening of the $p_T$ spectra in the multiple re-scattering of hadrons or partons colliding with the nucleus[28].
Finally, in the region $x_2 \leq 0.1$, a nuclear suppression of the production rate occurs and is usually interpreted as a shadowing of inner nucleons by the surface of the nucleus or a saturation of target scattering centers[26].
Leaving behind the first two effects, one can ask, whether remaining effects originate in coherent interaction of target nucleons with incident particle or they have other explanation. It is tempting to interpret it as a result of constructive or destructive interference between amplitudes coming from the scattering of incident particles on different nucleons, since the light-front momentum in the target is low. Nevertheless, the magnitude of $x_2$ is not decisive quantity to manifest the strength of the coherence effects. The magnitude of coherence effects is controlled by the coherence length $l_c = K/m_N x_2$(see corresponding section for details), which can be interpreted as a length of the propagation of a quark fluctuation or as a time needed to distinguish a radiated particle from the static field of the quark. The longer the coherence length is the stronger coherence effects are. The formula for coherence length depends on the reference frame and, therefore, the explanation of coherence effects has to be treated separately for each coordinate system. The QCD predicts $K = 1/2$ and so the continuous decrease of the coherence length with $x_2$ and rise with $x_1$ in the infinite momentum frame. Thus, coherence effects should be dominant at forward rapidities(low $x_2$) and the $x_2$ scaling is presumed for the magnitude of coherence effects. But the evaluation of the coherence length in the rest frame of the target leads to the formula (4.13), which actually drops with $x_1 \to 1$ breaking the $x_2$ scaling(see corresponding section).
The Cronin effect is usually interpreted as a result of multiple interactions of the parton in the nucleus[27, 28]. However, in the infinite momentum frame it should be interpreted as a modification of parton distribution function in the nucleus due to enhanced transverse momentum of a parton inside colliding hadrons[28]. Since the original parton model does not contain information about the transverse motion of partons, one has to include an ad-hoc distribution of the soft primordial transverse momentum of a parton inside the hadron resulting in an enhanced mean transverse momentum of interacting particles and so to an enhancement of the cross-section of particles produced with "middle" $p_T$. In the rest frame of the target, the underlying mechanism is dependent on the coherence length. In the regime of small coherence length, the hard fluctuation is created deep inside the nucleus right before loosing coherence. Meanwhile, the incident hadron can have multiple soft interactions in the nucleus. It does not lead to the production of any particle, but the mean transverse

momentum of partons is changed. It can be viewed as if the propagating fluctuation were subject to "Brownian motion" in the transverse momentum plane induced by multiple soft re-scatterings leading to enhanced probability to produce particle with higher $p_T$ than in one hard scattering[9]. In the regime of long coherence length, the nuclear broadening is due to the color filtering of the nucleus. The fluctuation is created long before entering nucleus and due to Lorentz time dilatation components of the fluctuation cannot influence each other, and so, no change of transverse momenta can be transferred from the interaction of the quark in the nucleus to the photon. Nevertheless, the harder(smaller) the fluctuation is, the stronger the transverse momentum transfer is needed to disrupt the coherence. Large fluctuations have high probability to lose coherence on the surface of the nucleus while small fluctuations can be still resolved due to addition of small sub-threshold momentum transfers from multiple re-scattering in the nucleus. Therefore, the nucleus can disrupt smaller fluctuations than the nucleon target and so the cross-section on the nucleus is enhanced at "middle" $p_T$. In other words, the nucleus acts like a color filter[29]. As one can see, the Cronin enhancement occur regardless on coherence length. However, in the latter limit it is reduced by the effect of shadowing.

The suppression of the production rate at $x_2 \leq 0.1$ was predicted by Gribov[13] as a result of the nuclear shadowing, where nucleons compete on releasing the particle in a hard interaction. The explanation of the shadowing in the rest frame of the target is rather intuitive. If the coherence length is longer than nuclear radius, the fluctuation is created before it enters the nucleus and it is disrupted in a hard interaction on a surface nucleons. Even if there is another hard interaction after the emission of a particle, the incident parton cannot radiate another particle before it re-creates it's color field and develop another fluctuation. Therefore, the incident particle cannot radiate in each successive interactions inside the nucleus. This behaviour is known from the quantum electrodynamics as the Landau-Pomeranchuk and Migdal effect[14]. This limit is naturally incorporated in the optical Glauber model of high-energy multiple re-scatterings inside the nucleus. It was formulated within the non-relativistic quantum mechanics as the eikonal approximation with the assumption that phases from different scattering combine additively. Nevertheless, in reality the eikonal model overpowers the magnitude of shadowing because it does not allow for the interference between amplitudes. This was elaborated by Gribov[13] within the quantum field theory, which lead to Gribov corrections for the Glauber model. As one goes to lower coherence length, the coherent production of particles is weaker and if the coherence length is shorter than mean inter-nucleon spacing, then each inelastic collision contributes to the production of particles and so shadowing vanishes. This limit corresponds to the Bethe-Heitler regime[15].

In the infinite momentum frame the description of the shadowing is due to partonic fusion[30]. As one moves to very small $x_2$ an extremely accelerated nucleus is Lorentz contracted in the longitudinal direction. Therefore, the distance between nucleons is contracted too and as the number of gluons seen in the nucleon increase during the acceleration, gluon clouds starts to overlap in the transverse plane.

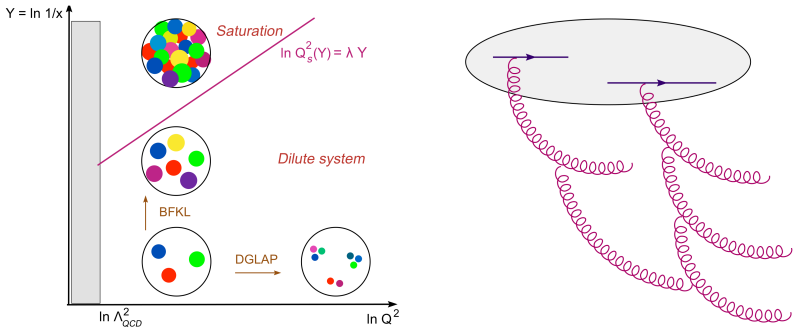


Figure 2.5: Sketch of the gluon density evolution in highly accelerated nucleons and the transition to CGC regime. Figures are taken from [30]

Eventually, from certain energy (called saturation scale) the gluon density is so high that the probability of gluon fusion ($qg \to q$ or $gg \to g$) overweights the probability to radiate more gluons and the number of gluons in the target actually drops, and so, the cross-section of the production of certain particle on a nucleus is suppressed. This effect is called the Color Glass Condensate(CGC) and it is controlled by the target gluon density, which is proportional to the light-front momentum fraction of the target $x_2$, and so, it predicts the $x_2$ scaling. In the rest frame of the target the effect of suppression due to the gluon fusion is related to different Fock components in the incoming hadron. Multiple interactions of those fluctuations give rise to the quark and gluon shadowing[31](see corresponding section).
Indeed, the nuclear suppression was observed in several experiments mainly at large rapidities(small $x_2$) - e.g. in BRAHMS experiment[32] at RHIC for charged hadron production, in NA49[33] experiment at SPS for the pion and charmonium production and even in E772 experiment[11] at FNAL for the dilepton and charmonium production

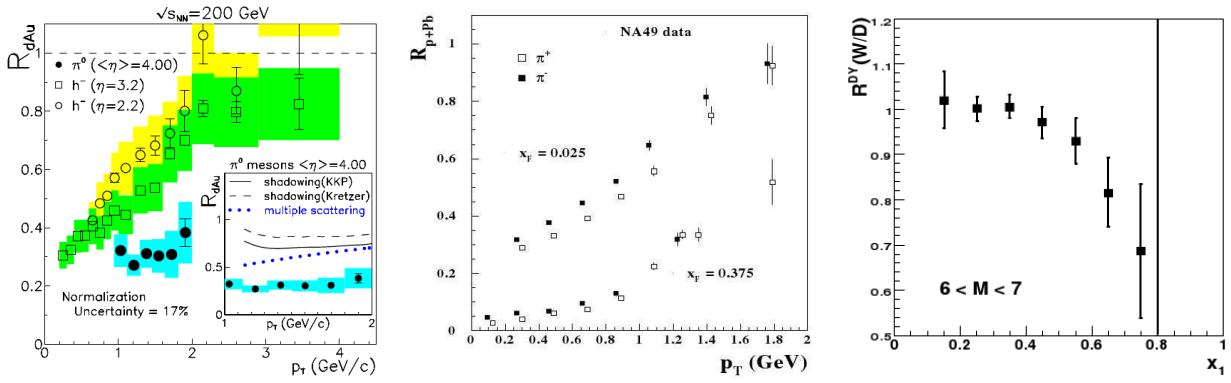


Figure 2.6: Collection of data indicating common suppression pattern at forward rapidities. Figures are taken from [32, 33, 11]

Nevertheless, the presence of the suppression at low energy experiments cannot be explained only by the parton fusion, since valence quarks dominate in this energy range. Models based on the Color Glass Condensate can describe the suppression at forward rapidities at high energies since the partonic composition is dominated by gluons. Nevertheless, the interpretation of large rapidity suppression is not so straightforward since there is no consensus so far about the strength of the gluon shadowing and CGC. The BRAHMS data at $y = 3.2$ are fitted rather than explained(see [31]) within this model - if one fixes the saturation scale to reproduce correctly data for one rapidity, it completely fails to describe other rapidities. Moreover, inclusion of BRAHMS data into nuclear parton distribution parametrizations[34] leads to grossly exaggerated gluon shadowing which conflicts with the unitarity bound[35]. In addition, careful analysis of available data shows[36, 19] that the $x_2$ scaling is broken and suggest the presence of the $x_F$ scaling

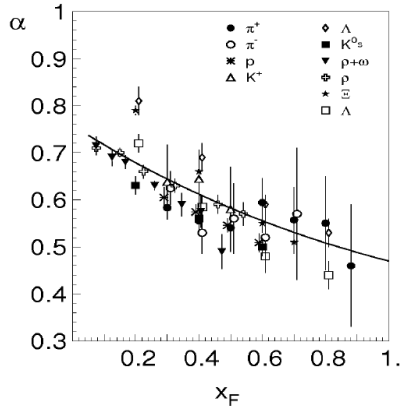


Figure 2.7: Collection of data in the energy range from 70 to $400GeV$ indicating that the suppression scales with $x_F$. The variable $\alpha$ has a meaning of exponent in the approximation $R_{pA} = A^{\alpha}$. Figure is taken from [19]

Therefore, apart from coherence effects(CGC and shadowing) there is an evidence in data for energy independent effect that scales with $x_F$ and that is present for any particle produced in the interaction. Such mechanism is proposed as a result of the energy conservation restrictions in multiple parton re-scatterings inside the nuclear medium[19, 17, 18] and is formulated in corresponding section.

# Chapter 3

# Dilepton and direct photon production in proton-proton collisions

## 3.1 Quantum chromodynamics on the light-cone

A fundamental theory that is used for the description of physics of hadron and nuclear collisions is the quantum chromodynamics(QCD). In principle, it describes a hadron structure and dynamics using quark and gluon degrees of freedom. In practice, the use of QCD to describe phenomena in hadron or even nuclear collisions is rather difficult because of the complexity of the whole theory and interplay of perturbative effects with non-perturbative effects such as color confinement or coherence. In most applications such as large momentum transfer processes one can make predictions using the factorization theorem that separate hard perturbative dynamics from the non-perturbative physics included in the hadron and nuclear binding. In other applications, such as the passage of hadrons through nuclear matter or low momentum transfer processes, the use of factorization is problematic and one is forced to use other formulations.
The form of Lorentz invariant observables has to be equal in any reference frame. A usual way to parametrize the space-time(called instant form) is that the system is fully described at some initial time $t = 0$. From this initial state the system can be propagated to any time using equations of motion. Other parametrizations can be reached by means of Lorentz transformation. Nevertheless, there is a parametrization not accessible by Lorentz transformation, that has some remarkable features. Namely, a frame of reference that is boosted at a velocity $v = c$ is called a light-cone frame. The system described by the theory on the light cone has to be specified at some fixed light-cone time.
Let's denote an instant form of the four-vector $x = (x^0, x^1, x^2, x^3)$, where $x^0 = ct$ is a time component and $x^i, i \in 1..3$ are spatial components. Light cone components can be defined as

$$\begin{aligned} x^+ &= x^0 + x^3 \\ x^- &= x^0 - x^3 \\ \vec{x}^T &= (x^1, x^2), \end{aligned} \tag{3.1}$$

where $x^+$ is called "light-cone time". The metric tensor in this basis has a form

$$g^{\mu\nu} = \begin{pmatrix} 0 & 0 & 0 & 2 \\ 0 & -1 & 0 & 0 \\ 0 & 0 & -1 & 0 \\ 2 & 0 & 0 & 0 \end{pmatrix}. \tag{3.2}$$

The scalar product can be re-written as

$$x \cdot y = \frac{1}{2}(x^+ y^- + x^- y^+) - \vec{x}^T \cdot \vec{y}^T. \tag{3.3}$$

The four-momentum vector $p = (E, \vec{p}c)$ can be re-defined in the same way, but now $p^-$ represents the light-cone energy, as it conjugates with the light-cone time $x^+$(for details see Appendix A). The on-shell condition then reads

$$p^2 = m^2 \quad \Rightarrow \quad p^- = \frac{p_T^2 + m^2}{p^+}. \tag{3.4}$$

This type of quantization is particularly suitable for relativistic bound state problems. One of remarkable features is that the ground state of the free theory is also a ground state of the theory with the interaction, and so, the Fock expansion of the vacuum state provides a complete basis for diagonalizing the full theory. Moreover, light-cone wave functions $\Psi_n$ that describe a probability of having any particular quark and gluon state $|n\rangle$ inside the hadron or nuclei are frame independent[37].
Essential variables for the formulation of the light-cone wave function are the boost-invariant light-cone momentum fractions

$$x_i = \frac{p_i^+}{p_h^+}, \tag{3.5}$$

where $p_h^\pm = p_h^0 \pm p_h^3$ and $p_i^\pm = p_i^0 \pm p_i^3$ are hadron and quark light-cone momenta. The internal transverse momentum variables are $\vec{k}_i^T = \vec{p}_i^T - x_i \vec{p}_h^T$ with constraints $\sum_i \vec{k}_i^T = 0$ and $\sum_i x_i = 1$. The light-cone momentum fractions $x_i$ and transverse momenta $\vec{k}_i^T$ can be viewed as relative coordinates of internal degrees of freedom(quarks and gluons) inside the hadronic system, and so, they are independent on it's total four-momentum $p$.
The entire spectrum of hadrons and their scattering states is given by the set of eigenstates of the light-cone hamiltonian of QCD defined as $H_{LC} = p_h^- p_h^+ - p_T^2$

$$H_{LC}|\Psi_h\rangle = M_h^2|\Psi_h\rangle \tag{3.6}$$

and an individual hadron $h$ can be described by the eigenfunction $|\Psi_h\rangle$ with the eigenvalue $M_h^2$ using complete set of quark and gluon states $|n\rangle = |qqq\rangle, |qqqg\rangle \ldots$ (assuming they are eigenstates of free hamiltonian and they preserve all quantum numbers of the hadron $h$)[37]

$$|\Psi_h\rangle = \sum_n \Psi_n(x_i, \vec{k}_i^T, \lambda_i)|n\rangle, \tag{3.7}$$

where $\lambda_i$ are helicities of constituents.
Since the number of particles in relativistic quantum systems is not an invariant quantity, the sum representing a wave function of a hadron runs over Fock states of arbitrary particle number and one can see a hadron as a second quantized sum over fluctuations of color singlet partonic states of different momenta and number of constituents. Consequently, probability coefficients of these fluctuations are light-cone wave functions $\Psi_n$. The invariant mass of partons in a given Fock state is then

$$M^2 = \sum_i \frac{(k_i^T)^2 + m_i^2}{x_i}. \tag{3.8}$$

The hadron wave function is generally dominated by configurations with minimum values of $M^2$ since the probability for the occurrence of heavier fluctuations decrease strongly. Using light-cone wave functions $\Psi_n$, every hadronic dynamical quantity can be calculated by the convolution with appropriate quark and gluon matrix element[37]

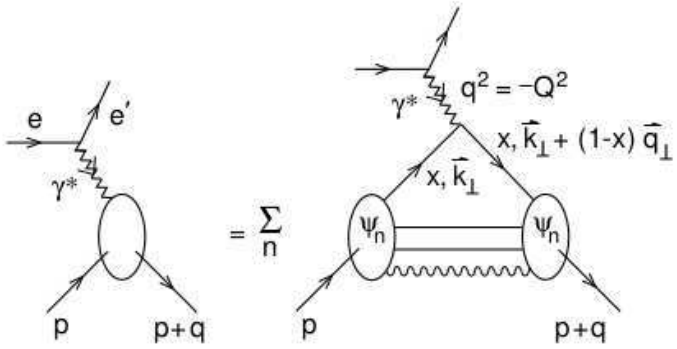


Figure 3.1: The deep inelastic scattering written in terms of the scattering on Fock components of the proton in the light-cone approach. Figure is taken from [37].

## 3.2 The color dipole approach to dilepton and direct photon production

One of many interesting processes in hadron-hadron collisions is the production of hard electromagnetic radiation - either lepton pairs coming from the decay of massive virtual photon or direct real massless photon production. The former process is usually called the Drell-Yan process[38]. This process corresponds to the annihilation of a quark and an anti-quark from each hadron in the parton model formulated in the infinite momentum frame.

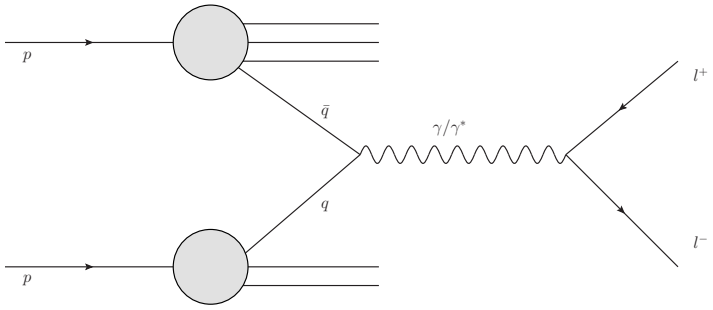


Figure 3.2: Sketch of the partonic process leading to dilepton or real photon production in the parton model.

Nevertheless, the same process viewed in the rest frame of one hadron looks like a bremsstrahlung from an incident quark. The virtual photon then decays into a dilepton. This radiation can occur before or after the quark scatters off the target.

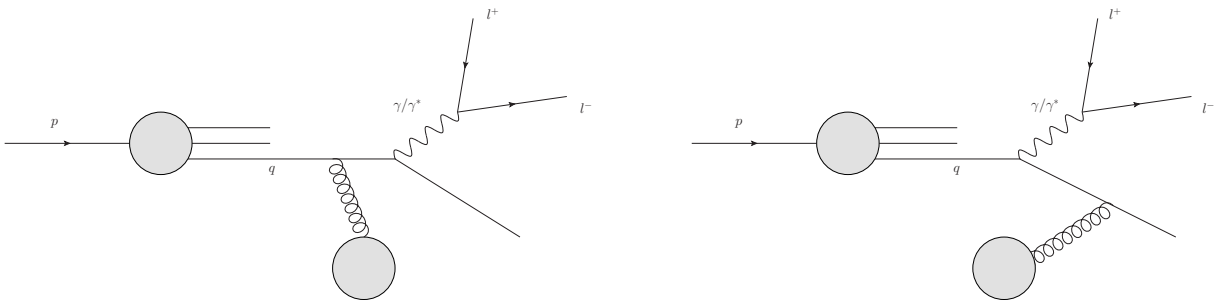


Figure 3.3: Sketch of the partonic process leading to dilepton or real photon production in the rest frame of the target. There are two possibilities - the photon is produced either before or after the interaction with target color field.

Although the cross-section is Lorentz invariant quantity, the space-time interpretation of the process is not Lorentz invariant and, therefore, depends on a reference frame. For the

description of this type of processes in the rest frame of the target, the color dipole approach was formulated[4, 5].
In this model, the projectile quark can be expanded into the Fock series[4]

$$|q\rangle = \sqrt{Z_2}|q_{bare}\rangle + \Psi^{T,L}_{\gamma q}|q\gamma\rangle + \Psi^{T,L}_{\gamma qG}|q\gamma G\rangle + \dots, \tag{3.9}$$

where $Z_2$ is the renormalization constant for the wave function of a fermion and $\Psi^{T,L}_{\gamma q}$ gives the probability to develop transversely or longitudinally polarized state $|q\gamma\rangle$. Assuming that the transverse separation between particles in Fock state is fixed during the interaction than these Fock states correspond to eigenstates of the interaction. In order to produce a photon, the interaction of an incoming quark with the color field of the target has to distinguish between different states. Since the first two states in the expansion are most probable, one can restrict the description to them as a lowest approximation. Thus, the interaction cannot distinguish these two states since only quark can interact with the strong color field of the target. Therefore, the difference between interacting states has to come from the relative displacement of a quark in each state in the transverse plane. The development of the $|q\gamma\rangle$ state can be understood in such way that the incoming quark is substituted with coherent state of a quark and a virtual photon, while the center of mass of the fluctuation in the transverse plane coincides to the incident quark. If $\rho$ is the transverse separation between a quark and a photon, the distance between a quark or a photon and a center of gravity respectively in transverse plane is $(1-\alpha)\rho$ or $\alpha\rho$ respectively, where $\alpha$ is a fraction of the light-cone momentum of the initial quark taken by the photon.

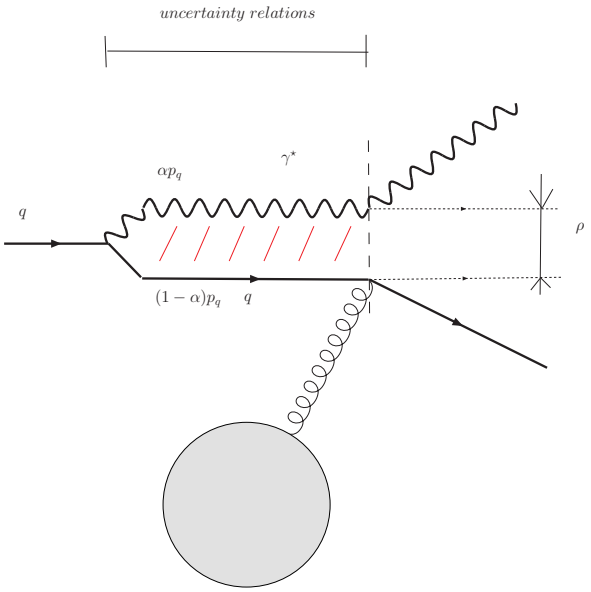


Figure 3.4: A detailed look on a fluctuation propagation and its consecutive disruption.

The coherence of the fluctuation is interrupted by the interaction with the target color field and the photon is released on mass shell and, eventually, decays into a lepton pair. In contrast to the parton model the formulation in the rest frame of the target consists of two diagrams where photon can be emitted before or after the quark is scattered on a nucleon[4]. In each configuration the incident quark comes to the point of the interaction with the color field at different transverse distance. Interference between both amplitudes gives rise to the situation that can be viewed as a quark dipole scattering off the color field. Therefore, the cross-section can be formulated in factorized form using the color dipole cross-section from the deep inelastic scattering[4, 5, 39](see Appendix B)

$$\frac{\mathrm{d}\sigma(qp \to \gamma X)}{\mathrm{d}\ln\alpha} = \int \mathrm{d}^2\rho |\Psi_{\gamma q}(\alpha,\rho)|^2 \sigma^N_{q\bar{q}}(\alpha\rho, x_2), \tag{3.10}$$

where $\sigma^N_{q\bar{q}}$ is a dipole cross-section(for details see next section) and $\Psi_{\gamma q}$ is a light-cone wave function, i.e. $|\Psi_{\gamma q}(\alpha,\rho)|^2$ gives the probability that incident quark develops into a $\gamma q$ fluctuation with transverse separation $\rho$ and relative part of light-cone momentum of a photon and quark is $\alpha$ and $1-\alpha$, respectively. Furthermore, the summation over longitudinally and transversely polarized photons has to be accounted. The light-cone wave function of the $\gamma q$ fluctuation for transversely and longitudinally polarized photons can be expressed as [39]

$$\Psi^{T,L}_{\gamma q}(\alpha,\rho) = \frac{\sqrt{\alpha_{em}}}{2\pi}(\bar{\chi}_f \hat{\mathcal{O}}^{T,L}_{\gamma q}\chi_i)K_0(\varepsilon\rho), \tag{3.11}$$

where $\chi_{f,i}$ are 2-component spinors of the final and initial quarks, $\varepsilon^2 = m_q^2\alpha^2 + M^2(1-\alpha)$ and $K_0$ is a modified Bessel function. Operators $\hat{\mathcal{O}}$ can be expressed as[39]

$$\begin{aligned}
\hat{\mathcal{O}}^T_{\gamma q} &= i m_q \alpha^2 \vec{e}^{\,*}(\vec{n}\times\vec{\sigma}) - i(2-\alpha)(\vec{e}^{\,*}\cdot\vec{\nabla}_p) + \alpha\vec{e}^{\,*}(\vec{\sigma}\times\vec{\nabla}_\rho) \\
\hat{\mathcal{O}}^L_{\gamma q} &= 2M(1-\alpha),
\end{aligned} \tag{3.12}$$

where $\vec{e}$ is a polarization vector of the photon, $\vec{n}$ is a unit vector along the projectile momentum, $\vec{\sigma}$ is a vector of Dirac matrices, $m_q$ is an effective quark mass and $M$ is an invariant mass of the photon. An exact form of the square of the wave function can be calculated using[39]

$$\begin{aligned}
\Psi^{T*}_{\gamma q}(\alpha,\rho_1)\Psi^T_{\gamma q}(\alpha,\rho_2) &= \frac{\alpha_{em}}{2\pi^2}\left(m_q^2\alpha^4 K_0(\varepsilon\rho_1)K_0(\varepsilon\rho_2) + (1+(1-\alpha)^2)\varepsilon^2\frac{\vec{\rho}_1\cdot\vec{\rho}_2}{\rho_1\rho_2}K_1(\varepsilon\rho_1)K_1(\varepsilon\rho_2)\right) \\
\Psi^{L*}_{\gamma q}(\alpha,\rho_1)\Psi^L_{\gamma q}(\alpha,\rho_2) &= \frac{\alpha_{em}}{2\pi^2}\left(2M^2(1-\alpha)^2 K_0(\varepsilon\rho_1)K_0(\varepsilon\rho_2)\right)
\end{aligned} \tag{3.13}$$

that leads to the formula

$$
\begin{aligned}
|\Psi_{\gamma q}(\alpha,\rho)|^2 &= |\Psi^T_{\gamma q}(\alpha,\rho)|^2 + |\Psi^L_{\gamma q}(\alpha,\rho)|^2 = \\
&= \frac{\alpha_{em}}{2\pi^2}\left((m_q^2\alpha^4 + 2M^2(1-\alpha)^2)K_0^2(\epsilon\rho) + (1+(1-\alpha)^2)\varepsilon^2 K_1^2(\varepsilon\rho)\right). \quad (3.14)
\end{aligned}
$$

In order to form a hadronic cross-section, it is essential to identify light-cone variables on parton level using macroscopically measured quantities in the rest frame of the target. Let's denote 4-momentum of measured real/virtual photon $p^\mu_\gamma$, incident proton $p^\mu_p$ and target proton $p^\mu_{p'}$

$$
\begin{aligned}
p^\mu_\gamma = (E_\gamma, \vec{p}^{\,T}_\gamma, p^z_\gamma) \qquad & E^2_\gamma - (p^T_\gamma)^2 - (p^z_\gamma)^2 = M^2 \\
p^\mu_p = (E_p, 0, p^z_p) \qquad & E^2_p - (p^z_p)^2 = m^2_N \\
p^\mu_{p'} = (E_{p'}, 0, 0) = (m_N, 0, 0) \qquad & E^2_{p'} = m^2_N. \quad (3.15)
\end{aligned}
$$

One can characterize hadron collision using parton model kinematic variables for projectile $x_1$ and target $x_2$ together with invariant square of cms energy $s$ and square of the photon momentum $q^2 = p^2_\gamma$ defined as

$$
x_1 = \frac{2p^\mu_{p'}(p_\gamma)_\mu}{s}; \quad x_2 = \frac{2p^\mu_p(p_\gamma)_\mu}{s}; \quad s = (p_p + p_{p'})^2 = 2m^2_N + 2m_N E^{LAB}; \quad q^2 = M^2, \quad (3.16)
$$

where $E^{LAB}$ is the energy of the collision in the laboratory frame, $m_N$ is a mass of the nucleon and $x_F = \frac{p^z_\gamma|_{cms}}{p^z_\gamma|_{cms}^{max}}$ is the Feynman variable. The relation between kinematic variables can be expressed as[21](neglecting proton mass)

$$
\begin{aligned}
x_1 &= \frac{\sqrt{x_F^2 + 4\frac{M^2+\vec{p}_T^{\,2}}{s}} + x_F}{2} = \sqrt{\frac{p_T^2 + M^2}{s}}e^{\eta} \\
x_2 &= \frac{\sqrt{x_F^2 + 4\frac{M^2+\vec{p}_T^{\,2}}{s}} - x_F}{2} = \sqrt{\frac{p_T^2 + M^2}{s}}e^{-\eta} \\
x_1 x_2 &= \frac{M^2 + \vec{p}_T^{\,2}}{s} \qquad x_F = x_1 - x_2, \quad (3.17)
\end{aligned}
$$

where the photon transverse momentum $\vec{p}^{\,T}_\gamma$ is denoted as $\vec{p}_T$(this holds from now on through the text), $\eta$ is a pseudo-rapidity of the photon and the definition of light-cone variables $x_1$ and $x_2$ was used

$$
x_1 = \frac{p^+_\gamma}{p^+_p} = \frac{E_\gamma + p^z_\gamma}{E_p + p^z_p} \qquad x_2 = \frac{p^+_\gamma}{p^+_{p'}} = \frac{E_\gamma + p^z_\gamma}{E_{p'} + p^z_{p'}}. \quad (3.18)
$$

Taking into account the definition of $\alpha = \frac{p_\gamma^+}{p_q^+} = \frac{E_\gamma + p_\gamma^z}{E_q + p_q^z}$, one can see a manifestation of non-invariance of the space-time description, since in contrast to parton model, where $x_1$ is a part of momentum of incident quark that annihilates with and anti-quark, taken away by photon, here, $x_1$ is a part of momentum of proton carried away by photon. Therefore, parton distribution of proton is probed at $x_q = \frac{p_q^+}{p_p^+} = \frac{x_1}{\alpha}$ with invariant energy on the parton level being $s_q = s x_q$.
The hadronic cross-section is formed by summing up partonic cross-sections from incident quarks and anti-quarks weighted with corresponding parton distribution functions in the projectile hadron integrated over quark or anti-quark momentum fractions inside the hadron[4]

$$\begin{aligned}
\frac{\mathrm{d}\sigma(pp \to \gamma/\gamma^* X)}{\mathrm{d}M^2 \mathrm{d}x_F} &= \frac{\mathrm{d}\sigma(\gamma^* \to l^+ l^-)}{\mathrm{d}M^2} \frac{x_1}{x_1 + x_2} \int\limits_{x_1}^{1} \frac{\mathrm{d}\alpha}{\alpha^2} \sum_q Z_q^2 \left( f_q\left(\frac{x_1}{\alpha}\right) + f_{\bar{q}}\left(\frac{x_1}{\alpha}\right)\right) \frac{\mathrm{d}\sigma(qp \to \gamma X)}{\mathrm{d}\ln\alpha} \\
&= \frac{\mathrm{d}\sigma(\gamma^* \to l^+ l^-)}{\mathrm{d}M^2} \frac{1}{x_1 + x_2} \int\limits_{x_1}^{1} \frac{\mathrm{d}\alpha}{\alpha} F_2^p\left(\frac{x_1}{\alpha}, Q^2\right) \frac{\mathrm{d}\sigma(qp \to \gamma X)}{\mathrm{d}\ln\alpha} \\
\frac{\mathrm{d}\sigma(\gamma^* \to l^+ l^-)}{\mathrm{d}M^2} &= \frac{\alpha_{em}}{3\pi M^2}, \qquad (3.19)
\end{aligned}$$

where $f_q$ and $f_{\bar{q}}$ are parton distribution functions(PDFs) of quarks and anti-quarks and $F_2^p$ is a proton structure function

$$F_2^p(x, Q^2) = \sum_q Z_q^2 (x f_q(x, Q^2) + x f_{\bar{q}}(x, Q^2)), \qquad (3.20)$$

$Q^2 = p_T^2 + (1 - x_1) M^2$ is a scale of the process[40], $Z_q$ is a fractional charge of the quark flavour and $\alpha_{em}$ is a fine structure constant.
The dependence of the cross-section on the transverse momentum of the photon is given by four-fold Fourier transformation[39](see Appendix B)

$$\begin{aligned}
\frac{\mathrm{d}\sigma(qp \to \gamma X)}{\mathrm{d}\ln\alpha \mathrm{d}^2 p_T} &= \frac{1}{(2\pi)^2} \int \mathrm{d}^2\rho_1 \mathrm{d}^2\rho_2 e^{i\vec{p}_T \cdot (\vec{\rho}_1 - \vec{\rho}_2)} \Psi_{\gamma q}^*(\alpha, \rho_1) \Psi_{\gamma q}(\alpha, \rho_2) \times \\
&\quad \times \frac{1}{2} \left( \sigma_{q\bar{q}}^N(\alpha\rho_1, x_2) + \sigma_{q\bar{q}}^N(\alpha\rho_2, x_2) - \sigma_{q\bar{q}}^N(\alpha|\vec{\rho}_1 - \vec{\rho}_2|, x_2)\right) \\
\frac{\mathrm{d}\sigma(pp \to \gamma/\gamma^* X)}{\mathrm{d}M^2 \mathrm{d}x_F \mathrm{d}^2 p_T} &= \frac{\mathrm{d}\sigma(\gamma^* \to l^+ l^-)}{\mathrm{d}M^2} \frac{1}{x_1 + x_2} \int\limits_{x_1}^{1} \frac{\mathrm{d}\alpha}{\alpha} F_2^p\left(\frac{x_1}{\alpha}, Q^2\right) \frac{\mathrm{d}\sigma(qp \to \gamma X)}{\mathrm{d}\ln\alpha \mathrm{d}^2 p_T} \\
\Psi_{\gamma q}^*(\alpha, \rho_1) \Psi_{\gamma q}(\alpha, \rho_2) &= \Psi_{\gamma q}^{T*}(\alpha, \rho_1) \Psi_{\gamma q}^T(\alpha, \rho_2) + \Psi_{\gamma q}^{L*}(\alpha, \rho_1) \Psi_{\gamma q}^L(\alpha, \rho_2), \qquad (3.21)
\end{aligned}$$

where $\rho_1$ and $\rho_2$ are quark-photon transverse separations corresponding to two different amplitudes contributing to the cross-section. The formula is already integrated over final

quark transverse momenta. Integration of the above formula over the photon transverse momenta recover the formula for $x_F$ dependence as expected.
Note that in reality, the fraction $\alpha$ of the momentum of the quark taken by the photon cannot reach 1, since then the quark could not form the fluctuation and the photon would be instantly created out of the quark, which violates conservation laws. Alternatively, the condition for the upper bound of $\alpha$ can be determined from the fact that the invariant mass of the final state cannot exceed the total available energy of the quark-nucleon system, i.e.

$$s_q \geq \frac{M^2}{\alpha} + \frac{m_q^2}{(1-\alpha)} + \frac{p_T^2}{\alpha(1-\alpha)} \tag{3.22}$$

leading to the condition(neglecting the mass of the quark $m_q$)

$$\alpha \leq 1 - \frac{p_T^2}{x_1 s - M^2}. \tag{3.23}$$

This realistic bound is important at low or moderate energies since the integrand is peaked around $\alpha = 1$. Nevertheless, the impact of the realistic bound is very small at sufficiently high energies.
Let's denote that apart from phenomenologically determined functions $\sigma_{q\bar{q}}^N$ and $f_q(f_{\bar{q}})$ the only free parameter in the color dipole approach is the effective quark mass $m_q = 0.2\,GeV$. For the discussion on a value of the effective quark mass see [41, 29], but the influence on the calculation is limited.

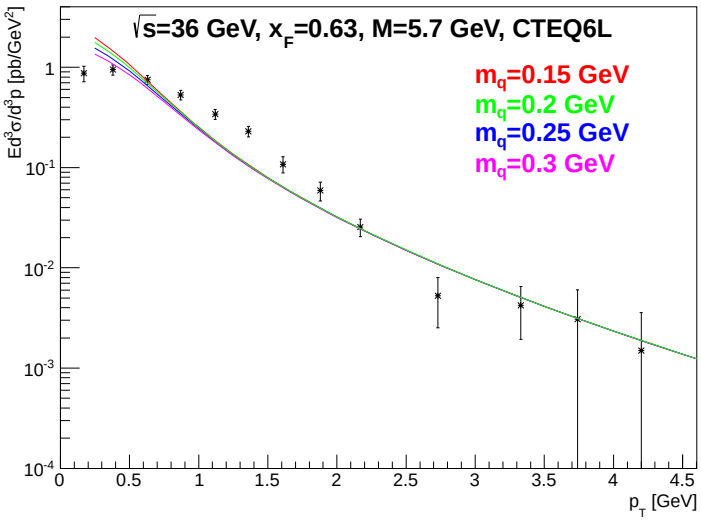


Figure 3.5: The $p_T$ spectrum of the Drell-Yan process at energy corresponding to E866 experiment for different effective quark masses. Data are taken from E866 experiment[42].

The quark mass plays a role of a global cut-off in order to reproduce finite cross-section at the kinematic limit $p_T \to 0$. In standard approach this limit leads to logarithmic divergences leaving the cross-section infinite.
The formula for transverse momentum distribution can be simplified by performing three of four integrals analytically(see Appendix C) to final form

$$\begin{aligned}
\frac{\mathrm{d}\sigma(qp \to \gamma X)}{\mathrm{d}\ln\alpha \mathrm{d}^2 p_T} &= \frac{\alpha_{em}}{2\pi^2}\left( (m_q^2\alpha^4 + 2M^2(1-\alpha)^2)\left(\frac{I_1}{p_T^2+\varepsilon^2} - \frac{I_2}{4\varepsilon}\right) + \right. \\
&\left. (1+(1-\alpha)^2)\left(\frac{\varepsilon p_T}{p_T^2+\varepsilon^2} I_3 - \frac{I_1}{2} + \frac{\varepsilon}{4} I_2\right)\right) \\
I_1 &= \int_0^\infty \mathrm{d}\rho\, \rho J_0(p_T\rho) K_0(\varepsilon\rho)\sigma_{q\bar{q}}(\alpha\rho, x_2) \\
I_2 &= \int_0^\infty \mathrm{d}\rho\, \rho^2 J_0(p_T\rho) K_1(\varepsilon\rho)\sigma_{q\bar{q}}(\alpha\rho, x_2) \\
I_3 &= \int_0^\infty \mathrm{d}\rho\, \rho J_1(p_T\rho) K_1(\varepsilon\rho)\sigma_{q\bar{q}}(\alpha\rho, x_2)
\end{aligned} \tag{3.24}$$

where $J_0$ resp. $J_1$ and $K_0$ resp. $K_1$ are Bessel functions of the first kind and modified Bessel functions of the second kind.
For comparison with data, it is useful to review some facts. For the Drell-Yan process data are usually presented for several bins in invariant mass together with mean value of the invariant mass $\langle M \rangle$ for each bin. This corresponds to use of integrated virtual photon decay cross-section $\sigma(\gamma^* \to l^+l^-) = \int_{M^2_{min}}^{M^2_{max}} \mathrm{d}M^2 \frac{\mathrm{d}\sigma(\gamma^* \to l^+l^-)}{\mathrm{d}M^2}$ having

$$\frac{\mathrm{d}\sigma(pp \to \gamma^* X)}{\mathrm{d}x_F} = \sigma(\gamma^* \to l^+l^-)\frac{1}{x_1+x_2}\int_{x_1}^1 \frac{\mathrm{d}\alpha}{\alpha} F_2^p\left(\frac{x_1}{\alpha}, Q^2\right)\left.\frac{\mathrm{d}\sigma(qp \to \gamma X)}{\mathrm{d}\ln\alpha}\right|_{M^2=\langle M\rangle^2}. \tag{3.25}$$

Also, data are usually presented in the form of the invariant cross-section $E\frac{\mathrm{d}^3\sigma}{\mathrm{d}^3 p}$ or azimuthally integrated cross-section $\frac{\mathrm{d}^2\sigma}{\mathrm{d}p_T \mathrm{d}\eta}$. This can be expressed in terms of the above formulas together with

$$E = \sqrt{M^2 + p_\gamma^2} = \sqrt{M^2 + p_T^2 + \frac{s}{4}x_F^2} \tag{3.26}$$

to have[21]

$$E\frac{\mathrm{d}^3\sigma}{\mathrm{d}^3p} = E\frac{\mathrm{d}^3\sigma}{\mathrm{d}^2p_T\mathrm{d}p_L} = \sqrt{M^2 + p_T^2 + \frac{s}{4}x_F^2}\frac{2}{\sqrt{s}}\frac{\mathrm{d}^3\sigma}{\mathrm{d}^2p_T\mathrm{d}x_F} \tag{3.27}$$

$$\frac{\mathrm{d}^2\sigma}{\mathrm{d}p_T\mathrm{d}\eta} = \left|\left(\frac{\mathrm{d}\eta}{\mathrm{d}p_L}\right)_{p_T=konst.} = \frac{1}{E}\right| = E\frac{\mathrm{d}^2\sigma}{\mathrm{d}p_T\mathrm{d}p_L} = 2\pi p_T E\frac{\mathrm{d}^3\sigma}{\mathrm{d}^2p_T\mathrm{d}p_L} = 2\pi p_T E\frac{\mathrm{d}^3\sigma}{\mathrm{d}^3p}. \tag{3.28}$$

## 3.3 Phenomenological parametrizations

For the completeness of the color dipole approach calculation, phenomenological parametrizations of the dipole cross-section $\sigma^N_{q\bar{q}}$ and parton distribution functions $f_q$ have to be specified. The idea of the dipole cross-section comes from the theoretical description of the deep inelastic scattering and depends on the separation of the fluctuation $\rho$ and on Bjorken variable $x_{Bj}$. Since there is no Bjorken variable in hadron-hadron collisions, correct analogy of $x_{Bj}$ in the target rest frame has to be identified. The natural choice is to take $x_2$ since the dipole cross-section describes the interaction of a dipole with the target hadron[4]. In Born approximation the dipole cross-section is independent on energy. The energy dependence is generated by radiation of soft gluons, which can be re-summed in leading log approximation. Using Weizsäcker-Williams approximation, the dipole cross-section can be expressed for small separations using unintegrated gluon density G[41, 43]

$$\sigma^N_{q\bar{q}}(x_2,\rho) = \frac{4\pi}{3}\alpha_s\rho^2 \int \frac{\mathrm{d}^2k_T}{k_T^2}\frac{1-e^{i\vec{k}_T\cdot\vec{\rho}}}{k_T^2\rho^2}\frac{\partial G(x_2,k_T^2)}{\partial \ln k_T^2}, \tag{3.29}$$

where $\vec{k}_T$ is the transverse momentum of the dipole exchanged with the target and $\alpha_s$ is the strong coupling constant at the scale relevant for the process. The dipole cross-section, therefore, behave like $\sim \rho^2$ at small separations $\rho \to 0$. However, at large separations the dipole cross-section is presumed to be saturated in order to suppress contributions from very large dipoles. Nevertheless, the behaviour of the dipole cross-section at large separations is not known exactly and has to be extracted from data. Several parametrizations exist, but most of them do not take into account the QCD evolution of the gluon density, and, consequently, presume the scale of the process to be fixed to some value ($Q \sim 1GeV$).
One of parametrizations is provided by the saturation model of Golec-Biernat and Wüsthöff (GBW)[6]

$$\sigma^N_{q\bar{q}}(x_2,\rho) = \sigma_0\left(1-e^{-\frac{\rho^2Q_0^2}{4\left(\frac{x_2}{x_0}\right)^\lambda}}\right) \tag{3.30}$$

$$Q_0^2 = 1GeV^2 \quad \sigma_0 = 23.03mb \quad x_0 = 0.0003 \quad \lambda = 0.288 \tag{3.31}$$

This dipole cross-section vanishes like $\rho^2$ at small distances, whereas it levels of at large distances exponentially. This parametrization comes from global fit to HERA data(see [6]). More recent version of this parametrization was published by Kowalski-Motyka and Watt (GBWnew) [7]

$$\sigma^N_{q\bar{q}}(x_2,\rho) = \sigma_0\left(1-e^{-\frac{\rho^2Q_0^2}{4\left(\frac{x_2}{x_0}\right)^\lambda}}\right) \tag{3.32}$$

$$Q_0^2 = 1GeV^2 \quad \sigma_0 = 23.9mb \quad x_0 = 0.000111 \quad \lambda = 0.287 \tag{3.33}$$

Note, that both parametrizations account for one Pomeron exchange. As a consequence, the parametrization is accurate at high energies corresponding to $x_2 \leq 0.01$. In addition to Pomeron part, Reggeon part can be added (and consequently add an interaction with valence quarks in the target). Nevertheless, the extraction of Reggeon part from data is not as accurate as Pomeron part, and so, the improvement of the prediction power is disputable[29]. Another parametrization was published by Kopeliovich, Schäfer and Tarasov (KST)[8]

$$\sigma_{q\bar{q}}^N(s_q, \rho) = \sigma_0(s_q)\left(1 - e^{-\frac{\rho^2}{r_0^2(s_q)}}\right) \tag{3.34}$$

$$\sigma_0(s_q) = \sigma_{tot}^{\pi p}(s_q)\left(1 + \frac{3r_0^2(s_q)}{8\langle r_{ch}^2\rangle_\pi}\right) \tag{3.35}$$

$$r_0(s_q) = 0.88\left(\frac{s_q}{s_0}\right)^{-0.14} fm \qquad s_0 = 1000GeV^2 \tag{3.36}$$

$$\sigma_{tot}^{\pi p}(s_q) = 23.6\left(\frac{s_q}{s_0}\right)^{0.08} mb \qquad \langle r_{ch}^2\rangle_\pi = 0.44fm^2, \tag{3.37}$$

where all values depend on energy $s_q = sx_q$ rather than on $x_2$ and also an energy dependent parameter $\sigma_0(s_q)$ is introduced in order to correctly reproduce hadronic cross-sections. For the pion-proton total cross-section, the parametrization from [44] is used with fit parameters taken from [45]. This formula also contains only Pomeron part of the dipole cross-section, nevertheless, the Reggeon part can be easily added by considering full form of the pion-proton cross-section(FULLKST) in [45]

$$\sigma_{tot}^{\pi p}(s_q) = 23.6\left(\frac{s_q}{s_0}\right)^{0.08} + 1.425\left(\frac{s_q}{s_0}\right)^{-0.45} mb. \tag{3.38}$$

For parton distribution functions $f_q(x, Q^2)$ many parametrizations exist.One should use leading order PDFs in the dipole approach since they are scheme independent and have intuitive probabilistic interpretation. Moreover, gluon distribution functions are not taken into account here since there is no vertex in the QCD that produces photon bremsstrahlung out of the gluon. Following table summarizes some of parametrization used throughout this work

| PDF | $x$ range [1] | $Q^2$ range $[GeV^2]$ |
|---|---|---|
| GRV94LO[46] | $10^{-5} < x < 1$ | $0.4 < Q^2 < 10^6$ |
| GRV98LO[47] | $10^{-9} < x < 1$ | $0.8 < Q^2 < 10^6$ |
| GJR08LO[48] | $10^{-9} < x < 1$ | $0.3 < Q^2 < 10^8$ |
| CTEQ6L[49] | $10^{-6} < x < 1$ | $1.3 < Q^2 < 10^4$ |
| MSTW2008lo[50] | $10^{-6} < x < 1$ | $1 < Q^2 < 10^9$ |
| NNPDF21lo[51] | $10^{-9} < x < 1$ | $2 < Q^2 < 10^8$ |

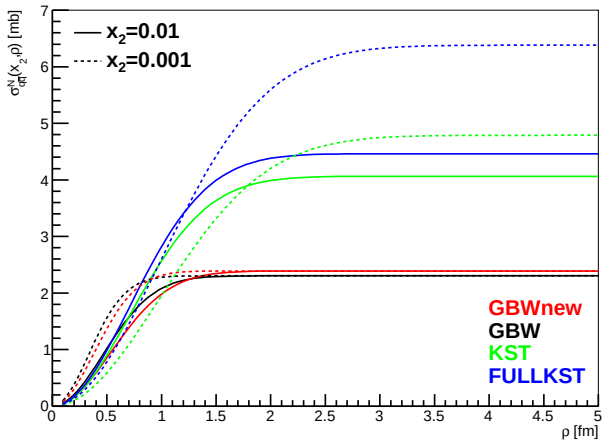


Figure 3.6: The dependence of the dipole cross-section from various parametrizations on the transverse separation of the dipole for two values of $x_2$.

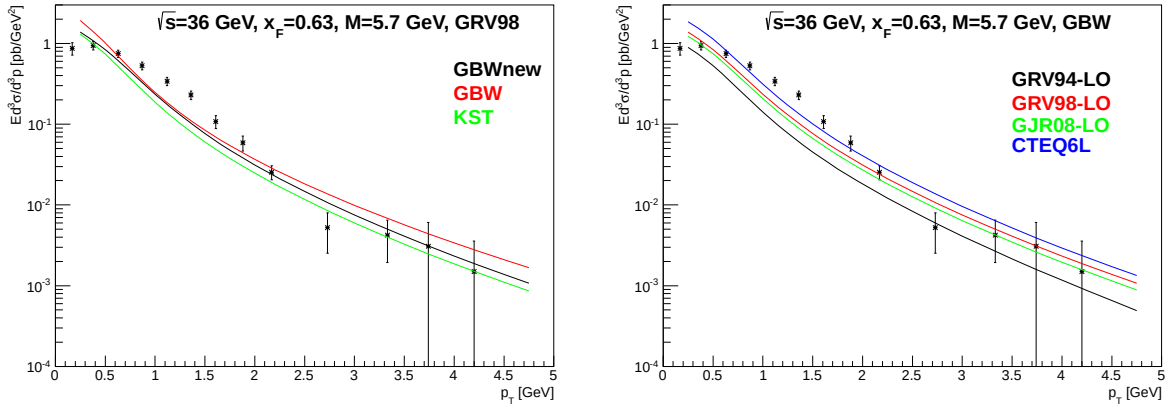


Figure 3.7: The $p_T$ spectrum of the Drell-Yan process at energy corresponding to E866 experiment for different dipole cross-sections and PDFs. Data are taken from E866 experiment[42].

# Chapter 4

# Coherence effects in proton-nucleus collisions

## 4.1 Coherence length

In previous chapter the Drell-Yan process and the direct photon production was treated in the rest frame of the target via the color dipole approach. According to this picture, a quark from the incident hadron interact with the target partonic field and radiate either a virtual photon $\gamma^*$ of a mass $M$ that subsequently decays into a Drell-Yan dilepton $\bar{l}l$ or a real hard massless photon $\gamma$[52, 53]. The photon is a part of the projectile fluctuations, which are frozen by time dilatation for the time $t_c$, called coherence time, that is fixed by uncertainty relations. It can be also interpreted as a lifetime of the $|q\gamma\rangle$ fluctuation in the projectile Fock state expansion. Assuming that the quark travels at a speed of light, one can also use a coherence length $l_c = t_c c$.
When the scattering takes place on a nucleus, multiple interactions with target nucleons can give rise to various nuclear medium effects. The coherence length control the magnitude of nuclear effects, that have its origin in coherent interaction of nucleons[53, 54].
One can distinguish two limiting cases. The short coherence length limit(SCL) that is reached when the coherence length is shorter than inter-particle spacing($\sim 1 - 2fm$) and, therefore, the fluctuation has time to interact with only one bound nucleon, and so, all nucleons contribute equally to the cross-section (Bethe-Heitler regime[15]). The long coherence length limit(LCL) that is reached when the coherence length is longer than the nuclear radius and different bound nucleons compete in freeing the photon in the fluctuation leading to either destructive or constructive interference between contributions of nucleons into the cross-section (Landau-Pomeranchuk-Migdal effect[14]).
The coherence length can be expressed from the uncertainty relations regarding a quark in the rest frame of the target before and after it develops a fluctuation

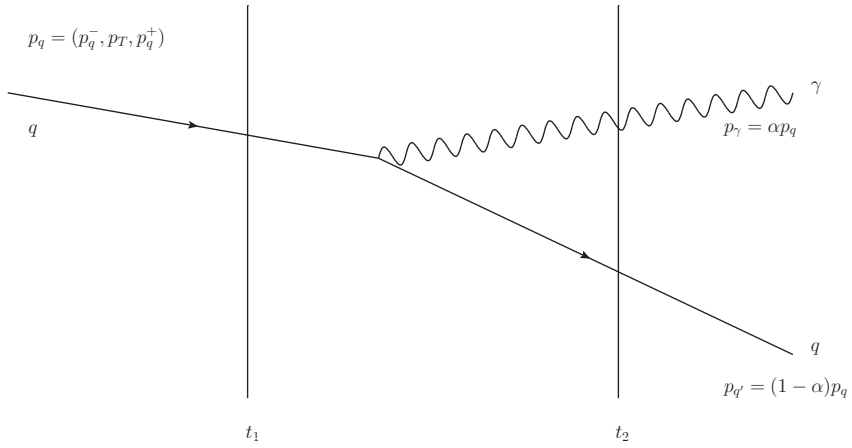


Figure 4.1: Sketch of the $|q\gamma\rangle$ fluctuation indicating the time that the fluctuation can propagate due to the energetic balance before and after developing certain fluctuation.

in the light-cone kinematics by the energy denominator

$$l_c = \frac{1}{\Delta p^-}, \tag{4.1}$$

where $\Delta p^-$ is the difference in the light-cone energy for the transition $q \to q\gamma$. It can be written in terms of light-cone energies $p^-$[55, 56]

$$\begin{aligned} m^2 = p^2 = \tfrac{1}{2}(p^- p^+ + p^+ p^-) - p_T^2 = p^+ p^- - p_T^2 \\ p^- = \tfrac{m^2 + p_T^2}{p^+}, \end{aligned} \tag{4.2}$$

where $m$ is a mass of the state and $p^+ = E + p^L$ is the light-cone momentum of the state. Assuming that the transverse and longitudinal momentum of the quark and the fluctuation is same, one can write

$$\Delta p^- = \frac{M_{q\gamma}^2 - m_q^2}{p_q^+} \tag{4.3}$$

having

$$l_c = \frac{p_q^+}{M_{q\gamma}^2 - m_q^2}, \tag{4.4}$$

where $M_{q\gamma}$ is an invariant mass of the fluctuation and $m_q$ is a mass of the bare quark. If the energy is conserved, the longitudinal momentum transfer between the initial state $|q\rangle$ and

the fluctuation $|q\gamma\rangle$ is $q_c = \frac{1}{l_c}$. Therefore, one can say that coherence length is the maximal longitudinal distance between fluctuations that are in the phase(and so they can interfere). Using a definition of the light-cone momentum of the incident quark $p_q^+ = E_q + p_q^L$ and assuming that $E_q \sim p_q^L$(high energy limit) one can write

$$l_c = \frac{2E_q}{M_{q\gamma}^2 - m_q^2}. \tag{4.5}$$

The mass of the fluctuation is [53, 54]

$$M_{q\gamma}^2 = \frac{M^2}{1-\alpha} + \frac{m_q^2}{\alpha} + \frac{p_T^2}{\alpha(1-\alpha)}, \tag{4.6}$$

where $M$ is an invariant mass of the photon, $p_T$ is a transverse momentum of the photon and $\alpha$ is the fraction of the light-cone momenta of the incident quark carried by the photon. Therefore,

$$l_c = \frac{2E_q\alpha(1-\alpha)}{(1-\alpha)M^2 + \alpha^2 m_q^2 + p_T^2}. \tag{4.7}$$

Since

$$\alpha = \frac{p_\gamma^+}{p_q^+} \quad x_1 = \frac{p_\gamma^+}{p_p^+} \quad \Rightarrow \quad p_\gamma^+ = \alpha p_q^+ = x_1 p_p^+ \tag{4.8}$$

and

$$E_q = x_q E_p = \frac{p_q^+}{p_p^+} E_p, \tag{4.9}$$

one can substitute $E_q$ by $\frac{x_1}{\alpha}E_p$ to

$$l_c = \frac{x_1 2E_p(1-\alpha)}{(1-\alpha)M^2 + \alpha^2 m_q^2 + p_T^2}, \tag{4.10}$$

where $E_p$ is the energy of incident proton, $x_1$ is a fraction of the light-cone momenta of the incident proton taken by the photon and $x_q$ is a fraction of the light-cone momenta of incident proton carried by the quark. The incident energy of the proton in the rest frame of the target can be expressed using the square of the invariant energy $s$ and the mass of the nucleon

$$s = 2m_N^2 + 2E_p m_N \sim 2E_p m_N, \tag{4.11}$$

where $m_N$ is a mass of the nucleon, as

$$l_c = \frac{x_1 s(1-\alpha)}{m_N((1-\alpha)M^2 + \alpha^2 m_q^2 + p_T^2)}. \tag{4.12}$$

The final formula can be obtained using a formula $x_1 x_2 = \frac{M^2+p_T^2}{s}$

$$l_c = \frac{1}{x_2 m_N} \frac{(M^2+p_T^2)(1-\alpha)}{(1-\alpha)M^2+\alpha^2 m_q^2 + p_T^2} = \frac{1}{x_2 m_N} K(\alpha, p_T). \tag{4.13}$$

In order to obtain the mean coherence length, one has to average the formula over $\alpha$ and over $p_T$

$$\begin{aligned}
\langle l_c \rangle &= \frac{1}{x_2 m_N} \left\langle \frac{(M^2+p_T^2)(1-\alpha)}{(1-\alpha)M^2+\alpha^2 m_q^2 + p_T^2} \right\rangle_{\alpha, p_T} = \frac{1}{x_2 m_N} \langle K(\alpha, p_T) \rangle_{\alpha, p_T} \\
\langle K(\alpha, p_T) \rangle_{\alpha, p_T} &= \frac{\sum_q \int_{x_1}^1 \frac{x_1 \mathrm{d}\alpha}{\alpha^2} \int \mathrm{d}^2 p_T f_q(\frac{x_1}{\alpha}, Q^2) |\Psi_{\gamma q}(\alpha, p_T)|^2 K(\alpha, p_T)}{\sum_q \int_{x_1}^1 \frac{x_1 \mathrm{d}\alpha}{\alpha^2} \int \mathrm{d}^2 p_T f_q(\frac{x_1}{\alpha}, Q^2) |\Psi_{\gamma q}(\alpha, p_T)|^2},
\end{aligned} \tag{4.14}$$

where $f_q^h$ is a parton distribution function of an incoming quark at the scale $Q^2 = (1-\alpha)M^2 + p_T^2$. The invariant mass is taken to be fixed - either $M = 0$ for real photon or $M \neq 0$ for the Drell-Yan pair.

It is expected that the mass of the quark should be taken as a current mass. However, it leads to large transverse separations between the parent and recoil quark when the radiated photon takes almost all quark momentum $(1-\alpha)M^2 \sim m_q^2$. In this case the separation becomes $\rho \sim \frac{1}{m_q}$ and it leads to a divergence in the case of unsaturated dipole cross-section. This divergence can be regularized by taking an effective value of a quark mass $m_q \sim 0.2 GeV$ from the analysis of DIS data that suppress the probability of large separations[54]. Moreover, the average is performed over the light-cone wave function squared which is known to diverge for transversally polarized photons at small separations $\rho$ (or for large $p_T$)[53]. That implies that the vacuum fluctuations are dominated by infinitely heavy $|q\gamma\rangle$ fluctuations. Such heavy fluctuations, however, do not contribute into the cross-section since they are too small to be resolved by the interaction, and so, they are not distinguishable from the bare quark. In order to avoid those small fluctuations, one has to include the dipole cross-section into the averaging procedure since it vanishes at $\rho \to 0$

$$\Psi_{\gamma q}^T(\alpha, p_T) = \int d^2\rho e^{i\vec{\rho}\cdot\vec{p}_T} \sigma_{q\bar{q}}^N(\alpha\rho, x) \Psi_{\gamma q}^T(\alpha, \rho), \tag{4.15}$$

where only transverse part of the wave function is taken since the longitudinal part is suppressed in the limit $x_1 \to 1$. The size-dependent wave function is discussed in previous chapter. The fourier transform can be performed analytically for the dipole cross-section in the form $\sigma_{q\bar{q}}(\rho, \alpha) = C(x)\rho^2$ leading to the formula [54]

$$\Psi_{\gamma q}^T(\alpha, p_T) = 2 Z_q \sqrt{\alpha_{em}} C(x) \vec{e} \cdot \vec{p}_T \frac{i\alpha^2 \varepsilon^2}{\pi(\varepsilon^2 + p_T^2)^3}, \tag{4.16}$$

where $\varepsilon^2 = (1-\alpha)M^2 + \alpha^2 m_q^2$, $\vec{e}$ is a polarization vector of a photon and $Z_q$ is a charge of the quark. Therefore, the square of the wave function can be expressed analytically and one can write

$$\langle K(\alpha, p_T)\rangle_{\alpha,p_T} = \frac{\int_{x_1}^{1} \frac{\mathrm{d}\alpha}{\alpha} \int \mathrm{d}^2 p_T F_2^h(\frac{x_1}{\alpha}, Q^2) \frac{p_T^2 \alpha^4 \varepsilon^4}{(\varepsilon^2 + p_T^2)^6} K(\alpha, p_T)}{\int_{x_1}^{1} \frac{\mathrm{d}\alpha}{\alpha} \int \mathrm{d}^2 p_T F_2^h(\frac{x_1}{\alpha}, Q^2) \frac{p_T^2 \alpha^4 \varepsilon^4}{(\varepsilon^2 + p_T^2)^6}}, \tag{4.17}$$

where $F_2^h$ is a structure function of the incoming hadron.
The usual approximation used for the calculation in the QCD has a form[54]

$$\langle K_{QCD}\rangle = 1/2 \tag{4.18}$$

which produce simple form of the coherence length

$$\langle l_c\rangle = \frac{1}{2x_2 m_N} \tag{4.19}$$

leading to the scaling of nuclear effects with $x_2$[54]. In contrast, the prediction of the scaling of nuclear effects in the rest frame of the target is more complicated, since the coherence length fall to zero in the limit $x_1 \to 1$ since $x_1 < \alpha$ and the factor $(1-\alpha)$ in the numerator suppresses the mean coherence length.

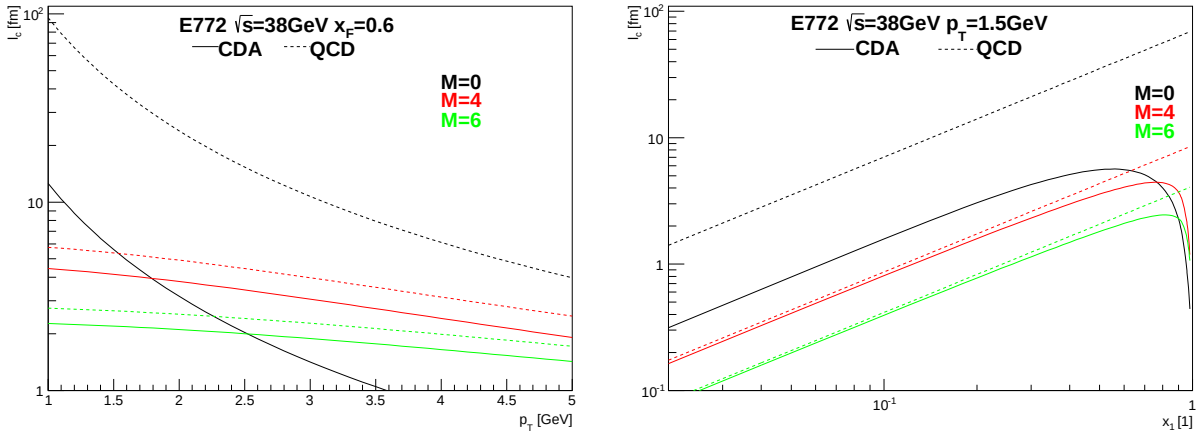


Figure 4.2: Dependence of the coherence length corresponding to E772 experiment on transverse momenta and on $x_1$ for various invariant masses of the photon. Solid line corresponds to the prediction using color dipole approach in the target rest frame, whereas dotted line corresponds to the prediction in QCD infinite momentum frame.

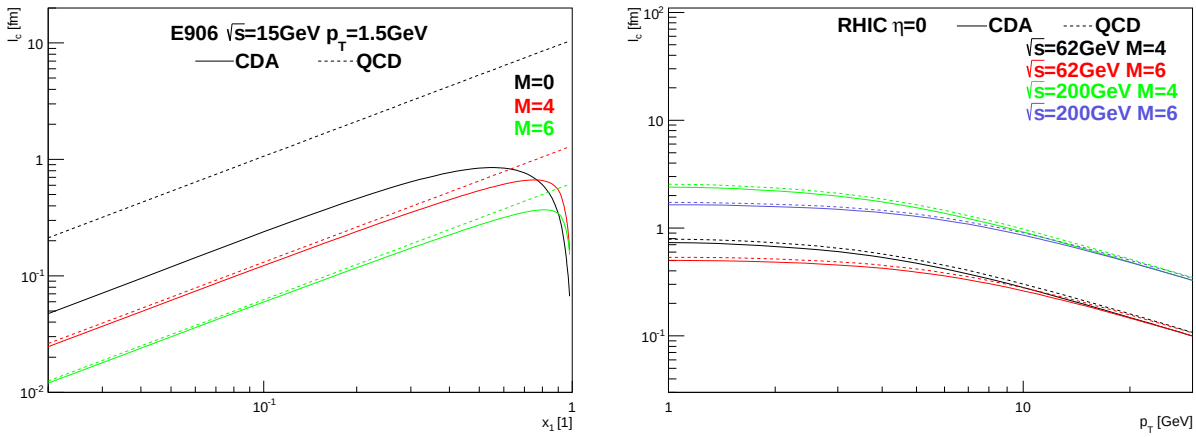


Figure 4.3: Dependence of the coherence length corresponding to E906 experiment on $x_1$ and to RHIC experiment on transverse momentum for various invariant masses of the photon. Solid line corresponds to the prediction using color dipole approach in the target rest frame, whereas dotted line corresponds to the prediction in QCD infinite momentum frame.

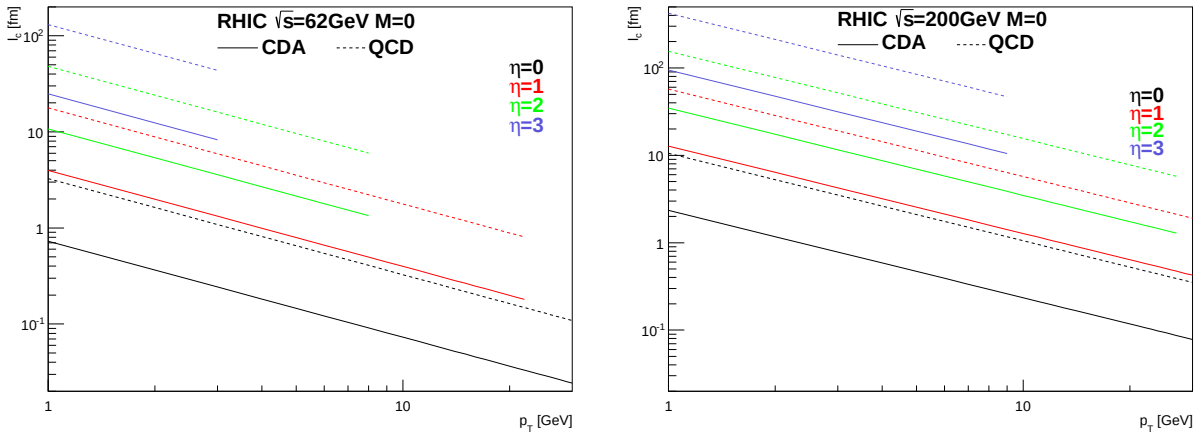


Figure 4.4: Dependence of the coherence length corresponding to RHIC experiment on transverse momenta for various pseudo-rapidities of the photon. Solid line corresponds to the prediction using color dipole approach in the target rest frame, whereas dotted line corresponds to the prediction in QCD infinite momentum frame.

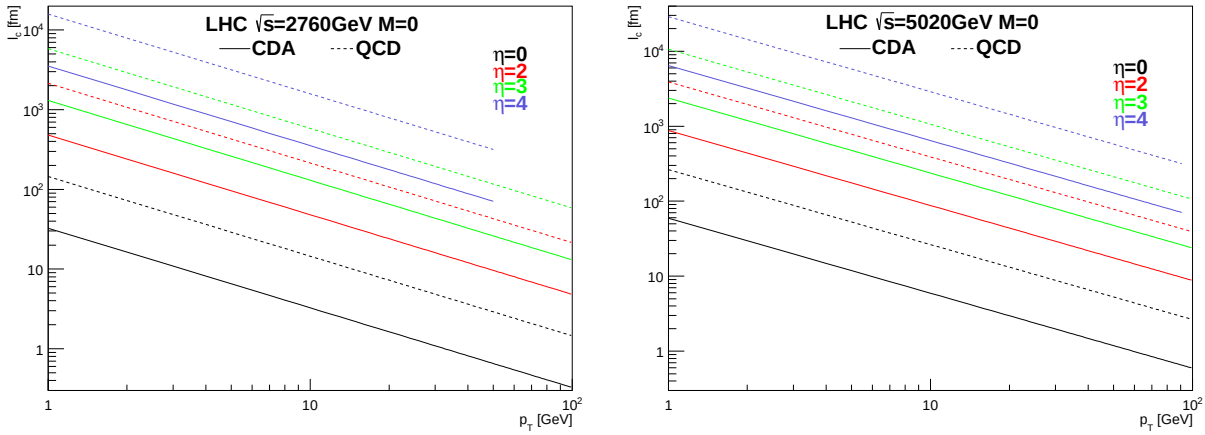


Figure 4.5: Dependence of the coherence length corresponding to LHC experiment on transverse momenta for various pseudo-rapidities of the photon. Solid line corresponds to the prediction using color dipole approach in the target rest frame, whereas dotted line corresponds to the prediction in QCD infinite momentum frame.

## 4.2 Geometrical Glauber model

The Glauber model [12, 21] consider the collision of two composite objects in terms of the individual interactions of its constituents. In case of nucleon-nucleus and nucleus-nucleus collisions those constituents correspond to nucleons. The quantitative consideration of the geometrical configuration of colliding nuclei leads to the multiple-collision model. After an incident projectile nucleon suffers a collision, the nucleon-like remnant can be treated loosely as the projectile that continue to make further collisions along its path through the nucleus. Although in principle a nucleon on its way can be excited and, therefore, the cross-section between projectile and target nucleons in successive interactions should be different only the situation, where projectile comes with sufficiently high energy is taken into account. Consequently, the time-scale of the interaction is much shorter than the effect of the excitation. In this so called "optical limit" the incident nucleon can be described as a plane wave and the overall phase shift of the incoming wave is taken as a sum over all possible two-nucleon phase shifts with the imaginary part of the phase shift related to the nucleon-nucleon scattering cross-section through the optical theorem[12]. Also, it is assumed that the colliding nucleon is undeflected as it pass through the nucleus. Furthermore, nucleons are supposed to move independently in the nucleus and the size of the nucleus is presumed to be large compared to the extent of the nucleon-nucleon interaction length.
Let's consider the situation, where nucleon and nucleus with $A$ nucleons are colliding at relativistic speeds with the impact parameter $\vec{b}$

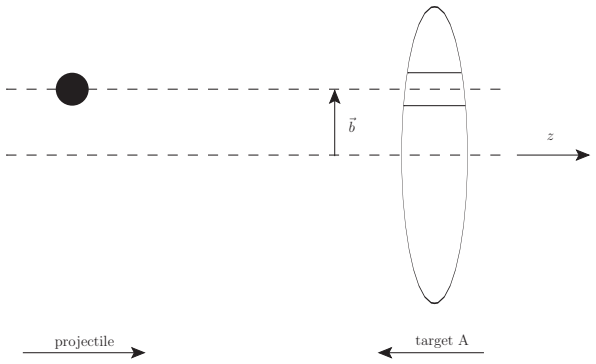


Figure 4.6: Schematic figure of a nucleon-nucleus collision in a side view.

The density of nucleons per unit transverse area $T_A$ at the impact parameter $\vec{b}$ is called nuclear thickness function

$$T_A(\vec{b}) = \int \rho_A(\vec{b}, z)\mathrm{d}z, \tag{4.20}$$

where $\rho_A(\vec{b}, z)$ is the spatial density of nucleons at the position $(\vec{b}, z)$ inside the nucleus. The

normalization of the nuclear thickness function is chosen such that

$$\int T_A(\vec{b})\mathrm{d}^2b = A. \tag{4.21}$$

Therefore, one can express the probability per unit transverse area that the nucleon is located in the nucleus at impact parameter $\vec{b}$ as

$$\frac{T_A(\vec{b})}{A} = \frac{1}{A}\int \rho_A(\vec{b},z)\mathrm{d}z, \tag{4.22}$$

where $\frac{\rho_A(\vec{b},z)}{A}$ corresponds to the probability per unit volume for finding a nucleon at the location $(\vec{b},z)$. For collisions of unpolarized nucleons, the interaction does not depend on the orientation of $\vec{b}$, and so, $T_A(\vec{b})$ depends only on the magnitude of $\vec{b}$.
The nucleon density $\rho_A(\vec{b})$ has to be parametrized for each nucleus as it cannot be calculated from the theory. Most common parametrizations for heavy nuclei are Wood-Saxon distribution and Fermi distribution

$$\rho_A^{WS}(r) = \rho_0\frac{1}{1+e^{\frac{r-R}{a}}} \qquad \rho_A^{F}(r) = \rho_0\frac{1+w(\frac{r}{R})^2}{1+e^{\frac{r-R}{a}}} \qquad r=\sqrt{b^2+z^2} \tag{4.23}$$

with independent parameters - nuclear radius $R$, skin depth $a$ and the deviation from spherical shape $w$. Parameter $\rho_0$ is fixed by the above normalization. Various nuclear parameters are taken from [57].

| | A | R$[fm]$ | a$[fm]$ | w[1] | $\rho_0[fm^{-3}]$ |
|---|---|---|---|---|---|
| Pb | 208 | 6.624 | 0.549 | 0 | 0.16008 |
| Au | 197 | 6.380 | 0.535 | 0 | 0.16943 |
| W | 184 | 6.510 | 0.535 | 0 | 0.14934 |
| Cu | 63 | 4.214 | 0.586 | 0 | 0.16886 |
| Fe | 56 | 3.980 | 0.569 | 0 | 0.17655 |
| Ca | 40 | 3.510 | 0.563 | 0 | 0.17619 |

Table 4.1: Nuclear parameters and corresponding normalization factors for heavy nuclei from [57].

For light nuclei apart from the deuteron, one can use a modified harmonic oscillator distribution

$$\rho_A(r) = \rho_0\left(1+\alpha\frac{r^2}{a^2}\right)e^{-\frac{r^2}{a^2}}, \tag{4.24}$$

where independent parameters $\alpha$ and $a$ are taken from [57].

| | A | $\alpha[1]$ | a$[fm]$ | $\rho_0[fm^{-3}]$ |
|---|---|---|---|---|
| C | 12 | 1.247 | 1.649 | 0.16752 |
| Be | 9 | 0.611 | 1.791 | 0.14687 |

Table 4.2: Nuclear parameters and corresponding normalization factors for light nuclei from [57].

Considering that the deuteron cannot be treated as bound nucleus but rather a loosely bound proton-neutron state with a consequently large spatial extent, a calculation of its nuclear density has to be made in a different way. The Hulthen wave function[58] of the deuteron is taken in a form which contains S and D - wave components

$$\psi_{J_z}(\vec{r}') = \frac{u(r')}{r'}\Phi_{1J_z0}(\Omega) + \frac{w(r')}{r'}\Phi_{1J_z2}(\Omega), \tag{4.25}$$

where $\vec{r}'$ is the distance between proton and neutron, $J_z$ is a z-component of the angular momentum of the deuteron and $\Phi$ corresponds to the spherical part of the wave function. For the radial functions $u$ and $w$, the Hulthen form[58] is used

$$u(r') = N\sqrt{1-\epsilon^2}(1-e^{-\beta(\alpha r'-x_c)})e^{-\alpha r'} \tag{4.26}$$

$$w(r') = N\epsilon(1-e^{-\gamma(\alpha r'-x_c)})^2\left(1+\frac{3}{\alpha r'}(1-e^{-\gamma\alpha r'})+\frac{3}{\alpha^2 r'^2}(1-e^{-\gamma\alpha r'})^2\right)e^{-\alpha r'}, \tag{4.27}$$

where $N$ is fixed by the normalization condition, $\alpha = 0.231696 fm^{-1}$ is calculated from the experimentally measured binding energy and parameters $\beta, \gamma, \epsilon, x_c$ are taken from fit to data. Two sets of fit parameters exist[59]

| | $\beta[1]$ | $\gamma[1]$ | $\epsilon[1]$ | $x_c[fm]$ | $\rho_0[fm^{-3}]$ |
|---|---|---|---|---|---|
| Set 1 | 9.045 | 4.799 | 0.02438 | 0.13 | 1.30363 |
| Set 2 | 4.680 | 2.494 | 0.03232 | 0 | 1.42315 |

Table 4.3: Nuclear parameters and corresponding normalization factors for deuteron from [57].

Using the wave function, the density distribution can be defined[59] as

$$\rho_D(r) = \left|\frac{u(2r)}{2r}\right|^2 + \left|\frac{w(2r)}{2r}\right|^2, \tag{4.28}$$

where $r$ is the distance between the cms and one of constituents and the normalization factor $\rho_0 = N^2$ is fixed by the same normalization condition as for other nuclei. One has to be cautious with integrating the distribution, since the distribution based on Hulthen wave function at large $r \sim 20 fm$ is even higher than the Wood-Saxon distribution of gold. Thus the range of applicability of the deuteron spatial distribution is approximately $10 fm$.

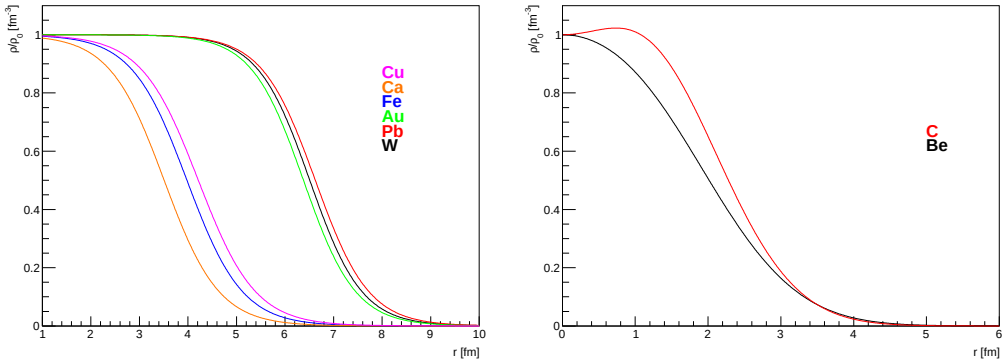


Figure 4.7: Nuclear density profiles at $b = 0$ for heavy and light nuclei.

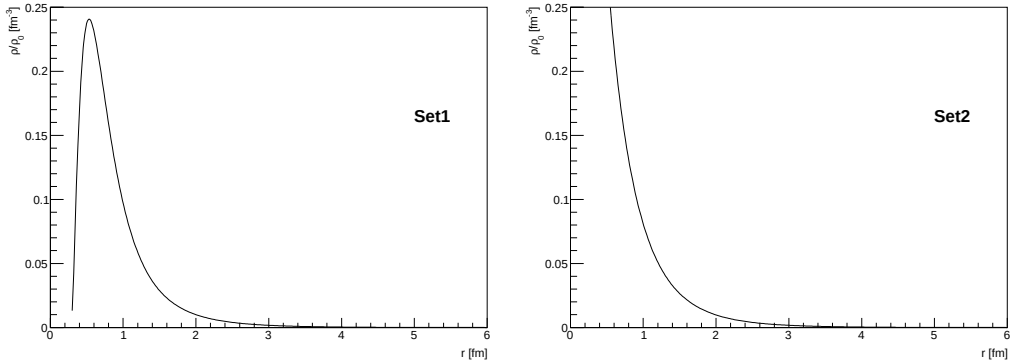


Figure 4.8: Nuclear density profiles at $b = 0$ for two sets of deuteron parametrizations.

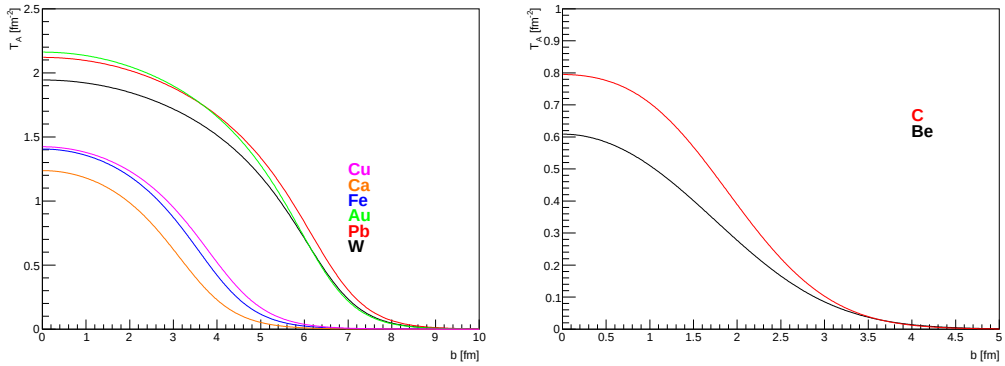


Figure 4.9: Nuclear thickness functions for heavy and light nuclei.

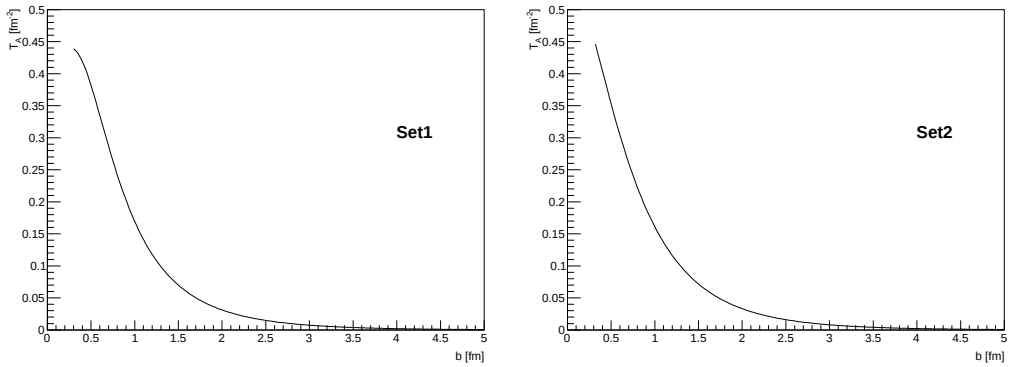


Figure 4.10: Nuclear thickness functions for two sets of deuteron parametrizations.

For the purpose of further calculations, the nuclear thickness function can be fitted by a phenomenological function for each nuclei. It is mainly used in the situation, where the calculation is numerically difficult to do and using a fit can take out one integration. Using a function

$$T_A(b) = c_1 e^{-c_2 b^2} + c_3 e^{-c_4 \left(\frac{b}{1fm}\right)^{5.7}} \tag{4.29}$$

the fit can be performed with results

| | $A[1]$ | $c_1[fm^{-2}]$ | $c_2[fm^{-2}]$ | $c_3[fm^{-2}]$ | $c_4[10^{-5}]$ | $\chi^2/ndf[10^{-5}]$ |
|---|---|---|---|---|---|---|
| Pb | 208.2739 | 0.638381 | 0.0492059 | 1.48963 | 2.67945 | 1.44211 |
| Au | 197.3194 | 0.663385 | 0.0520087 | 1.50604 | 3.31051 | 1.39676 |
| W | 184.2022 | 0.576938 | 0.0517207 | 1.37407 | 2.96327 | 1.28592 |
| Cu | 63.7889 | 0.774798 | 0.0771784 | 0.661432 | 28.96910 | 5.96136 |
| Fe | 56.7189 | 0.784233 | 0.0850787 | 0.6344 | 39.42770 | 6.16552 |
| Ca | 40.5435 | 0.76075 | 0.102056 | 0.48907 | 74.38160 | 5.59244 |
| C | 12.2421 | 0.60571 | 0.209875 | 0.203321 | 741.20200 | 4.09739 |
| Be | 9.1012 | 0.545389 | 0.21581 | 0.0676162 | 561.29700 | 0.465502 |

Table 4.4: Fit parameters for various nuclei using a phenomenological function. Here $A$ corresponds to the overall integral of the fit function.

For deuteron the phenomenological function can be taken in the form

$$T_A(b) = \frac{0.55}{2\pi\alpha} e^{-0.25\frac{b^2}{\alpha}} + \frac{0.45}{2\pi\beta} e^{-0.25\frac{b^2}{\beta}} fm^{-2} \tag{4.30}$$

with results

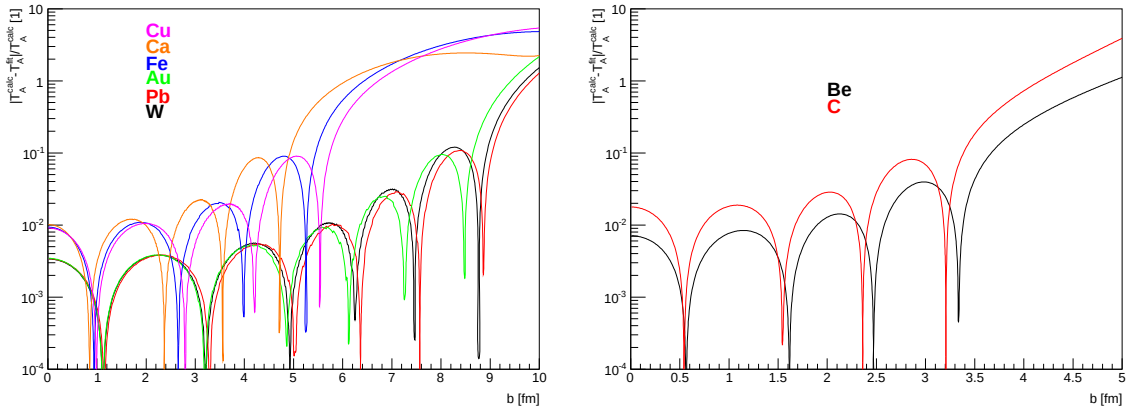


Figure 4.11: Estimation of an error made by using a parametrization of nuclear thickness function for heavy and light nuclei.

| | $A[1]$ | $\alpha[fm^2]$ | $\beta[fm^2]$ | $\chi^2/ndf[10^{-6}]$ |
|---|---|---|---|---|
| Set 1 | 1.999 | 0.901487 | 0.175899 | 1.08885 |
| Set 2 | 1.999 | 1.1056 | 0.17872 | 4.96544 |

Table 4.5: Fit parameters for deuteron using a phenomenological function. Here $A$ corresponds to the overall integral of the fit function.

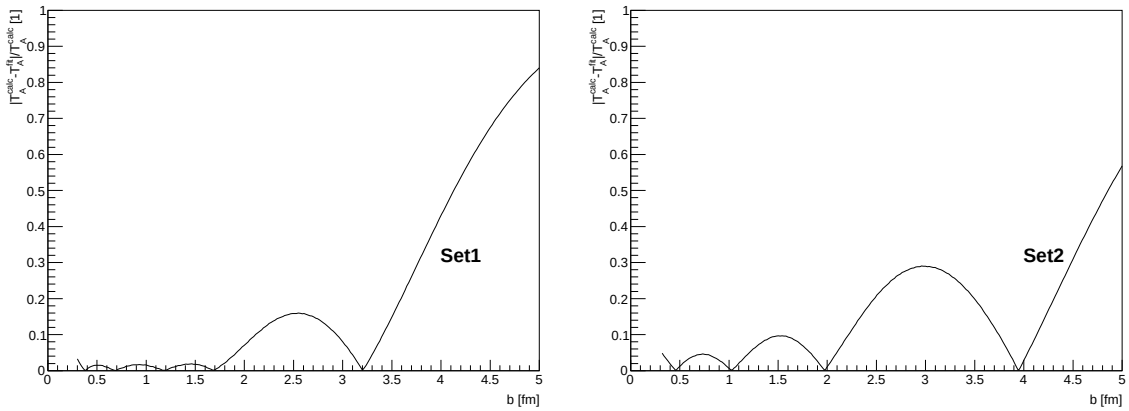


Figure 4.12: Estimation of an error made by using a parametrization of deuteron thickness function for two sets of parameters.

Using the above discussed nuclear thickness function $T_A(\vec{b})$ and considering that the probability $T_A/A$ that a nucleon is located in the nucleus at the impact parameter $\vec{b}$ has a unit

of inverse area, one can interpret it as the effective overlap area where an incident nucleon can interact with a nucleon in $A$. The probability that an interaction occur can be taken as $\frac{T_A(\vec{b})}{A}\sigma_{inel}^{NN}$, where $\sigma_{inel}^{NN}$ is the nucleon-nucleon inelastic cross section. Since the integrated inelastic cross-section includes contributions from all possible processes, mostly with low momentum transfer, it is impossible to calculate it using perturbative QCD. Thus, one has to use the measured $\sigma_{inel}^{NN}$ as an input. In general, the cross-section depends weakly on the collision energy $\sqrt{s}$, and so, it has to be taken from measurements of each experiment considered in the calculation[60, 61]

| | $\sqrt{s}[GeV]$ | $\sigma_{inel}^{NN}[mb]$ |
|---|---|---|
| RHIC | 62 | 36 |
| RHIC | 200 | 42 |
| LHC | 2760 | 62 |
| LHC | 5000 | 65 |
| LHC | 7000 | 70 |

Table 4.6: Measured integrated inelastic cross-sections used for the calculation corresponding to various energies from [60, 61].

The parametrization of $\sigma_{inel}^{NN}(s)$ exist in the form[62]

$$\sigma_{inel}^{NN}(s) = 32.4 - 1.2\ln(s[GeV^2]) + 0.21\ln^2(s[GeV^2]) \quad mb. \tag{4.31}$$

This type of formula is in very good agreement with data[62] and allows one to predict the cross-section for energies, where data are not available. The advantage of this logarithmic form is that it does not violate the Froissard unitarity bound at very high energies. During following calculation, whenever the measured cross-section is known, it is also used preferably. The diffraction and elastic processes are not taken into consideration, since they are significant at relatively large impact parameters, and so, they are suppressed by the nuclear distribution. In case of the situation, where the unintegrated cross-section has to be used, it has to be calculated using a model(see previous chapter).

Having the probability of an interaction of an incident nucleon with nuclei at impact parameter $\vec{b}$, the probability of having $n$ such interactions in the nucleus with $A$ nucleons is given by a binomial distribution

$$P(n,\vec{b}) = \binom{A}{n}\left(\frac{T_A(\vec{b})}{A}\sigma_{inel}^{NN}\right)^n\left(1-\frac{T_A(\vec{b})}{A}\sigma_{inel}^{NN}\right)^{A-n}, \tag{4.32}$$

where the first term refers to the number of combinations for finding $n$ collisions out of $A$ possible nucleon-nucleon encounters. The second term is the probability for having exactly

$n$ collisions and the last term corresponds to the probability of exactly $A-n$ misses. The total probability of an inelastic interaction between a nucleon and a nucleus $A$ is the sum of $P(n,\vec{b}\,)$ over all possible numbers of interactions

$$\begin{aligned}\frac{\mathrm{d}^2\sigma_{in}^{pA}}{\mathrm{d}^2b} &= \sum_{n=1}^{A} P(n,\vec{b}\,) = \sum_{n=0}^{A}\binom{A}{n}\left(\frac{T_A(\vec{b}\,)}{A}\sigma_{inel}^{NN}\right)^n\left(1-\frac{T_A(\vec{b}\,)}{A}\sigma_{inel}^{NN}\right)^{A-n} - \\ &\binom{A}{0}\left(1-\frac{T_A(\vec{b}\,)}{A}\sigma_{inel}^{NN}\right)^{A} = \left(\frac{T_A(\vec{b}\,)}{A}\sigma_{inel}^{NN}+1-\frac{T_A(\vec{b}\,)}{A}\sigma_{inel}^{NN}\right)^{A} - \\ &\left(1-\frac{T_A(\vec{b}\,)}{A}\sigma_{inel}^{NN}\right)^{A} = 1-\left(1-\frac{T_A(\vec{b}\,)}{A}\sigma_{inel}^{NN}\right)^{A}, \end{aligned} \tag{4.33}$$

where the binomial theorem has been used. Therefore, in case of unpolarized nucleons, one can write the total inelastic cross-section as

$$\sigma_{inel}^{pA} = \int \mathrm{d}^2b\left[1-\left(1-\frac{T_A(\vec{b}\,)}{A}\sigma_{inel}^{NN}\right)^{A}\right] = \int_0^{+\infty} 2\pi b\mathrm{d}b\left[1-\left(1-\frac{T_A(b)}{A}\sigma_{inel}^{NN}\right)^{A}\right]. \tag{4.34}$$

Using the probability for having $n$ inelastic collisions one can calculate the total number of collisions

$$\begin{aligned} N_{coll}(b) &= \sum_{n=0}^{A} nP(n,\vec{b}\,) = \sum_{n=0}^{A} n\binom{A}{n}\left(\frac{T_A(\vec{b}\,)}{A}\sigma_{inel}^{NN}\right)^n\left(1-\frac{T_A(\vec{b}\,)}{A}\sigma_{inel}^{NN}\right)^{A-n} = \\ &= \tau\frac{\partial}{\partial\tau}\sum_{n=0}^{A} n\binom{A}{n}\left(\tau\sigma_{inel}^{NN}\right)^n\left(1-\frac{T_A(\vec{b}\,)}{A}\sigma_{inel}^{NN}\right)^{A-n}\Big|_{\tau=\frac{T_A(\vec{b}\,)}{A}} = \\ &= \tau\frac{\partial}{\partial\tau}\left(1-\frac{T_A(\vec{b}\,)}{A}\sigma_{inel}^{NN}+\tau\sigma_{inel}^{NN}\right)^{A}\Big|_{\tau=\frac{T_A(\vec{b}\,)}{A}} = \\ &= \tau A\left(1-\frac{T_A(\vec{b}\,)}{A}\sigma_{inel}^{NN}+\tau\sigma_{inel}^{NN}\right)^{A-1}\sigma_{inel}^{NN}\Big|_{\tau=\frac{T_A(\vec{b}\,)}{A}} = \\ &= T_A(\vec{b}\,)\sigma_{inel}^{NN}. \end{aligned} \tag{4.35}$$

Detailed derivation of the Glauber eikonal formulas can be done based on quantum mechanical treatment of the optical approximation[12](see Appendix D).

Although the derivation of the geometrical Glauber model gives a formula for the total inelastic cross section, it can be applied to any inclusive process. When one considers hard scattering processes, the corresponding cross-section $\sigma_{hard}^{NN}$ is small and one can expand the formula for integrated cross-section in orders of $\sigma_{hard}^{NN} T_A(\vec{b})$ and, consequently, write in the first order

$$\sigma_{hard}^{pA} = \int 1 - \left(1 - \frac{T_A(\vec{b})\sigma_{hard}^{NN}}{A}\right)^A \mathrm{d}^2 b \sim \int T_A(\vec{b})\sigma_{hard}^{NN} \mathrm{d}^2 b. \tag{4.36}$$

The particle yield $N$ for an inclusive hard process with cross-section $\sigma_{hard}^{NN}$ in nucleon-nucleon collisions per interaction of a proton with nucleus $A$ with impact parameter $\vec{b}$ is[63]

$$N_{hard}^{pA}(\vec{b}) = \frac{\sigma_{hard}^{pA}(\vec{b})}{\sigma_{inel}^{pA}} = \frac{T_A(\vec{b})\sigma_{hard}^{NN}}{\sigma_{inel}^{pA}} = \frac{T_A(\vec{b})\sigma_{inel}^{NN} N_{hard}^{NN}}{\sigma_{inel}^{pA}} \tag{4.37}$$

$$N_{hard}^{NN} = \frac{\sigma_{hard}^{NN}}{\sigma_{inel}^{NN}}. \tag{4.38}$$

Since one cannot distinguish the impact parameter of particular interaction, it has to be integrated over the whole range. It leads to the minimum bias yield

$$\langle T_A \rangle = \frac{\int_0^{+\infty} 2\pi b T_A(b) \mathrm{d}b}{\sigma_{inel}^{pA}} = \frac{A}{\sigma_{inel}^{pA}} \tag{4.39}$$

$$\langle N_{coll} \rangle = \frac{\int_0^{+\infty} 2\pi b T_A(b) \mathrm{d}b\, \sigma_{inel}^{NN}}{\sigma_{inel}^{pA}} = \langle T_A \rangle \sigma_{inel}^{NN} \tag{4.40}$$

$$\langle N_{hard}^{pA} \rangle \sim \frac{\sigma_{hard}^{pA}}{\sigma_{inel}^{pA}} = \frac{\int_0^{+\infty} 2\pi b T_A(b) \mathrm{d}b\, \sigma_{hard}^{NN}}{\sigma_{inel}^{pA}} = \langle N_{coll} \rangle N_{hard}^{NN}. \tag{4.41}$$

If the particle yield is measured as a function of transverse momentum $p_T$, one has to know the $p_T$ dependence of the nucleon-nucleon hard cross-section, and so,

$$\frac{\mathrm{d}^2 N^{pA}_{hard}(\vec{b})}{\mathrm{d}^2 p_T} = \frac{\frac{\mathrm{d}^2\sigma^{pA}_{hard}(\vec{b})}{\mathrm{d}^2 p_T}}{\sigma^{pA}_{inel}} = \frac{\int T_A(\vec{b})\mathrm{d}^2 b \frac{\mathrm{d}^2\sigma^{NN}_{hard}}{\mathrm{d}^2 p_T}}{\sigma^{pA}_{inel}} = \frac{\int T_A(\vec{b})\mathrm{d}^2 b \sigma^{NN}_{inel}\frac{\mathrm{d}^2 N^{NN}_{hard}}{\mathrm{d}^2 p_T}}{\sigma^{pA}_{inel}} \quad (4.42)$$

$$\frac{\mathrm{d}^2 N^{NN}_{hard}}{\mathrm{d}^2 p_T} = \frac{\frac{\mathrm{d}^2\sigma^{NN}_{hard}}{\mathrm{d}^2 p_T}}{\sigma^{NN}_{inel}}. \quad (4.43)$$

The nuclear modification factor $R_{pA}$ is defined using invariant multiplicity of produced inclusive hard particles as

$$R_{pA}(p_T) = \frac{1}{\langle N_{coll}\rangle}\frac{\frac{\mathrm{d}^2 N^{pA}_{hard}}{\mathrm{d}^2 p_T}}{\frac{\mathrm{d}^2 N^{NN}_{hard}}{\mathrm{d}^2 p_T}} = \frac{1}{\langle T_A\rangle}\frac{\frac{\mathrm{d}^2 N^{pA}_{hard}}{\mathrm{d}^2 p_T}}{\frac{\mathrm{d}^2\sigma^{NN}_{hard}}{\mathrm{d}^2 p_T}} = \frac{1}{A}\frac{\frac{\mathrm{d}^2\sigma^{pA}_{hard}}{\mathrm{d}^2 p_T}}{\frac{\mathrm{d}^2\sigma^{NN}_{hard}}{\mathrm{d}^2 p_T}}. \quad (4.44)$$

## 4.3 Long coherence length

If the mean coherence length is greater than the nuclear radius($\langle l_c \rangle \gg R_A$), the fluctuation lives long enough to experience multiple re-scattering inside the nucleus before loosing coherence and can eventually pass through the whole nucleus without producing any particle on-shell. This is fully satisfied in the kinematic region, where $x_2 \lesssim 0.1$.

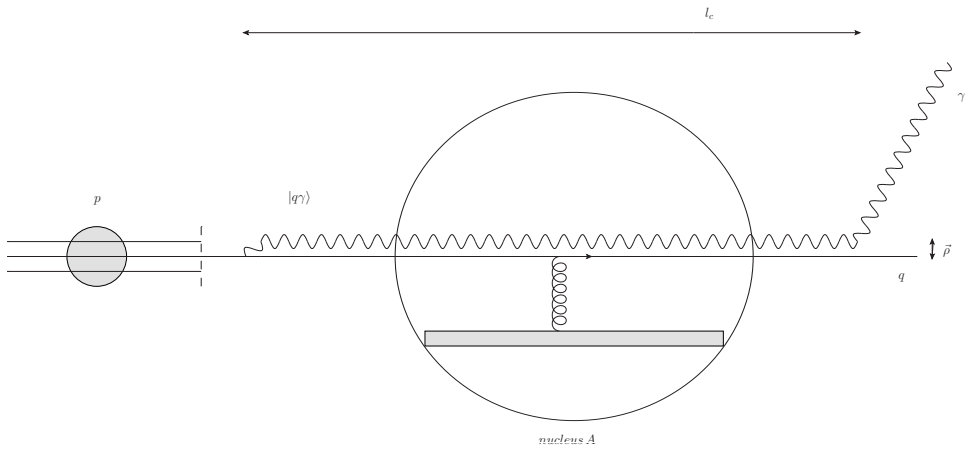


Figure 4.13: A fast quark undergoes a virtual fluctuation into a photon and a quark. Since the coherence length is large, the entire nucleus participates as a single entity

The fluctuation arises long before the quark enters the nucleus and is subject to maximal quark shadowing - all nucleons having the same impact parameter participate coherently in the production of the proton. In this limit, the incoming quark can be decomposed into a system of Fock states with fixed transverse separation $\rho$. Since parton configurations with constant transverse separation in the impact parameter space are eigenstates of the interaction [64], the cross-section of the photon(or dilepton) production in proton-nucleus scattering can be calculated by replacing the dipole cross-section $\sigma^N_{q\bar{q}}$ in the formula for proton-proton cross-section by the dipole cross-section $\sigma^A_{q\bar{q}}$ on the nucleus $A$ that can be calculated using Glauber model eikonalization [65, 29]

$$\sigma^N_{q\bar{q}}(\rho, x_2) \to \sigma^A_{q\bar{q}}(\rho, x_2) = 2 \int \mathrm{d}^2 b \left( 1 - \left( 1 - \frac{1}{2A} \sigma^N_{q\bar{q}}(\rho, x_2) T_A(\vec{b}) \right)^A \right), \tag{4.45}$$

where $T_A(\vec{b})$ is the nuclear thickness function at impact parameter $\vec{b}$ defined in previous section. Only the contribution from the Fock component $|q\gamma\rangle$ is considered since the probability for more complex components is suppressed. Nevertheless, due to the ability of the nucleus to resolve higher Fock components via multiple re-scattering, one has to include also the contribution from these components by the procedure discussed in the section with the gluon

shadowing. As one can see, at small $\rho$ the exponent $\sigma^N_{q\bar{q}}(\rho,x_2)T_A(\vec{b}) \ll 1$ since $\sigma^N_{q\bar{q}}(\rho,x_2)$ is small. Therefore, one can expand the exponential and the cross-section in proton-nucleus collisions is equal to $A$ times the cross-section in proton-proton collisions. This is the Bethe-Heitler limit for the photon bremsstrahlung. In the opposite limit $\sigma^N_{q\bar{q}}(\rho,x_2)T_A(\vec{b}) \gg 1$ one can neglect the exponential for $b \leq R_A$ and the cross-section in the proton-nucleus collisions is equal to $A^{\frac{2}{3}}$ times the cross-section in proton-proton collisions. This is the limit of full coherence, where the whole row of nucleons with the same impact parameter is seen by an incident quark as single scattering center. As the transverse momentum $p_T$ of a bremsstrahlung in the fluctuation is inversely proportional to the transverse size of the fluctuation $\rho$, it can be expected that the limit of maximal coherence is reached for small $p_T$ and the Bethe-Heitler limit for large $p_T$. Therefore, the nuclear target acts like a color filter for wide fluctuations.

Final formula for the photon(dilepton) production cross-section in pA collisions is then[65]

$$\begin{aligned}
\frac{\mathrm{d}^2\sigma(pA\to\gamma X)}{\mathrm{d}x_F\mathrm{d}M^2} &= \frac{\mathrm{d}\sigma(\gamma^*\to l^+l^-)}{\mathrm{d}M^2}\frac{x_1}{x_1+x_2}\int\limits_{x_1}^1\frac{\mathrm{d}\alpha}{\alpha^2}\sum_q Z_q^2\left(f_q\left(\frac{x_1}{\alpha},Q^2\right)+f_{\bar{q}}\left(\frac{x_1}{\alpha},Q^2\right)\right)\times \\
&\times\frac{\mathrm{d}\sigma(qA\to\gamma X)}{\mathrm{d}\ln\alpha} = \frac{\mathrm{d}\sigma(\gamma^*\to l^+l^-)}{\mathrm{d}M^2}\frac{1}{x_1+x_2}\int\limits_{x_1}^1\frac{\mathrm{d}\alpha}{\alpha}F_2^p\left(\frac{x_1}{\alpha}\right)\frac{\mathrm{d}\sigma(qA\to\gamma X)}{\mathrm{d}\ln\alpha} \\
\frac{\mathrm{d}\sigma(qA\to\gamma X)}{\mathrm{d}\ln\alpha} &= 2\int\mathrm{d}^2b\int\mathrm{d}^2\rho|\Psi_{q\gamma}(\rho,\alpha)|^2\left(1-\left(1-\frac{1}{2A}\sigma^N_{q\bar{q}}(\alpha\rho,x_2)T_A(\vec{b})\right)^A\right), \quad (4.46)
\end{aligned}$$

and for the transverse momentum distribution of produced photons(dileptons)

$$\begin{aligned}
\frac{\mathrm{d}^2\sigma(pA\to\gamma X)}{\mathrm{d}^2p_T\mathrm{d}M^2\mathrm{d}x_F} &= \frac{\mathrm{d}\sigma(\gamma^*\to l^+l^-)}{\mathrm{d}M^2}\frac{x_1}{x_1+x_2}\int\limits_{x_1}^1\frac{\mathrm{d}\alpha}{\alpha^2}\sum_q Z_q^2\left(f_q\left(\frac{x_1}{\alpha},Q^2\right)+f_{\bar{q}}\left(\frac{x_1}{\alpha},Q^2\right)\right)\times \\
&\times\frac{\mathrm{d}\sigma(qA\to\gamma X)}{\mathrm{d}\ln\alpha\mathrm{d}^2p_T} = \frac{\mathrm{d}\sigma(\gamma^*\to l^+l^-)}{\mathrm{d}M^2}\frac{1}{x_1+x_2}\int\limits_{x_1}^1\frac{\mathrm{d}\alpha}{\alpha}F_2^p\left(\frac{x_1}{\alpha}\right)\frac{\mathrm{d}\sigma(qA\to\gamma X)}{\mathrm{d}\ln\alpha\mathrm{d}^2p_T} \\
\frac{\mathrm{d}\sigma(qA\to\gamma X)}{\mathrm{d}\ln\alpha\mathrm{d}^2p_T} &= \frac{1}{(2\pi)^2}\int\mathrm{d}^2\rho_1\int\mathrm{d}^2\rho_2 e^{i\vec{p}_T(\vec{\rho}_1-\vec{\rho}_2)}\Psi^*_{q\gamma}(\rho_1,\alpha)\Psi_{q\gamma}(\rho_2,\alpha)\Sigma^A_{q\bar{q}}(\rho_1,\rho_2,\alpha,x_2) \\
\Sigma^A_{q\bar{q}}(\rho_1,\rho_2,\alpha,x_2) &= \int\mathrm{d}^2b\left[1-\left(1-\frac{1}{2A}\sigma^N_{q\bar{q}}(\alpha\rho_1,x_2)T_A(\vec{b})\right)^A-\left(1-\frac{1}{2A}\sigma^N_{q\bar{q}}(\alpha\rho_2,x_2)T_A(\vec{b})\right)^A\right. \\
&\left.+\left(1-\frac{1}{2A}\sigma^N_{q\bar{q}}(\alpha|\vec{\rho}_1-\vec{\rho}_2|,x_2)T_A(\vec{b})\right)^A\right]. \quad (4.47)
\end{aligned}$$

## 4.4 Short coherence length

The short coherence length limit corresponds to the situation, where the mean coherence length $\langle l_c \rangle$ is shorter than the mean inter-nucleon separation ($\sim 1 - 2\, fm$). In that case, the separation of the fluctuation cannot be taken as "fixed" through the whole nucleus, and one has to account for each possible change in the fluctuation size. That is a reason why the Glauber eikonalization method cannot be used, since only configurations with fixed separations form eigenstates of the interaction and, therefore, can be taken independently. The fluctuation is then resolved immediately after it arises, and so, nucleons cannot act coherently on it. As a consequence, there is no nuclear shadowing in this limit due to very short duration of the $|\gamma q\rangle$ fluctuation. The corresponding theory for the description of the behaviour of the fluctuation in this limit is reviewed in Appendix E, and it is based on [9, 53].

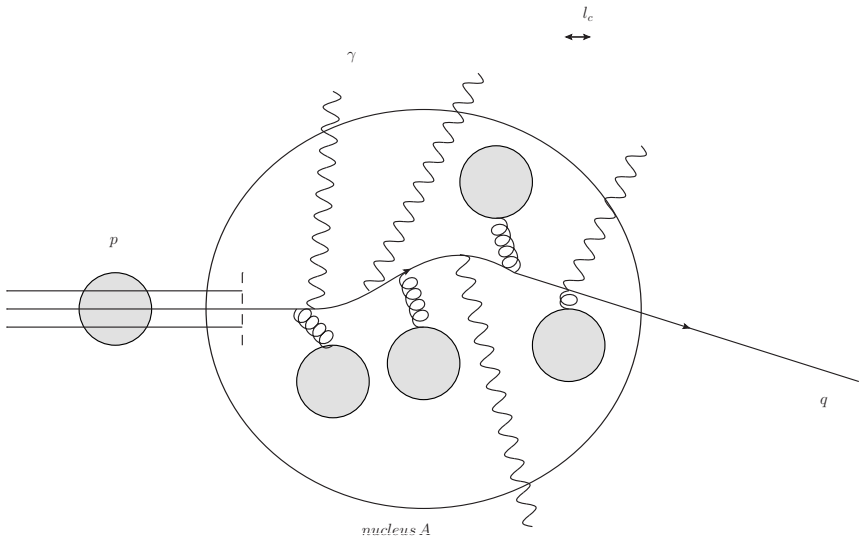


Figure 4.14: Sketch of the propagation of a quark through the nucleus in the short coherence length limit. Each inelastic scattering leads to the production of hard particle, since the $|\gamma q\rangle$ fluctuation is formed before a quark can interact with successive nucleons.

One has to proceed from the probability distribution $W_A^q(\vec{k}_T, x_q, \vec{b}, z) = \frac{\mathrm{d}^2 N_q}{\mathrm{d}^2 k_T}$ that a valence quark arriving at the position $(\vec{B}, z)$ in the nucleus $A$ will have acquired the transverse momentum $k_T$[9]. It can be written in terms of the quark density matrix describing the impact parameter distribution of the quark in the incident hadron

$$\Omega_q(\vec{b}, \vec{b}') = \frac{b_0^2}{\pi} e^{-\frac{b_0^2(b^2+b'^2)}{2}} \tag{4.48}$$

as

$$W_A^q(\vec{k}_T, x_q, \vec{B}, z) = \frac{1}{(2\pi)^2}\int \mathrm{d}^2b\mathrm{d}^2b' e^{i\vec{k}_T(\vec{b}-\vec{b}')}\Omega_q(\vec{b},\vec{b}')e^{-\frac{1}{2}\sigma_{q\bar{q}}^N(\vec{b}-\vec{b}',x_q)T_A\left(\frac{\vec{b}+\vec{b}'}{2}+\vec{B},z\right)}, \tag{4.49}$$

where $b_0^2 = \frac{2}{3\pi\langle r_{ch}^2\rangle}$ is the mean value of the primordial transverse momentum squared of the quark, $x_q$ is a fraction of the proton momentum carried by the quark, $\langle r_{ch}^2\rangle = 0.79 \pm 0.03 fm^2$[66] represents the mean square charge radius of a proton and $T_A(\vec{b}, z)$ is a partial nuclear thickness function

$$T_A(\vec{b}, z) = \int_{-\infty}^{z} \mathrm{d}z' \rho_A(\vec{b}, z'). \tag{4.50}$$

In contrast to the long coherence length limit, the nuclear thickness function $T_A(\vec{b})$ depends on the point, where the fluctuation occurs. To obtain the probability distribution per one nucleon $W^{qA}$ that a quark will have acquired transverse momentum $k_T$ after passing through the whole nucleus $A$ is obtained by averaging $W_A^q$ over the nuclear density $\rho_A(b, z)$[53]

$$W^{qA}(\vec{k}_T, x_q) = \frac{1}{A}\int \mathrm{d}^2B \int \mathrm{d}z \rho_A(\vec{B}, z) W_A^q(\vec{k}_T, x_q, \vec{B}, z). \tag{4.51}$$

The cross-section $\sigma^{qA}$ for an incident quark to produce a photon on a nucleus $A$ with transverse momentum $p_T$ can be expressed as a convolution of the probability $W^{qA}$ with the quark-nucleon cross-section $\sigma^{qN}$

$$\sigma^{qA}(\alpha, \vec{p}_T) = \int \mathrm{d}^2k_T W^{qA}(\vec{k}_T, x_q)\sigma^{qN}(\alpha, |\vec{p}_T - \alpha\vec{k}_T|), \tag{4.52}$$

where $\alpha = \frac{x_1}{x_q}$ is a fraction of quark momentum taken by a photon and $p_T$ is a transverse momentum of a photon. To obtain the transverse momentum distribution for an incident proton one should integrate over $\alpha$ using parton distribution functions as a quark momentum distributions inside the proton

$$\begin{aligned}\frac{\mathrm{d}^3\sigma(pA\to\gamma X)}{\mathrm{d}^2p_T\mathrm{d}x_F\mathrm{d}M^2} &= \frac{\mathrm{d}\sigma(\gamma^*\to l^+l^-)}{\mathrm{d}M^2}\frac{x_1}{x_1+x_2}\int_{x_1}^1\frac{\mathrm{d}\alpha}{\alpha^2}\sum_q Z_q^2\left(f_q\left(\frac{x_1}{\alpha},Q^2\right)+f_{\bar{q}}\left(\frac{x_1}{\alpha},Q^2\right)\right)\sigma^{qA}(\alpha,p_T)\\ &= \frac{\mathrm{d}\sigma(\gamma^*\to l^+l^-)}{\mathrm{d}M^2}\frac{1}{x_1+x_2}\int_{x_1}^1\frac{\mathrm{d}\alpha}{\alpha}F_2^p\left(\frac{x_1}{\alpha}\right)\sigma^{qA}(\alpha,p_T).\end{aligned} \tag{4.53}$$

Putting all formulas together one has to evaluate the formula

$$\sigma^{qA}(\alpha,p_T) = \frac{1}{A}\int \mathrm{d}^2k_T \int \mathrm{d}^2B \int \mathrm{d}z\rho_A(B,z)\frac{b_0^2}{(2\pi)^2\pi}\int \mathrm{d}^2b \int \mathrm{d}^2b' e^{i\vec{k}_T(\vec{b}-\vec{b}')} \times$$
$$\times e^{-\frac{1}{2}b_0^2(b^2+b'^2)} e^{-\frac{1}{2}\sigma_{q\bar{q}}^N(\vec{b}-\vec{b}',x_q)T_A\left(\frac{\vec{b}+\vec{b}'}{2}+\vec{B},z\right)}\sigma^{qN}(\alpha,|\vec{p}_T-\alpha\vec{k}_T|) \qquad (4.54)$$

that can be simplified using substitutions

$$\begin{aligned} \vec{r}_T &= \vec{b}-\vec{b}' & & \\ \vec{R} &= \frac{1}{2}(\vec{b}+\vec{b}') & \Rightarrow \qquad & b^2+b'^2 = 2R^2+\frac{r_T^2}{2} \\ \vec{\rho} &= \vec{R}+\vec{B} & & \frac{\vec{b}+\vec{b}'}{2}+\vec{B} = \vec{\rho} \end{aligned} \qquad (4.55)$$

having

$$\sigma^{qA}(\alpha,p_T) = \frac{b_0^2}{(2\pi)^2\pi A}\int \mathrm{d}^2k_T \int \mathrm{d}^2\rho \int \mathrm{d}z \int \mathrm{d}^2r_T \int \mathrm{d}^2R\ \rho_A(\vec{R}-\vec{\rho},z)e^{i\vec{k}_T\cdot\vec{r}_T} \times$$
$$\times e^{-\frac{1}{4}b_0^2r_T^2}e^{-b_0^2R^2}e^{-\frac{1}{2}\sigma_{q\bar{q}}^N(\vec{r}_T,x_q)T_A(\rho,z)}\sigma^{qN}(\alpha,|\vec{p}_T-\alpha\vec{k}_T|). \qquad (4.56)$$

This formula can be split into two parts

$$\begin{aligned} \sigma^{qA}(\alpha,\vec{p}_T) &= \frac{b_0^2}{(2\pi)^2\pi A}\int \mathrm{d}^2k_T \int \mathrm{d}^2r_T e^{i\vec{k}_T\cdot\vec{r}_T}e^{-\frac{1}{4}b_0^2r_T^2}U(r_T)\sigma^{qN}(\alpha,|\vec{p}_T-\alpha\vec{k}_T|) \\ U(r_T) &= \int \mathrm{d}^2\rho \int \mathrm{d}z \int \mathrm{d}^2R\ \rho_A(\vec{R}-\vec{\rho},z)e^{-b_0^2R^2}e^{-\frac{1}{2}\sigma_{q\bar{q}}^N(\vec{r}_T,x_q)T_A(\rho,z)}. \end{aligned} \qquad (4.57)$$

The last formula can be solved by applying procedure from [53] that leads to the substitution in the integration over $(\vec{B},z)$ using the nuclear thickness in the form

$$T_A(\vec{B},z) \Rightarrow \frac{\langle T_A\rangle}{2}, \qquad (4.58)$$

where the average thickness function $\langle T_A\rangle$ is defined as

$$\langle T_A\rangle = \frac{1}{A}\int \mathrm{d}^2b\, T_A^2(b). \qquad (4.59)$$

The factor one-half comes from the fact that $T_A(B,z) = \int\limits_{-\infty}^{z} \rho_A(B,z')\mathrm{d}z'$ should be averaged over the whole range of longitudinal variable $z$ from $-\infty$ to $+\infty$. Since the nuclear density

is symmetric in $z$, the average corresponds to the value $z = 0$, and so, one has to take one-half of the average. The uncertainty coming from the application of this approximation is less than one percent, and decrease with rising $p_T$[53]. Substituting the average thickness function leads to

$$U(r_T) = \int \mathrm{d}^2\rho \int \mathrm{d}z \int \mathrm{d}^2R\ \rho_A(\vec{R} - \vec{\rho}, z) e^{-b_0^2 R^2} e^{-\frac{1}{4}\sigma_{q\bar{q}}^N(\vec{r}_T, x_q)\langle T_A\rangle}. \tag{4.60}$$

Now, the transformation $\vec{\rho}_1 = \vec{R} - \vec{\rho}$ and $\vec{\rho}_2 = \vec{R}$ can be used

$$\begin{aligned} U(r_T) &= \int \mathrm{d}^2\rho_1 \int \mathrm{d}^2\rho_2\ T_A(\vec{\rho}_1) e^{-b_0^2\rho_2^2} e^{-\frac{1}{4}\sigma_{q\bar{q}}^N(\vec{r}_T, x_q)\langle T_A\rangle} \\ &= A2\pi \int_0^{+\infty} \rho_2 \mathrm{d}\rho_2\ e^{-b_0^2\rho_2^2} e^{-\frac{1}{4}\sigma_{q\bar{q}}^N(\vec{r}_T, x_q)\langle T_A\rangle} \\ &= \frac{A\pi}{b_0^2} e^{-\frac{1}{4}\sigma_{q\bar{q}}^N(\vec{r}_T, x_q)\langle T_A\rangle}. \end{aligned} \tag{4.61}$$

This solution can be substituted into the formula for $\sigma^{qA}$ having

$$\begin{aligned} \sigma^{qA}(\alpha, \vec{p}_T) &= \frac{1}{(2\pi)^2} \int \mathrm{d}^2k_T \int \mathrm{d}^2r_T e^{i\vec{k}_T\cdot\vec{r}_T} e^{-\frac{1}{4}b_0^2 r_T^2} e^{-\frac{1}{4}\sigma_{q\bar{q}}^N(\vec{r}_T, x_q)\langle T_A\rangle} \sigma^{qN}(\alpha, |\vec{p}_T - \alpha\vec{k}_T|) \\ &= \frac{1}{2\pi} \int \mathrm{d}^2k_T \int r_T \mathrm{d}r_T J_0(k_T r_T) e^{-\frac{1}{4}b_0^2 r_T^2} e^{-\frac{1}{4}\sigma_{q\bar{q}}^N(\vec{r}_T, x_q)\langle T_A\rangle} \sigma^{qN}(\alpha, |\vec{p}_T - \alpha\vec{k}_T|), \end{aligned} \tag{4.62}$$

where $J_0$ is a modified Bessel function. The final formula has a form

$$\begin{aligned} \sigma^{qA}(\alpha, \vec{p}_T) &= \frac{1}{2\pi} \int k_T \mathrm{d}k_T \int \mathrm{d}\varphi \int r_T \mathrm{d}r_T J_0(k_T r_T) e^{\frac{-r_T^2 b_0^2}{4}} e^{-\frac{1}{4}\sigma_{q\bar{q}}^N(r_T, x_q)\langle T_A\rangle} \times \\ &\quad \times \sigma^{qp}(\alpha, \sqrt{p_T^2 + \alpha^2 k_T^2 - 2\alpha k_T p_T \cos\varphi}), \end{aligned} \tag{4.63}$$

where $\sigma^{qp}$ can be calculated from the color dipole approach(see previous chapter).
In order to calculate the average thickness function, one can use models discussed in the chapter with the Glauber model.
Since the cross-section formula is already calculated per one nucleon, the normalization factor can be omitted and the nuclear modification factor has a form

$$R_{pA}(p_T) = \frac{\frac{\mathrm{d}^2\sigma(pA\to\gamma X)}{\mathrm{d}^2p_T}}{\frac{\mathrm{d}^2\sigma(pp\to\gamma X)}{\mathrm{d}^2p_T}}. \tag{4.64}$$

| | A[1] | $\langle T_A \rangle [fm^{-2}]$ |
|---|---|---|
| Pb | 208 | 1.46109 |
| Au | 197 | 1.48688 |
| W | 184 | 1.34126 |
| Cu | 63 | 0.88964 |
| Fe | 56 | 0.87307 |
| Ca | 40 | 0.74843 |
| C | 12 | 0.45236 |
| Be | 9 | 0.32271 |
| D(set 1) | 2 | 0.15909 |
| D(set 2) | 2 | 0.14400 |

Table 4.7: Average thickness function for various nuclei using nuclear densities discussed in the Glauber model chapter.

## 4.5 Formfactor

The transition region between the short coherence length limit($\langle l_c \rangle \sim 1 - 2fm$ or $x_2 \sim 0.1$) and the long coherence length limit ($\langle l_c \rangle \gg R_A$ or $x_2 \ll \frac{1}{2m_N R_A}$, where $m_N$ is a mass of the nucleon) is quite complicated and needs a calculation based on the path-integral approach using Green function technique[67, 68, 69]. Nevertheless, if quark shadowing corrections included in the long coherence length limit are not strong, one can use a linear interpolation between these limits performed by means of the nuclear longitudinal formfactor $F_A(q_c, b)$. The connection in the region between these limits has a form[54, 70, 71]

$$\sigma^{pA}(p_T) = \int \mathrm{d}^2 b \left( \left(1 - \left\langle F_A^2(q_c, b) \right\rangle \right) \sigma^{pA}_{l_c \ll 2fm}(p_T, b) + \left\langle F_A^2(q_c, b) \right\rangle \sigma^{pA}_{l_c \gg R_A}(p_T, b) \right), \quad (4.65)$$

where $q_c = 1/l_c$ is a longitudinal momentum transfer and the nuclear longitudinal formfactor $F_A(q_c, b)$ can be expressed as

$$F_A^2(q_c, b) = \frac{1}{T_A^2(b)} \left| \int_{-\infty}^{+\infty} dz e^{izq_c} \rho_A(b, z) \right|^2. \quad (4.66)$$

Here $\sigma^{pA}(p_T, b)$ is the unintegrated impact parameter dependent contribution to the cross-section and the longitudinal formfactor is averaged over $\alpha$ and $p_T$ weighted with the cross-section at fixed $p_T$ and varying initial and final parton momenta[72].
In order to simplify the calculation, one can use the averaged coherence length $\langle l_c \rangle_{\alpha, p_T}$ rather than average the whole formfactor. This approximation is sufficiently accurate, see [68]. One can write

$$\sigma^{pA}(p_T) = \int \mathrm{d}^2 b \left(1 - F_A^2(\langle q_c \rangle, b)\right) \sigma^{pA}_{l_c \ll 2fm}(p_T, b) + F_A^2(\langle q_c \rangle, b) \sigma^{pA}_{l_c \gg R_A}(p_T, b), \quad (4.67)$$

$$F_A^2(\langle q_c \rangle, b) = \frac{1}{T_A^2(b)} \left| \int_{-\infty}^{+\infty} dz e^{iz\langle q_c \rangle} \rho_A(b, z) \right|^2 = \frac{1}{T_A^2(b)} \left( 2 \int_0^{+\infty} dz \cos(\langle q_c \rangle z) \rho_A(b, z) \right)^2. \quad (4.68)$$

The connection formula can be understand in the following way. If the $l_c$ is short, no shadowing occur ($F_A^2(q_c) \to 0$) and the $\sigma^{pA}$ is dominated by the short coherence length contribution. In the opposite limit $l_c \gg R_A$, the shadowing has a full strength ($F_A^2(q_c) \to 1$) and the $\sigma^{pA}$ is dominated by the long coherence length contribution. The nuclear modification factor can be written as

$$R_{pA}(p_T) = \int \mathrm{d}^2 b \left( \left(1 - \left\langle F_A^2(q_c, b) \right\rangle \right) R_{pA}^{l_c \ll 2fm}(p_T, b) + \left\langle F_A^2(q_c, b) \right\rangle R_{pA}^{l_c \gg R_A}(p_T, b) \right), \quad (4.69)$$

## 4.6 Gluon shadowing

In order to account the nuclear shadowing into the calculation correctly, one has to include also a correction for higher Fock state $|\gamma qG\rangle$. The nuclear shadowing of gluons then modify the dipole cross-section $\sigma_{q\bar{q}}^N$ in the following way[29]

$$\begin{aligned} \sigma_{q\bar{q}}^N(\rho, x) &\Rightarrow \sigma_{q\bar{q}}^N(\rho, x) R_G(x, Q^2) \\ R_G(x, Q^2) &= \frac{G_A(x, Q^2)}{A G_N(x, Q^2)}. \end{aligned} \tag{4.70}$$

The correction factor for this Fock component is very difficult to calculate, although, the physical meaning of the shadowing term corresponds to the shadowing of the gluon part of the particular state. Therefore, the shadowing term should be universal and it can be calculated e.g. from DIS, where the similar calculation can be done easily. The factor $R_G(x, Q^2)$ is, therefore, calculated in the light-cone Green function approach developed in [16], where gluon shadowing is calculated from shadowing of the $|q\bar{q}G\rangle$ Fock component of a longitudinally polarized photons, since they can serve to measure the gluon density[29]. This can be understood in a way that the light-cone wave function for the transition $\gamma_L \to q\bar{q}$ suppress the probability for large aligned jet configurations with $\alpha \to 0.1$. Therefore, all $q\bar{q}$ dipoles from longitudinal photons have a small transverse size $\sim \frac{1}{Q^2}$. Nevertheless, the gluon can propagate quite far from the $q\bar{q}$ dipole, and so, the $|q\bar{q}G\rangle$ Fock state can be approximated by the $|GG\rangle$ state and the shadowing correction to the longitudinal cross-section is the same as the gluon shadowing

$$\frac{G_A(x, Q^2)}{A G_N(x, Q^2)} \sim \frac{\sigma_L^{\gamma A}(x, Q^2)}{A \sigma_L^{\gamma p}(x, Q^2)} = 1 - \frac{\Delta \sigma_L^{\gamma A}(x, Q^2)}{A \sigma_L^{\gamma p}(x, Q^2)}. \tag{4.71}$$

The magnitude of the gluon shadowing is determined by distance that the gluon can propagate from the dipole in the impact parameter space. The mean dipole distance was extracted from data to be rather small [16] $\rho_0 \sim 0.3 fm$. The value of $\rho_0$ also limits the range, where the above mentioned approximation is valid. It has to be assured that $Q^2 \gg \frac{1}{\rho^2}$ throughout the calculation, otherwise the $q\bar{q}$ pair is not point-like compared to the size of the Fock state.

The nuclear shadowing of photons corresponds to the inelastic nuclear shadowing introduced for hadrons by V.N.Gribov [73], where the shadowing term of the total photoabsorption cross-section $\Delta \sigma^{\gamma A} = \sigma_{tot}^{\gamma A} - A \sigma^{\gamma p}$ is related to the diffractive dissociation cross-section $\gamma N \to$

$XN$[73, 74], where one can write to the lowest order

$$\Delta\sigma^{\gamma A} = 8\pi\mathfrak{Re}\int \mathrm{d}^2b \int\limits_{-\infty}^{+\infty} \mathrm{d}z_1 \int\limits_{-\infty}^{+\infty} \mathrm{d}z_2 \Theta(z_2 - z_1)\rho_A(b, z_1)\rho_A(b, z_2) \times \int \mathrm{d}M_X^2 e^{-iq_L(z_2-z_1)} \frac{\mathrm{d}^2\sigma(\gamma N \to XN)}{\mathrm{d}M_X^2 \mathrm{d}q_T^2}\bigg|_{q_T=0} \tag{4.72}$$

and $q_L = \frac{Q^2+M_X^2}{2E_\gamma}$ resp. $q_T$ is the longitudinal resp. transversal momentum transfer, $E_\gamma$ is the photon energy in the rest frame of the target, $M_X$ is an invariant mass of the particular excited state, $\rho_A$ is a nuclear density function(for details see the Glauber model section), $\vec{b}$ is an impact parameter and $z_1$ resp. $z_2$ are longitudinal coordinates of nucleons $N_1$ resp. $N_2$ participating in the diffractive transitions $\gamma N_1 \to XN_1$ and $XN_2 \to \gamma N_2$. Since the masses of diffractive intermediate states are not well defined, one has to use a path integral technique while changing intermediate states with certain mass by Fock states $X = |q\bar{q}\rangle, |q\bar{q}G\rangle, \ldots$ [31]

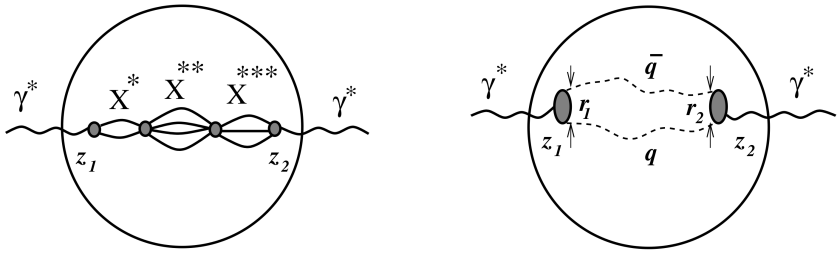


Figure 4.15: Sketch of the equivalence between diffractive dissociation(left) to intermediate states $X^*, X^{**}\ldots$ and path integral approach(right) with $|q\bar{q}\rangle$ fluctuation that effectively sum all orders of Gribov corrections. The figure is taken from [31]

Even then, the calculation is difficult and only first two states can be included. For the lowest state $|q\bar{q}\rangle$[16]

$$8\pi\mathfrak{Re}\int \mathrm{d}M_X^2 e^{-iq_L(z_2-z_1)} \frac{\mathrm{d}^2\sigma(\gamma N \to XN)}{\mathrm{d}M_X^2 \mathrm{d}q_T^2}\bigg|_{q_T=0} =$$

$$= \tfrac{1}{2}\mathfrak{Re}\int \mathrm{d}^2\rho_1 \int \mathrm{d}^2\rho_2 \int\limits_0^1 \mathrm{d}\alpha \Psi^\dagger_{q\bar{q}}(\vec{\rho}_2, \alpha)\sigma^N_{q\bar{q}}(\rho_2) G^0_{q\bar{q}}(\vec{\rho}_2, z_2, \vec{\rho}_1, z_1)\Psi_{q\bar{q}}(\vec{\rho}_1, \alpha)\sigma^N_{q\bar{q}}(\rho_1) \tag{4.73}$$

where

$$G^0_{q\bar{q}}(\vec{\rho}_2, z_2, \vec{\rho}_1, z_1) = \tfrac{1}{(2\pi)^2}\int \mathrm{d}^2k_T e^{-i\vec{k}_T(\vec{\rho}_2-\vec{\rho}_1) - \frac{ik_T^2(z_2-z_1)}{2E_\gamma\alpha(1-\alpha)}}$$
$$G^0_{q\bar{q}}(\vec{\rho}_2, z_1, \vec{\rho}_1, z_1) = \delta(\vec{\rho}_2 - \vec{\rho}_1) \tag{4.74}$$

is the Green function of the free propagation of the $q\bar{q}$ pair between points $z_1$ and $z_2$, $\Psi_{q\bar{q}}$ and $\sigma^N_{q\bar{q}}$ are defined in previous chapter, and $\alpha$ is a fraction of photon momentum carried by a quark. Note, that according to [16] the Green function in the coordinate representation lacks the information about absorption of the intermediate state in contrast to previous formulas. Thus, one should replace it with the solution of the Schrödinger equation

$$i\frac{\mathrm{d}}{\mathrm{d}z_2}G_{q\bar{q}}(\vec{\rho}_2,z_2,\vec{\rho}_1,z_1)=\left(\frac{\varepsilon^2-\Delta_r}{2E_\gamma\alpha(1-\alpha)}+V_{q\bar{q}}(b,z_2,\vec{\rho},\alpha)\right)G_{q\bar{q}}(\vec{\rho}_2,z_2,\vec{\rho}_1,z_1) \tag{4.75}$$

with $\varepsilon$ defined in previous chapter and with the imaginary potential

$$\mathfrak{Im}V_{q\bar{q}}(b,z_2,\vec{\rho},\alpha)=-\frac{\sigma^N_{q\bar{q}}(\rho)}{2}\rho_A(b,z_2). \tag{4.76}$$

Consequently, for the state $|q\bar{q}G\rangle$[16]

$$\begin{aligned}8\pi\mathfrak{Re}\int\mathrm{d}M_X^2e^{-iq_L(z_2-z_1)}\frac{\mathrm{d}^2\sigma(\gamma N\to XN)}{\mathrm{d}M_X^2\mathrm{d}q_T^2}\bigg|_{q_T=0}=\\ =\tfrac{1}{2}\mathfrak{Re}\int\mathrm{d}^2x_1\int\mathrm{d}^2y_1\int\mathrm{d}^2x_2\int\mathrm{d}^2y_2\int\mathrm{d}\alpha_q\int\mathrm{d}\ln\alpha_G\times\\ \times F^\dagger_{q\bar{q}G}(\vec{x}_2,\vec{y}_2,\alpha_q,\alpha_G)G_{q\bar{q}G}(\vec{x}_2,\vec{y}_2,z_2,\vec{x}_1,\vec{y}_1,z_1)F_{q\bar{q}G}(\vec{x}_1,\vec{y}_1,\alpha_q,\alpha_G)\end{aligned} \tag{4.77}$$

where $F$ is the amplitude of diffraction in the coordinate space, $\alpha_q$ and $\alpha_G$ are fractions of photon light-cone momenta carried by the quark and gluon, respectively. The coordinates in impact parameter space have following meaning.

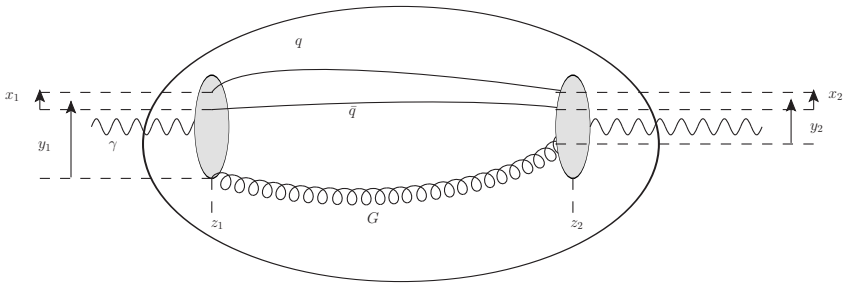


Figure 4.16: Coordinates used for the description of the propagation of $|q\bar{q}G\rangle$ fluctuation in the nucleus. The variable $\vec{x}_1$ and $\vec{x}_2$ describe the transverse separation of the $q\bar{q}$ part of the Fock state at the beginning and at the end respectively. The variable $\vec{y}_1$ and $\vec{y}_2$ corresponds to the distance of the gluon from the center of mass of the $q\bar{q}$ part of the Fock state.

The Schrödinger equation needed for the evaluation of the Green function describing propagation of the $|q\bar{q}G\rangle$ state through an interacting medium reads[16]

$$i\frac{\mathrm{d}}{\mathrm{d}z_2}G_{q\bar{q}G}(\vec{x}_2,\vec{y}_2,z_2,\vec{x}_1,\vec{y}_1,z_1)=\Bigg(\frac{Q^2}{2E_\gamma}-\frac{\alpha_q+\alpha_{\bar{q}}}{2E_\gamma\alpha_q\alpha_{\bar{q}}}\Delta(\vec{x}_2)-\frac{1}{2E_\gamma\alpha_G(1-\alpha_G)}\Delta(\vec{y}_2)$$
$$+V(b,\vec{x}_2,\vec{y}_2,z_2,\alpha_q,\alpha_G)\Bigg)G_{q\bar{q}G}(\vec{x}_2,\vec{y}_2,z_2,\vec{x}_1,\vec{y}_1,z_1) \quad (4.78)$$

with boundary condition

$$G_{q\bar{q}G}(\vec{x}_2,\vec{y}_2,z_1,\vec{x}_1,\vec{y}_1,z_1)=\delta(\vec{x}_2-\vec{x}_1)\delta(\vec{y}_2-\vec{y}_1). \quad (4.79)$$

The imaginary part of the potential can be expressed as [16]

$$2\mathfrak{Im}V(b,\vec{x}_2,\vec{y}_2,z_2,\alpha_q,\alpha_G)=$$
$$\Bigg(\tfrac{1}{8}\sigma^N_{q\bar{q}}(\vec{x}_2)-\tfrac{9}{8}\big(\sigma^N_{q\bar{q}}(\vec{y}_2-\tfrac{\alpha_q}{1-\alpha_G}\vec{x}_2)+\sigma^N_{q\bar{q}}(\vec{y}_2-\tfrac{\alpha_{\bar{q}}}{1-\alpha_G}\vec{x}_2)\big)\Bigg)\rho_A(b,z_2). \quad (4.80)$$

Now, the assumption that $q\bar{q}$ separation $\vec{x}$ can be neglected, and so, the dipole does not contribute to the potential can be used. Moreover, as soon as the separation is negligible, the dipole interacts as a gluon, which allows to look at the potential and the Green function as of the $GG$ dipole

$$\mathfrak{Im}V(b,\vec{x}_2,\vec{y}_2,z_2,\alpha_q,\alpha_G)=-\frac{\frac{9}{4}\sigma^N_{q\bar{q}}(y_2)}{2}\rho_A(b,z_2)=-\frac{\sigma^N_{GG}(y_2)}{2}\rho_A(b,z_2). \quad (4.81)$$

$$G_{q\bar{q}G}(\vec{x}_2,\vec{y}_2,z_2,\vec{x}_1,\vec{y}_1,z_1)=G^0_{q\bar{q}}(\vec{x}_2,z_2,\vec{x}_1,z_1)G_{GG}(\vec{y}_2,z_2,\vec{y}_1,z_1), \quad (4.82)$$

where the $G^0_{q\bar{q}}$ is a solution for the $q\bar{q}$ dipole without interacting medium and $G_{GG}$ is a solution for the $GG$ dipole with the above potential. Moreover, assuming that gluon carries very small part of the photon momenta ($\alpha_G\to 0$), one can express the amplitude $F$ in a way[16]

$$F_{q\bar{q}G}(\vec{x},\vec{y},\alpha_q,\alpha_G)=-\Psi^L_{q\bar{q}}(\vec{x},\alpha_q)\vec{x}\cdot\vec{\nabla}\Psi_{qG}(\vec{y})\sigma^N_{GG}(y), \quad (4.83)$$

where

$$\Psi_{qG}(\vec{y})=\lim_{\alpha_G\to 0}\Psi_{qG}(\vec{y},\alpha_G). \quad (4.84)$$

In order to evaluate the Green function one has to use a simple form of the dipole cross-section $\sigma^N_{GG}(y)=C_{GG}y^2$, where

$$C_{GG}=\left.\frac{\mathrm{d}^2\sigma_{GG}(y)}{\mathrm{d}^2y}\right|_{y=0} \quad (4.85)$$

and the Green function formula is

$$G_{GG}(\vec{y}_2, z_2, \vec{y}_1, z_1) = \frac{B}{2\pi \sinh(\Omega\Delta z)} e^{-\frac{B}{2}\left((y_2^2+y_1^2)\coth(\Omega\Delta z) - \frac{2\vec{y}_1\cdot\vec{y}_2}{\sinh(\Omega\Delta z)}\right)}, \tag{4.86}$$

where

$$\begin{aligned} B &= \sqrt{\tilde{b}^4 - i\alpha_G(1-\alpha_G)E_\gamma C_{GG}\rho_A} \\ \Omega &= \frac{iB}{\alpha_G(1-\alpha_G)E_\gamma} \\ \Delta z &= z_2 - z_1 \\ \tilde{b}^2 &= (0.65GeV)^2 + \alpha_G Q^2. \end{aligned} \tag{4.87}$$

Taking the quark-gluon wave function in the form

$$\psi_{qG}(\vec{y}\,) = \frac{2}{\pi}\sqrt{\frac{\alpha_s(Q^2)}{3}}\frac{\vec{e}\cdot\vec{y}}{y^2}e^{-\frac{b^2}{2}y^2}, \tag{4.88}$$

where $\alpha_s$ is a running coupling constant, and $\vec{e}$ is a polarization vector, one can perform the integration and write the final formula as[16]

$$\begin{aligned} &8\pi\mathfrak{Re}\int \mathrm{d}M_X^2 e^{-iq_L\Delta z}\frac{\mathrm{d}^2\sigma(\gamma N\to XN)}{\mathrm{d}M_X^2\mathrm{d}q_T^2}\bigg|_{q_T=0} = \\ &\mathfrak{Re}\int \mathrm{d}\alpha_q \int \mathrm{d}\ln\alpha_G \frac{16\alpha_{em}\sum\limits_q Z_q^2\alpha_s(Q^2)C_{GG}^2}{3\pi^2Q^2\tilde{b}^2}\left((1-2\xi-\xi^2)e^{-\xi}+\xi^2(3+\xi)E_1(\xi)\right)\times \\ &\times\left(\frac{t}{w}+\frac{\sinh(\Omega\Delta z)}{t}\ln\left(1-\frac{t^2}{u^2}\right)+\frac{2t^3}{uw^2}+\frac{t\sinh(\Omega\Delta z)}{w^2}+\frac{4t^3}{w^3}\right), \end{aligned} \tag{4.89}$$

where $Z_q$ is a fractional charge of a quark, $\alpha_{em}$ is a fine structure constant, $E_1$ is the exponential integral function and

$$\begin{aligned} \xi &= ixm_N\Delta z \\ t &= \frac{B}{\tilde{b}^2} \\ u &= t\cosh(\Omega\Delta z)+\sinh(\Omega\Delta z) \\ w &= (1+t^2)\sinh(\Omega\Delta z)+2t\cosh(\Omega\Delta z). \end{aligned} \tag{4.90}$$

The integration ranges are $0 \le \alpha_q \le 1$ and $x \le \alpha_G \le 0.1$[29], since one has to ensure the smallness of the momentum fraction taken by gluon that was used in approximations above.

The integration over $\alpha_q$ is trivial, since the integrand does not depend on $\alpha_q$ now. The running coupling constant was taken from [75] in the form

$$\alpha_s(Q^2) = \frac{4\pi}{9\ln\left(\frac{Q^2+0.25GeV^2}{(200MeV)^2}\right)}. \tag{4.91}$$

Instead of constant $C_{GG}$ in the dipole cross-section, one can take the effective value $C_{eff}(\tilde{x})$ dependent on the fraction of light-cone momenta of gluon taken from the proton $\tilde{x}$

$$C_{GG} = C_{eff}(\tilde{x}) \qquad \tilde{x} = \frac{x}{\alpha_G}, \tag{4.92}$$

where $x$ is the Bjorken variable of the gluon. To preserve the validity of the dipole model, the value of $\tilde{x}$ should not exceed 0.1 as $\alpha_G \to x$. The parameter $C_{eff}$ is determined from the asymptotic condition[29]

$$\frac{\int \mathrm{d}^2b \int \mathrm{d}^2\rho |\Psi_{qG}(\rho)|^2 \left(1 - e^{-\frac{1}{2}C_{eff}(\tilde{x})\rho^2 T_A(b)}\right)}{\int \mathrm{d}^2b \int \mathrm{d}^2\rho |\Psi_{qG}(\rho)|^2 C_{eff}(\tilde{x})\rho^2} = \frac{\int \mathrm{d}^2b \int \mathrm{d}^2\rho |\Psi_{qG}(\rho)|^2 \left(1 - e^{-\frac{9}{8}\sigma^N_{\bar{q}q}(\rho,\tilde{x})T_A(b)}\right)}{\int \mathrm{d}^2b \int \mathrm{d}^2\rho |\Psi_{qG}(\rho)|^2 \frac{9}{4}\sigma^N_{\bar{q}q}(\rho,\tilde{x})}, \tag{4.93}$$

where for the dipole cross-section a saturated parametrization was used[6]. Using constant nuclear density $\rho_A$ the shadowing term can be expressed as[29]

$$\Delta\sigma_L^{\gamma A}(x,Q^2) = \frac{\pi}{12}\rho_A^2 \int_0^{2R_A} \mathrm{d}L(L^3 - 12R_A^2 L + 16R_A^3) 8\pi \mathfrak{Re} \int \mathrm{d}M_X^2 e^{-iq_L L} \frac{\mathrm{d}^2\sigma(\gamma N \to XN)}{\mathrm{d}M_X^2 \mathrm{d}q_T^2}\bigg|_{q_T=0}, \tag{4.94}$$

where $L = 2\sqrt{R_A^2 - b^2}$ is a length of the propagation of the fluctuation inside the medium and $R_A$ is the nuclear radius. The gluon shadowing factor dependent of the impact parameter can be written as[29]

$$R_G(x,Q^2,b) = 1 - \frac{\Delta\sigma_L^{\gamma A}(x,Q^2,b)}{T_A(b)\sigma_L^{\gamma p}(x,Q^2)}, \tag{4.95}$$

where

$$\Delta\sigma_L^{\gamma A}(x,Q^2,b) = \rho_A^2 \int_0^L \mathrm{d}z(L-z) 8\pi \mathfrak{Re} \int \mathrm{d}M_X^2 e^{-iq_L z} \frac{\mathrm{d}^2\sigma(\gamma N \to XN)}{\mathrm{d}M_X^2 \mathrm{d}q_T^2}\bigg|_{q_T=0} \tag{4.96}$$

and the scale is

$$Q^2 = \frac{1}{\rho^2} + 4GeV^2. \tag{4.97}$$

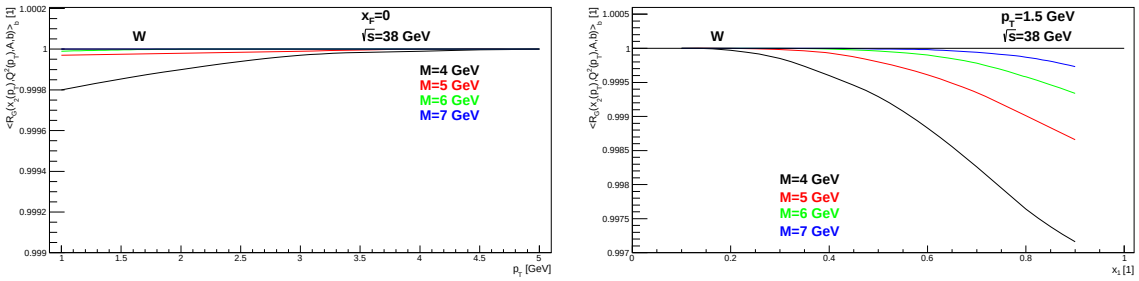


Figure 4.17: The gluon shadowing correction for the kinematic range accessible at the E772/E866 experiment for tungsten nucleus. Left figure corresponds to mean value of $R_G$ vs. $p_T$ for fixed $x_F = 0$, while the right figure corresponds to mean value of $R_G$ vs. $x_1$ for fixed $p_T = 1.5GeV$.

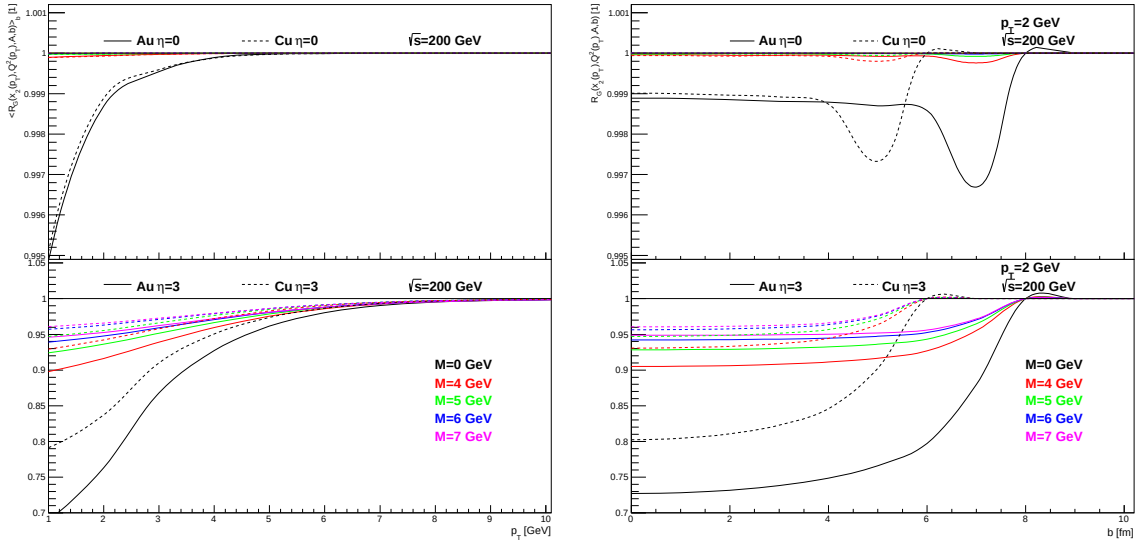


Figure 4.18: The gluon shadowing correction for the kinematic range accessible at the RHIC accelerator for mid and forward rapidity and for two kinds of nuclei. Left figure corresponds to mean value of $R_G$ vs. $p_T$, while the right figure corresponds to the dependence of $R_G$ on the impact parameter $b$ for fixed $p_T = 2GeV$.

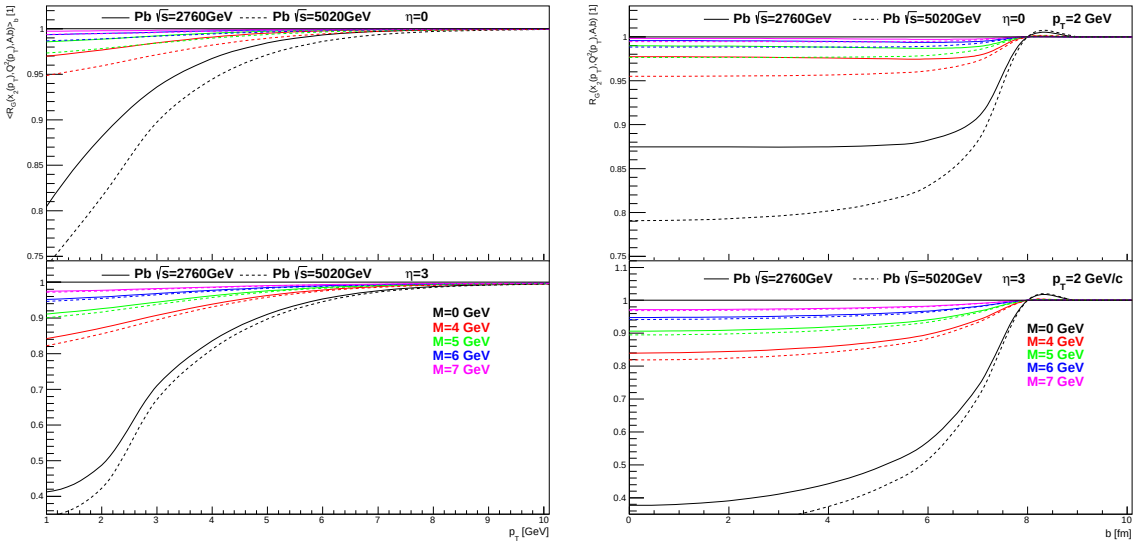


Figure 4.19: The gluon shadowing correction for the kinematic range accessible at the LHC accelerator for mid and forward rapidity and for two different energies used. Left figure corresponds to mean value of $R_G$ vs. $p_T$, while the right figure corresponds to the dependence of $R_G$ on the impact parameter $b$ for fixed $p_T = 2GeV$.

# Chapter 5

# Additional nuclear modifications

## 5.1 Izospin corrections

There is another effect that has to be accounted in nucleon-nucleus collisions, but more importantly in nucleus-nucleus collisions which is called an izospin effect. It comes from the fact that the interaction between a proton and nucleus differ from the interaction between a neutron and nucleus due to different valence quark composition of protons and neutrons. Therefore, one has to account properly parton distributions in the structure function used for the calculation. Assuming that sea quark distribution is equal to anti-sea quark distribution, the structure function of the nucleon can be written as

$$\begin{aligned} F_2(x,Q^2) &= \left(\frac{2}{3}\right)^2 x f_{u_v}(x,Q^2) + \left(\frac{1}{3}\right)^2 x f_{d_v}(x,Q^2) + \\ &+ \left(\frac{2}{3}\right)^2 2x f_{u_s}(x,Q^2) + \left(\frac{1}{3}\right)^2 2x f_{d_s}(x,Q^2) + \\ &+ \left(\frac{1}{3}\right)^2 2x f_{s_s}(x,Q^2) + \dots \end{aligned} \tag{5.1}$$

with the normalization for the proton

$$\int_0^1 f_{u_v}(x,Q)\mathrm{d}x = 2 \qquad \int_0^1 f_{d_v}(x,Q)\mathrm{d}x = 1, \tag{5.2}$$

whereas, for the neutron

$$\int_0^1 f_{u_v}(x,Q)\mathrm{d}x = 1 \qquad \int_0^1 f_{d_v}(x,Q)\mathrm{d}x = 2. \tag{5.3}$$

The variable $x$ is a fraction of nucleon momentum carried by a parton and $Q^2$ is a scale of the process. Parton distribution functions $f_q$ are taken from phenomenological parametrizations(see corresponding section).
For the case of incident deuteron, the nucleon structure function should correspond to the average between proton and neutron structure function

$$\begin{aligned} F_2^d(x,Q^2) &= \frac{1}{2}(F_2^p(x,Q^2)+F_2^n(x,Q^2)) = \\ &= \frac{1}{2}\Bigg( \left(\frac{2}{3}\right)^2 \frac{3}{2} x f_{u_v}(x,Q^2) + \left(\frac{1}{3}\right)^2 3 x f_{d_v}(x,Q^2) + \\ &+ \left(\frac{2}{3}\right)^2 4 x f_{u_s}(x,Q^2) + \left(\frac{1}{3}\right)^2 4 x f_{d_s}(x,Q^2) + \\ &+ \left(\frac{1}{3}\right)^2 4 x f_{s_s}(x,Q^2) + \dots \Bigg). \end{aligned} \tag{5.4}$$

For the case of a nuclear projectile with $Z$ protons and $N$ neutrons($A = Z + N$), there are $2Z$ valence $u$-quarks and $Z$ valence $d$-quarks from protons and $2N$ valence $d$-quarks and $N$ valence $u$-quarks from neutrons inside the projectile. Therefore, there are $A + Z$ valence $u$-quarks and $2A - Z$ valence $d$-quarks in total. The average structure function then reads

$$\begin{aligned} F_2^A(x,Q^2) &= \frac{1}{A}(ZF_2^p(x,Q^2)+NF_2^n(x,Q^2)) = \\ &= \frac{1}{A}\Bigg( \left(\frac{2}{3}\right)^2 \frac{A+Z}{2} x f_{u_v}(x,Q^2) + \left(\frac{1}{3}\right)^2 (2A-Z) x f_{d_v}(x,Q^2) + \\ &+ \left(\frac{2}{3}\right)^2 2A x f_{u_s}(x,Q^2) + \left(\frac{1}{3}\right)^2 2A x f_{d_s}(x,Q^2) + \\ &+ \left(\frac{1}{3}\right)^2 2A x f_{s_s}(x,Q^2) + \dots \Bigg). \end{aligned} \tag{5.5}$$

This effect slightly suppresses the nuclear modification factor for projectiles different from the proton at high $p_T$, since

$$R_{pA}(p_T \to +\infty) \sim \frac{F_2^p}{F_2^p} = 1 \tag{5.6}$$

and

$$R_{AA}(p_T \to +\infty) \sim \frac{F_2^A}{AF_2^p} = \frac{\left(\frac{2}{3}\right)^2 2\frac{A+Z}{2} + \left(\frac{1}{3}\right)^2 (2A-Z)}{A\left(\left(\frac{2}{3}\right)^2 2 + \left(\frac{1}{3}\right)^2 1\right)} = \left(\frac{2}{3}\right)^2 \left(1+\frac{Z}{A}\right) + \left(\frac{1}{3}\right)^2 \left(2-\frac{Z}{A}\right). \tag{5.7}$$

In the case of the deuteron $R_{dA} \sim \frac{5}{6}$. Note that only valence quarks are taken into the structure function at $p_T \to +\infty$, since also $x \to 1$ and sea component is negligible. Moreover, the structure function is integrated over $x$ in this limit.

## 5.2 Energy conservation restrictions in multiple parton re-scatterings

The purpose of this section is to discuss a feature common to all reactions on nuclear targets. As a quark passes through the medium, it is subject to induced energy loss, which can be remarkably strong in certain kinematics. Therefore, when a quark reaches the point of a particle emission, its energy is lower than at the beginning, and so, it cannot emit particle as energetic as the theory predicts. This is a reason why one has to include a correction for the energy conservation of the photon emission in multiple parton re-scattering [19, 17, 18]. One way how to do it is to parametrize the energy loss per unit of quark path in the medium and lower the energy of emitting quark as in [54]. Rather than that it is advantageous to treat it as a change of the probability that quark can emit certain particle in the multiple parton re-scattering. This class of events is usually called large rapidity gap processes. Obviously, the restriction of energy conservation leads to a substantial suppression, similar to what is known from QED as the Sudakov formfactor related to elastic electron scattering with no bremsstrahlung. Especially, if a large-$x$ particle $c$ is produced in the process $a + b \to c + X$, the rapidity interval to be kept empty is

$$\Delta y = -\ln(1 - x). \tag{5.8}$$

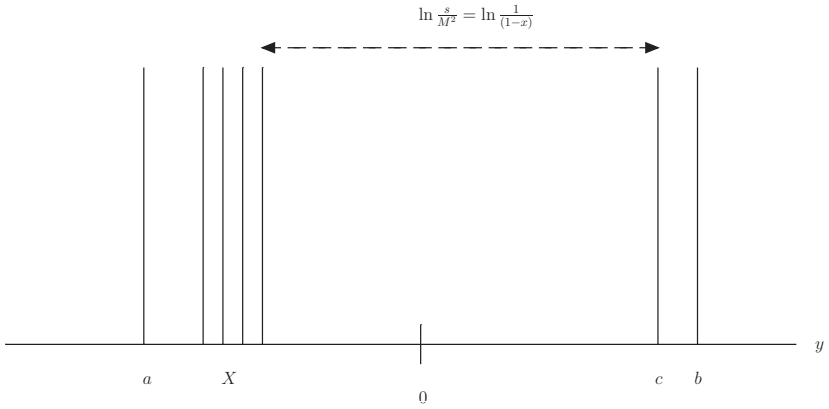


Figure 5.1: Sketch of the width of the rapidity gap in the interaction, where large-$x$ particle is produced.

The production of particles is treated via perturbative gluon radiation [77] following with a non-perturbative hadronization. Assuming an uncorrelated Poisson distribution for gluons, the Sudakov suppression factor, i.e. the probability to have a rapidity gap $\Delta y$, becomes[18]

$$S(\Delta y) = e^{-\langle n_G(\Delta y)\rangle}, \tag{5.9}$$

where $n_G(\Delta y)$ is the mean number of gluons that would be radiated within $\Delta y$, if it is allowed by energy conservation. Note, that even if gluons are not radiated within the rapidity gap, the hadronization can easily fill the gap with observed particles. The probability that this does not happen is another suppression factor which, however, is independent of target and cancels in the nuclear modification factor. The mean number $\langle n_G(\Delta y)\rangle$ of gluons radiated in the rapidity interval $\Delta y$ is related to the height of the plateau in the gluon spectrum

$$\langle n_G(\Delta y)\rangle = \Delta y \frac{\mathrm{d}n_G}{\mathrm{d}y}. \tag{5.10}$$

Thus, the Sudakov factor acquires the simple form,

$$S(x) = (1-x)^{\frac{\mathrm{d}n_G}{\mathrm{d}y}}. \tag{5.11}$$

The height of the gluon plateau was estimated in [77] as,

$$\frac{\mathrm{d}n_G}{\mathrm{d}y} = \frac{3\alpha_s}{\pi} \ln\left(\frac{m_\rho^2}{\Lambda_{QCD}^2}\right), \tag{5.12}$$

where $m_\rho$ is a mass of the $\rho$ meson from the $\rho$ dominance model and $\Lambda_{QCD} \sim 0.2GeV$. The value of $\alpha_S$ was fitted to data on pion multiplicity in $e^+e^-$ annihilation leading to the value $\alpha_S = 0.45$[77]. Other determination of the $\alpha_S$ has been realized in several sources (see [19]) leading to the values varying within an interval from 0.38[78, 79] to 0.45. For further calculations, the value $\alpha_S = 0.4$ is taken, which gives with high accuracy $\frac{\mathrm{d}n_G}{\mathrm{d}y} = 1$, i.e. the Sudakov factor is

$$S(x) = 1 - x, \tag{5.13}$$

where

$$x = \sqrt{x_T + x_L} \qquad x_T = \frac{2p_T}{\sqrt{s}} \qquad x_L = x_F. \tag{5.14}$$

This coincides with the suppression factor applied to every additional Pomeron exchange in the quark-gluon string [80, 81] and dual parton [82] models based on the Regge approach.

On a nuclear target, the Sudakov factor should fall more steeply as $x \to 1$ since multiple interactions enhance the transverse momentum given to the projectile parton and therefore tend to radiate more gluons. This can be understood in terms of the Fock state decomposition. The projectile hadron can be expanded over different states that form fluctuations of this hadron. In the system of the infinite momentum frame those fluctuations live infinitely long. One can probe the Fock state expansion by the interaction with a target. The interaction modifies weights of Fock states - some of them are enhanced, some are suppressed. As an example, one can see the wave function of the transversely polarized photon. In vacuum,

it is dominated by the $|q\bar{q}\rangle$ Fock states with very small separation leading to an ultraviolet divergent normalization of the wave function. However, the smaller is the size of the fluctuation, the smaller is the interaction cross-section of the particular Fock state leaving the overall photoabsorption cross-section finite. In each Fock component the hadron momentum is shared by constituents, and so, the momentum distribution depends on their multiplicity - the more constituents are involved, the smaller energy per constituent parton is and the softer the fractional energy distribution of the leading parton is. Especially, according to the Brodsky-Farrar counting rules [83, 84], the behaviour of the single parton distribution function for $x \to 1$ depends on the number of constituents in the particular Fock state. A nucleus having higher resolution (controlled by the saturation scale $Q_s$ [85, 86, 87]) resolves more constituents and thus results in steeper fall off of the distribution function toward $x = 1$. If one parton in the multiparton Fock state takes the main part of the momenta ($x \to 1$), other partons has to be within small phase space cell of the magnitude $1 - x$. The more partons is in the Fock state the less is the probability that these partons can fit to a small phase space $(1 - x)^{n(A)}$[83], where $n(A)$ is the number of partons in the relevant Fock state. Therefore, in this kinematical region the parton distribution has to fall more steeply as $x \to 1$ and $f_q^A \sim (1 - x)^{n(A)}$[84]. This result suggest a non-trivial conclusion that the effective parton distribution function in the beam hadron depends on the target. Such a process-dependence constitutes an apparent breakdown of QCD factorization and is a leading twist effect.
In case of hard reaction on the nucleus, the softening of the projectile parton momentum distribution can be viewed as an effective energy loss of the leading parton in the nuclear medium, because the initial state multiple interactions enhance weight factors for higher Fock states in the projectile hadron[31]. As discussed above, the mean energy of the leading parton decreases compared to lower Fock states that dominate the hard reaction. This reduction of the mean energy of the leading parton can be treated as an effective energy loss proportional to the initial energy of a hadron. Nevertheless, there is an important difference between this effect and energy loss of a single parton propagating through the medium and producing induced gluon radiation. In the former case, the mean fraction of energy carried by radiated gluons vanishes with initial energy as $\frac{1}{E}$ in contrast to the latter case, where the mean energy loss is independent of the initial energy of a quark[31].
Nevertheless, treating the problem in any way, one arrive at the conclusion that every additional inelastic interaction contributes an extra suppression factor $S(x)$. The probability of an n-fold inelastic collision is related to the Glauber model coefficients via the Abramovsky-Gribov-Kancheli (AGK) cutting rules [88]. Correspondingly, the survival probability at impact parameter $\vec{b}$ reads

$$W_{LRG}^{NA}(\vec{b}) = e^{-\sigma_{inc}^{NA} T_A(\vec{b})} \sum_{n=1}^{A} \frac{1}{n!} (\sigma_{inc}^{NN} T_A(\vec{b}))^n S^{n-1}(x) \tag{5.15}$$

and, consequently, the cross-sections of a hard reaction on a nuclear target $A$ and on a nucleon target $N$ are related as

$$\frac{\mathrm{d}^3\sigma_A}{\mathrm{d}x\mathrm{d}^2b} = \frac{\mathrm{d}\sigma_N}{\mathrm{d}x}\frac{e^{-\sigma_{eff}T_A(\vec{b})}}{\sigma_{eff}}\sum_{n=1}^{A}\frac{n}{n!}(\sigma_{eff}T_A(\vec{b}))^n S^{n-1}(x) \to \frac{\mathrm{d}\sigma_N}{\mathrm{d}x}T_A(\vec{b})e^{-(1-S(x))\sigma_{eff}T_A(\vec{b})}. \quad (5.16)$$

In this expression particles are assumed to be produced independently in multiple re-scattering, i.e. in Bethe-Heitler regime. It should be in principle corrected for effects of coherence. Indeed, at small $x$ the Sudakov factor $S(x \to 0) \to 1$, and the probability takes the form of the Glauber expression for absorptive hadron-nucleus cross section. In this case coherence effects are referred as Gribov inelastic shadowing corrections which are known to be small [89]. In another limiting case $x \to 1$ energy conservation allows only radiation of low-energy particles having short coherence time. Therefore, particles are produced incoherently in multiple interactions and the formula for the probability holds.
The probability of an n-fold inelastic collision leads to the following form of the quark distribution in the nucleus

$$f_q^A(x, Q^2, \vec{b}, z) = \sum_{n=0}^{\infty} v_n(\vec{b}, z) f_q^n(x, Q^2), \quad (5.17)$$

where the coefficients $v_n$ read

$$v_n(\vec{b}, z) = \frac{(\sigma_{eff}T_A(\vec{b}, z))^n}{(1 + \sigma_{eff}T_A(\vec{b}, z))^{n+1}} \quad (5.18)$$

with the effective cross section

$$\sigma_{eff} = 20mb \quad (5.19)$$

as was evaluated in [19]. The quark distribution functions $f_q^n$ are also given by usual parton distribution functions, but contain extra suppression factor $S^n(x) = (1-x)^n$ corresponding to an n-fold inelastic collision

$$f_q^n(x, Q^2) = C_n f_q(x, Q^2) S^n(x), \quad (5.20)$$

where the normalization factors $C_n$ are fixed by the Gottfried sum rule

$$\int_0^1 \mathrm{d}x(f_q^A(x, Q^2) - f_{\bar{q}}^A(x, Q^2)) = n_q, \quad (5.21)$$

where $n_q$ are numbers of valence quarks of given flavour $q$($n_u = 2$ a $n_d = 1$ for a proton). Summing up the expression for the parton distribution function in the nucleus $f_q^A$ leads to the formula

$$
\begin{aligned}
f_q^A(x,Q^2) &= C_n f_q(x,Q^2)\frac{\int \mathrm{d}^2b(e^{-x\sigma_{eff}T_A(\vec{b})}-e^{-\sigma_{eff}T_A(\vec{b})})}{(1-x)\int \mathrm{d}^2b(1-e^{-\sigma_{eff}T_A(\vec{b})})} \\
&= C_n f_q(x,Q^2)\int \mathrm{d}^2b\, e^{-(1-S(x))\sigma_{eff}T_A(\vec{b})}
\end{aligned}
\tag{5.22}
$$

However, the expression for the Sudakov formfactor was derived for the situation, where $x \to 1$ and as far as one goes to the production of particles with lower $x$, the other limit $x \to 0$ starts to contribute to the attenuation factor. Therefore, one should modify the formfactor to account both limits. This interpolation was taken to reproduce well available data for the Drell-Yan production in the form

$$
S(x) = (1-x)\sum_{i=1}^{k} x^{i-1}, \tag{5.23}
$$

where $k = 5$ is free parameter that takes into account that a weight of the limit $x \to 0$ is stronger than the weight of the limit $x \to 1$. The modified formula for the formfactor correctly reproduce both limiting cases

$$
S(x \to 0) = 1 \tag{5.24}
$$

and

$$
S(x \to 1) \sim 1 - x. \tag{5.25}
$$

# Chapter 6

# Coherence effects in nucleus-nucleus collisions

## 6.1 Geometrical Glauber model in heavy-ion collisions

Let's consider the situation where the target nucleus with $A$ nucleons collide with projectile nucleus with $B$ nucleons at impact parameter $\vec{b}$.

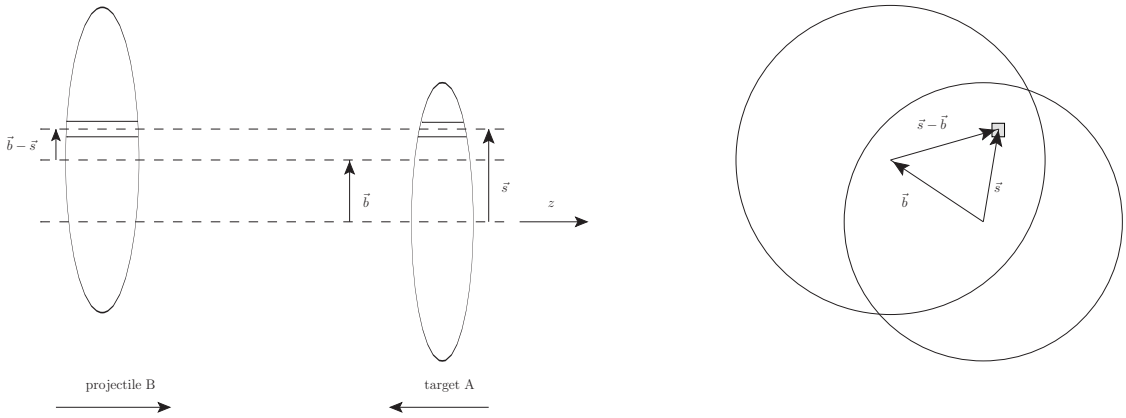


Figure 6.1: Schematic figure of a nucleus-nucleus collision in a side view(left) and a front view(right).

Then one can focus on two "flux tubes" located at a displacement $\vec{s}$ with respect to the center of the target nucleus and a distance $\vec{s}-\vec{b}$ from the center of the projectile nucleus. These tubes form an overlapping region, where the probability of the interaction between nucleons is considered. Using definitions from chapter 4.2 the probability per unit transverse area that the nucleon is located in the nucleus $A$ resp. $B$ at the impact parameter $\vec{s}$ resp.

$\vec{b} - \vec{s}$ is

$$\frac{T_A(\vec{s})}{A} \qquad \text{resp.} \qquad \frac{T_B(\vec{b}-\vec{s})}{B}. \tag{6.1}$$

The joint probability per unit area of nucleons being located in the respective overlapping flux tubes of differential area $\mathrm{d}^2 s$ is given by the product

$$\frac{T_A(\vec{s})}{A}\frac{T_B(\vec{b}-\vec{s})}{B}\mathrm{d}^2 s. \tag{6.2}$$

Integrating over all possible values of $\vec{s}$ defines the so called nuclear overlap function $T_{AB}(\vec{b})$

$$\frac{1}{AB}\int T_A(\vec{s})T_B(\vec{b}-\vec{s})\mathrm{d}^2 s = \frac{1}{AB}T_{AB}(\vec{b}) \tag{6.3}$$

which is normalized as $\int T_{AB}(\vec{b})\mathrm{d}^2 b = AB$.

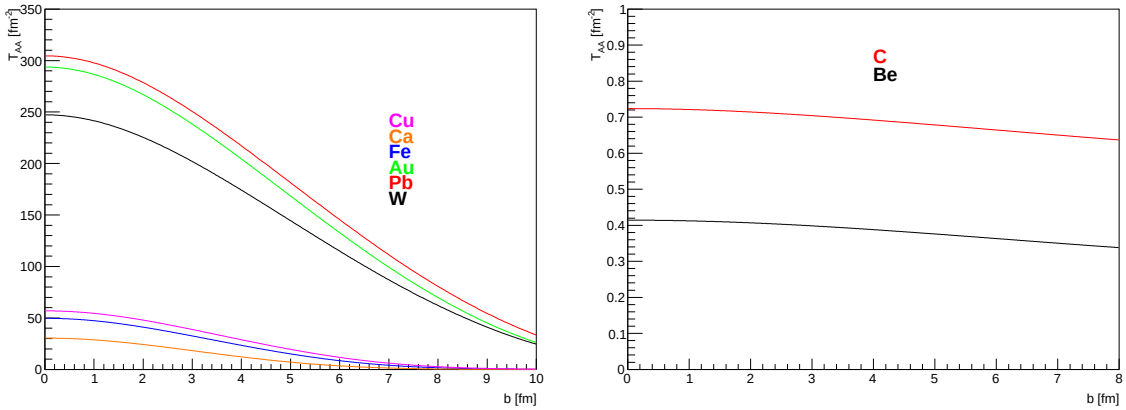


Figure 6.2: Nuclear overlap functions for heavy and light nuclei.

Since the overlap function adds up one more integration into the calculation, it is usually advantageous to fit the overlap function with some phenomenological function. The thickness function is taken in the form discussed in previous chapter - Wood-Saxon parametrization for heavy nuclei and modified harmonic oscillator for light nuclei. Using a function

$$T_{AA}(b) = c_1 e^{-c_2 b^2} + c_3 e^{-c_4 b^3} \tag{6.4}$$

the fit can be performed with results in Tab. 6.1
Again, having the probability that the nucleons are located in an overlap region, one can write the probability that an interaction occur in this region as $T_{AB}(\vec{b})\sigma_{inel}^{NN}$ and, therefore,

| | $A \times A[1]$ | $c_1[fm^{-2}]$ | $c_2[fm^{-2}]$ | $c_3[fm^{-2}]$ | $c_4[fm^{-3}]$ | $\chi^2/ndf$ |
|---|---|---|---|---|---|---|
| Pb | 43431.395 | 112.04 | 0.0566697 | 192.227 | 0.00177108 | 0.0835684 |
| Au | 38953.656 | 108.387 | 0.0605959 | 184.966 | 0.00197237 | 0.0731961 |
| W | 33990.553 | 90.7452 | 0.0590111 | 156.283 | 0.00187234 | 0.0574234 |
| Cu | 4022.634 | 64.4888 | 0.0479192 | -7.2313 | 0.032057 | 0.041711 |
| Fe | 3176.542 | 56.0495 | 0.0528486 | -6.08894 | 0.0376543 | 0.0296631 |
| Ca | 1616.632 | 33.7477 | 0.0630581 | -3.1447 | 0.0521694 | 0.00794242 |
| C | 135.187 | 0.701256 | 0.0015327 | 0.0217845 | 0.0338789 | $1.55812.10^{-7}$ |
| Be | 74.425 | 0.396348 | 0.00252686 | 0.017371 | 0.0280931 | $7.18765.10^{-8}$ |

Table 6.1: Fit parameters for various nuclei using a phenomenological function. Here $A \times A$ corresponds to the overall integral of the fit function.

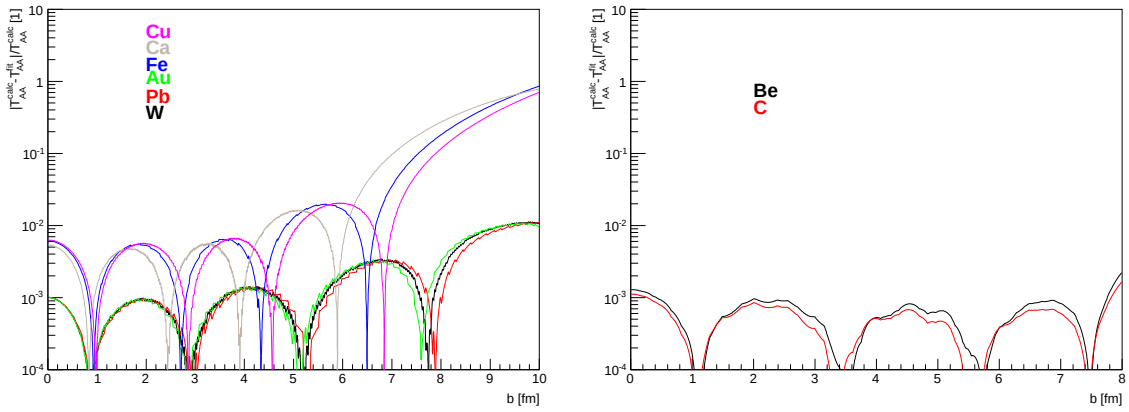


Figure 6.3: Estimation of an error made by using a parametrization of nuclear overlap function for heavy and light nuclei.

the probability to have $n$ inelastic interactions between nucleus $A$ and $B$ is given by binomial distribution

$$P(n,\vec{b}) = \binom{AB}{n} \left(\frac{T_{AB}(\vec{b})}{AB}\sigma_{inel}^{NN}\right)^n \left(1 - \frac{T_{AB}(\vec{b})}{AB}\sigma_{inel}^{NN}\right)^{AB-n} \tag{6.5}$$

Summation over all possible inelastic collisions gives a total probability of an interaction between $A$ and $B$

$$\frac{\mathrm{d}^2\sigma_{inel}^{AB}}{\mathrm{d}^2 b} = \sum_{n=1}^{AB} P(n,\vec{b}) = 1 - \left(1 - \frac{T_{AB}(\vec{b})}{AB}\sigma_{inel}^{NN}\right)^{AB} \tag{6.6}$$

and the respective total cross-section is

$$\sigma_{inel}^{AB} = \int \mathrm{d}^2 b \left[ 1 - \left( 1 - \frac{T_{AB}(\vec{b})}{AB} \sigma_{inel}^{NN} \right)^{AB} \right] = \int_0^{+\infty} 2\pi b \mathrm{d}b \left[ 1 - \left( 1 - \frac{T_{AB}(b)}{AB} \sigma_{inel}^{NN} \right)^{AB} \right]. \tag{6.7}$$

Using the probability for having $n$ inelastic collisions, one can calculate the total number of collisions

$$N_{coll}(\vec{b}) = \sum_{n=0}^{AB} n P(n, \vec{b}) = T_{AB}(\vec{b}) \sigma_{inel}^{NN}. \tag{6.8}$$

The number of nucleons in the target and projectile nuclei that interact is called number of participants or number of wounded nucleons. It can be calculated as

$$\begin{aligned} N_{part}(\vec{b}) &= \int T_A(\vec{s}) \left( 1 - \left( 1 - \frac{T_B(\vec{b} - \vec{s})}{B} \sigma_{inel}^{NN} \right)^B \right) \mathrm{d}^2 s + \\ &\quad + \int T_B(\vec{b} - \vec{s}) \left( 1 - \left( 1 - \frac{T_A(\vec{s})}{A} \sigma_{inel}^{NN} \right)^A \right) \mathrm{d}^2 s \\ &= \int T_A(\vec{s}) \frac{\mathrm{d}\sigma^{pB}}{\mathrm{d}^2 s}(\vec{b} - \vec{s}) \mathrm{d}^2 s + \int T_B(\vec{b} - \vec{s}) \frac{\mathrm{d}\sigma^{pA}}{\mathrm{d}^2 s}(\vec{s}) \mathrm{d}^2 s. \end{aligned} \tag{6.9}$$

In principle, $N_{part}$ and $N_{coll}$ are not directly measurable in experiment, and so, one has to use so called centrality classes to characterize the collision. The basic assumption underlying centrality classes is that the impact parameter $b$ is monotonically related to particle multiplicity, both at mid and forward rapidity. For large $b$(peripheral events)low multiplicity at mid-rapidity and large number of spectators at beam rapidity is expected. For small $b$(central events) large multiplicity at mid-rapidity and small number of spectators at beam rapidity is expected.

In the simplest case, one takes a cross-section dependence on $\vec{b}$ and integrates it over the entire range. This corresponds to the minimum bias situation in the experiment and is denoted as the centrality class 100%. Centrality class $k$% corresponds to an impact parameter $b_k$, where the following formula holds

$$\frac{\int_0^{b_k} 2\pi b \mathrm{d}b \frac{\mathrm{d}\sigma}{\mathrm{d}b}}{\int_0^{+\infty} 2\pi b \mathrm{d}b \frac{\mathrm{d}\sigma}{\mathrm{d}b}} = 0.01k. \tag{6.10}$$

Therefore, one can say that a process belongs to the centrality class $(k_1 - k_2)$% when

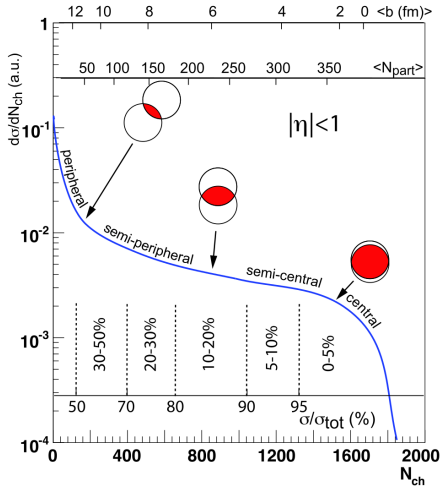


Figure 6.4: Schematic figure published in [90] relating impact parameter $b$ to centrality classes and number of charged particles $N_{ch}$ measured in the final state.

$$\frac{\int_0^{b_{k_2}} 2\pi b \mathrm{d}b \frac{\mathrm{d}\sigma}{\mathrm{d}b} - \int_0^{b_{k_1}} 2\pi b \mathrm{d}b \frac{\mathrm{d}\sigma}{\mathrm{d}b}}{\int_0^{+\infty} 2\pi b \mathrm{d}b \frac{\mathrm{d}\sigma}{\mathrm{d}b}} = \frac{\int_{b_{k_1}}^{b_{k_2}} 2\pi b \mathrm{d}b \frac{\mathrm{d}\sigma}{\mathrm{d}b}}{\int_0^{+\infty} 2\pi b \mathrm{d}b \frac{\mathrm{d}\sigma}{\mathrm{d}b}} = 0.01(k_2 - k_1). \tag{6.11}$$

Since the differential cross-section depends weakly on the energy of the collision, one has to calculate centrality classes for each experiment considered. Following table summarizes mapping between centrality classes and impact parameter for various nuclei and collision energies.

In principle, as a consequence of the factorization the number of inclusive hard processes between point-like constituents of the nucleons in the nucleus-nucleus collision is proportional to the nuclear overlap function $T_{AB}(b)$, since

$$\sigma_{hard}^{AB} = \int \left(1 - \left(1 - \frac{T_{AB}(\vec{b})\sigma_{hard}^{NN}}{AB}\right)^{AB}\right) \mathrm{d}^2 b \sim \int T_{AB}(\vec{b})\sigma_{hard}^{NN} \mathrm{d}^2 b \tag{6.12}$$

The particle yield $N$ for an inclusive hard process with cross-section $\sigma_{hard}^{NN}$ in nucleon-nucleon collisions per interaction of two nuclei $A$ and $B$ with impact parameter $\vec{b}$ is[63, 90]

| | $\sqrt{s}[GeV]$ | 0% | 10% | 20% | 30% | 40% | 50% | 60% | 70% | 80% | 90% | 100% |
|---|---|---|---|---|---|---|---|---|---|---|---|---|
| Cu | 62 | 0 | 3.32 | 4.71 | 5.77 | 6.66 | 7.45 | 8.16 | 8.82 | 9.46 | 10.23 | 12.63 |
| Cu | 200 | 0 | 3.36 | 4.76 | 5.83 | 6.74 | 7.53 | 8.25 | 8.92 | 9.56 | 10.32 | 12.63 |
| Au | 62 | 0 | 4.69 | 6.64 | 8.14 | 9.40 | 10.51 | 11.51 | 12.44 | 13.30 | 14.18 | 19.13 |
| Au | 200 | 0 | 4.72 | 6.69 | 8.19 | 9.46 | 10.58 | 11.59 | 12.52 | 13.39 | 14.27 | 19.13 |
| Pb | 2760 | 0 | 4.94 | 6.99 | 8.57 | 9.90 | 11.07 | 12.12 | 13.10 | 14.00 | 14.90 | 19.85 |
| Pb | 5500 | 0 | 4.96 | 7.03 | 8.61 | 9.95 | 11.12 | 12.19 | 13.16 | 14.07 | 14.98 | 19.85 |

Table 6.2: Impact parameters in $fm$ corresponding to centralities for several nuclei and energies of the collision.

$$N^{AB}_{hard}(\vec{b}) = \frac{\sigma^{AB}_{hard}(\vec{b})}{\sigma^{AB}_{inel}} = \frac{T_{AB}(\vec{b})\sigma^{NN}_{hard}}{\sigma^{AB}_{inel}} = \frac{T_{AB}(\vec{b})\sigma^{NN}_{inel}N^{NN}_{hard}}{\sigma^{AB}_{inel}} \tag{6.13}$$

$$N^{NN}_{hard} = \frac{\sigma^{NN}_{hard}}{\sigma^{NN}_{inel}}. \tag{6.14}$$

Averaging over certain centrality class $k$ one gets

$$\langle T_{AB}\rangle|_k = \frac{\int_0^{b_k} 2\pi b T_{AB}(b)\mathrm{d}b}{\sigma^{AB}_{inel}} \tag{6.15}$$

$$\langle N_{coll}\rangle|_k = \frac{\int_0^{b_k} 2\pi b T_{AB}(b)\mathrm{d}b\,\sigma^{NN}_{inel}}{\sigma^{AB}_{inel}} = \langle T_{AB}\rangle|_k\sigma^{NN}_{inel} \tag{6.16}$$

$$\langle N^{AB}_{hard}\rangle|_k = \frac{\sigma^{AB}_{hard}(b_k)}{\sigma^{AB}_{inel}} = \frac{\int_0^{b_k} 2\pi b T_{AB}(b)\mathrm{d}b\,\sigma^{NN}_{hard}}{\sigma^{AB}_{inel}} \sim \langle N_{coll}\rangle|_k N^{NN}_{hard}. \tag{6.17}$$

If the particle yield is measured as a function of transverse momentum $p_T$, one has to know the $p_T$ dependence of the nucleon-nucleon hard cross-section and so

$$\frac{\mathrm{d}^2N^{AB}_{hard}(\vec{b})}{\mathrm{d}^2p_T} = \frac{\frac{\mathrm{d}^2\sigma^{AB}_{hard}(\vec{b})}{\mathrm{d}^2p_T}}{\sigma^{AB}_{inel}} = \frac{\int T_{AB}(\vec{b})\mathrm{d}^2b\frac{\mathrm{d}^2\sigma^{NN}_{hard}}{\mathrm{d}^2p_T}}{\sigma^{AB}_{inel}} = \frac{\int T_{AB}(\vec{b})\mathrm{d}^2b\sigma^{NN}_{inel}\frac{\mathrm{d}^2N^{NN}_{hard}}{\mathrm{d}^2p_T}}{\sigma^{AB}_{inel}} \tag{6.18}$$

$$\frac{\mathrm{d}^2N^{NN}_{hard}}{\mathrm{d}^2p_T} = \frac{\frac{\mathrm{d}^2\sigma^{NN}_{hard}}{\mathrm{d}^2p_T}}{\sigma^{NN}_{inel}}. \tag{6.19}$$

The invariant multiplicity of produced inclusive hard particles with transverse momentum $p_T$ per inelastic collision of nuclei $A$ and $B$ with impact parameter $b$ is defined as

$$\frac{1}{N_{coll}}\frac{\mathrm{d}^2 N_{hard}^{AB}(\vec{b})}{\mathrm{d}^2 p_T} = \frac{1}{N_{coll}}\frac{\int T_{AB}(\vec{b})\mathrm{d}^2 b \frac{\mathrm{d}^2\sigma_{hard}^{NN}}{\mathrm{d}^2 p_T}}{\sigma_{inel}^{AB}} \tag{6.20}$$

and the nuclear modification factor $R_{AB}$ is defined as

$$R_{AB}(p_T) = \frac{1}{\langle N_{coll}\rangle|_k}\frac{\frac{\mathrm{d}^2 N_{hard}^{AB}}{\mathrm{d}^2 p_T}}{\frac{\mathrm{d}^2 N_{hard}^{NN}}{\mathrm{d}^2 p_T}} = \frac{1}{\langle T_{AB}\rangle|_k}\frac{\frac{\mathrm{d}^2 N_{hard}^{AB}}{\mathrm{d}^2 p_T}}{\frac{\mathrm{d}^2 \sigma_{hard}^{NN}}{\mathrm{d}^2 p_T}} = \frac{1}{\int_0^{b_k} 2\pi b T_{AB}(b)\mathrm{d}b}\frac{\frac{\mathrm{d}^2 \sigma_{hard}^{AB}}{\mathrm{d}^2 p_T}}{\frac{\mathrm{d}^2 \sigma_{hard}^{NN}}{\mathrm{d}^2 p_T}}. \tag{6.21}$$

## 6.2 Long coherence length in heavy-ion collisions

In order to apply the long coherence length limit calculation to the nucleus-nucleus collisions, one has to carefully identify the role of proton-nucleus cross-section in the target rest frame. The condition for the onset of shadowing in this limit is that the coherence length exceeds the nuclear radius $R_A$ as in the case of proton-nucleus collisions. Therefore, the eikonalization of the dipole cross-section can be used to incorporate shadowing effects. Relying on the sketch of the nucleus-nucleus collision in the rest frame of the target

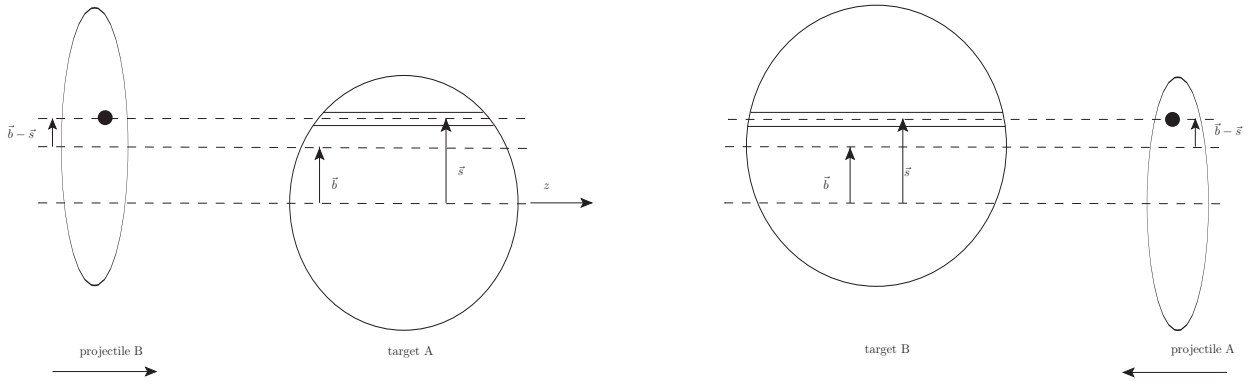


Figure 6.5: A sketch of the nucleus-nucleus collision in the rest frame of one nucleus.

one can see that the situation resembles the nucleon-nucleus collision in the sense that one nucleon from the nucleus $B$ with the impact parameter distribution $T_B(\vec{b}-\vec{s})$ is scattered on the nucleus $A$ at impact parameter $\vec{s}$. Due to the fact that the cross-section has to be symmetric on the interchange of the nuclei, one has to include also the part where the nucleon from the nucleus $A$ with the distribution $T_A(\vec{s})$ is scattered on the nucleus $B$ at impact parameter $\vec{b}-\vec{s}$. Therefore, if the dipole cross-section modification for the nucleon-nucleus collision is denoted as

$$\sigma^A_{q\bar{q}}(\rho, x_2) = 2\int \mathrm{d}^2 s\, \sigma^A_{q\bar{q}}(\vec{s}) \qquad \sigma^A_{q\bar{q}}(\vec{s}) = \left(1 - \left(1 - \frac{1}{2A}\sigma^N_{q\bar{q}}(\rho, x_2) T_A(\vec{s})\right)^A\right), \tag{6.22}$$

one can calculate the cross-section for the real/virtual photon production by changing the dipole cross-section in nucleon-nucleon cross-section with

$$\sigma^N_{q\bar{q}}(\rho, x_2) \to \sigma^{AB}_{q\bar{q}}(\rho, x_2) = \int \mathrm{d}^2 b \mathrm{d}^2 s \left(\sigma^A_{q\bar{q}}(\vec{s}) T_B(\vec{b}-\vec{s}) + \sigma^B_{q\bar{q}}(\vec{b}-\vec{s}) T_A(\vec{s})\right), \tag{6.23}$$

where $T_A$ and $T_B$ are nuclear thickness functions defined in previous section. The correspondence between Glauber calculation in the infinite momentum frame and in the rest

frame of the target can be seen in the Bethe-Heitler limit(see proper section in proton-nucleus collisions chapter), where one can expand both exponentials and the cross-section in nucleus-nucleus collisions is equal to

$$\begin{aligned}
\sigma^{AB}_{q\bar{q}}(\rho,x_2) &= \int \mathrm{d}^2b\mathrm{d}^2s\left(\sigma^A_{q\bar{q}}(\vec{s})T_B(\vec{b}-\vec{s})+\sigma^B_{q\bar{q}}(\vec{b}-\vec{s})T_A(\vec{s})\right)\sim \\
&\sim \int \mathrm{d}^2b\mathrm{d}^2s\left(\frac{1}{2}\sigma^N_{q\bar{q}}(\rho,x_2)T_A(\vec{s})T_B(\vec{b}-\vec{s})+\frac{1}{2}\sigma^N_{q\bar{q}}(\rho,x_2)T_B(\vec{b}-\vec{s})T_A(\vec{s})\right)= \\
&= \int \mathrm{d}^2b\mathrm{d}^2s\sigma^N_{q\bar{q}}(\rho,x_2)T_A(\vec{s})T_B(\vec{b}-\vec{s})= \\
&= \int \mathrm{d}^2b\sigma^N_{q\bar{q}}(\rho,x_2)T_{AB}(\vec{b}). \qquad (6.24)
\end{aligned}$$

Final formula for the photon(dilepton) production cross-section in nucleus-nucleus collisions is then

$$\begin{aligned}
\frac{\mathrm{d}\sigma(AB\to\gamma X)}{\mathrm{d}x_F\mathrm{d}M^2} &= \frac{\mathrm{d}\sigma(\gamma^*\to l^+l^-)}{\mathrm{d}M^2}\frac{x_1}{x_1+x_2}\int\limits_{x_1}^1\frac{\mathrm{d}\alpha}{\alpha^2}\sum_q Z_q^2\left(f_q\left(\frac{x_1}{\alpha},Q^2\right)+f_{\bar{q}}\left(\frac{x_1}{\alpha},Q^2\right)\right)\times \\
&\quad\times\int \mathrm{d}^2b\mathrm{d}^2s\left(\frac{\mathrm{d}\sigma(qA\to\gamma X)}{\mathrm{d}\ln\alpha}(\vec{s})T_B(\vec{b}-\vec{s})+\frac{\mathrm{d}\sigma(qB\to\gamma X)}{\mathrm{d}\ln\alpha}(\vec{b}-\vec{s})T_A(\vec{s})\right) \\
\frac{\mathrm{d}\sigma(qA\to\gamma X)}{\mathrm{d}\ln\alpha}(\vec{s}) &= \int \mathrm{d}^2\rho|\Psi_{q\gamma}(\rho,\alpha)|^2\left(1-\left(1-\frac{1}{2A}\sigma^N_{q\bar{q}}(\alpha\rho,x_2)T_A(\vec{s})\right)^A\right) \qquad (6.25)
\end{aligned}$$

and for the transverse momentum distribution of produced photons(dileptons)

$$\begin{aligned}
\frac{\mathrm{d}\sigma(AB\to\gamma X)}{\mathrm{d}^2p_T\mathrm{d}M^2\mathrm{d}x_F} &= \frac{\mathrm{d}\sigma(\gamma^*\to l^+l^-)}{\mathrm{d}M^2}\frac{x_1}{x_1+x_2}\int\limits_{x_1}^1\frac{\mathrm{d}\alpha}{\alpha^2}\sum_q Z_q^2\left(f_q\left(\frac{x_1}{\alpha},Q^2\right)+f_{\bar{q}}\left(\frac{x_1}{\alpha},Q^2\right)\right)\times \\
&\quad\times\int \mathrm{d}^2b\mathrm{d}^2s\left(\frac{\mathrm{d}\sigma(qA\to\gamma X)}{\mathrm{d}\ln\alpha\mathrm{d}^2p_T}(\vec{s})T_B(\vec{b}-\vec{s})+\frac{\mathrm{d}\sigma(qB\to\gamma X)}{\mathrm{d}\ln\alpha\mathrm{d}^2p_T}(\vec{b}-\vec{s})T_A(\vec{s})\right) \\
\frac{\mathrm{d}\sigma(qA\to\gamma X)}{\mathrm{d}\ln\alpha\mathrm{d}^2p_T}(\vec{s}) &= \frac{1}{(2\pi)^2}\int \mathrm{d}^2\rho_1\int \mathrm{d}^2\rho_2 e^{i\vec{p}_T(\vec{\rho}_1-\vec{\rho}_2)}\Psi^*_{q\gamma}(\rho_1,\alpha)\Psi_{q\gamma}(\rho_2,\alpha)\Sigma^A_{q\bar{q}}(\rho_1,\rho_2,\alpha,x_2,\vec{s}) \\
\Sigma^A_{q\bar{q}}(\rho_1,\rho_2,\alpha,x_2,\vec{s}) &= 1-\left(1-\frac{1}{2A}\sigma^N_{q\bar{q}}(\alpha\rho_1,x_2)T_A(\vec{s})\right)^A-\left(1-\frac{1}{2A}\sigma^N_{q\bar{q}}(\alpha\rho_2,x_2)T_A(\vec{s})\right)^A \\
&\quad+\left(1-\frac{1}{2A}\sigma^N_{q\bar{q}}(\alpha|\vec{\rho}_1-\vec{\rho}_2|,x_2)T_A(\vec{s})\right)^A. \qquad (6.26)
\end{aligned}$$

## 6.3 Short coherence length in heavy-ion collisions

The short coherence length limit of the cross-section calculation in nucleus-nucleus collisions corresponds to the same situation as in proton-nucleus collisions, namely $\langle l_c \rangle \sim 1 - 2fm$. Using the same mechanism as for the long coherence length limit in nucleus-nucleus collisions, one has to account for both parts corresponding to the sketch in the previous section. If the cross-section for the interaction of a quark from the incident nucleon with the nucleus $A$ is taken as

$$\begin{aligned}
\sigma^{qA}(\alpha, p_T) &= \int \mathrm{d}^2 s \sigma^{qA}(\alpha, p_T, \vec{s}) \\
\sigma^{qA}(\alpha, p_T, \vec{s}) &= \int \mathrm{d}^2 k_T \int \mathrm{d}z \rho_A(s,z) \frac{b_0^2}{(2\pi)^2 \pi} \int \mathrm{d}^2 b' \int \mathrm{d}^2 b'' e^{i\vec{k}_T(\vec{b}'-\vec{b}'')} \times \\
&\quad \times e^{-\frac{1}{2}b_0^2(b'^2+b''^2)} e^{-\frac{1}{2}\sigma_{q\bar{q}}^N(\vec{b}'-\vec{b}'', x_q) T_A\left(\frac{\vec{b}'+\vec{b}''}{2}+\vec{s}, z\right)} \sigma^{qN}(\alpha, |\vec{p}_T - \alpha \vec{k}_T|) \quad (6.27)
\end{aligned}$$

then one can write the cross-section for the interaction of a quark from the nucleon inside the nucleus $A$ with nucleus $B$ and vice versa as

$$\begin{aligned}
\sigma^{q(A)B}(\alpha, p_T) &= \int \mathrm{d}^2 b \mathrm{d}^2 s \left( \sigma^{qA}(\alpha, p_T, \vec{s}) T_B(\vec{b}-\vec{s}) + \sigma^{qB}(\alpha, p_T, \vec{b}-\vec{s}) T_A(\vec{s}) \right) \\
\frac{\mathrm{d}\sigma(pA \to \gamma X)}{\mathrm{d}^2 p_T \mathrm{d}x_F \mathrm{d}M^2} &= \frac{\mathrm{d}\sigma(\gamma^* \to l^+ l^-)}{\mathrm{d}M^2} \frac{1}{x_1 + x_2} \int_{x_1}^{1} \frac{\mathrm{d}\alpha}{\alpha} F_2^p \left( \frac{x_1}{\alpha}, Q^2 \right) \sigma^{q(A)B}(\alpha, p_T). \quad (6.28)
\end{aligned}$$

The procedure for simplifying the calculation as written in the chapter for proton-nucleus collisions can be used on each part separately having

$$\begin{aligned}
\sigma^{q(A)B}(\alpha, p_T) &= \frac{1}{(2\pi)^2} \int \mathrm{d}^2 b T_{AB}(\vec{b}) \times \\
&\times \left( \int \mathrm{d}^2 k_T \int \mathrm{d}^2 r_T e^{i\vec{k}_T \cdot \vec{r}_T} e^{-\frac{1}{4}b_0^2 r_T^2} e^{-\frac{1}{4}\sigma_{q\bar{q}}^N(r_T, x_q)\langle T_A \rangle} \sigma^{qN}(\alpha, |\vec{p}_T - \alpha \vec{k}_T|) \right. \\
&+ \left. \int \mathrm{d}^2 k_T \int \mathrm{d}^2 r_T e^{i\vec{k}_T \cdot \vec{r}_T} e^{-\frac{1}{4}b_0^2 r_T^2} e^{-\frac{1}{4}\sigma_{q\bar{q}}^N(r_T, x_q)\langle T_B \rangle} \sigma^{qN}(\alpha, |\vec{p}_T - \alpha \vec{k}_T|) \right) = \\
&= \frac{1}{(2\pi)^2} \int \mathrm{d}^2 b T_{AB}(\vec{b}) \int \mathrm{d}^2 k_T \int \mathrm{d}^2 r_T e^{i\vec{k}_T \cdot \vec{r}_T} e^{-\frac{1}{4}b_0^2 r_T^2} \left( e^{-\frac{1}{4}\sigma_{q\bar{q}}^N(r_T, x_q)\langle T_A \rangle} + \right. \\
&+ \left. e^{-\frac{1}{4}\sigma_{q\bar{q}}^N(r_T, x_q)\langle T_B \rangle} \right) \sigma^{qN}(\alpha, |\vec{p}_T - \alpha \vec{k}_T|). \quad (6.29)
\end{aligned}$$

The final formula can be, therefore, written as

$$\begin{aligned}
\sigma^{q(A)B}(\alpha, p_T) &= \frac{1}{2\pi}\int \mathrm{d}^2 b T_{AB}(\vec{b}\,)\int k_T \mathrm{d}k_T \int \mathrm{d}\varphi \int \mathrm{d}r_T J_0(k_T r_T) e^{-\frac{1}{4}b_0^2 r_T^2}\Bigg(e^{-\frac{1}{4}\sigma_{q\bar{q}}^N(r_T,x_q)\langle T_A\rangle} + \\
&+ e^{-\frac{1}{4}\sigma_{q\bar{q}}^N(r_T,x_q)\langle T_B\rangle}\Bigg)\sigma^{qN}\left(\alpha, \sqrt{p_T^2+\alpha^2 k_T^2 - 2\alpha k_T p_T \cos\varphi}\right) \\
\frac{\mathrm{d}\sigma(AB\to\gamma X)}{\mathrm{d}^2 p_T \mathrm{d}x_F \mathrm{d}M^2} &= \frac{\mathrm{d}\sigma(\gamma^*\to l^+l^-)}{\mathrm{d}M^2}\frac{1}{x_1+x_2}\int\limits_{x_1}^{1}\frac{\mathrm{d}\alpha}{\alpha}F_2^p\left(\frac{x_1}{\alpha}, Q^2\right)\sigma^{q(A)B}(\alpha, p_T), \qquad (6.30)
\end{aligned}$$

where again $\sigma^{qp}$ can be calculated from the color dipole approach.
The cross-section formula is not normalized to one nucleon as in the case of proton-nucleus collisions formula, and so, the proper formula for the nuclear modification factor is

$$R_{AB}(p_T) = \frac{\frac{\mathrm{d}^2\sigma(AB\to\gamma X)}{\mathrm{d}^2 p_T}}{\int\limits_{centr.}\mathrm{d}^2 b T_{AB}(\vec{b}\,)\frac{\mathrm{d}^2\sigma(pp\to\gamma X)}{\mathrm{d}^2 p_T}}. \qquad (6.31)$$

## 6.4 Gluon shadowing in heavy-ion collisions

The gluon shadowing in proton-nucleus collisions corresponds to multiple interactions of higher Fock states containing gluons in the projectile proton. In nucleus-nucleus collisions the situation is similar in the sense that nucleons from the projectile nucleus propagate through the target nucleus(having it's higher components shadowed) as well as nucleons from target nucleus propagate through the projectile nucleus. In other words, the lifetime of the gluonic fluctuation produced by a nucleon in the nucleus $A$ may be sufficiently long only relative to the nucleus $B$ and vice versa. Therefore, no gluonic fluctuations undergo double color filtering[31]. In terms of the inelastic shadowing it means that the diffractive excitation of the nucleons of $A$ propagate through the $B$ independently of the excitations of $B$ propagating through $A$. That is why one can take a factorized form of the gluonic shadowing ratio $R_g^{AB}$ as [76]

$$R_g^{AB}(\vec{b},\vec{s},x_1,x_2) = R_g^A(\vec{s},x_1)R_g^B(\vec{b}-\vec{s},x_2). \tag{6.32}$$

The meaning of variables is shown at figure in Glauber model section.

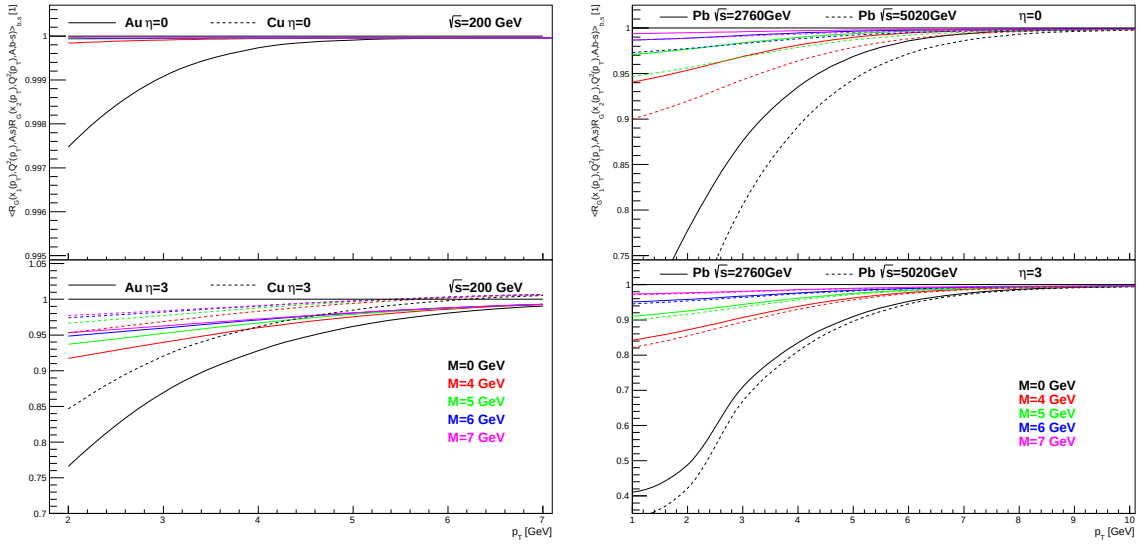


Figure 6.6: The gluon shadowing correction for the kinematic range accessible at the RHIC(left) and LHC(right) accelerators for mid and forward rapidity and various nuclei. The figure corresponds to mean value of $R_G^{AB}$ vs. $p_T$

.

# Chapter 7

# Summary

In this work, coherence effects in the production of direct photons and Drell-Yan lepton pairs in collisions on proton and nuclear targets are studied in the rest frame of the target using the color dipole approach. The production process in the rest frame of the target looks like a bremsstrahlung of virtual or real photon from the incoming quark. The virtual photon decays later to a dilepton. In the color dipole approach, the incoming quark is decomposed into a superposition of Fock states, where the lowest non-trivial state is $|q\gamma\rangle$ fluctuation. Each Fock state scatter with different amplitudes off the target disrupting the coherence between Fock states and releasing the photon. The corresponding production cross-section in the proton-proton collisions can be written using the dipole cross-section and light-cone wave-function representing the probability to develop the $|q\gamma\rangle$ fluctuation. It was demonstrated that the color dipole model needs only one free parameter - effective mass of the quark $m_q = 200MeV$. Published results of calculations for dilepton and photon production in proton-proton collisions are in a good agreement with available data in a wide energy range from the fixed target E772 up to collider RHIC experiments.
The rest frame of the target is also very convenient for description of coherence effects. Most prominent manifestation of coherence effects at high energies is the nuclear shadowing. In photon production this shadowing is caused by multiple scatterings of the $|q\gamma\rangle$ fluctuation inside the nucleus controlled by the time scale(length) called the coherence length. If the coherence length exceeds the nuclear radius, the shadowing in photon production is due to the Landau-Pomeranchuk-Migdal suppression of bremsstrahlung. The quark shadowing is calculated in the limit of long coherence length within the Glauber-Gribov eikonal model. As expected, the magnitude of the quark shadowing is maximal in the long coherence length limit and vanishes, when nucleons participate incoherently to the bremsstrahlung. In the latter case, the production cross-section can be calculated using quark scattering matrix.
Gluon shadowing is a leading twist correction to coherence effects. It corresponds to the shadowing of higher Fock components containing one or more gluons. The calculation of the gluon shadowing correction is performed within the same color dipole approach using the Green functions formalism. According to equation 4.7, higher Fock components containing

gluons are heavier and have a shorter coherence time than the lower state $|q\gamma\rangle$. Consequently, gluon shadowing dominates at higher energies, i.e. at small values of Bjorken $x \leq 0.01$.
Besides coherence effects, an unified approach to large $x_F(x_T)$ nuclear suppression based on restrictions coming from the energy conservation near kinematic limit in multiple initial state interactions inside the nucleus is presented. As a result, this leads to nuclear modification of quark distribution functions of the incoming proton in contrast with the QCD factorization. This mechanism is applicable to any process at any energy and causes a suppression in kinematic regions where no coherence effects are possible.
In the calculation also izospin effects are included. They lead to the attenuation of the cross-section for deuteron-nucleus or nucleus-nucleus collisions.
First, the significant suppression at large $x_F$ in a good agreement with the data for Drell-Yan process from E772 and E866 experiments at FNAL was predicted. The FNAL energy range and large invariant masses of the dileptons allow to minimize the effects of coherence. Consequently, the observed large-$x_F$ suppression is a manifestation of net ISI effects. Predictions for the large-$x_F$ suppression can be further verified by new experiment E906 at FNAL. A strong large-$x_F$ suppression induced by ISI effects can be seen also in the RHIC energy range. Nuclear effects for the second class of processes - production of direct photons off nuclei - are calculated. In comparison with the Drell-Yan production processes with direct photons have much longer coherence length leading to much stronger manifestation of coherence effects. Published results for d+Au collisions are consistent with PHENIX data at midrapidity. Besides coherence effects, a strong rise of ISI effects at forward rapidities is demonstrated. Predicted large $p_T$ suppression is in contrast with the fact that nuclear effects are not expected at large $p_T$, since photons have no final state interactions. At small Bjorken $x$, the importance of gluon shadowing was shown leading to the additional suppression. Production of direct photons was studied also in heavy ion collisions. An unexpected strong suppression of large-$p_T$ photons at midrapidity indicated by the PHENIX experiment in most central collisions is presented to be a manifestation of ISI effects. Predictions for strong suppression can be tested by the future data at LHC at different rapidities. Here a mixing of coherence and ISI effects is expected. Further tests of the calculation can be done in the future by the considered forward calorimeter detector upgrade(FOCAL) of ALICE experiment or by newly planed fixed target experiment AFTER at LHC.

# Appendices

# Appendix A

# Light-cone kinematics

Some features of light-cone kinematics are reviewed here. Parametrization used here follow Lepage-Brodsky convention[91, 92].

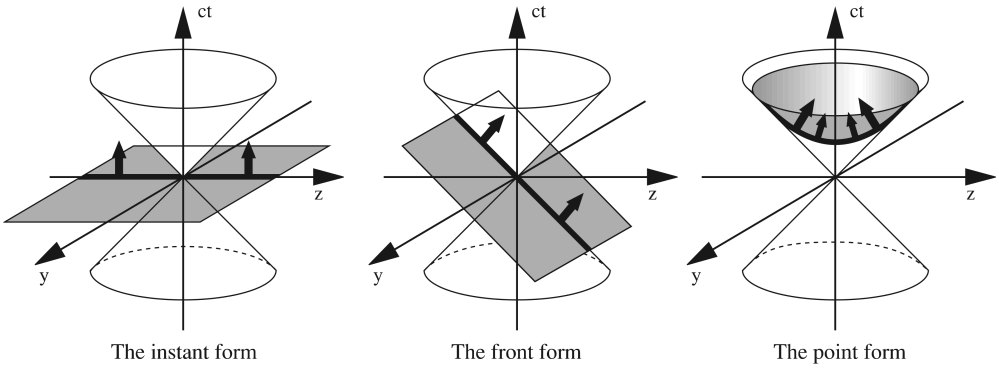


Figure 1: Three different forms of parametrizations used for the spacetime description - instant form, light-cone(or light-front) form and point form. Figure is taken from [37].

Let's review the instant form first. The contravariant four-vector of position $x^\mu$ is

$$x^\mu = (x^0, x^1, x^2, x^3) = (ct, x, y, z).$$

The metric tensor is given by

$$g^{\mu\nu} = \begin{pmatrix} 1 & 0 & 0 & 0 \\ 0 & -1 & 0 & 0 \\ 0 & 0 & -1 & 0 \\ 0 & 0 & 0 & -1 \end{pmatrix}.$$

Scalar product has a form

$$x \cdot y = x^0 y_0 + x^1 y_1 + x^2 y_2 + x^3 y_3 = x^0 y^0 - x^1 y^1 - x^2 y^2 - x^3 y^3 = x^0 y^0 - \vec{x} \cdot \vec{y}.$$

The four-momentum $p^\mu = (p^0, p^1, p^2, p^3) = (E, \vec{p}c)$ couples to position four-vector as

$$x \cdot p = (Et - \vec{x} \cdot \vec{p})c.$$

A boost to the speed $v$ in the direction of $x^3$ is given by Lorentz transformations

$$\begin{aligned}
\gamma &= \frac{1}{\sqrt{1-\frac{v^2}{c^2}}} \\
x'^0 &= (x^0 + \frac{v}{c}x^3)\gamma \\
x'^1 &= x^1 \\
x'^2 &= x^2 \\
x'^3 &= (x^3 + \frac{v}{c}x^0)\gamma.
\end{aligned}$$

Light-cone coordinates can be defined as

$$\begin{aligned}
x^+ &= x^0 + x^3 \\
x^- &= x^0 - x^3 \\
\vec{x}^T &= (x^1, x^2),
\end{aligned}$$

where $(x^0, x^1, x^2, x^3)$ are coordinates in the instant form. The covariant vectors $x_\mu = (x_+, x_-, \vec{x}_T)$ are obtained from contravariant ones $x^\mu = (x^+, x^-, \vec{x}^T)$ using metric tensor

$$g^{\mu\nu} = \begin{pmatrix} 0 & 0 & 0 & 2 \\ 0 & -1 & 0 & 0 \\ 0 & 0 & -1 & 0 \\ 2 & 0 & 0 & 0 \end{pmatrix}.$$

Scalar product is defined as

$$x \cdot y = \frac{1}{2}(x^+ y_+ + x^- y_-) + \vec{x}^T \vec{y}_T = \frac{1}{2}(x^+ y^- + x^- y^+) - \vec{x}^T \cdot \vec{y}^T.$$

The four-momentum vector $p^\mu = (p^-, p^+, \vec{p}^T)$ couples to position four-vectors as

$$x \cdot p = \frac{1}{2}(x^+ p^- + x^- p^+) - \vec{x}^T \cdot \vec{p}^T.$$

The interpretation of $x^\pm$ is generally a matter of convention. It is usually prefered to take $x^+$ as light-cone time and $x^-$ as light-cone spatial coordinate.
A boost in the $x^3$ direction is given by formulas

$$\begin{aligned}
x'^+ &= x^+ e^\psi \\
x'^- &= x^- e^{-\psi} \\
\vec{x}'^T &= \vec{x}^T \\
\psi &= \frac{1}{2}\ln\frac{1+v}{1-v}.
\end{aligned}$$

If the particle is moving in the $x^3$ direction with velocity $v$, the definition of variables can be re-written to

$$\begin{aligned} x^- &= (1-v)t \\ & \qquad \Rightarrow \quad x^- = \tfrac{1-v}{1+v}x^+ \\ x^+ &= (1+v)t \end{aligned}$$

and one can identify a light-cone velocity as

$$\frac{\mathrm{d}x^-}{\mathrm{d}x^+} = \frac{1-v}{1+v}.$$

In the case of four-momentum vector it is not straightforward to identify the meaning of $p^+$ and $p^-$. Usual assumption is to identify the light-cone energy as $p^-$ and light-cone momentum as $p^+$, since $p^-$ couples to light-cone time in the scalar product

$$x \cdot p = \frac{1}{2}(x^- p^+ + x^+ p^-) - \vec{x}^T \cdot \vec{p}^T.$$

Moreover, if one consider a particle moving in the direction $x^3$, the light-cone velocity $\frac{\mathrm{d}x^-}{\mathrm{d}x^+}$ is small and so shall be the light-cone energy. Since

$$p^\pm = p^0 \pm p^3 \qquad p^0 = \sqrt{(p^3)^2 + m^2 + (p^T)^2} \sim p^3 \left(1 + \frac{m^2 + (p^T)^2}{2(p^3)^2}\right),$$

and so,

$$p^+ = 2p^3 \qquad p^- = \frac{m^2 + (p^T)^2}{2p^3}.$$

Therefore $p^-$ is small in contrast to $p^+$, which is large.
If the definition of rapidity is used

$$y = \frac{1}{2}\ln\frac{p^+}{p^-} = \frac{1}{2}\ln\frac{E+p^3}{E-p^3} = \frac{1}{2}\ln\frac{1+v}{1-v},$$

one can write

$$p^+ = \sqrt{m^2 + (p^T)^2}e^y \qquad p^- = \sqrt{m^2 + (p^T)^2}e^{-y}.$$

# Appendix B

## Formula for the cross-section in proton-proton collisions

A sketch of detailed derivation of the formula for the photon production and the Drell-Yan process cross-section in the rest frame of the target via a color dipole approach is presented here. The formula was derived at [4] but here the covariant Feynman perturbation framework is used as was presented in [3]. In perturbation theory, two Feynman diagrams correspond to the dilepton/photon production in the target rest frame.

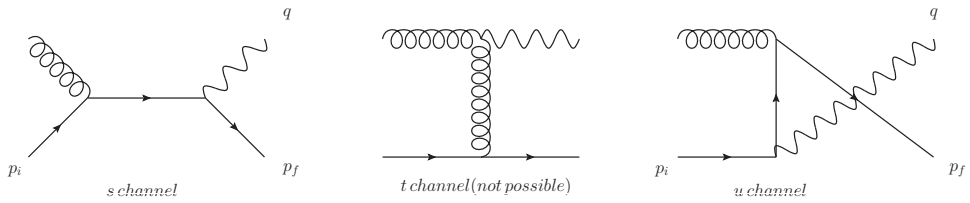


Figure 2: Possible Feynman diagrams contributing to the bremsstrahlung cross-section. Since bremsstrahlung is a scattering on static potential rather than two-particle scattering, the gluon is depicted only to remind that the interaction is strong.

Therefore, the cross-section formula is

$$\begin{aligned} \mathrm{d}\sigma(qp \to \gamma X \to l^+l^- X) &= \sum_{\lambda\lambda' X} \varepsilon^*_\mu(\lambda)\varepsilon_\nu(\lambda')\overline{\mathfrak{M}}^{\mu\nu} \frac{\mathrm{d}\alpha \mathrm{d}^2 p_f^T \mathrm{d}^2 q_T}{8(2\pi)^5 (p_i^0)^2 \alpha(1-\alpha)} \times \\ &\times \alpha_{em}\varepsilon_\kappa(\lambda)\varepsilon^*_\rho(\lambda') L^{\kappa\rho} \frac{\mathrm{d}^2 M \mathrm{d}\Omega}{16\pi^2 M^4}, \end{aligned}$$

where the first part corresponds to the production of a photon with mass $q^2 = M^2$ from the quark with four-momentum $p_i$ leaving the quark in the final state with four-momentum $p_f$ and the second part describes potential decay of this photon (if $M^2 > 0$) into a dilepton to the angle $\mathrm{d}\Omega$. The sum runs over all final states $X$ and over all polarizations $\lambda, \lambda' \in \{-1, 0, 1\}$ and the energy-momentum conservation law is presumed in the calculation. The first part of the formula can be obtained from the well known quantum field theory formula for the cross-section

$$\begin{aligned} \mathrm{d}\sigma(qp \to \gamma X) &= \sum_{\lambda\lambda' X} \frac{1}{|\vec{v}_i|} \frac{1}{2p_i^0} \varepsilon^*_\mu(\lambda)\varepsilon_\nu(\lambda')\overline{\mathfrak{M}}^{\mu\nu} \frac{\mathrm{d}^3 p_f \mathrm{d}^3 q}{(2\pi)^3 2p_f^0 (2\pi)^3 2q^0} 2\pi\delta(p_f^0 + q^0 - p_i^0) \\ &= \sum_{\lambda\lambda' X} \frac{1}{|\vec{v}_i|} \varepsilon^*_\mu(\lambda)\varepsilon_\nu(\lambda')\overline{\mathfrak{M}}^{\mu\nu} \frac{\mathrm{d}^3 p_f \mathrm{d}^3 q}{8(2\pi)^5 p_f^0 q^0 p_i^0} \delta(p_f^0 + q^0 - p_i^0) \end{aligned}$$

Since only longitudinal part of the momenta is considered in the Feynman model and one can neglect the mass of the quark, so $|p_f^0| = |p_f^L|$ and $|p_i^0| = |p_i^L|$, therefore,

$$\mathrm{d}^3 p_f = \mathrm{d}p_f^L \mathrm{d}^2 p_f^T = \mathrm{d}p_f^0 \mathrm{d}^2 p_f^T \qquad |\vec{v}_i| = \frac{p_i^0}{p_i^L} = 1$$

and the integral over the delta function can be performed

$$\begin{aligned}
\mathrm{d}\sigma(qp \to \gamma X) &= \sum_{\lambda\lambda' X} \frac{1}{|\vec{v}_i|} \varepsilon_\mu^*(\lambda)\varepsilon_\nu(\lambda')\overline{\mathfrak{M}}^{\mu\nu} \frac{\mathrm{d}^3 p_f \mathrm{d}^3 q}{8(2\pi)^5 p_f^0 q^0 p_i^0} \delta(p_f^0 + q^0 - p_i^0) = \\
&= \sum_{\lambda\lambda' X} \varepsilon_\mu^*(\lambda)\varepsilon_\nu(\lambda')\overline{\mathfrak{M}}^{\mu\nu} \frac{\mathrm{d}^2 p_f^T \mathrm{d}q^0 \mathrm{d}^2 q_T}{8(2\pi)^5 (p_i^0 - q^0) q^0 p_i^0} = \\
&= \sum_{\lambda\lambda' X} \varepsilon_\mu^*(\lambda)\varepsilon_\nu(\lambda')\overline{\mathfrak{M}}^{\mu\nu} \frac{\mathrm{d}^2 p_f^T \mathrm{d}\alpha \mathrm{d}^2 q_T}{8(2\pi)^5 (p_i^0 - q^0) q^0} = \\
&= \sum_{\lambda\lambda' X} \varepsilon_\mu^*(\lambda)\varepsilon_\nu(\lambda')\overline{\mathfrak{M}}^{\mu\nu} \frac{\mathrm{d}^2 p_f^T \mathrm{d}\alpha \mathrm{d}^2 q_T}{8(2\pi)^5 (1-\alpha)\alpha (p_i^0)^2},
\end{aligned}$$

where $\alpha = \frac{q^0}{p_i^0}$. The decay part can be derived from standard photon to 2-fermion decay cross-section(see e.g. [21]).
The scattering amplitude is averaged over initial quarks(helicity $\sigma_i$ and color $c_i$) and summed over final quarks($\sigma_f$ and $c_f$)

$$\overline{\mathfrak{M}}^{\mu\nu} = \frac{1}{2}\frac{1}{N_c} \sum_{\sigma_i c_i} \sum_{\sigma_f c_f} (\mathfrak{M}_s + \mathfrak{M}_u)^2,$$

where $\mathfrak{M}_s$ and $\mathfrak{M}_u$ are contributions from $s$ channel and $u$ channel(see figure above) and $N_c = 3$ is the number of colors. The $t$ channel does not contribute since the gluon cannot radiate electromagnetic bremsstrahlung. The lepton tensor summed over helicities is given as

$$L^{\mu\nu} = 4(p_{l^+}^\mu p_{l^-}^\nu + p_{l^+}^\nu p_{l^-}^\mu - g^{\mu\nu} p_{l^+} p_{l^-}).$$

Now, the integration over the dilepton scattering angle $\mathrm{d}\Omega = \mathrm{d}\phi \mathrm{d}\cos\theta = \sin\theta \mathrm{d}\theta \mathrm{d}\phi$ and over remaining final quark phase space can be performed

$$\begin{aligned}
\mathrm{d}\sigma(qp \to l^+ l^- X) &= \int \mathrm{d}^2 p_f^T \sum_{\lambda\lambda' X} \varepsilon_\mu^*(\lambda)\varepsilon_\nu(\lambda')\overline{\mathfrak{M}}^{\mu\nu} \frac{\mathrm{d}\alpha \mathrm{d}^2 q_T}{8(2\pi)^5 (1-\alpha)\alpha (p_i^0)^2} \\
&\times \int \mathrm{d}\Omega \alpha_{em} \varepsilon_\kappa(\lambda) \varepsilon_\rho^*(\lambda') L^{\kappa\rho} \frac{\mathrm{d}^2 M}{16\pi^2 M^4}
\end{aligned}$$

and using the fact that $\mathrm{d}\ln\alpha = \frac{\mathrm{d}\alpha}{\alpha}$ one gets

$$\begin{aligned}\mathrm{d}\sigma(qp\to l^+l^-X) &= \int \mathrm{d}^2p_f^T \sum_{\lambda X} \varepsilon^*_\mu(\lambda)\varepsilon_\nu(\lambda)\overline{\mathfrak{M}}^{\mu\nu}\frac{\mathrm{d}\ln\alpha\mathrm{d}^2q_T}{8(2\pi)^5(1-\alpha)(p_i^0)^2}\\ &\times \int \mathrm{d}\cos\theta\alpha_{em}\varepsilon_\kappa(\lambda)\varepsilon^*_\rho(\lambda)L^{\kappa\rho}\frac{\mathrm{d}^2M}{8\pi M^4}.\end{aligned}$$

The decay part of the cross-section can be now calculated using standard approach, e.g. from [21] to be independent on polarization

$$\mathrm{d}\sigma(qp\to l^+l^-X) = \int \mathrm{d}^2p_f^T \sum_{\lambda X} \varepsilon^*_\mu(\lambda)\varepsilon_\nu(\lambda)\overline{\mathfrak{M}}^{\mu\nu}\frac{\mathrm{d}\ln\alpha\mathrm{d}^2q_T}{8(2\pi)^5(1-\alpha)(p_i^0)^2}\frac{\alpha_{em}\mathrm{d}^2M}{3\pi M^2}.$$

Therefore, one can write

$$\begin{aligned}\frac{\mathrm{d}\sigma(qp\to l^+l^-X)}{\mathrm{d}\ln\alpha\mathrm{d}^2q_T\mathrm{d}^2M} &= \frac{\alpha_{em}}{3\pi M^2}\Big[\int \mathrm{d}^2p_f^T \sum_{\lambda\in\{\pm1\}X} \varepsilon^*_\mu(\lambda)\varepsilon_\nu(\lambda)\overline{\mathfrak{M}}^{\mu\nu}\frac{1}{8(2\pi)^5(1-\alpha)(p_i^0)^2}\\ &+ \int \mathrm{d}^2p_f^T \sum_{X} \varepsilon^*_\mu(0)\varepsilon_\nu(0)\overline{\mathfrak{M}}^{\mu\nu}\frac{1}{8(2\pi)^5(1-\alpha)(p_i^0)^2}\Big] =\\ &= \frac{\alpha_{em}}{3\pi M^2}\left[\frac{\mathrm{d}\sigma_T(qp\to l^+l^-X)}{\mathrm{d}\ln\alpha\mathrm{d}^2q_T} + \frac{\mathrm{d}\sigma_L(qp\to l^+l^-X)}{\mathrm{d}\ln\alpha\mathrm{d}^2q_T}\right],\end{aligned}$$

where parts corresponding to transversal and longitudinal photons are separated.
Now, the scattering amplitude for the $s$ channel can be expressed using the propagator of the quark in the intermediate state

$$\frac{\not{p}_f + \not{q} + m_q}{(p_f+q)^2 - m_q^2} = \sum_\sigma \frac{u_\sigma(p_f+q)\bar{u}_\sigma(p_f+q)}{(p_f+q)^2-m_q^2} - \frac{\gamma^+}{2(p_f^+ + q^+)},$$

where the sum runs over helicities of the state described by Dirac spinor $u_\sigma$ and the last term comes from the fact that the quark is off-shell. This term can be neglected in the high-energy approximation, which allows to write the scattering amplitude as

$$i\mathfrak{M}_s^\mu = e\sum_\sigma \frac{\bar{u}_\sigma(p_f)\gamma^\mu u_\sigma(p_f+q)}{(p_f+q)^2-m_q^2} t_{q,\sigma,\sigma_i}((p_f^0+q^0),\vec{k}_T),$$

where

$$t_{q,\sigma,\sigma_i}((p_f^0+q^0),\vec{k}_T) = \bar{u}_\sigma(p_f+q)\gamma^0 V_q(\vec{k}_T)u_{\sigma_i}(p_i) \sim 2p_i^0\delta_{\sigma\sigma_i}V_q(\vec{k}_T)$$

is the scattering amplitude of the quark on a nucleon in the rest frame of the nucleon and the matrix in the color space $V_q(\vec{k}_T)$ describes the interaction of the nucleon with incident quark with exchanged transverse momentum $\vec{k}_T = \vec{p}_f^{\,T} + \vec{q}_T - \vec{p}_i^{\,T}$. The same amplitude transformed into the impact parameter space is given by the Fourier transformation(neglecting the quark charge $e$)

$$\begin{aligned}
\mathfrak{M}_s^\mu(\vec{b},\vec{\rho}) &= \int \frac{\mathrm{d}^2 l_T \mathrm{d}^2 k_T}{(2\pi)^4} e^{-i\vec{l}_T\alpha\vec{\rho}} e^{-i\vec{k}_T\vec{b}} \mathfrak{M}_s^\mu = \\
&= \int \frac{\mathrm{d}^2 l_T \mathrm{d}^2 k_T}{(2\pi)^4} e^{-i\vec{l}_T\alpha\vec{\rho}} e^{-i\vec{k}_T\vec{b}} \frac{\bar{u}_{\sigma_f}(p_f)\gamma^\mu u_{\sigma_i}(p_f+q)}{(p_f+q)^2 - m_q^2} 2p_i^0 V_q(\vec{k}_T) = \\
&= \int \frac{\mathrm{d}^2 l_T}{(2\pi)^2} e^{-i\vec{l}_T\alpha\vec{\rho}} \frac{\bar{u}_{\sigma_f}(p_f)\gamma^\mu u_{\sigma_i}(p_f+q)}{(p_f+q)^2 - m_q^2} 2p_i^0 \tilde{V}_q(\vec{b}) = \\
&= -i\sqrt{4\pi}\frac{\sqrt{1-\alpha}}{\alpha^2} \Psi_{\gamma q}^\mu(\alpha,\vec{\rho}) 2p_i^0 \tilde{V}_q(\vec{b}),
\end{aligned}$$

where

$$\begin{aligned}
\vec{l}_T &= \vec{p}_f^{\,T} - \frac{1-\alpha}{\alpha}\vec{q}_T \\
\tilde{V}_q(\vec{b}) &= \frac{1}{(2\pi)^2}\int \mathrm{d}^2 k_T e^{-\vec{k}_T\vec{b}} V_q(\vec{k}_T) \\
\Psi_{\gamma q}^\mu(\alpha,\vec{\rho}) &= \alpha^3\sqrt{1-\alpha}\int \frac{\mathrm{d}^2 l_T}{(2\pi^2)} e^{-i\vec{l}_T\alpha\vec{\rho}} \sqrt{\alpha_{em}} \frac{\bar{u}_{\sigma_f}(p_f)\gamma^\mu u_{\sigma_i}(p_f+q)}{\alpha^2 l_T^2 + (1-\alpha)M^2 + \alpha^2 m_q^2}.
\end{aligned}$$

The $u$ channel can be treated in similar way, but the quark scattering amplitude will be shifted in the impact parameter space

$$\mathfrak{M}_u^\mu(\vec{b},\vec{\rho}) = -i\sqrt{4\pi}\frac{\sqrt{1-\alpha}}{\alpha^2}\Psi_{\gamma q}^\mu(\alpha,\vec{\rho}) 2p_i^0 \tilde{V}_q(\vec{b}+\alpha\vec{\rho}).$$

Putting all formulas together one has

$$\begin{aligned}\frac{\mathrm{d}\sigma(qp\to l^+l^-X)}{\mathrm{d}\ln\alpha\mathrm{d}^2q_T\mathrm{d}^2M} &= \frac{\alpha_{em}}{3\pi M^2}\int\mathrm{d}^2p_f^T\frac{1}{(2\pi)^4}\int\mathrm{d}^2b_1\int\mathrm{d}^2b_2\int\mathrm{d}^2\rho_1\int\mathrm{d}^2\rho_2 e^{i\vec{l}_T\alpha(\vec{\rho}_1-\vec{\rho}_2)+i\vec{k}_T(\vec{b}_1-\vec{b}_2)}\times\\ &\times\left(\sum_{\lambda\in\{\pm1\}}\frac{1}{2}\sum_{\sigma_f\sigma_i}\varepsilon^*_\mu(\lambda)\Psi^\mu_{\gamma q}(\alpha,\vec{\rho}_1)\varepsilon_\nu(\lambda)\Psi^{\mu*}_{\gamma q}(\alpha,\vec{\rho}_2)+\right.\\ &+\left.\frac{1}{2}\sum_{\sigma_f\sigma_i}\varepsilon^*_\mu(0)\Psi^\mu_{\gamma q}(\alpha,\vec{\rho}_1)\varepsilon_\nu(0)\Psi^{\mu*}_{\gamma q}(\alpha,\vec{\rho}_2)\right)\times\\ &\times\sum_X\frac{1}{N_c}\sum_{c_fc_i}(\tilde{V}_q(\vec{b}_1)-\tilde{V}_q(\vec{b}_1+\alpha\vec{\rho}_1))(\tilde{V}^\dagger_q(\vec{b}_2)-\tilde{V}^\dagger_q(\vec{b}_2+\alpha\vec{\rho}_2)).\end{aligned}$$

The contraction of LC wave functions with polarization vectors can be calculated [4] as

$$\begin{aligned}\Psi^T_{\gamma q}(\alpha,\vec{\rho}_1)\Psi^T_{\gamma q}(\alpha,\vec{\rho}_2) &= \sum_{\lambda\in\{\pm1\}}\frac{1}{2}\sum_{\sigma_f\sigma_i}\varepsilon^*_\mu(\lambda)\Psi^\mu_{\gamma q}(\alpha,\vec{\rho}_1)\varepsilon_\nu(\lambda)\Psi^{\mu*}_{\gamma q}(\alpha,\vec{\rho}_2)\\ \Psi^L_{\gamma q}(\alpha,\vec{\rho}_1)\Psi^L_{\gamma q}(\alpha,\vec{\rho}_2) &= \frac{1}{2}\sum_{\sigma_f\sigma_i}\varepsilon^*_\mu(0)\Psi^\mu_{\gamma q}(\alpha,\vec{\rho}_1)\varepsilon_\nu(0)\Psi^{\mu*}_{\gamma q}(\alpha,\vec{\rho}_2)\end{aligned}$$

having

$$\begin{aligned}\frac{\mathrm{d}\sigma(qp\to l^+l^-X)}{\mathrm{d}\ln\alpha\mathrm{d}^2q_T\mathrm{d}^2M} &= \frac{\alpha_{em}}{3\pi M^2}\int\mathrm{d}^2p_f^T\frac{1}{(2\pi)^4}\int\mathrm{d}^2b_1\int\mathrm{d}^2b_2\int\mathrm{d}^2\rho_1\int\mathrm{d}^2\rho_2 e^{i\vec{l}_T\alpha(\vec{\rho}_1-\vec{\rho}_2)+i\vec{k}_T(\vec{b}_1-\vec{b}_2)}\\ &\times\Psi^*_{\gamma q}(\alpha,\vec{\rho}_1)\Psi_{\gamma q}(\alpha,\vec{\rho}_2)\sum_X\frac{1}{N_c}\sum_{c_fc_i}(\tilde{V}_q(\vec{b}_1)-\tilde{V}_q(\vec{b}_1+\alpha\vec{\rho}_1))(\tilde{V}^\dagger_q(\vec{b}_2)-\tilde{V}^\dagger_q(\vec{b}_2+\alpha\vec{\rho}_2)).\end{aligned}$$

The dipole cross-section is defined as

$$\sigma^N_{\bar{q}q}(\alpha\rho)=\sum_X\frac{1}{N_c}\sum_{c_fc_i}\int\mathrm{d}^2b\left|\tilde{V}_q(\vec{b})-\tilde{V}_q(\vec{b}+\alpha\vec{\rho})\right|^2$$

and one can obtain the final formula by performing the integration over $\vec{p}_f^T$. Since the integrand is real, it can be symmetrized with respect to $\vec{\rho}_1$ and $\vec{\rho}_2$ to have

$$\begin{aligned}\frac{\mathrm{d}\sigma(qp\to l^+l^-X)}{\mathrm{d}\ln\alpha\mathrm{d}^2q_T\mathrm{d}^2M} &= \frac{\alpha_{em}}{3\pi M^2}\frac{1}{(2\pi)^2}\int\mathrm{d}^2\rho_1\int\mathrm{d}^2\rho_2 e^{i\vec{q}_T(\vec{\rho}_1-\vec{\rho}_2)}\Psi^*_{\gamma q}(\alpha,\vec{\rho}_1)\Psi_{\gamma q}(\alpha,\vec{\rho}_2)\\ &\times\frac{1}{2}\left(\sigma^N_{\bar{q}q}(\alpha\rho_1)+\sigma^N_{\bar{q}q}(\alpha\rho_2)-\sigma^N_{\bar{q}q}(\alpha(\rho_1-\rho_2)\right).\end{aligned}$$

Integration over the photon transverse momentum reproduce the formula for the $x_F$ dependent cross-section.

# Appendix C

# Reduction of the formula for $p_T$ distribution of photons in proton-proton collisions

Starting from

$$\begin{aligned}
\frac{\mathrm{d}^3\sigma(pp\to\gamma/\gamma^*X)}{\mathrm{d}M^2\mathrm{d}x_F\mathrm{d}^2p_T} &= \frac{\mathrm{d}\sigma(\gamma^*\to l^+l^-)}{\mathrm{d}M^2}\frac{1}{x_1+x_2}\int\limits_{x_1}^{1}\frac{\mathrm{d}\alpha}{\alpha}F_2^p\left(\frac{x_1}{\alpha},Q^2\right)\frac{\mathrm{d}\sigma(qp\to\gamma X)}{\mathrm{d}\ln\alpha\mathrm{d}^2p_T}\\
\frac{\mathrm{d}^3\sigma(qp\to\gamma X)}{\mathrm{d}\ln\alpha\mathrm{d}^2p_T} &= \frac{1}{(2\pi)^2}\int\mathrm{d}^2\rho_1\mathrm{d}^2\rho_2 e^{i\vec{p}_T(\vec{\rho}_1-\vec{\rho}_2)}\Psi^*_{\gamma q}(\alpha,\rho_1)\Psi_{\gamma q}(\alpha,\rho_2)\times\\
&\quad\times\frac{1}{2}\left(\sigma^N_{q\bar{q}}(\alpha\rho_1,x_2)+\sigma^N_{q\bar{q}}(\alpha\rho_2,x_2)-\sigma^N_{q\bar{q}}(\alpha|\vec{\rho}_1-\vec{\rho}_2|,x_2)\right)\\
\Psi^*_{\gamma q}(\alpha,\rho_1)\Psi_{\gamma q}(\alpha,\rho_2) &= \frac{\alpha_{em}}{2\pi^2}\Bigg((m_q^2\alpha^4+2M^2(1-\alpha)^2)K_0(\varepsilon\rho_1)K_0(\varepsilon\rho_2)+\\
&\quad(1+(1-\alpha)^2)\varepsilon^2\frac{\vec{\rho}_1\vec{\rho}_2}{\rho_1\rho_2}K_1(\varepsilon\rho_1)K_1(\varepsilon\rho_2)\Bigg)
\end{aligned}$$

one can separate the integral to six parts[93](dependence of the dipole cross-section on $x_2$ is omitted)

$$\begin{aligned}
\frac{\mathrm{d}^3\sigma(qp\to\gamma X)}{\mathrm{d}\ln\alpha\mathrm{d}^2p_T} &= \frac{\alpha_{em}}{(2\pi)^2(2\pi)^2}\Bigg[\\
&\quad\int\mathrm{d}^2\rho_1\mathrm{d}^2\rho_2 e^{i\vec{p}_T(\vec{\rho}_1-\vec{\rho}_2)}(m_q^2\alpha^4+2M^2(1-\alpha)^2)K_0(\varepsilon\rho_1)K_0(\varepsilon\rho_2)\sigma^N_{q\bar{q}}(\alpha\rho_1)\\
&+\int\mathrm{d}^2\rho_1\mathrm{d}^2\rho_2 e^{i\vec{p}_T(\vec{\rho}_1-\vec{\rho}_2)}(m_q^2\alpha^4+2M^2(1-\alpha)^2)K_0(\varepsilon\rho_1)K_0(\varepsilon\rho_2)\sigma^N_{q\bar{q}}(\alpha\rho_2)\\
&-\int\mathrm{d}^2\rho_1\mathrm{d}^2\rho_2 e^{i\vec{p}_T(\vec{\rho}_1-\vec{\rho}_2)}(m_q^2\alpha^4+2M^2(1-\alpha)^2)K_0(\varepsilon\rho_1)K_0(\varepsilon\rho_2)\sigma^N_{q\bar{q}}(\alpha|\vec{\rho}_1-\vec{\rho}_2|)\\
&+\int\mathrm{d}^2\rho_1\mathrm{d}^2\rho_2 e^{i\vec{p}_T(\vec{\rho}_1-\vec{\rho}_2)}(1-(1-\alpha)^2)\varepsilon^2\frac{\vec{\rho}_1\vec{\rho}_2}{\rho_1\rho_2}K_1(\varepsilon\rho_1)K_1(\varepsilon\rho_2)\sigma^N_{q\bar{q}}(\alpha\rho_1)\\
&+\int\mathrm{d}^2\rho_1\mathrm{d}^2\rho_2 e^{i\vec{p}_T(\vec{\rho}_1-\vec{\rho}_2)}(1-(1-\alpha)^2)\varepsilon^2\frac{\vec{\rho}_1\vec{\rho}_2}{\rho_1\rho_2}K_1(\varepsilon\rho_1)K_1(\varepsilon\rho_2)\sigma^N_{q\bar{q}}(\alpha\rho_2)\\
&-\int\mathrm{d}^2\rho_1\mathrm{d}^2\rho_2 e^{i\vec{p}_T(\vec{\rho}_1-\vec{\rho}_2)}(1-(1-\alpha)^2)\varepsilon^2\frac{\vec{\rho}_1\vec{\rho}_2}{\rho_1\rho_2}K_1(\varepsilon\rho_1)K_1(\varepsilon\rho_2)\sigma^N_{q\bar{q}}(\alpha|\vec{\rho}_1-\vec{\rho}_2|)\Bigg].
\end{aligned}$$

The first part can be re-formulated using the integral definition of modified Bessel function of the second kind[94] $K_0(\varepsilon\rho)=\frac{1}{2\pi}\int\mathrm{d}^2l\frac{e^{i\vec{l}\vec{\rho}}}{l^2+\varepsilon^2}$

$$\int \mathrm{d}^2\rho_1\mathrm{d}^2\rho_2 e^{i\vec{p}_T(\vec{\rho}_1-\vec{\rho}_2)}(m_q^2\alpha^4+2M^2(1-\alpha)^2)K_0(\varepsilon\rho_1)K_0(\varepsilon\rho_2)\sigma_{q\bar{q}}^N(\alpha\rho_1) =$$

$$= \quad (m_q^2\alpha^4+2M^2(1-\alpha)^2)\frac{1}{(2\pi)^2}\int \mathrm{d}^2\rho_1\mathrm{d}^2\rho_2\mathrm{d}^2l_1\mathrm{d}^2l_2 e^{i\vec{p}_T(\vec{\rho}_1-\vec{\rho}_2)}\frac{e^{i\vec{l}_1\vec{\rho}_1}}{l_1^2+\varepsilon^2}\frac{e^{i\vec{l}_2\vec{\rho}_2}}{l_2^2+\varepsilon^2}\sigma_{q\bar{q}}^N(\alpha\rho_1) =$$

The integral over $\vec{\rho}_2$ can be performed leading to delta function $\delta^{(2)}(\vec{x}\pm\vec{y}) = \frac{1}{(2\pi)^2}\int \mathrm{d}^2\rho e^{i\vec{\rho}(\vec{x}\pm\vec{y})}$.

$$= \quad (m_q^2\alpha^4+2M^2(1-\alpha)^2)\int \mathrm{d}^2\rho_1\mathrm{d}^2l_1\mathrm{d}^2l_2 e^{i\vec{p}_T\vec{\rho}_1}\frac{e^{i\vec{l}_1\vec{\rho}_1}}{l_1^2+\varepsilon^2}\frac{1}{l_2^2+\varepsilon^2}\sigma_{q\bar{q}}^N(\alpha\rho_1)\delta^{(2)}(\vec{l}_2-\vec{p}_T) =$$

$$= \quad (m_q^2\alpha^4+2M^2(1-\alpha)^2)\int \mathrm{d}^2\rho_1\mathrm{d}^2l_1 e^{i\vec{p}_T\vec{\rho}_1}\frac{e^{i\vec{l}_1\vec{\rho}_1}}{l_1^2+\varepsilon^2}\frac{1}{p_T^2+\varepsilon^2}\sigma_{q\bar{q}}^N(\alpha\rho_1) =$$

$$= \quad (m_q^2\alpha^4+2M^2(1-\alpha)^2)\frac{2\pi}{p_T^2+\varepsilon^2}\int \mathrm{d}^2\rho_1 e^{i\vec{p}_T\vec{\rho}_1}K_0(\varepsilon\rho_1)\sigma_{q\bar{q}}^N(\alpha\rho_1) =$$

Remaining two-dimensional integral can be reduced using the definition of the Bessel function of the first kind[94] $J_0(p_T\rho) = \frac{1}{2\pi}\int \mathrm{d}\phi\, e^{i\vec{p}_T\vec{\rho}} = \frac{1}{2\pi}\int \mathrm{d}\phi\, e^{ip_T\rho\cos\phi}$ to

$$= (m_q^2\alpha^4+2M^2(1-\alpha)^2)\frac{(2\pi)^2}{p_T^2+\varepsilon^2}\int \mathrm{d}\rho_1\,\rho_1 J_0(p_T\rho_1)K_0(\varepsilon\rho_1)\sigma_{q\bar{q}}^N(\alpha\rho_1).$$

The second integral can be treated in the same way

$$\int \mathrm{d}^2\rho_1\mathrm{d}^2\rho_2 e^{i\vec{p}_T(\vec{\rho}_1-\vec{\rho}_2)}(m_q^2\alpha^4+2M^2(1-\alpha)^2)K_0(\varepsilon\rho_1)K_0(\varepsilon\rho_2)\sigma_{q\bar{q}}^N(\alpha\rho_2) =$$

$$= \quad (m_q^2\alpha^4+2M^2(1-\alpha)^2)\frac{(2\pi)^2}{p_T^2+\varepsilon^2}\int \mathrm{d}\rho_2\,\rho_2 J_0(p_T\rho_2)K_0(\varepsilon\rho_2)\sigma_{q\bar{q}}^N(\alpha\rho_2).$$

The third integral has to be first substituted using $\vec{r}_1 = \vec{\rho}_1 - \vec{\rho}_2$ and $\vec{r}_2 = \vec{\rho}_2$

$$\int \mathrm{d}^2\rho_1\mathrm{d}^2\rho_2 e^{i\vec{p}_T(\vec{\rho}_1-\vec{\rho}_2)}(m_q^2\alpha^4+2M^2(1-\alpha)^2)K_0(\varepsilon\rho_1)K_0(\varepsilon\rho_2)\sigma_{q\bar{q}}^N(\alpha|\vec{\rho}_1-\vec{\rho}_2|) =$$

$$= \quad (m_q^2\alpha^4+2M^2(1-\alpha)^2)\frac{1}{(2\pi)^2}\int \mathrm{d}^2r_1\mathrm{d}^2r_2\mathrm{d}^2l_1\mathrm{d}^2l_2 e^{i\vec{p}_T\vec{r}_1}\frac{e^{i\vec{l}_1(\vec{r}_1+\vec{r}_2)}}{l_1^2+\varepsilon^2}\frac{e^{i\vec{l}_2\vec{r}_2}}{l_2^2+\varepsilon^2}\sigma_{q\bar{q}}^N(\alpha r_1) =$$

The rest of the treatment is the same as in preceding case

$$= \quad (m_q^2\alpha^4+2M^2(1-\alpha)^2)\int \mathrm{d}^2r_1\mathrm{d}^2l_1\mathrm{d}^2l_2 e^{i\vec{p}_T\vec{r}_1}\frac{e^{i\vec{l}_1\vec{r}_1}}{l_1^2+\varepsilon^2}\frac{1}{l_2^2+\varepsilon^2}\sigma_{q\bar{q}}^N(\alpha r_1)\delta^{(2)}(\vec{l}_1+\vec{l}_2) =$$

$$= \quad (m_q^2\alpha^4+2M^2(1-\alpha)^2)\int \mathrm{d}^2r_1\mathrm{d}^2l_1 e^{i\vec{p}_T\vec{r}_1}\frac{e^{i\vec{l}_1\vec{r}_1}}{(l_1^2+\varepsilon^2)^2}\sigma_{q\bar{q}}^N(\alpha r_1) =$$

Now the definition of modified Bessel function $K_1$ can be used[94]

$$K_1(\varepsilon r) = -\frac{1}{\varepsilon}\frac{\mathrm{d}}{\mathrm{d}r}K_0(\varepsilon r) = -\frac{1}{r}\frac{\mathrm{d}}{\mathrm{d}\varepsilon}K_0(\varepsilon r) = -\frac{1}{2\pi\varepsilon}\int \mathrm{d}^2 l \frac{e^{i\vec{l}\vec{r}}}{l^2+\varepsilon^2}\frac{\vec{l}\vec{r}}{r} = \frac{1}{2\pi r}\int \mathrm{d}^2 l \frac{e^{i\vec{l}\vec{r}}}{(l^2+\varepsilon^2)^2}2\varepsilon$$

to have

$$\begin{aligned} &= (m_q^2\alpha^4 + 2M^2(1-\alpha)^2)\int \mathrm{d}^2 r_1 e^{i\vec{p}_T\vec{r}_1}\frac{\pi r_1}{\varepsilon}K_1(\varepsilon r_1)\sigma^N_{q\bar{q}}(\alpha r_1) = \\ &= (m_q^2\alpha^4 + 2M^2(1-\alpha)^2)\frac{2\pi^2}{\varepsilon}\int \mathrm{d}r_1\, r_1^2 J_0(p_T r_1)K_1(\varepsilon r_1)\sigma^N_{q\bar{q}}(\alpha r_1). \end{aligned}$$

Fourth and fifth integral can be re-formulated using above definition of $K_1$ to

$$\begin{aligned} &\int \mathrm{d}^2\rho_1 \mathrm{d}^2\rho_2 e^{i\vec{p}_T(\vec{\rho}_1-\vec{\rho}_2)}(1-(1-\alpha)^2)\varepsilon^2\frac{\vec{\rho}_1\vec{\rho}_2}{\rho_1\rho_2}K_1(\varepsilon\rho_1)K_1(\varepsilon\rho_2)\sigma^N_{q\bar{q}}(\alpha\rho_1) = \\ &= (1-(1-\alpha)^2)\varepsilon^2\frac{1}{(2\pi)^2}\int \mathrm{d}^2\rho_1\mathrm{d}^2\rho_2\mathrm{d}^2 l_1\mathrm{d}^2 l_2 e^{i\vec{p}_T(\vec{\rho}_1-\vec{\rho}_2)}\frac{\vec{\rho}_1\vec{\rho}_2\vec{\rho}_1\vec{\rho}_2}{\varepsilon^2\rho_1^2\rho_2^2}\frac{e^{i\vec{l}_1\vec{\rho}_1}}{l_1^2+\varepsilon^2}\vec{l}_1\vec{l}_2\frac{e^{i\vec{l}_2\vec{\rho}_2}}{l_2^2+\varepsilon^2}\sigma^N_{q\bar{q}}(\alpha\rho_1) = \\ &= (1-(1-\alpha)^2)\int \mathrm{d}^2\rho_1\mathrm{d}^2 l_1\mathrm{d}^2 l_2 e^{i\vec{p}_T\vec{\rho}_1}\frac{e^{i\vec{l}_1\vec{\rho}_1}}{l_1^2+\varepsilon^2}\frac{\vec{l}_1\vec{l}_2}{l_2^2+\varepsilon^2}\sigma^N_{q\bar{q}}(\alpha\rho_1)\delta^{(2)}(\vec{l}_2-\vec{p}_T) = \\ &= (1-(1-\alpha)^2)\int \mathrm{d}^2\rho_1\mathrm{d}^2 l_1 e^{i\vec{p}_T\vec{\rho}_1}\frac{e^{i\vec{l}_1\vec{\rho}_1}}{l_1^2+\varepsilon^2}\frac{\vec{l}_1\vec{p}_T}{p_T^2+\varepsilon^2}\sigma^N_{q\bar{q}}(\alpha\rho_1) = \\ &= -(1-(1-\alpha)^2)\frac{2\pi\varepsilon}{p_T^2+\varepsilon^2}\int \mathrm{d}^2\rho_1 e^{i\vec{p}_T\vec{\rho}_1}\frac{\vec{\rho}_1\vec{p}_T}{\rho_1}K_1(\varepsilon\rho_1)\sigma^N_{q\bar{q}}(\alpha\rho_1) = \\ &= (1-(1-\alpha)^2)\frac{(2\pi)^2\varepsilon p_T}{p_T^2+\varepsilon^2}\int \mathrm{d}\rho_1\,\rho_1 J_1(p_T\rho_1)K_1(\varepsilon\rho_1)\sigma^N_{q\bar{q}}(\alpha\rho_1) \end{aligned}$$

and

$$\begin{aligned} &\int \mathrm{d}^2\rho_1\mathrm{d}^2\rho_2 e^{i\vec{p}_T(\vec{\rho}_1-\vec{\rho}_2)}(1-(1-\alpha)^2)\varepsilon^2\frac{\vec{\rho}_1\vec{\rho}_2}{\rho_1\rho_2}K_1(\varepsilon\rho_1)K_1(\varepsilon\rho_2)\sigma^N_{q\bar{q}}(\alpha\rho_2) \\ &= (1-(1-\alpha)^2)\frac{(2\pi)^2\varepsilon p_T}{p_T^2+\varepsilon^2}\int \mathrm{d}\rho_2\,\rho_2 J_1(p_T\rho_2)K_1(\varepsilon\rho_2)\sigma^N_{q\bar{q}}(\alpha\rho_2), \end{aligned}$$

where[94]

$$J_1(p_T\rho) = -\frac{\mathrm{d}}{\mathrm{d}\rho}J_0(p_T\rho) = -\frac{\mathrm{d}}{\mathrm{d}p_T}J_0(p_T\rho) = -\frac{1}{2\pi}\int \mathrm{d}\phi e^{ip_T\rho\cos\phi}\cos\phi = \frac{1}{2\pi}\int \mathrm{d}\phi e^{i\vec{p}_T\vec{\rho}}\frac{\vec{p}_T\vec{\rho}}{p_T\rho}.$$

The last integral has to be again substituted with $\vec{r}_1 = \vec{\rho}_1 - \vec{\rho}_2$ and $\vec{r}_2 = \vec{\rho}_2$

$$\begin{aligned}
&\int \mathrm{d}^2\rho_1\mathrm{d}^2\rho_2 e^{i\vec{p}_T(\vec{\rho}_1-\vec{\rho}_2)}(1-(1-\alpha)^2)\varepsilon^2\frac{\vec{\rho}_1\vec{\rho}_2}{\rho_1\rho_2}K_1(\varepsilon\rho_1)K_1(\varepsilon\rho_2)\sigma^N_{q\bar{q}}(\alpha|\vec{\rho}_1-\vec{\rho}_2|) = \\
= \;& (1-(1-\alpha)^2)\frac{1}{(2\pi)^2}\int \mathrm{d}^2r_1\mathrm{d}^2r_2\mathrm{d}^2l_1\mathrm{d}^2l_2 e^{i\vec{p}_T\vec{r}_1}\frac{e^{i\vec{l}_1(\vec{r}_1+\vec{r}_2)}}{l_1^2+\varepsilon^2}\vec{l}_1\vec{l}_2\frac{e^{i\vec{l}_2\vec{r}_2}}{l_2^2+\varepsilon^2}\sigma^N_{q\bar{q}}(\alpha r_1) = \\
= \;& (1-(1-\alpha)^2)\int \mathrm{d}^2r_1\mathrm{d}^2l_1\mathrm{d}^2l_2 e^{i\vec{p}_T\vec{r}_1}\frac{e^{i\vec{l}_1\vec{r}_1}}{l_1^2+\varepsilon^2}\frac{\vec{l}_1\vec{l}_2}{l_2^2+\varepsilon^2}\sigma^N_{q\bar{q}}(\alpha r_1)\delta^{(2)}(\vec{l}_1+\vec{l}_2) = \\
= \;& (1-(1-\alpha)^2)\int \mathrm{d}^2r_1\mathrm{d}^2l_1 e^{i\vec{p}_T\vec{r}_1}l_1^2\frac{e^{i\vec{l}_1\vec{r}_1}}{(l_1^2+\varepsilon^2)^2}\sigma^N_{q\bar{q}}(\alpha r_1) =
\end{aligned}$$

At this point the integral can be split to two

$$\begin{aligned}
= \;& (1-(1-\alpha)^2)\Bigg[\int \mathrm{d}^2r_1\mathrm{d}^2l_1 e^{i\vec{p}_T\vec{r}_1}(l_1^2+\varepsilon^2)\frac{e^{i\vec{l}_1\vec{r}_1}}{(l_1^2+\varepsilon^2)^2}\sigma^N_{q\bar{q}}(\alpha r_1) - \\
- \;& \int \mathrm{d}^2r_1\mathrm{d}^2l_1 e^{i\vec{p}_T\vec{r}_1}\varepsilon^2\frac{e^{i\vec{l}_1\vec{r}_1}}{(l_1^2+\varepsilon^2)^2}\sigma^N_{q\bar{q}}(\alpha r_1)\Bigg] = \\
= \;& (1-(1-\alpha)^2)\Bigg[\int \mathrm{d}^2r_1 e^{i\vec{p}_T\vec{r}_1}2\pi K_0(\varepsilon r_1)\sigma^N_{q\bar{q}}(\alpha r_1) - \int \mathrm{d}^2r_1 e^{i\vec{p}_T\vec{r}_1}\frac{2\pi\rho\varepsilon^2}{2\varepsilon}K_1(\varepsilon r_1)\sigma^N_{q\bar{q}}(\alpha r_1)\Bigg] = \\
= \;& (1-(1-\alpha)^2)(2\pi)^2\int \mathrm{d}r_1 r_1 J_0(p_T r_1)K_0(\varepsilon r_1)\sigma^N_{q\bar{q}}(\alpha r_1) - \\
- \;& (1-(1-\alpha)^2)2\pi^2\varepsilon\int \mathrm{d}r_1 r_1^2 J_0(p_T r_1)K_1(\varepsilon r_1)\sigma^N_{q\bar{q}}(\alpha r_1).
\end{aligned}$$

Putting all formulas together and denoting

$$\begin{aligned}
I_1(p_T,\alpha) &= \int_0^\infty \mathrm{d}\rho\,\rho J_0(p_T\rho)K_0(\varepsilon\rho)\sigma_{q\bar{q}}(\alpha\rho) \\
I_2(p_T,\alpha) &= \int_0^\infty \mathrm{d}\rho\,\rho^2 J_0(p_T\rho)K_1(\varepsilon\rho)\sigma_{q\bar{q}}(\alpha\rho) \\
I_3(p_T,\alpha) &= \int_0^\infty \mathrm{d}\rho\,\rho J_1(p_T\rho)K_1(\varepsilon\rho)\sigma_{q\bar{q}}(\alpha\rho)
\end{aligned}$$

one has

$$\begin{aligned}
\frac{\mathrm{d}\sigma(qp\to\gamma X)}{\mathrm{d}\ln\alpha\mathrm{d}^2p_T} &= \frac{\alpha_{em}}{(2\pi)^2(2\pi)^2}\Bigg[(m_q^2\alpha^4+2M^2(1-\alpha)^2)\Bigg(\frac{(2\pi)^2}{p_T^2+\varepsilon^2}I_1(p_T,\alpha)+\frac{(2\pi)^2}{p_T^2+\varepsilon^2}I_1(p_T,\alpha)- \\
&\quad -\frac{2\pi^2}{\varepsilon}I_2(p_T,\alpha)\Bigg)+(1+(1-\alpha)^2)\Bigg(\frac{\varepsilon p_T(2\pi)^2}{p_T^2+\varepsilon^2}I_3(p_T,\alpha)+\frac{\varepsilon p_T(2\pi)^2}{p_T^2+\varepsilon^2}I_3(p_T,\alpha)- \\
&\quad -(2\pi)^2I_1(p_T,\alpha)+2\pi^2\varepsilon I_2(p_T,\alpha)\Bigg)\Bigg]= \\
&= \frac{\alpha_{em}}{2\pi^2}\Bigg((m_q^2\alpha^4+2M^2(1-\alpha)^2)\Bigg(\frac{I_1(p_T,\alpha)}{p_T^2+\varepsilon^2}-\frac{I_2(p_T,\alpha)}{4\varepsilon}\Bigg)+ \\
&\quad +(1+(1-\alpha)^2)\Bigg(\frac{\varepsilon p_T}{p_T^2+\varepsilon^2}I_3(p_T,\alpha)-\frac{I_1(p_T,\alpha)}{2}+\frac{\varepsilon}{4}I_2(p_T,\alpha)\Bigg)\Bigg).
\end{aligned}$$

# Appendix D

# Optical Glauber model

The optical Glauber model[12] is reviewed here based on proper quantum mechanical treatment. Let's begin with elastic scattering of a particle with mass $m$ on a static field represented by the potential $V(\vec{r})$. Energy of the particle has a form

$$E = \frac{\hbar^2 k^2}{2m},$$

where $\vec{k}$ is a wave vector. The Schödinger equation describing that system is

$$\begin{aligned} \hat{H}\psi(\vec{r}) &= E\psi(\vec{r}) \\ \left(-\frac{\hbar^2\nabla^2}{2m} + V(\vec{r})\right)\psi(\vec{r}) &= E\psi(\vec{r}) \\ (\nabla^2 + k^2)\psi(\vec{r}) &= \frac{2mV(\vec{r})}{\hbar^2}\psi(\vec{r}) \end{aligned}$$

with asymptotic boundary conditions

$$\psi(\vec{r})|_{t\to-\infty} \sim e^{i\vec{k}\vec{r}} \qquad \psi(\vec{r})|_{t\to+\infty} \sim e^{i\vec{k}\vec{r}} + f(\theta)\frac{e^{i\vec{k}\vec{r}}}{r},$$

where $f(\theta)$ is a scattering amplitude. Choosing an incident wave in the form of the plane wave $\psi(\vec{r}) = Ne^{i\vec{k}\vec{r}}$ results in a probability density of a form $|\psi|^2 = |N|^2$ and if the normalization constant is chosen as $|N|^2 = 1$ than the incident flux of particles is equal to the incident velocity $\vec{v}$. The flux of particles scattered into fixed angle $\mathrm{d}\Omega$ is

$$|f(\theta)|^2\frac{1}{r^2}vr^2\mathrm{d}\Omega.$$

The differential cross-section is

$$\mathrm{d}\sigma = |f(\theta)|^2\mathrm{d}\Omega.$$

A solution of this type of equation can be found using a Green function defined as a solution of a wave equation

$$(\nabla^2 + k^2)G(\vec{r},\vec{r}\,') = \frac{2m}{\hbar^2}\delta(\vec{r}-\vec{r}\,').$$

In general, this equation has a solution in a form

$$G(\vec{r},\vec{r}\,') = -\frac{2m}{4\pi\hbar^2}\frac{\alpha e^{ik|\vec{r}-\vec{r}\,'|}+\beta e^{-ik|\vec{r}-\vec{r}\,'|}}{|\vec{r}-\vec{r}\,'|} \qquad \alpha+\beta=1.$$

If the Green function is chosen such that it corresponds to the amplitude of coherent source emission located at $\vec{r}\,'$, the form of the Green function reduces to

$$G(\vec{r},\vec{r}\,') = -\frac{2m}{4\pi\hbar^2}\frac{e^{ik|\vec{r}-\vec{r}\,'|}}{|\vec{r}-\vec{r}\,'|}.$$

Now, the solution of a Schrödinger equation can be written as

$$\psi(\vec{r}) = e^{i\vec{k}\vec{r}} + \int G(\vec{r},\vec{r}\,')V(\vec{r}\,')\psi(\vec{r}\,')\mathrm{d}\vec{r}\,',$$

where boundary conditions are fulfilled automatically, since $t\to+\infty \Rightarrow |\vec{r}|\to+\infty$ and

$$|\vec{r}-\vec{r}\,'|^2 = r^2 + r\,'^2 - 2\vec{r}\vec{r}\,' \to r^2(1-2\frac{\vec{r}\vec{r}\,'}{r^2}) \to r^2(1-\frac{\vec{r}\vec{r}\,'}{r^2})^2.$$

A fraction in the last formula is small due to the fact that $\vec{r}\,'$ is limited to the region where $V(\vec{r}\,')\neq 0$ and, therefore, can be neglected. Now, let's define a vector $\vec{k}_r$ in the direction of $\vec{r}$ as

$$\vec{k}_r = |\vec{k}|\frac{\vec{r}}{r},$$

and so, the solution can be re-written in the asymptotic form

$$\begin{aligned}\psi(\vec{r})|_{t\to+\infty} &= e^{i\vec{k}\vec{r}} - \frac{2m}{4\pi\hbar^2}\int\frac{e^{ik|\vec{r}-\vec{r}\,'|}}{|\vec{r}-\vec{r}\,'|}V(\vec{r}\,')\psi(\vec{r}\,')\mathrm{d}\vec{r}\,' \to \\ & e^{i\vec{k}\vec{r}} + \frac{e^{ikr}}{r}\left(-\frac{2m}{4\pi\hbar^2}\int e^{-i\vec{k}_r\vec{r}\,'}V(\vec{r}\,')\psi(\vec{r}\,')\mathrm{d}\vec{r}\,'\right)\end{aligned}$$

$$f(k,k') = -\frac{2m}{4\pi\hbar^2}\int e^{-i\vec{k}\,'\vec{r}}V(\vec{r})\psi(\vec{r})\mathrm{d}\vec{r},$$

where the scattering amplitude has been re-written as dependent on incident wave vector $\vec{k}$ and reflected wave vector $\vec{k}'$.
Now comes the assumption that scattering happens at high energy and essentially very fast. To say it more explicitly, the absolute height of a potential barrier has to be much smaller than the incident energy and the wavelength of an incoming particle has to be much shorter than the width of the potential barrier. If the back-scattering of an incident particle can be neglected, the wave function can be separated to an outgoing plane wave and a very slowly varying function

$$\psi(\vec{r}) = e^{i\vec{k}\vec{r}}\varphi(\vec{r})$$

and substituting to the wave equation gives

$$\varphi(\vec{r}) = 1 - \frac{2m}{4\pi\hbar^2}\int \frac{e^{ik|\vec{r}-\vec{r}'|-i\vec{k}(\vec{r}-\vec{r}')}}{|\vec{r}-\vec{r}'|}V(\vec{r}')\varphi(\vec{r}')\mathrm{d}\vec{r}'$$

or with a substitution $\vec{r}'' = \vec{r} - \vec{r}'$

$$\varphi(\vec{r}) = 1 - \frac{2m}{4\pi\hbar^2}\int \frac{e^{i(kr''-\vec{k}\vec{r}'')}}{r''}V(\vec{r}-\vec{r}'')\varphi(\vec{r}-\vec{r}'')\mathrm{d}\vec{r}''.$$

Again, the presumption is that $V(\vec{r})$ and $\varphi(\vec{r})$ vary slowly - on a scale $d$ that is much larger than the wavelength of the particle $\frac{1}{k}$.
The integration over $\vec{r}''$ can be done using a substitution

$$\mathrm{d}\vec{r}'' = r''^2\mathrm{d}r''\mathrm{d}\mu\mathrm{d}\phi \qquad \mu = \cos\sphericalangle\vec{k},\vec{r}$$

where $\phi$ is the azimuthal angle of a rotation of $\vec{r}$ around $\vec{k}$

$$\begin{aligned}\varphi(\vec{r}) &= 1 - \frac{2m}{4\pi\hbar^2}\int \frac{e^{i(kr''-kr''\mu)}}{r''}V(\vec{r}-\vec{r}'')\varphi(\vec{r}-\vec{r}'')r''^2\mathrm{d}r''\mathrm{d}\mu\mathrm{d}\phi \\ &= 1 + \frac{2m}{4\pi\hbar^2}\int r''\mathrm{d}r''\mathrm{d}\phi\left[\frac{e^{ikr''(1-\mu)}}{ikr''}V(\vec{r}-\vec{r}'')\varphi(\vec{r}-\vec{r}'')\right]_{\mu=-1}^{\mu=1} + O\left(\frac{1}{kd}\right).\end{aligned}$$

The limit $\mu = -1$ corresponds to the situation, where $\vec{r}''$ is anti-parallel to $\vec{k}$. But the exponential in this limit strongly oscillate and due to slow variation of the rest of the integral the whole limit behave as $O(\frac{1}{kd})$. Therefore,

$$\varphi(\vec{r}) = 1 - \frac{i}{\hbar v}\int_0^{+\infty} V(r-r'')\varphi(r-r'')|_{\vec{r}''||\vec{k}}\mathrm{d}r''.$$

Now, the change of variables to Cartesian coordinates can be made

$$\begin{aligned}\vec{k} &= (0,0,|\vec{k}|) \\ \vec{r}'' &= (0,0,|\vec{r}''|) \\ \vec{r} &= (x,y,z)\end{aligned}$$

leading to

$$\varphi(\vec{r}) = 1 - \frac{i}{\hbar v}\int\limits_0^{+\infty} V(x,y,z-r'')\varphi(x,y,z-r'')\mathrm{d}r'' = 1 - \frac{i}{\hbar v}\int\limits_{-\infty}^{z} V(x,y,z')\varphi(x,y,z')\mathrm{d}z'.$$

This integral equation can be transformed into a differential equation

$$\frac{\partial}{\partial z}\varphi(x,y,z) = -\frac{i}{\hbar v}V(x,y,z)\varphi(x,y,z),$$

which has a solution in the form

$$\varphi(x,y,z) = e^{-\frac{i}{\hbar v}\int\limits_{-\infty}^{z} V(x,y,z')\mathrm{d}z'}$$

and, therefore,

$$\psi(x,y,z) = e^{ikz-\frac{i}{\hbar v}\int\limits_{-\infty}^{z} V(x,y,z')\mathrm{d}z'}.$$

This solution was obtained in the region, where $V \neq 0$ and, therefore, does not contain all parts one would expect from the wave function, such as outgoing spherical wave etc. Nevertheless, the ultimate goal is to calculate the scattering amplitude(or the cross-section), which has an integral form, and so, only parts of the wave function that correspond to non-zero potential are needed for the calculation. Now, let's choose coordinate vectors $\vec{b}, \hat{k} = \frac{\vec{k}}{|\vec{k}|}$ so that $\vec{r} = \vec{b} + \hat{k}z$ hold

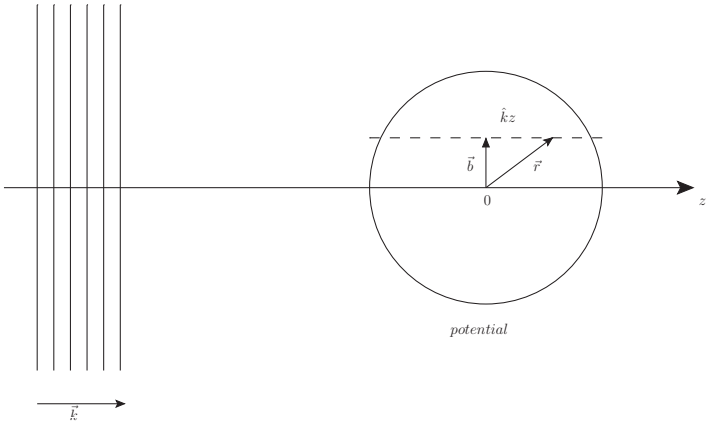


Using this notation the wave function can be written as

$$\psi(\vec{r}) = e^{i\vec{k}\vec{r}-\frac{i}{\hbar v}\int\limits_{-\infty}^{z} V(\vec{b}+\hat{k}z')\mathrm{d}z'}$$

and can be substituted into the formula for scattering amplitude

$$f(\vec{k}',\vec{k}) = -\frac{2m}{4\pi\hbar^2}\int e^{i(\vec{k}-\vec{k}')\vec{r}}V(\vec{r})e^{-\frac{i}{\hbar v}\int\limits_{-\infty}^{z} V(\vec{b}+\hat{k}z')\mathrm{d}z'}\mathrm{d}z\mathrm{d}^2b.$$

The energy conservation in elastic scattering implies $|\vec{k}| = |\vec{k}'|$ so for small angles ($dk\theta << 1$) $\vec{k}-\vec{k}'$ is almost perpendicular to $\vec{k}$ and the term $i(\vec{k}-\vec{k}')\hat{k}z$ can be neglected, which allows to perform the integration over $z$

$$\begin{aligned} f(\vec{k}',\vec{k}) &= -\frac{2m}{4\pi\hbar^2}\int e^{i(\vec{k}-\vec{k}')\vec{b}}V(\vec{b}+\hat{k}z)e^{-\frac{i}{\hbar v}\int\limits_{-\infty}^{z} V(\vec{b}+\hat{k}z')\mathrm{d}z'}\mathrm{d}z\mathrm{d}^2b = \\ &= -\frac{mv}{2\pi\hbar i}\int e^{i(\vec{k}-\vec{k}')\vec{b}}\frac{\partial}{\partial z}\left(e^{-\frac{i}{\hbar v}\int\limits_{-\infty}^{z} V(\vec{b}+\hat{k}z')\mathrm{d}z'}\right)\mathrm{d}z\mathrm{d}^2b = \\ &= \frac{k}{2\pi i}\int e^{i(\vec{k}-\vec{k}')\vec{b}}\left(e^{-\frac{i}{\hbar v}\int\limits_{-\infty}^{+\infty} V(\vec{b}+\hat{k}z')\mathrm{d}z'} - 1\right)\mathrm{d}^2b. \end{aligned}$$

One can imagine that the formula express the situation, where each part of an incoming wave goes through the potential along a straight trajectory and the potential performs a phase shift characteristic for each trajectory. This is a final formula for elastic scattering that can be related to the cross-section using an optical theorem

$$\sigma_{tot} = \frac{4\pi}{k}\mathfrak{Im}f(\vec{k},\vec{k}).$$

Let's revise conditions that has to be fulfilled so that all approximations up to now can be used. It was presumed that the potential times slow modulating function $V\varphi$ does change significantly on the distance $d$ so that terms $\sim \frac{1}{kd}$ can be neglected. Potential $V$ should change significantly on the distance $a$. According to the formula for $\varphi$ it change significantly on the distance $\frac{\hbar v}{V}$, therefore $d$ should have an order of smaller one from numbers $a$ and $\frac{\hbar v}{V}$

$$\begin{aligned} \frac{1}{kd} \quad \Rightarrow \quad & ka >> 1 \qquad d = a \\ & \frac{V}{E} << 1 \qquad d = \tfrac{\hbar v}{V}. \end{aligned}$$

Furthermore, the relation on the scattering angle $\theta^2 kd << 1$ must hold, and so, one can formulate a constrain

$$\theta < O\left(\sqrt{\frac{1}{ka}}\right) \qquad d = a$$
$$\theta < O\left(\sqrt{\frac{V}{E}}\right) \qquad d = \frac{\hbar v}{V}.$$

## Time-dependent interactions

Let's take the time dependent potential $V(x,t)$, where only one spatial dimension is considered. The Schrödinger wave equation has a form

$$\left(\frac{\hbar^2}{2m}\frac{\partial^2}{\partial^2 x} + i\hbar\frac{\partial}{\partial t}\right)\psi(x,t) = V(x,t)\psi(x,t)$$

and the wave function is taken in the form

$$\psi(x,t) = e^{i(kx-\omega t)}\varphi(x,t) \qquad \omega = \frac{E}{\hbar} = \frac{\hbar k^2}{2m}.$$

Glauber's approximation corresponds to very slow change of the function $\varphi$ with respect to $x$ and, therefore, one can omit terms $\frac{\partial^2\varphi}{\partial^2 x}$ and have

$$\left(\frac{\partial}{\partial x} + \frac{1}{v}\frac{\partial}{\partial t}\right)\varphi(x,t) = -\frac{i}{\hbar v}V(x,t)\varphi(x,t).$$

Using a substitution $t \to s = t - \frac{x}{v}$ the form of equation is the same as for static potential. So, the only condition that has to be fulfilled to be able to solve the equation as for the static potential is that the incoming wave in the absence of the potential is plane wave

$$\varphi(-\infty, t) = 1 \quad \forall t.$$

One can then immediately write the solution in the form

$$\varphi(x,t) = e^{-\frac{i}{\hbar v}\int\limits_{-\infty}^{x} V(x', t-\frac{x-x'}{v})\mathrm{d}x'}.$$

Since the time dependence of the wave function is not as simple as $e^{-i\omega t}$, and so, higher Fourier components are involved, each trajectory can be deflected in different way, and so, the scattering is no longer elastic. Therefore, one has to reformulate conditions used for the derivation. During the calculation it was presumed that the change in wave vector $\vec{k}$ is small, but $|\vec{k}| = |\vec{k}'|$. For inelastic scattering the last equation no longer holds, nevertheless, the change of the magnitude of $\vec{k}$ has to be small in order to use the approximation. Therefore, only not-so-inelastic scattering is taken into account ($\frac{\Delta E}{E} << 1$) and one has to restrict

on those potentials $V(x,t)$ whose dominant frequencies are much smaller than $\omega$. Furthermore, it is possible that potentials in different coordinates no longer comute and rather than exponential it is better to use a functional form

$$\begin{aligned}\varphi(x,t) &= 1-\frac{i}{\hbar v}\int\limits_{-\infty}^{x} V(x',t-\frac{x-x'}{v})\mathrm{d}x' + \\ &+\left(\frac{i}{\hbar v}\right)^2\int\limits_{-\infty}^{x}\mathrm{d}x'\int\limits_{-\infty}^{x'}\mathrm{d}x''V(x',t-\frac{x-x'}{v})V(x'',t-\frac{x'-x''}{v})+\cdots = \\ &=\left\{e^{-\frac{i}{\hbar v}\int\limits_{-\infty}^{x}V(x',t-\frac{x-x'}{v})\mathrm{d}x'}\right\}_+ .\end{aligned}$$

## Scattering on bound particles

Consider the situation, where the potential is produced by particles that are not free but as a result of the interaction they can change to different bound state, but not arbitrarily. Let's consider only one spatial dimension, where particle has a coordinate $q$ and hamiltonian $H(q)$ with eigenvalues and eigenvectors $\varepsilon_j$ and $u_j$, respectively. Let's presume that one of those states (called initial $u_i$) is bound and so the movement of the particle is restricted to small interval around $q$. Let's suppose that the incoming particle has a coordinate $x$ and interacts with the bound particle through the potential $V(x-q)$. In order to discuss the behaviour of incoming and target particle one has to switch to time-dependent Schrödinger equation and to the Heisenberg picture. Let $\Omega$ be the state of the whole system (including the time dependence). Then

$$\left(-\frac{\hbar^2}{2m}\frac{\partial^2}{\partial^2 x}+V(x-q)+H(q)\right)\Omega=-i\hbar\frac{\partial}{\partial t}\Omega,$$

where the time dependence of the state $\Omega$ can be separated to

$$\Omega=e^{-iH(q)\frac{t}{\hbar}}\psi,$$

and so,

$$\left(-\frac{\hbar^2}{2m}\frac{\partial^2}{\partial^2 x}+e^{iH(q)\frac{t}{\hbar}}V(x-q)e^{-iH(q)\frac{t}{\hbar}}\right)\psi=i\hbar\frac{\partial}{\partial t}\psi.$$

The time-dependent coordinate operator in the Heisenberg picture has a form

$$\hat{q}(t)=e^{iH(q)\frac{t}{\hbar}}qe^{-iH(q)\frac{t}{\hbar}}.$$

Since $x$ and $q$ comute, the equation is reduced to

$$\left(\frac{\hbar^2}{2m}\frac{\partial^2}{\partial^2 x}+i\hbar\frac{\partial}{\partial t}\right)\psi = V(x-\hat{q}(t))\psi,$$

which is close to the equation for time-dependent interaction. In analogy, one can write

$$\begin{aligned}
\psi(x,\hat{q},t) &= e^{i(kx-\omega t)}\varphi(x,\hat{q},t)u_i \\
\left(\frac{\partial}{\partial x}+\frac{1}{v}\frac{\partial}{\partial t}\right)\varphi(x,\hat{q},t) &= -\frac{i}{\hbar v}V(x-\hat{q}(t))\varphi(x,\hat{q},t) \\
\varphi(x,\hat{q},t) &= \left\{ e^{-\frac{i}{\hbar v}\int\limits_{-\infty}^{x} V(x'-q(t-\frac{x-x'}{v}))\mathrm{d}x'} \right\}_+ .
\end{aligned}$$

The approximation was done under the condition that the change of incident wave vector magnitude is small and it implies that the change in the coordinate $q$ is small, and so, the Hamiltonian $H(q)$ is weak. Moreover, the strength of the binding force has to be small compared to incident energy. That leads to the assumption that one has to restrict to collisions with small momentum transfer. Consequently, the scattering angle and the recoil of the target particle is small. The assumption that the target particle barely moves imply that the operator $\hat{q}$ does not actually depend on time. The last assumption one has to make to ease up the calculation is a neglecting of the so called retardation effect and, therefore, the velocity of the target particle has to be small compared to incident particle. Finally, the approximation has a form

$$\varphi(x,q,t) = \left\{ e^{-\frac{i}{\hbar v}\int\limits_{-\infty}^{x} V(x'-q)\mathrm{d}x'} \right\}_+ .$$

This form allows direct generalization to

$$\begin{aligned}
\varphi(\vec{r},\vec{q},t) &= \left\{ e^{-\frac{i}{\hbar v}\int\limits_{-\infty}^{z} V(\vec{b}+\hat{k}z'-\vec{q})\mathrm{d}z'} \right\}_+ \\
\psi(\vec{r},\vec{q},t) &= e^{i\vec{k}\vec{r}-\frac{i}{\hbar v}\int\limits_{-\infty}^{z} V(\vec{b}+\hat{k}z'-\vec{q})\mathrm{d}z'} u_i(q).
\end{aligned}$$

For each collision, one has to specify initial and final state of the target particle $(u_i, u_f)$ and initial and final wave vectors of incident particle $\vec{k}$ and $\vec{k}'$. The scattering amplitude is then

$$F_{fi}(\vec{k},\vec{k}') = -\frac{2m}{4\pi\hbar^2}\int e^{-i\vec{k}'\vec{r}}u_f^*(\vec{q})V(\vec{r}-\vec{q})\psi(\vec{r},\vec{q})\mathrm{d}^2r\mathrm{d}^2q.$$

If the transverse component of $\vec{q}$ (perpendicular to $\hat{k}$) is denoted $\vec{s}$, so

$$\vec{s} = \vec{q} - \hat{k}(\hat{k}.\vec{q})$$

and the phase shift is denoted $\chi(\vec{b}-\vec{s}) = -\frac{1}{\hbar v}\int_{\Re} V(\vec{b}-\vec{s}+\hat{k}z)\mathrm{d}z$ leading to

$$F_{fi}(\vec{k},\vec{k}') = \frac{k}{2\pi i}\int e^{i(\vec{k}-\vec{k}')\vec{b}}\int u_f^*(\vec{q})\left(e^{i\chi(\vec{b}-\vec{s})}-1\right)u_i(\vec{q})\mathrm{d}^2b\mathrm{d}^2q.$$

## Scattering on a multi-particle system

Let's change the one-particle wave function by a multi-particle one

$$u(\vec{q}) \to u(\vec{q}_1,\vec{q}_2,\dots\vec{q}_N)$$

and a one-particle phase shift by a shift produced by a pass through the target configuration. If an incident particle interact only through the two-particle interaction, the phase shift is equal to the sum of individual phase shifts

$$\chi(\vec{b}-\vec{s}) = \sum_{j=1}^{N}\chi_j(\vec{b}-\vec{s}_j),$$

where $\vec{s}_j$ are components of $\vec{q}_j$ perpendicular to $\hat{k}$. Therefore,

$$F_{fi}(\vec{k},\vec{k}') = \frac{k}{2\pi i}\int e^{i(\vec{k}-\vec{k}')\vec{b}}\int u_f^*(\vec{q}_1,\vec{q}_2,\dots\vec{q}_N)\left(e^{i\sum\limits_{j=1}^{N}\chi_j(\vec{b}-\vec{s}_j)}-1\right)u_i(\vec{q}_1,\vec{q}_2,\dots\vec{q}_N)\mathrm{d}^2b\prod_{j=1}^{N}\mathrm{d}^2q_j.$$

The formula does not correspond to successive interaction amplitudes with each individual particle, but rather to the superposition of individual phase shifts from each particle. Consider now, that the multi-particle system corresponds to the nucleus and coordinates of individual particles are denoted $\vec{q}_1,\vec{q}_2,\dots\vec{q}_N$. If the nucleus is in the initial state $i$, the elastic scattering amplitude is

$$F_{ii}(\vec{k},\vec{k}') = \frac{k}{2\pi i}\int e^{i(\vec{k}-\vec{k}')\vec{b}}\int |u_i(\vec{q}_1,\vec{q}_2,\dots\vec{q}_N)|^2\left(e^{i\chi(\vec{b},\vec{s}_1,\vec{s}_2,\dots,\vec{s}_N)}-1\right)\mathrm{d}^2b\prod_{j=1}^{N}\mathrm{d}^2q_j$$

$$\chi(\vec{b},\vec{s}_1,\vec{s}_2,\dots,\vec{s}_N) = \sum_{j=1}^{N}\chi_j(\vec{b}-\vec{s}_j).$$

The nucleus plays quite passive role since it merely produce an instant phase shift of an incoming wave. Question is, whether one can formulate such inert model of the nucleus(denoted

by the so called optical potential $\chi_{opt}$) so that corresponding scattering amplitude is formally equivalent to single elastic scattering

$$F_{ii}(\vec{k},\vec{k}') = \tfrac{k}{2\pi i}\int e^{i(\vec{k}-\vec{k}')\vec{b}}\int |u_i(\vec{q}_1,\vec{q}_2,\dots\vec{q}_N)|^2\left(e^{i\chi(\vec{b},\vec{s}_1,\vec{s}_2,\dots,\vec{s}_N)}-1\right)\mathrm{d}^2b\prod_{j=1}^N\mathrm{d}^2q_j$$

$$\wr$$

$$f(\vec{k},\vec{k}') = \tfrac{k}{2\pi i}\int e^{i(\vec{k}-\vec{k}')\vec{b}}\left(e^{i\chi_{opt}(\vec{b})}-1\right)\mathrm{d}^2b$$

$$\Rightarrow \qquad e^{i\chi_{opt}(\vec{b})} = \int |u_i(\vec{q}_1,\vec{q}_2,\dots\vec{q}_N)|^2 e^{i\sum\limits_{j=1}^N\chi_j(\vec{b}-\vec{s}_j)}\prod_{j=1}^N\mathrm{d}^2q_j,$$

where $|u_i(\vec{q}_1,\vec{q}_2,\dots\vec{q}_N)|^2$ corresponds to the probability of an initial state of the nucleus, and so, one can see it as an average over each initial configuration

$$e^{i\chi_{opt}(\vec{b})} = \left\langle e^{i\chi(\vec{b},\vec{s}_1,\vec{s}_2,\dots,\vec{s}_N)}\right\rangle_i.$$

Although, the phase shift is real, the optical potential is generally complex with non-zero imaginary part. It can be understood in the sense that not every colliding particle undergoes an elastic collision. Particles that undergo inelastic collision must be absent in the elastic scattering amplitude and so an optical potential cover the lack of particles in elastic scattering as an absorption. Let's rewrite the last equation

$$\begin{aligned}
\chi_{opt}(\vec{b}) &= -i\ln\left\langle e^{i\chi(\vec{b},\vec{s}_1,\vec{s}_2,\dots,\vec{s}_N)}\right\rangle_i = \\
&= -i\ln\left(1+i\left\langle\chi(\vec{b},\vec{s}_1,\vec{s}_2,\dots,\vec{s}_N)\right\rangle_i-\frac{1}{2}\left\langle\chi^2(\vec{b},\vec{s}_1,\vec{s}_2,\dots,\vec{s}_N)\right\rangle_i+\dots\right) = \\
&= \left\langle\chi(\vec{b},\vec{s}_1,\vec{s}_2,\dots,\vec{s}_N)\right\rangle_i+\frac{i}{2}\left\{\left\langle\chi^2(\vec{b},\vec{s}_1,\vec{s}_2,\dots,\vec{s}_N)\right\rangle_i-\left\langle\chi(\vec{b},\vec{s}_1,\vec{s}_2,\dots,\vec{s}_N)\right\rangle_i^2\right\}+\dots
\end{aligned}$$

The first part of $\chi_{opt}$ is simply an average of $\chi(\vec{b},\vec{s}_1,\vec{s}_2,\dots,\vec{s}_N)$ over all nuclear configurations, the imaginary part of $\chi_{opt}$ corresponds to the absorption and comes from the fact that nucleons in the nucleus are not fixed. Should they have a fixed configuration, the imaginary part vanish. From the optical theorem, one can write

$$\sigma_{inel} = \int\mathrm{d}^2b\left(1-\left|\int|u_i(\vec{q}_1,\vec{q}_2,\dots\vec{q}_N)|^2e^{i\sum\limits_{j=1}^N\chi_j(\vec{b}-\vec{s}_j)}\prod_{j=1}^N\mathrm{d}^2q_j\right|^2\right) = \int\mathrm{d}^2b\left(1-|e^{i\chi_{opt}(\vec{b})}|^2\right)$$

which is an absorption cross-section for an equivalent single-particle problem. Therefore, particles that are present as absorbed during the propagation through the nucleus are transformed as particles present in the inelastic scattering. This formula is still not usable for

the calculation, since the optical theorem is not known. Let's presume, that particles inside the nucleus behave independently. Furthermore, let's suppose that functions $\chi_j$ for the interaction of an incoming particle with individual nucleons are known. If we denote $\Gamma_j(\vec{b}) = 1 - e^{i\chi_j(\vec{b})}$, the scattering amplitude of an incoming particle on a nucleon $l$(isolated from others $j \neq l$) is

$$f_l(\vec{k}', \vec{k}) = \frac{ik}{2\pi} \int e^{i(\vec{k}-\vec{k}')\vec{b}} \Gamma_l(\vec{b}) \mathrm{d}^2 b.$$

Now, multiple re-scattering has to be included. Let $\vec{q}_j$ be a coordinate of a nucleon, $\vec{s}_j$ it's transverse coordinate, $u_i(\vec{q}_1, \ldots, \vec{q}_N)$ is a wave function of an initial state of the nucleus. Since

$$e^{i \sum_{j=1}^{N} \chi_j(\vec{b}-\vec{s}_j)} = \prod_{j=1}^{N} (1 - \Gamma_j(\vec{b} - \vec{s}_j))$$

the scattering amplitude is

$$F_{ii}(\vec{k}, \vec{k}') = \frac{k}{2\pi i} \int e^{i(\vec{k}-\vec{k}')\vec{b}} \left( \int |u_i(\vec{q}_1, \vec{q}_2, \ldots \vec{q}_N)|^2 \prod_{j=1}^{N} \Big(1 - \Gamma_j(\vec{b} - \vec{s}_j)\Big) \mathrm{d}^2 q_j - 1 \right) \mathrm{d}^2 b.$$

The product can be decomposed to

$$\prod_{j=1}^{N} (1 - \Gamma_j) = 1 - \sum_{j=1}^{N} \Gamma_j + \sum_{l \neq j=1}^{N} \Gamma_j \Gamma_l - \ldots (-1)^N \prod_{j=1}^{N} \Gamma_j.$$

The first two terms in the decomposition correspond to the single scattering

$$F_{ii}(\vec{k}, \vec{k}') \sim \sum_{j=1}^{N} f_j(\vec{k}, \vec{k}') \int e^{i(\vec{k}-\vec{k}')\vec{s}_j} |u_i(\vec{q}_1, \ldots, \vec{q}_N)|^2 \prod_{j'=1}^{N} \mathrm{d}^2 q_{j'}.$$

Other terms describe corrections on multi-particle re-scattering effects including interferences coming from configurations, where nucleons lie in the shadow of the others. Due to the presumption of independent nucleons, the wave function can be factorized using normalized density of finding a particle $j$ inside the nucleus $\rho_j(\vec{q}_j)$ as

$$|u_i(\vec{q}_1,\ldots,\vec{q}_N)|^2 = \prod_{j=1}^{N} \rho_j(\vec{q}_j)$$

$$\Downarrow$$

$$e^{i\chi_{opt}(\vec{b})} = \int |u_i(\vec{q}_1,\ldots,\vec{q}_N)|^2 \prod_{j=1}^{N} \left(1-\Gamma_j(\vec{b}-\vec{s}_j)\right) \mathrm{d}^2 q_j = \prod_{j=1}^{N} \left(1-\int \rho_j(\vec{q}_j)\Gamma_j(\vec{b}-\vec{s}_j)\mathrm{d}^2 q_j\right)$$

$$\Downarrow$$

$$\chi_{opt}(\vec{b}) = -i\sum_{j=1}^{N} \ln\left(1-\int \rho_j(\vec{q}_j)\Gamma_j(\vec{b}-\vec{s}_j)\mathrm{d}^2 q_j\right).$$

Now, one has to make the assumption, that the distance between particles and the interaction length is much smaller than the radius $R$ of the nucleus. That allows to make a series in $\int \rho_j(\vec{q}_j)\Gamma_j(\vec{b}-\vec{s}_j)\mathrm{d}^2 q_j$ in the interval $b < R$

$$\chi_{opt}(\vec{b}) = i\sum_{j=1}^{N} \int \rho_j(\vec{q}_j)\Gamma_j(\vec{b}-\vec{s}_j)\mathrm{d}^2 q_j + \ldots$$

Since only protons and neutrons are present in the nucleus, there will be two types of $\Gamma_j$ in general, but the strong interaction does not distinguish between them, and so, one can have only one $\Gamma(\vec{q})$. Furthermore, let's introduce an average particle density $\rho(\vec{q}) = \frac{1}{N}\sum_{j=1}^{N} \rho_j(\vec{q})$ having

$$\chi_{opt}(\vec{b}) = iN \int \rho(\vec{q})\Gamma(\vec{b}-\vec{s})\mathrm{d}^2 q = iN \int \rho(\vec{s},z)\Gamma(\vec{b}-\vec{s})\mathrm{d}^2 s\mathrm{d}z.$$

Expanding remaining $\Gamma$ and dropping higher terms leads to

$$\chi_{opt}(\vec{b}) = iN \int\limits_{\mathfrak{R}} \rho(\vec{s},z)\mathrm{d}z \int \Gamma(\vec{s})\mathrm{d}^2 s.$$

The scattering amplitude for forward scattering on one nucleon is $f(0) = \frac{ik}{2\pi}\int \Gamma(\vec{b})\mathrm{d}^2 b$, and so,

$$\chi_{opt}(\vec{b}) \sim \frac{2\pi N}{k} f(0) \int\limits_{\mathfrak{R}} \rho(\vec{b},z)\mathrm{d}z.$$

Up to now, only the inelastic scattering amplitude of a particle on multi-particle state has been considered, where final states are the same as initial. Now, consider that the final state of the nucleus is not far from the initial. Then,

$$F_{fi}(\vec{k}',\vec{k}) = \frac{k}{2\pi i}\int e^{i(\vec{k}-\vec{k}')\vec{b}}\mathrm{d}^2 b \int u_f^*(\vec{q}_1,\ldots,\vec{q}_N)\left(e^{i\sum\limits_{j=1}^{N}\chi_j(\vec{b}-\vec{s}_j)} - 1\right) u_i(\vec{q}_1,\ldots,\vec{q}_N)\prod_{j=1}^{N}\mathrm{d}^2 q_j.$$

The approximation using static densities cannot be used, since the distribution of nucleons inside the nucleus can change. Rather one consider the change of small number of nucleons (preferably only one) and the rest of nucleons is unchanged in a kind of "closed shells." Therefore one consider the interaction of incoming particle with a small number of nucleons inside an optical potential well produced by remaining nucleons. For one such particle

$$\begin{aligned} u_i(\vec{q}_1,\ldots,\vec{q}_N) &= v_i(\vec{q}_1)u(\vec{q}_2,\ldots,\vec{q}_N) \\ u_f(\vec{q}_1,\ldots,\vec{q}_N) &= v_f(\vec{q}_N)u(\vec{q}_2,\ldots,\vec{q}_N) \\ e^{i\chi_{opt}^{(N-1)}(\vec{b})} &= \int |u(\vec{q}_2,\ldots,\vec{q}_N)|^2 e^{i\sum\limits_{j=2}^{N}\chi_j(\vec{b}-\vec{s}_j)} \prod_{j=2}^{N} \mathrm{d}^2 q_j \end{aligned}$$

$$\Downarrow$$

$$\begin{aligned} F_{fi}(\vec{k}',\vec{k}) &= \frac{k}{2\pi i}\int e^{i(\vec{k}-\vec{k}')\vec{b}}\mathrm{d}^2 b \int v_f^*(\vec{q}_1)\left(e^{i\chi_{opt}^{(N-1)}(\vec{b})+i\chi_{opt}^{1}(\vec{b}-\vec{s}_1)}-1\right)v_i(\vec{q}_1)\mathrm{d}^2 q_1 = \\ &= \int v_f^*(\vec{q}_1)e^{i(\vec{k}-\vec{k}')\vec{s}_1}v_i(\vec{q}_1)\bar{f}(\vec{k}',\vec{k},\vec{s}_1)\mathrm{d}^2 q_1, \end{aligned}$$

where $\bar{f}$ is the scattering amplitude of first nucleon not considered as isolated, but lying at an impact parameter $\vec{s}_1$ in the optical potential made by $N-1$ nucleons. Direct generalization is difficult but considering the inelastic cross-section one can write

$$\begin{aligned} \left.\frac{\mathrm{d}\sigma}{\mathrm{d}\Omega}\right|_{inel} = \sum_{f\neq i}|F_{fi}(\vec{k}',\vec{k})|^2 &= \left(\frac{k}{2\pi}\right)^2 \int e^{i(\vec{k}-\vec{k}')(\vec{b}-\vec{b}')}\left(\left\langle e^{i\sum\limits_{j=1}^{N}\chi_j(\vec{b}-\vec{s}_j)} e^{-i\sum\limits_{l=1}^{N}\chi_l^*(\vec{b}'-\vec{s}_l)}\right\rangle_i \right. \\ &\left. - \left\langle e^{i\sum\limits_{j=1}^{N}\chi_j(\vec{b}-\vec{s}_j)}\right\rangle_i \left\langle e^{-i\sum\limits_{l=1}^{N}\chi_l^*(\vec{b}'-\vec{s}_l)}\right\rangle_i\right)\mathrm{d}^2 b\mathrm{d}^2 b' \\ &= \left(\frac{k}{2\pi}\right)^2 \int e^{i(\vec{k}-\vec{k}')(\vec{b}-\vec{b}')}\left(\left\langle \prod_{j=1}^{N}(1-\Gamma_j(\vec{b}-\vec{s}_j))(1-\Gamma_j^*(\vec{b}'-\vec{s}_j))\right\rangle_i \right. \\ &\left. - \left\langle \prod_{j=1}^{N}(1-\Gamma_j(\vec{b}-\vec{s}_j))\right\rangle_i \left\langle \prod_{l=1}^{N}(1-\Gamma_l^*(\vec{b}'-\vec{s}_l))\right\rangle_i\right)\mathrm{d}^2 b\mathrm{d}^2 b'. \end{aligned}$$

Employing $\vec{B}=\frac{1}{2}(\vec{b}-\vec{b}')$, $\vec{\beta}=\vec{b}-\vec{b}'$, $\vec{\lambda}=\vec{k}-\vec{k}'$, one has

$$\left.\frac{\mathrm{d}\sigma}{\mathrm{d}\Omega}\right|_{inel} = \left(\frac{k}{2\pi}\right)^2 \int \mathrm{d}^2 B e^{-\sigma\int_{\Re} n(\vec{B},z)\mathrm{d}z} \int \mathrm{d}^2\beta e^{i(\vec{k}-\vec{k}')\vec{\beta}}\left(e^{\frac{1}{k^2}\int e^{i\vec{\gamma}\vec{\beta}}|f(\lambda)|^2\mathrm{d}^2\lambda\int_{\Re} n(\vec{B},z)\mathrm{d}z}-1\right).$$

Integration over the direction of $\vec{k}'$ one gets

$$\begin{aligned}\sigma_{inel} &= \int \mathrm{d}^2 B e^{-\sigma \int\limits_{\mathfrak{R}} n(\vec{B},z)\mathrm{d}z} \left( e^{-\int |f(\lambda)|^2 \mathrm{d}^2\lambda \frac{1}{k^2} \int\limits_{\mathfrak{R}} n(\vec{B},z)\mathrm{d}z} - 1 \right) = \\ &= \int \mathrm{d}^2 B e^{-\sigma \int\limits_{\mathfrak{R}} n(\vec{B},z)\mathrm{d}z} \left( e^{-\sigma_{scatt} \int\limits_{\mathfrak{R}} n(\vec{B},z)\mathrm{d}z} - 1 \right).\end{aligned}$$

Since $\sigma = \sigma_{abs} + \sigma_{scatt}$ one has the final formula

$$\sigma_{inel} = \int \mathrm{d}^2 B e^{-\sigma_{abs} \int\limits_{\mathfrak{R}} n(\vec{B},z)\mathrm{d}z} \left( 1 - e^{-\sigma_{scatt} \int\limits_{\mathfrak{R}} n(\vec{B},z)\mathrm{d}z} \right).$$

So, the inelastic cross-section is an integral over impact parameter of the probability that the incident particle both escapes absorption and undergoes at least one scattering collision. If the absorption is not an issue($\sigma_{abs} = 0$) and the normalized nucleon density is denoted $n(\vec{B}, z) = \frac{\rho_A(\vec{B},z)}{A}$, where $A$ is the number of nucleons in the nucleus, the formula has a form

$$\sigma_{inel} = \int \mathrm{d}^2 B \left( 1 - e^{-\sigma_{scatt} \int\limits_{\mathfrak{R}} \frac{\rho_A(\vec{B},z)}{A}\mathrm{d}z} \right).$$

# Appendix E

# Transverse momentum distribution of a quark in the short coherence length limit

It is known that a high energy parton propagating through a medium experiences multiple interactions that increase its transverse momentum. If the coherence time of the photon production process is short, produced photons(or dileptons) carry undisturbed information about the transverse momentum of the projectile quark which undergoes initial state interactions. The nucleus supplies the fluctuating quark with larger mean value of the momentum transfer than a nucleon target, therefore, it can resolve fluctuations with larger intrinsic transverse momenta. That is why the short coherence length limit leads to broadening of the transverse momentum spectra since the nucleus behave like size-dependent color filter producing an attenuation of color dipoles propagating through the nuclear matter. The goal of this section is to derive a general expression for the transverse momentum distribution of one of projectile quarks $W_A^q = \frac{\mathrm{d}N_q}{\mathrm{d}^2k_T}$. It can be expressed in terms of the density matrix of the final quark $\Omega_f^q(\vec{b},\vec{b}')$, where $\vec{b}$ is an impact parameter

$$\frac{\mathrm{d}N_q}{\mathrm{d}^2k_T} = \int \mathrm{d}^2b\mathrm{d}^2b' e^{i\vec{k}_T(\vec{b}-\vec{b}')}\Omega_f^q(\vec{b},\vec{b}') \qquad \int \frac{\mathrm{d}N_q}{\mathrm{d}^2k_T}\mathrm{d}^2k_T = 1.$$

The final density matrix is related to the initial one as[9]

$$\Omega_f^q(\vec{b},\vec{b}') = \mathrm{Tr}\hat{S}^\dagger(\vec{b}'+\vec{B})\Omega_{in}^q(\vec{b},\vec{b}')\hat{S}(\vec{b}+\vec{B}),$$

where $\hat{S}(\vec{b}+\vec{B})$ is the S-matrix for a quark-nucleus collision with impact parameter $\vec{b}+\vec{B}$, $\vec{B}$ is the impact parameter between the center of gravity of the projectile hadron and the center of the nucleus and $\vec{b}$ is the impact parameter between the center of gravity of the projectile hadron and the center of the quark. Taking the trace over color indices of the quark, the initial density matrix reads[9]

$$\Omega_{in}^q(\vec{b}_1,\vec{b}_1') = \sum_{n,polar.,color} |C_n|^2 \int \mathrm{d}^2b_2\mathrm{d}^2b_3\ldots\mathrm{d}^2b_n\psi_n^\dagger(\vec{b}_1,\vec{b}_2,\ldots,\vec{b}_n)\psi_n(\vec{b}_1',\vec{b}_2,\ldots,\vec{b}_n),$$

where the sum over different Fock components of hadrons containing different number of quarks $n$ with weight factors $|C_n|^2$ is performed. Also sum runs over all initial state polarizations and colors of all quarks. As a result the matrix $\Omega_{in}^q(\vec{b}_1,\vec{b}_1')$ is diagonal in color space. The longitudinal part of momenta of all quarks is presumed to be integrated and so it does not appear in the hadronic wave function. The S-matrix of a quark-nucleon collision can be treated in the approximation where all coordinates $\vec{r}_i$ of bound nucleons and intrinsic quark coordinates $\vec{\rho}_i$ in nucleons are fixed during the interaction time. Therefore, the S-matrix can be eikonalized[9]

$$\hat{S}(\vec{b}+\vec{B},\vec{r}_i,\vec{\rho}_i,\mu_i)=\sum_{perm}\Theta(z_2-z_1)\dots\Theta(z_A-z_{A-1})\hat{s}_1(\vec{b}+\vec{B}-\vec{r}_{T1},\vec{\rho}_1,\mu_1)\dots\hat{s}_A(\vec{b}+\vec{B}-\vec{r}_{TA},\vec{\rho}_A,\mu_A),$$

where the sum runs over all permutations of nucleons, $\mu_i$ denotes color indices in the $i$-th nucleon an $\hat{s}_i$ corresponds to single quark-$i$-th nucleon S-matrix

$$\hat{s}_i(\vec{b}+\vec{B}-\vec{r}_{Ti},\vec{\rho}_i,\mu_i)=e^{\frac{i}{4}\sum\limits_{j=1}^{3}\hat{\lambda}_a\hat{\lambda}_a(j)\chi(\vec{b}+\vec{B}-\vec{r}_{Tj})}$$

$$\chi(\vec{b})=\int\limits_{\Lambda^2}^{+\infty}\frac{\mathrm{d}^2q}{q^2}\alpha_s(q^2)J_0(b.q),$$

where $\hat{\lambda}_a$ are Gell-Mann matrices and the index $j$ denotes a quark inside the nucleon, $\vec{q}$ is the transverse momentum of the gluon exchanged in the t-channel and $\Lambda^2$ is an infrared cut-off. Now, the product $\hat{S}^\dagger\hat{S}$ can be averaged over colors $\mu_i$, coordinates $\vec{\rho}_i$ of quarks in the target nucleons and also over positions of nucleons $\vec{r}$

$$\left\langle\left\langle\hat{S}^\dagger(\vec{b'}+\vec{B},\vec{r}_i,\vec{\rho}_i,\mu_i)\hat{S}(\vec{b'}+\vec{B},\vec{r}_i,\vec{\rho}_i,\mu_i)\right\rangle_{\vec{\rho},\mu}\right\rangle_{\vec{r}}=\left\langle\sum_{perm}\Theta(z_2-z_1)\dots\Theta(z_A-z_{A-1})\right.$$

$$\left\langle\hat{s}_1^\dagger(\vec{b'}+\vec{B}-\vec{r}_{T1})\left\langle\hat{s}_2^\dagger(\vec{b'}+\vec{B}-\vec{r}_{T2})\dots\left\langle\hat{s}_A^\dagger(\vec{b'}+\vec{B}-\vec{r}_{TA})\right.\right.\right.$$

$$\left.\left.\left.\hat{s}_A(\vec{b}+\vec{B}-\vec{r}_{TA})\right\rangle_{\vec{\rho}_A,\mu_A}\dots\hat{s}_2(\vec{b}+\vec{B}-\vec{r}_{T2})\right\rangle_{\vec{\rho}_2,\mu_2}\hat{s}_1(\vec{b}+\vec{B}-\vec{r}_{T1})\right\rangle_{\vec{\rho}_1,\mu_1}\Bigg\rangle_{\vec{r}}.$$

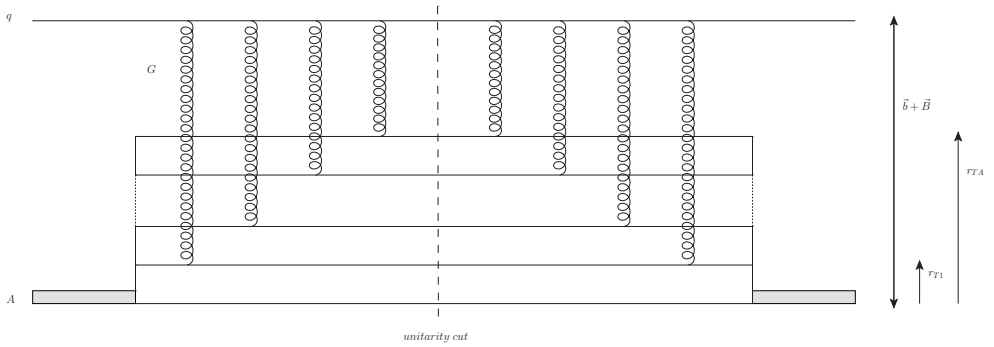


Figure 3: The probability of multiple interactions via one-gluon exchange for the quark in the nucleus

Let's define a function $U_k$ as

$$U_k(\vec{b'}+\vec{B}-\vec{r}_{Tk},\vec{b}+\vec{B}-\vec{r}_{Tk}) = \left\langle \hat{s}_k^\dagger(\vec{b'}+\vec{B}-\vec{r}_{Tk})\hat{s}_k(\vec{b}+\vec{B}-\vec{r}_{Tk})\right\rangle_{\vec{\rho}_k,\mu_k}.$$

These functions commute with each other and so after averaging over $\vec{r}_k$ they became independent of the index $k$

$$\begin{gathered}\left\langle U(\vec{b'}+\vec{B}-\vec{r}_T,\vec{b}+\vec{B}-\vec{r}_T)\right\rangle_{\vec{r}} = \tfrac{1}{A}\int \mathrm{d}^3r\rho_A(\vec{r}_T,z)U(\vec{b'}+\vec{B}-\vec{r}_T,\vec{b}+\vec{B}-\vec{r}_T) = \\ = \tfrac{1}{A}\int \mathrm{d}^3r\rho_A(\vec{r}_T,z) - \tfrac{1}{A}\int \mathrm{d}^3r\rho_A(\vec{r}_T,z)(1-U(\vec{b'}+\vec{B}-\vec{r}_T,\vec{b}+\vec{B}-\vec{r}_T)) = \\ = 1-\tfrac{1}{A}\int \mathrm{d}^2rT_A(\vec{r}_T)(1-U(\vec{b'}+\vec{B}-\vec{r}_T,\vec{b}+\vec{B}-\vec{r}_T)).\end{gathered}$$

Using an expression for the total cross-section for the interaction of a $q\bar{q}$ dipole with transverse separation $\vec{b}-\vec{b'}$ with a nucleon [64]

$$\sigma_{q\bar{q}}(\vec{b}-\vec{b'}) = \frac{2}{A}\int \mathrm{d}^2r_T\left(1-U(\vec{b'}+\vec{B}-\vec{r}_T,\vec{b}+\vec{B}-\vec{r}_T)\right),$$

one can get an approximation[9]

$$\left\langle U(\vec{b'}+\vec{B}-\vec{r}_T,\vec{b}+\vec{B}-\vec{r}_T)\right\rangle_{\vec{r}_T} \sim 1-\frac{1}{2A}T_A\left(\frac{\vec{b}+\vec{b'}}{2}+\vec{B}\right)\sigma_{\bar{q}q}(\vec{b}-\vec{b'}).$$

Moreover, the sum over permutations of nucleon coordinates of the product of $\Theta$ function equals one. Therefore,

$$\begin{gathered}\Omega_f^q(\vec{b},\vec{b'}) = \Omega_{in}^q(\vec{b},\vec{b'})\left(1-\tfrac{1}{2A}T_A\left(\tfrac{\vec{b}+\vec{b'}}{2}+\vec{B}\right)\sigma_{\bar{q}q}(\vec{b}-\vec{b'})\right)^A \sim \Omega_{in}^q(\vec{b},\vec{b'})e^{-\frac{1}{2}T_A\left(\frac{\vec{b}+\vec{b'}}{2}+\vec{B}\right)\sigma_{\bar{q}q}(\vec{b}-\vec{b'})} \\ \frac{\mathrm{d}N}{\mathrm{d}^2k_T} = \int \mathrm{d}^2b\mathrm{d}^2b'e^{i\vec{k}_T(\vec{b}-\vec{b'})}\Omega_{in}^q(\vec{b},\vec{b'})e^{-\frac{1}{2}T_A\left(\frac{\vec{b}+\vec{b'}}{2}+\vec{B}\right)\sigma_{\bar{q}q}(\vec{b}-\vec{b'})}\end{gathered}$$

is a final formula for the transverse momentum distribution of a quark that has propagated through the nucleus. One can use gaussian hadronic wave function to evaluate the density matrix of the initial quark in the proton[9]

$$\Omega_{in}^q(\vec{b},\vec{b'}) = \frac{2}{3\pi < r_{ch}^2 >}e^{-\frac{b^2+b'^2}{3<r_{ch}^2>}},$$

where $< r_{ch}^2 >$ is the mean square of the proton charge radius.

# Bibliography


[1] Greiner, W. and Schramm, S. and Stein, E., Quantum Chromodynamics, Springer, Berlin, 2007

[2] S. D. Drell and T. -M. Yan, Annals Phys. **66** (1971) 578 [Annals Phys. **281** (2000) 450].

[3] J. Raufeisen, J. C. Peng and G. C. Nayak, Phys. Rev. D **66**, 034024 (2002)

[4] B. Kopeliovich, In *Hirschegg 1995, Proceedings, Dynamical properties of hadrons in nuclear matter* 102-112 [arXiv:hep-ph/9609385]

[5] S. J. Brodsky, A. Hebecker and E. Quack, Phys. Rev. D **55**, 2584 (1997)

[6] K. J. Golec-Biernat and M. Wusthoff, Phys. Rev. D **59** (1998) 014017

[7] H. Kowalski, L. Motyka and G. Watt, Phys. Rev. D **74** (2006) 074016

[8] B. Z. Kopeliovich, A. Schafer and A. V. Tarasov, Phys. Rev. D **62** (2000) 054022

[9] M. B. Johnson, B. Z. Kopeliovich and A. V. Tarasov, Phys. Rev. C **63** (2001) 035203 [hep-ph/0006326].

[10] EM collaboration, J. Achmann *et al.*, Phys. Lett. **202B** (1988) 603.

[11] D. M. Alde, H. W. Baer, T. A. Carey, G. T. Garvey, A. Klein, C. Lee, M. J. Leitch and J. W. Lillberg *et al.*, Phys. Rev. Lett. **64** (1990) 2479.

[12] R. J. Glauber, Lectures in Theoretical Physics (Interscience Publishers, Inc., N. Y., 1959), Vol. 1, p. 315.

[13] V. N. Gribov, Sov. Phys. JETP **30** (1970) 709 [Zh. Eksp. Teor. Fiz. **57** (1969) 1306].

[14] L. D. Landau and I. Pomeranchuk, Dokl. Akad. Nauk Ser. Fiz. **92**, 535 (1953); A. B. Migdal, Phys. Rev. **103**, 1811 (1956)

[15] H. Bethe and W. Heitler, Proc. Roy. Soc. Lond. A **146** (1934) 83.

[16] B. Z. Kopeliovich, A. Schafer, A. V. Tarasov and , Phys. Rev. D **62** (2000) 054022 [hep-ph/9908245].

[17] J. Nemchik, V. Petracek, I. K. Potashnikova and M. Sumbera, Phys. Rev. C **78** (2008) 025213 [arXiv:0805.4267 [hep-ph]].

[18] B. Z. Kopeliovich, J. Nemchik, I. K. Potashnikova, M. B. Johnson and I. Schmidt, Nucl. Phys. Proc. Suppl. **146** (2005) 171.

[19] B. Z. Kopeliovich, J. Nemchik, I. K. Potashnikova, M. B. Johnson and I. Schmidt, Phys. Rev. C **72** (2005) 054606 [hep-ph/0501260].

[20] R. J. Fries and C. Nonaka, Prog. Part. Nucl. Phys. **66** (2011) 607 [arXiv:1012.1881 [nucl-th]].

[21] C. Y. Wong, Introduction to High-Energy Heavy-Ion Collisions, World Scientific, 1994.

[22] J. P. Vary, K. E. Lassila and M. S. Sandel, Print-79-0106 (IOWA STATE).

[23] A. Szczurek and A. Budzanowski, Mod. Phys. Lett. A **19** (2004) 1669 [nucl-th/0311025].

[24] J. Ashman *et al.* [European Muon Collaboration], Phys. Lett. B **202** (1988) 603.

[25] J. Arrington [JLab E03-103 Collaboration], J. Phys. Conf. Ser. **69** (2007) 012024 [nucl-ex/0701017].

[26] N. Armesto, J. Phys. G **32** (2006) R367 [hep-ph/0604108].

[27] J. W. Cronin, H. J. Frisch, M. J. Shochet, J. P. Boymond, R. Mermod, P. A. Piroue and R. L. Sumner, Phys. Rev. D **11** (1975) 3105.

[28] A. Accardi, hep-ph/0212148.

[29] B. Z. Kopeliovich, J. Raufeisen, A. V. Tarasov and M. B. Johnson, Phys. Rev. C **67** (2003) 014903 [hep-ph/0110221].

[30] E. Iancu, arXiv:1205.0579 [hep-ph].

[31] B. Z. Kopeliovich and J. Nemchik, J. Phys. G **38** (2011) 043101.

[32] I. Arsene *et al.* [BRAHMS Collaboration], Phys. Rev. Lett. **91** (2003) 072305 [nucl-ex/0307003].

[33] B. Boimska, CERN-THESIS-2004-035.

[34] K. J. Eskola, H. Paukkunen and C. A. Salgado, JHEP **0807** (2008) 102 [arXiv:0802.0139 [hep-ph]].

[35] B. Z. Kopeliovich, E. Levin, I. K. Potashnikova and I. Schmidt, Phys. Rev. C **79** (2009) 064906 [arXiv:0811.2210 [hep-ph]].

[36] A. Adare *et al.* [PHENIX Collaboration], Phys. Rev. C **77** (2008) 024912 [Erratum-ibid. C **79** (2009) 059901] [arXiv:0711.3917 [nucl-ex], arXiv:0903.4845 [nucl-ex]].

[37] S. J. Brodsky, H. -C. Pauli and S. S. Pinsky, Phys. Rept. **301** (1998) 299 [hep-ph/9705477].

[38] S. D. Drell and T. -M. Yan, Annals Phys. **66** (1971) 578 [Annals Phys. **281** (2000) 450].

[39] B. Z. Kopeliovich, A. Schafer and A. V. Tarasov, Phys. Rev. C **59**, 1609 (1999).

[40] B. Z. Kopeliovich and A. H. Rezaeian, Int. J. Mod. Phys. E **18** (2009) 1629

[41] B. Z. Kopeliovich, J. Raufeisen and A. V. Tarasov, Phys. Lett. B **503** (2001) 91

[42] J. C. Webb *et al.* [NuSea Collaboration], arXiv:hep-ex/0302019.

[43] N. N. Nikolaev and B. G. Zakharov, Phys. Lett. B **332** (1994) 177

[44] A. Donnachie and P. V. Landshoff, Phys. Lett. B **296** (1992) 227

[45] R. M. Barnett *et al.* [Particle Data Group], Phys. Rev. D **54** (1996) 1.

[46] M. Gluck, E. Reya and A. Vogt, Z. Phys. C **67** (1995) 433.

[47] M. Gluck, E. Reya and A. Vogt, Eur. Phys. J. C **5** (1998) 461 [arXiv:hep-ph/9806404]

[48] M. Gluck, P. Jimenez-Delgado and E. Reya, Eur. Phys. J. C **53** (2008) 355

[49] J. Pumplin, D. R. Stump, J. Huston, H. L. Lai, P. Nadolsky, W. K. Tung, JHEP 0207:012(2002), [arxiv:hep-ph/0201195]

[50] A. D. Martin, W. J. Stirling, R. S. Thorne and G. Watt, Eur. Phys. J. C **63** (2009) 189

[51] L. Del Debbio *et al.* [NNPDF Collaboration], JHEP **0703** (2007) 039

[52] M. B. Johnson, Eur. Phys. J. A **19** (2004) 105 [hep-ph/0309151].

[53] M. B. Johnson, B. Z. Kopeliovich and I. Schmidt, Phys. Rev. C **75** (2007) 064905 [arXiv:hep-ph/0701015].

[54] M. B. Johnson *et al.*, Phys. Rev. C **65** (2002) 025203 [arXiv:hep-ph/0105195].

[55] T. Hyer, Phys. Rev. D **49** (1994) 2074.

[56] S. J. Brodsky, In *Miami Beach 1996, Neutrino mass, dark matter, gravitational waves, monopole condensation, and light cone quantization* 153-181 [hep-ph/9604391].

[57] H. De Vries, C. W. De Jager and C. De Vries, Atomic Data and Nuclear Data Tables,Volume 36,Issue 3,pages 495-536

[58] L. Hulthen, M. Sugawara, "Handbuch der Physik", vol.39 (1957).

[59] Ramona Vogt, Ultrarelativistic Heavy-ion Collisions, Oxford: Elsevier, 2007.

[60] A. Toia, J. Phys. G **38** (2011) 124007 [arXiv:1107.1973 [nucl-ex]].

[61] B. Abelev *et al.* [ALICE Collaboration], [arXiv:1208.4968 [hep-ex]].

[62] T. Wibig and D. Sobczynska, J. Phys. G **24** (1998) 2037 [J. Phys. G G **24** (1998) 2037] [hep-ph/9809494].

[63] F. Arleo, P. Aurenche, F. W. Bopp, I. Dadic, G. David, H. Delagrange, D. G. d'Enterria and K. J. Eskola *et al.*, hep-ph/0311131.

[64] B. Z. Kopeliovich, L. I. Lapidus and A. B. Zamolodchikov, JETP Lett. **33** (1981) 595 [Pisma Zh. Eksp. Teor. Fiz. **33** (1981) 612].

[65] B. Z. Kopeliovich, A. V. Tarasov and A. Schafer, Phys. Rev. C **59** (1999) 1609 [hep-ph/9808378].

[66] R. Rosenfelder, Phys. Lett. B **479** (2000) 381 [nucl-th/9912031].

[67] B. Z. Kopeliovich, J. Raufeisen and A. V. Tarasov, Phys. Lett. B **440** (1998) 151 [hep-ph/9807211].

[68] B. Z. Kopeliovich, J. Raufeisen and A. V. Tarasov, Phys. Rev. C **62** (2000) 035204 [hep-ph/0003136].

[69] J. Nemchik, Phys. Rev. C **68** (2003) 035206 [hep-ph/0301043].

[70] J. M. Moss, G. T. Garvey, M. B. Johnson, M. J. Leitch, P. L. McGaughey, J. C. Peng, B. Z. Kopeliovich and I. K. Potashnikova, Phys. Rev. Lett. **86** (2001) 4483-4487 [hep-ex/0109014].

[71] B. Z. Kopeliovich, J. Nemchik, A. Schafer and A. V. Tarasov, Phys. Rev. Lett. **88** (2002) 232303 [hep-ph/0201010].

[72] B. Kopeliovich and B. Povh, Phys. Lett. B **367** (1996) 329 [hep-ph/9509362].

[73] V. N. Gribov, Sov. Phys. JETP **29** (1969) 483 [Zh. Eksp. Teor. Fiz. **56** (1969) 892].

[74] V. A. Karmanov, L. A. Kondratyuk and , Pisma Zh. Eksp. Teor. Fiz. **18** (1973) 451.

[75] Y. L. Dokshitzer, G. Marchesini and B. R. Webber, Nucl. Phys. B **469** (1996) 93 [hep-ph/9512336].

[76] B. Z. Kopeliovich, I. K. Potashnikova, H. J. Pirner and I. Schmidt, Phys. Rev. C **83** (2011) 014912 [arXiv:1008.4272 [hep-ph]].

[77] J. F. Gunion and G. Bertsch, Phys. Rev. D **25** (1982) 746.

[78] B. Z. Kopeliovich, I. K. Potashnikova, B. Povh and E. Predazzi, Phys. Rev. D **63** (2001) 054001 [hep-ph/0009008].

[79] B. Z. Kopeliovich, I. K. Potashnikova, B. Povh and E. Predazzi, Phys. Rev. Lett. **85** (2000) 507 [hep-ph/0002241].

[80] A. B. Kaidalov, JETP Lett. **32** (1980) 474 [Pisma Zh. Eksp. Teor. Fiz. **32** (1980) 494].

[81] A. B. Kaidalov, Phys. Lett. B **116** (1982) 459.

[82] A. Capella, U. Sukhatme, C-ITan and J. Tran Thanh Van, Phys. Rept. **236** (1994) 225.

[83] S. J. Brodsky and G. R. Farrar, Phys. Rev. Lett. **31** (1973) 1153.

[84] R. Blankenbecler and S. J. Brodsky, Phys. Rev. D **10** (1974) 2973.

[85] A. H. Mueller, Eur. Phys. J. A **1** (1998) 19 [hep-ph/9710531].

[86] L. D. McLerran and R. Venugopalan, Phys. Rev. D **49** (1994) 3352 [hep-ph/9311205].

[87] L. D. McLerran and R. Venugopalan, Phys. Rev. D **49** (1994) 2233 [hep-ph/9309289].

[88] V. A. Abramovsky, V. N. Gribov and O. V. Kancheli, Yad. Fiz. **18** (1973) 595 [Sov. J. Nucl. Phys. **18** (1974) 308].

[89] B. Z. Kopeliovich, Phys. Rev. C **68** (2003) 044906 [nucl-th/0306044].

[90] M. L. Miller, K. Reygers, S. J. Sanders and P. Steinberg, Ann. Rev. Nucl. Part. Sci. **57** (2007) 205

[91] G. P. Lepage and S. J. Brodsky, Phys. Rev. D **22** (1980) 2157.

[92] G. P. Lepage, S. J. Brodsky, T. Huang and P. B. Mackenzie, CLNS-82-522.

[93] J. Raufeisen, arXiv:hep-ph/0009358.

[94] Abramowitz, Milton; Stegun, Irene A., eds. (1972), Handbook of Mathematical Functions with Formulas, Graphs, and Mathematical Tables, New York: Dover Publications, ISBN 978-0-486-61272-0

# Published results

## Publication list

[1] Cepila J.; Nemchik J., Nuclear suppression of dileptons at large x(F), NUCLEAR PHYSICS B-PROCEEDINGS SUPPLEMENTS 198 (2009) 30-34,
doi: 10.1016/j.nuclphysbps.2009.12.006

[2] Cepila J.; Nemchik J., Nuclear suppression of dileptons at forward rapidities, J. Phys.: Conf. Ser. 312 (2011) 022011, doi:10.1088/1742-6596/312/2/022011

[3] Cepila J.; Nemchik J.; Sumbera M., QCD factorization at forward rapidities, J. Phys.: Conf. Ser. 312 (2011) 012013, doi:10.1088/1742-6596/312/1/012013

[4] Cepila J.; Nemchik J., Direct Photon Production in Proton-Nucleus and Nucleus-Nucleus Collisions, Nuclear Physics A 862-863CF (2011) 445-448, doi:10.1016/j.nuclphysa.2011.06.004

[5] Cepila J., Calculation of direct photon production in nuclear collisions, CERN-proceedings-2012-001,ISBN:9789290833734, pp.135-139, http://cds.cern.ch/record/1471004/

[6] Cepila J.; Nemchik J., Direct photons at large pT : from RHIC to LHC, 25th International Nuclear Physics Conference, Firenze, Italy, 2-7 June 2013, submitted to EPJ Web of Conferences

+ 4 posters presented at international conferences

# Nuclear Suppression of Dileptons at Large $x_F$

J. Cepila[a] * and J. Nemchik[ab] †

[a] Czech Techn. University in Prague, FNSPE, Břehová 7,11519 Prague, Czech Republic

[b] Institute of Experimental Physics SAS, Watsonova 47,04001 Košice, Slovakia

We study a significant nuclear suppression of the relative production rates (p(d)+A)/(p+d(p)) for the Drell-Yan process at large Feynman $x_F$. Since this is the region of minimal values for the light-front momentum fraction variable $x_2$ in the target nucleus, it is tempting to interpret this as a manifestation of coherence or of a Color Glass Condensate. We demonstrate, however, that this suppression mechanism is governed by the energy conservation restrictions in multiple parton rescatterings in nuclear matter. To eliminate nuclear shadowing effects coming from the coherence, we calculate nuclear suppression in the light-cone dipole approach at large dilepton masses and at energy accessible at FNAL. Our calculations are in a good agreement with data from the E772 experiment. Using the same mechanism we predict also nuclear suppression at forward rapidities in the RHIC energy range.

## 1. INTRODUCTION

Recent study of small-$x$ physics is realized at RHIC by measurements of high-$p_T$ particles in $d+Au$ collisions at forward rapidities $y>0$ [1,2]. If a particle with mass $m_h$ and transverse momentum $p_T$ is produced in a hard reaction then the corresponding values of Bjorken variable in the beam and the target are $x_{1,2}=(m_h^2+p_T^2)\,e^{\pm y}/\sqrt{s}$. Thus, at forward rapidities the target $x_2$ is $e^y$-times smaller than at midrapidities. This allows to study coherent phenomena (shadowing, Color Glass Condensate (CGC)), which are expected to suppress particle yields.

However, a significant suppression at large $y$ for any reaction is observed so far at any energy. Namely, all fixed target experiments (see examples in [3]) have too low energy for the onset of coherence effects since $x_2$ is large. The rise of suppression with $y$ (with Feynman $x_F$) shows the same pattern as observed at RHIC. This allows to favor another mechanism common for all reactions arising at any energy. Such a common mechanism based on energy conservation effects in initial state parton rescatterings and leading to $x_F$ scaling of nuclear effects was proposed in [3].

The projectile hadron can be decomposed over different Fock states. A nucleus has a higher resolution than a proton due to multiple interactions and so can resolve higher Fock components containing more constituents. Corresponding parton distributions fall off steeper at $x\to 1$ where any hard reaction can be treated as a large rapidity gap (LRG) process where no particle is produced within rapidity interval $\Delta y=-\ln(1-x)$. The suppression factor as a survival probability for LRG was estimated in [3], $S(x)\sim 1-x$. Each of multiple interactions of projectile partons produces an extra $S(x)$ and the weight factors are given by the AGK cutting rules [4]. As was shown in [3] the effective projectile parton distribution correlates with the nuclear target and reads

$$f_{q/N}^{(A)}(x)=C\,f_{q/N}(x)\\ \times\frac{\int d^{\,2}b\,\left[e^{-x\,\sigma_{eff}T_A(b)}-e^{-\sigma_{eff}T_A(b)}\right]}{(1-x)\int d^{\,2}b\,\left[1-e^{-\sigma_{eff}T_A(b)}\right]}\,, \qquad (1)$$

where $T_A(b)$ is the nuclear thickness function, $\sigma_{eff}$ was evaluated in [3] and the normalization factor $C$ is fixed by the Gottfried sum rule.

In this paper we study the rise of suppression with $y$ ($x_1$) at FNAL reported by the E772 Collaboration [5] for the Drell-Yan (DY) process. We predict similar nuclear effects also at RHIC in the forward region expecting the same suppression pattern as seen at FNAL.

*This work was supported by the Grant LC 07048 (Ministry of Education of the Czech Republic).

†This work was supported in part by the Slovak Funding Agency, Grant 2/7058/27 and by Grants VZ MŠMT 6840770039 and LC 07048 (Ministry of Education of the Czech Republic).

## 2. THE COLOR DIPOLE APPROACH

The DY process in the target rest frame can be treated as radiation of a heavy photon/dilepton by a projectile quark. The transverse momentum $p_T$ distribution of photon bremsstrahlung in quark-nucleon interactions, $\sigma^{qN}(\alpha,\vec{p}_T)$, reads [6]:

$$\frac{d\sigma(qN\to\gamma^* X)}{d(ln\,\alpha)\,d^2p_T}=\frac{1}{(2\pi)^2}\sum_{in,f}\int d^2r_1\,d^2r_2$$
$$e^{i\vec{p}_T\cdot(\vec{r}_1-\vec{r}_2)}\Phi^*_{\gamma^*q}(\alpha,\vec{r}_1)\Phi_{\gamma^*q}(\alpha,\vec{r}_2)\;\times \qquad (2)$$
$$\frac{1}{2}\Big\{\sigma_{\bar{q}q}(x,\alpha r_1)+\sigma_{\bar{q}q}(x,\alpha r_2)-\sigma_{\bar{q}q}(x,\alpha|\vec{r}_1-\vec{r}_2|)\Big\},$$

where $\alpha=p^+_{\gamma^*}/p^+_q$ and the light-cone (LC) wave functions of the projectile quark $q+\gamma^*$ fluctuation $\Phi^*_{\gamma^*q}(\alpha,\vec{r})$ are presented in [6]. Feynman variable is given as $x_F=x_1-x_2$ and in the target rest frame $x_1=p^+_{\gamma^*}/p^+_p$. For the dipole cross section $\sigma_{\bar{q}q}(x,\alpha r)$ in Eq. (2) we used parametrization from [7].

The hadron cross section is given convolving the parton cross section, Eq. (2) with the corresponding parton distribution functions (PDFs) $f_q$ and $f_{\bar{q}}$ [6,8],

$$\frac{d\sigma(pp\to\gamma^*X)}{dx_F\,d^2p_T\,dM^2}=\frac{\alpha_{em}}{3\,\pi\,M^2}\frac{x_1}{x_1+x_2}\int_{x_1}^1\frac{d\alpha}{\alpha^2}\sum_q Z_q^2$$
$$\times\Big\{f_q\big(\frac{x_1}{\alpha},Q^2\big)+f_{\bar{q}}\big(\frac{x_1}{\alpha},Q^2\big)\Big\}\frac{d\sigma(qN\to\gamma^*X)}{d(ln\,\alpha)\,d^2p_T}, \qquad (3)$$

where $Z_q$ is the fractional quark charge, PDFs $f_q$ and $f_{\bar{q}}$ are used with the lowest order (LO) parametrization from [9] at the scale $Q^2=p_T^2+(1-x_1)M^2$ and the factor $\alpha_{em}/(3\pi\,M^2)$ accounts for decay of the photon into a dilepton.

## 3. DILEPTON PRODUCTION ON NUCLEAR TARGETS

The rest frame of the nucleus is very convenient for study of coherence effects. The dynamics of the DY process is regulated by the coherence length $l_c$ related to the longitudinal momentum transfer, $q_L=1/l_c$, which controls the interference between amplitudes of the hard reaction occurring on different nucleons. The condition for the onset of shadowing in a hard reaction is sufficiently long coherence length (LCL) in comparison with the nuclear radius, $l_c\gtrsim R_A$, where

$$l_c=\frac{2E_q\,\alpha(1-\alpha)}{(1-\alpha)\,M^2+\alpha^2\,m_q^2+p_T^2}\;, \qquad (4)$$

and $E_q=x_qs/2m_N$ and $m_q$ is the energy and mass of the projectile quark. The fraction of the proton momentum $x_q$ carried by the quark is related to $x_1$ as $\alpha x_q=x_1$. In the LCL limit the special advantage of the color dipole approach allows to incorporate nuclear shadowing effects via a simple eikonalization of $\sigma_{\bar{q}q}(x,r)$ [10], i.e. replacing $\sigma_{\bar{q}q}(x,r)$ in Eq. (2) by $\sigma^A_{\bar{q}q}(x,r)$:

$$\sigma^A_{\bar{q}q}=2\int d^2b\left\{1-\left[1-\frac{1}{2\,A}\,\sigma_{\bar{q}q}\,T_A(b)\right]^A\right\}. \qquad (5)$$

The corresponding predictions for nuclear broadening in DY reaction based on the theory [6] for LCL limit were presented in [11].

In the short coherence length (SCL) regime the coherence length is shorter than the mean internucleon spacing, $l_c\lesssim 1\div 2\,$fm. In this limit there is no shadowing due to very short duration of the $\gamma^*+q$ fluctuation. The corresponding theory for description of the quark transverse momentum broadening can be found in [12,13]. Here the probability distribution $W^q_A(\vec{k}_T,x_q,\vec{b},z)=dn_q/d^2k_T$ that a valence quark arriving at the position $(\vec{b},z)$ in the nucleus $A$ will have acquired transverse momentum $\vec{k}_T$ can be written in term of the quark density matrix, $\Omega_q(\vec{r}_1,\vec{r}_2)=(b_0^2/\pi)\,\exp(-b_0^2(r_1^2+r_2^2)/2)$,

$$W^q_A(\vec{k}_T,x_q,\vec{b},z)=\frac{1}{(2\pi)^2}\int d^2r_1d^2r_2\,e^{i\,\vec{k}_T\cdot(\vec{r}_1-\vec{r}_2)}$$
$$\times\,\Omega_q(\vec{r}_1,\vec{r}_2)\,e^{-\frac{1}{2}\,\sigma_{\bar{q}q}(x_q,\vec{r}_1-\vec{r}_2)\,T_A(\frac{\vec{r}_1+\vec{r}_2}{2}+\vec{b},z)}\;, \qquad (6)$$

where $b_0^2=\frac{2}{3\,\langle r^2_{ch}\rangle}$ with $\langle r^2_{ch}\rangle=0.79\pm0.03\,\mathrm{fm}^2$ representing the mean-square charge radius of the proton. $T_A(b,z)$ in Eq. (6) is the partial nuclear thickness function, $T_A(b,z)=\int_{-\infty}^z dz'\,\rho_A(b,z')$.

Transverse momentum acquired by a quark on the nucleus, $W^{qA}(\vec{k}_T,x_q)$, is obtained averaging Eq. (6) over the nuclear density $\rho_A(b,z)$:

$$W^{qA}=\frac{1}{A}\int d^2bdz\rho_A(b,z)\,W^q_A(\vec{k}_T,x_q,\vec{b},z)\,. \qquad (7)$$

The cross section, $\sigma^{qA}(\alpha,p_T)$, for an incident quark to produce a photon on a nucleus $A$

with transverse momentum $p_T$ can be expressed convolving the probability function $W^{qA}(\vec{k}_T, x_q)$ with the cross section $\sigma^{qN}(\alpha, k_T)$ (see Eq. (2)),

$$\sigma^{qA}(\alpha, p_T) = \int d^2k_T W^{qA}(\vec{k}_T, x_q)\sigma^{qN}(\alpha, \vec{l}_T)\,, \quad (8)$$

where $\vec{l}_T = \vec{p}_T - \alpha\vec{k}_T$. To obtain the transverse momentum distribution for an incident proton one should integrate over $\alpha$ similarly as in Eq. (3):

$$\frac{d\sigma(pA \to \gamma^* X)}{d\,x_F\,d^2p_T\,dM^2} = \frac{\alpha_{em}}{3\,\pi\,M^2}\frac{x_1}{x_1+x_2}\int_{x_1}^1 \frac{d\alpha}{\alpha^2}\sum_q Z_q^2$$

$$\times\left\{f_q\big(\frac{x_1}{\alpha}, Q^2\big) + f_{\bar{q}}\big(\frac{x_1}{\alpha}, Q^2\big)\right\}\sigma^{qA}(\alpha, p_T)\,. \quad (9)$$

Nuclear effects in $p + A$ collisions are usually investigated via the so called nuclear modification factor, defined as

$$R_A(p_T, x_F, M) = \frac{\frac{d\sigma(pA\to\gamma^* X)}{d\,x_F\,d^2p_T\,dM^2}}{A\,\frac{d\sigma(pN\to\gamma^* X)}{d\,x_F\,d^2p_T\,dM^2}}\,, \quad (10)$$

where the numerator is calculated in SCL and LCL regimes as described above. Corrections for the finite coherence length was realized by linear interpolation using nuclear longitudinal formfactor [14] (for more sophisticate Green function method see [6,15]).

Note that at RHIC energy and at forward rapidities (large $x_F$) the eikonal formula for LCL regime, Eqs. (3) and (5), is not exact since higher Fock components containing gluons lead to additional corrections, called gluon shadowing (GS). The corresponding suppression factor $R_G$ was derived in [14,11] and included in calculations replacing in Eq. (5) $\sigma_{\bar{q}q}$ by $R_G\,\sigma_{\bar{q}q}$. GS leads to reduction of the Cronin effect [16] at moderate $p_T$ and to additional suppression (see Fig. 3).

For elimination of the coherence effects one can study production of dileptons at large $M$ (see Eq. (4)) as has been realized by the E772 Collaboration [5]. Another possibility is to study the DY process at large $x_1 \to 1$, when also $\alpha \to 1$, and $l_c \to 0$ in this limit (see Eq. (4)).

## 4. NUCLEAR SUPPRESSION AT FNAL ENERGIES

We start with the DY process in $p + p$ collisions. Besides calculations based on Eq. (3) using GRV PDFs [9] (see the dashed line in Fig. 1) we present by the solid line also predictions using proton structure functions from [17]. Fig. 1 shows a reasonable agreement of the model with data from the E886 Collaboration [18]. This encourages us to apply the color dipole approach to nuclear targets as well.

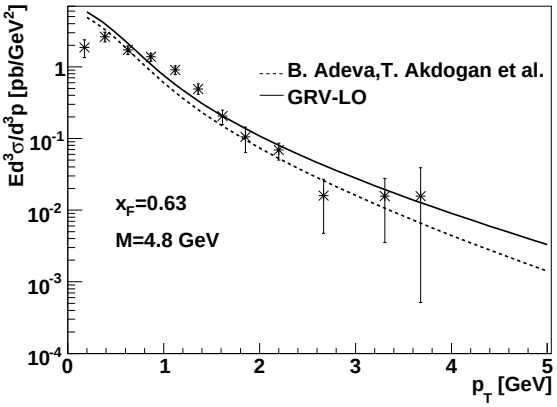


Figure 1. Differential cross section of dileptons in $p + p$ collisions at $x_F = 0.63$ and $M = 4.8\,\mathrm{GeV}$ vs. E886 data [18].

The E772 Collaboration [5] found a significant suppression of DY pairs at large $x_1$ (see Fig. 2). Large invariant masses of the photon allows to minimize shadowing effects (see a small differences between lines calculated in SCL and LCL regimes). If effects of energy conservation are not included one can not describe a strong suppression at large $x_1$. In the opposite case a reasonable agreement of our model with data is achieved.

Finally, we present also predictions for $p_T$ dependence of the nuclear modification factor $R_{d+Au}$ at RHIC energy and at several fixed values of $x_F$. Similarly as in [3] instead of usual Cronin enhancement, a suppression is found (see Fig. 3). The onset of isotopic effects at large $p_T$ gives a value $R_{d+Au} \sim 0.73 \div 0.79$ and can not explain strong nuclear effects. The predicted huge rise of suppression with $x_F$ in Fig. 3 reflects much smaller survival probability $S(x_F)$ at larger $x_F$ and can be tested in the future by the new data from RHIC. Note that effects of GS depicted in Fig. 3 by the thick lines lead to additional suppression which rises with $x_F$.

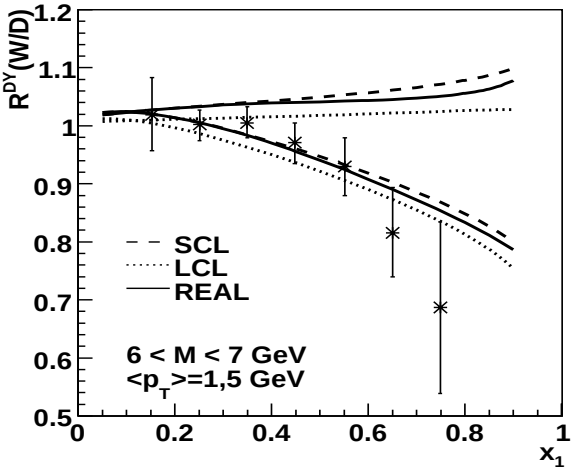


Figure 2. Ratio $R^{DY}(W/D)$ of Drell-Yan cross sections on W and D vs. E772 data for $6 < M < 7\,\mathrm{GeV}$. Predictions correspond to the long (LCL) and short coherence length (SCL) regimes, and their interpolation (REAL). The lower and upper series of curves are calculated with and without energy conservation effects, respectively.

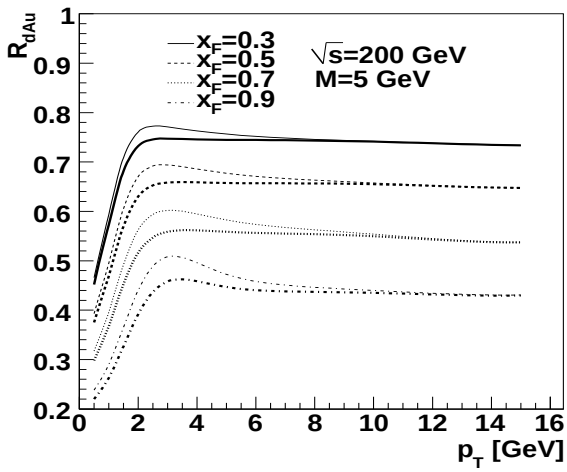


Figure 3. Predictions for the ratio $R_{d+Au}(p_T)$ at $\sqrt{s} = 200\,\mathrm{GeV}$ for several fixed values of $x_F$ with the energy conservation effects (thin lines). Thick lines additionally include gluon shadowing effects.

## 5. SUMMARY

We present unified approach to large $x_1$ ($x_F$) nuclear suppression based on energy conservation effects in multiple parton rescatterings. We apply this approach for the DY process and explain well a significant suppression at large $x_1$ in accordance with the E772 data. The FNAL energy range and large invariant masses of the photon allow to minimize the coherence effects, what does not leave much room for other mechanisms, such as CGC. We predict a significant suppression also in $d + Au$ collisions at RHIC in the forward region (see Fig. 3). At moderate $p_T$ we show an importance of GS effects and their rise with $x_F$.

## REFERENCES

1. BRAHMS Collaboration, I. Arsene, et al., Phys. Rev. Lett.**93**, 242303 (2004); Hongyan Yang, et al., J. Phys.**G34**, S619 (2007).
2. STAR Collaboration, J. Adams, et al., Phys. Rev. Lett. **97**, 152302 (2006).
3. B.Z. Kopeliovich, et al., Phys. Rev. **C72**, 054606 (2005); J. Nemchik, et al., Phys. Rev. **C78**, 025213 (2008).
4. A.V. Abramovsky, V.N. Gribov, and O.V. Kancheli, Yad. Fiz. **18**, 595 (1973).
5. E772 Collaboration, D.M. Alde, at al., Phys. Rev. Lett **64**, 2479 (1990).
6. B.Z. Kopeliovich, A. Schäfer, and A.V. Tarasov, Phys. Rev. **C59**, 1609 (1999).
7. H. Kowalski, L. Motyka, and G. Watt, Phys. Rev. **D74**, 074016 (2006).
8. B.Z. Kopeliovich, J. Raufeisen, and A.V. Tarasov, Phys. Lett. **B503**, 91 (2001).
9. M. Gluck, E. Reya, and A. Vogt, Z. Phys. **C67**, 433 (1995).
10. A.B. Zamolodchikov, et al., Sov. Phys. JETP Lett. **33**, 595 (1981).
11. B.Z. Kopeliovich, et al., Phys. Rev. **C67**, 014903 (2003).
12. M.B. Johnson, B.Z. Kopeliovich, and A.V. Tarasov, Phys. Rev. **C63**, 035203 (2001).
13. M.B. Johnson, B.Z. Kopeliovich, and I. Schmidt, Phys. Rev. **C75**, 064905 (2007).
14. B.Z. Kopeliovich, et al., Phys. Rev. **C65**, 035201 (2002).
15. J. Nemchik, Phys. Rev. **C68**, 035206 (2003).
16. B.Z. Kopeliovich, et al., Phys. Rev. Lett. **88**, 232303 (2002).
17. SMC Collaboration, B. Adeva, et al., Phys. Rev. **D58**, 112001 (1998).
18. E886 Collaboration, J.C.Webb, **FERMILAB -THESIS-2002-56**, hep-ex-0301031.

# Nuclear suppression of dileptons at forward rapidities

**J. Čepila**[1] **and J. Nemchik**[1,2]

[1] Czech Technical University in Prague, FNSPE, Břehová 7, 11519 Prague, Czech Republic
[2] Institute of Experimental Physics SAS, Watsonova 47, 04001 Košice, Slovakia

E-mail: jan.cepila@fjfi.cvut.cz; nemchik@saske.sk

**Abstract.** Data from E772 and E866 experiments on the Drell-Yan process exhibit a significant nuclear suppression at large Feynman $x_F$. We show that a corresponding kinematic region does not allow to interpret this as a manifestation of coherence or a Color Glass Condensate. We demonstrate, however, that this suppression can be treated alternatively as an effective energy loss proportional to initial energy. To eliminate suppression coming from the coherence, we perform predictions for nuclear effects also at large dilepton masses. Our calculations are in a good agreement with available data. Since the forward region can be also approached in transverse momenta $p_T$, we present in the RHIC energy range corresponding predictions for expected large-$p_T$ suppression as well. Since a new experiment E906 planned at FNAL will provide us with more precise data soon, we present also predictions for expected large-$x_F$ nuclear suppression in this kinematic region.

## 1. Introduction

In comparison with a central region of very small rapidities, $y \to 0$, the forward rapidity region allows to study processes corresponding to much higher initial energies accessible at mid rapidities. If a particle with mass $M$ and transverse momentum $p_T$ is produced in a hard reaction then the corresponding values of Bjorken variable in the beam and the target are $x_{1,2} = \sqrt{M^2 + p_T^2}\, e^{\pm y}/\sqrt{s}$. Thus, at forward rapidities the target $x_2$ is $e^y$- times smaller than at mid rapidities. This allows to study already at RHIC coherence phenomena (shadowing, Color Glass Condensate (CGC)), which are expected to suppress particle yields.

Forward rapidity physics, manifested itself as a strong nuclear suppression, has been already investigated in variety of processes at different energies: in production of different species of particles in $p + A$ collisions [1], in charge pion [2] and charmonium production [3, 4] at SPS, in the Drell-Yan process and charmonium production at Fermilab [5, 6] and later on at larger RHIC energies by measurements of high-$p_T$ particles in $d + Au$ collisions [7, 8].

Althought forward rapidity region at RHIC allows to investigate small-$x$ coherence phenomena, one should be carreful with interpretation of observed suppression. Such a suppression is arisen globally for any reaction studied so far at any energy. Namely, all fixed target experiments have too low energy for the onset of coherence effects since $x_2$ is not small. The rise of suppression with $y$ (with Feynman $x_F$) shows the same pattern as observed at RHIC.

This universality of suppression favors also another mechanism which should be common for all reactions studied at any energy. Such a mechanism was proposed in [9] and allows to describe a strong suppression via energy conservation effects in initial state parton rescatterings. It can be also interpreted alternatively as a parton effective energy loss proportional to initial energy leading so to $x_F$ scaling of nuclear effects.

The projectile hadron can be decomposed over different Fock states. A nucleus has a higher resolution than a proton due to multiple interactions and so can resolve higher Fock components containing more constituents. Corresponding parton distributions fall off steeper at $x \to 1$

where any hard reaction can be treated as a large rapidity gap (LRG) process where no particle is produced within rapidity interval $\Delta y = -\ln(1-x)$. The suppression factor as a survival probability for LRG was estimated in [9], $S(x) \sim 1-x$. Each of multiple interactions of projectile partons produces an extra $S(x)$ and the weight factors are given by the AGK cutting rules [10]. As was shown in [9, 11] the effective projectile parton distribution correlates with the nuclear target and reads

$$f^{(A)}_{q/N}(x,Q^2,\vec{b}) = C\, f_{q/N}(x,Q^2)\, exp\Big[-[1-S(x)]\,\sigma_{eff} T_A(\vec{b})\Big] \tag{1}$$

where $T_A(\vec{b})$ is the nuclear thickness function defined at nuclear impact parameter $\vec{b}$, $\sigma_{eff} = 20\,\mathrm{mb}$ [9] and the normalization factor $C$ is fixed by the Gottfried sum rule.

In this paper we study a suppression of the Drell-Yan (DY) process on a nucleus with respect to a nucleon target and the rise of this suppression with $y$ ($x_1$, $x_F$) in various kinematic regions. First we compare our predictions with data from the fixed target E772 experiment at FNAL [5]. Then similar nuclear effects are predicted also for the RHIC forward region expecting the same suppression pattern as seen at FNAL. Finally we perform for the first time predictions in the kinematic range corresponding to a new E906 experiment planned at FNAL where no coherence effects are expected.

## 2. The color dipole approach

The DY process in the target rest frame can be treated as radiation of a heavy photon/dilepton by a projectile quark. The transverse momentum $p_T$ distribution of photon bremsstrahlung in quark-nucleon interactions, $\sigma^{qN}(\alpha,\vec{p}_T)$, reads [12]:

$$\frac{d\sigma(qN\to\gamma^* X)}{d(ln\,\alpha)\,d^2p_T} = \frac{1}{(2\pi)^2}\sum_{in,f}\int d^2r_1\, d^2r_2\, e^{i\vec{p}_T\cdot(\vec{r}_1-\vec{r}_2)}\Phi^*_{\gamma^* q}(\alpha,\vec{r}_1)\Phi_{\gamma^* q}(\alpha,\vec{r}_2)\,\Sigma(\alpha,r_1,r_2) \tag{2}$$

where $\Sigma(\alpha,r_1,r_2) = \{\sigma_{\bar{q}q}(\alpha r_1) + \sigma_{\bar{q}q}(\alpha r_2) - \sigma_{\bar{q}q}(\alpha|\vec{r}_1-\vec{r}_2|)\}/2$, $\alpha = p^+_{\gamma^*}/p^+_q$ and the light-cone (LC) wave functions of the projectile $q+\gamma^*$ fluctuation $\Phi^*_{\gamma^* q}(\alpha,\vec{r})$ are presented in [12]. Feynman variable is given as $x_F = x_1 - x_2$ and in the target rest frame $x_1 = p^+_{\gamma^*}/p^+_p$. For the dipole cross section $\sigma_{\bar{q}q}(\alpha r)$ in Eq. (2) we used GBW [13] and KST [14] parametrizations.

The hadron cross section is given convolving the parton cross section, Eq. (2), with the corresponding parton distribution functions (PDFs) $f_q$ and $f_{\bar{q}}$ [12, 15],

$$\frac{d\sigma(pp\to\gamma^* X)}{dx_F\,d^2p_T\,dM^2} = \frac{\alpha_{em}}{3\,\pi\,M^2}\frac{x_1}{x_1+x_2}\int_{x_1}^1\frac{d\alpha}{\alpha^2}\sum_q Z_q^2\Big\{f_q(\frac{x_1}{\alpha},Q^2) + f_{\bar{q}}(\frac{x_1}{\alpha},Q^2)\Big\}\frac{d\sigma(qN\to\gamma^* X)}{d(ln\,\alpha)\,d^2p_T}, \tag{3}$$

where $Z_q$ is the fractional quark charge, PDFs $f_q$ and $f_{\bar{q}}$ are used with the lowest order (LO) parametrization from [16] at the scale $Q^2 = p_T^2 + (1-x_1)M^2$ and the factor $\alpha_{em}/(3\pi\,M^2)$ accounts for decay of the photon into a dilepton.

## 3. Dilepton production on nuclear targets

The rest frame of the nucleus is very convenient for study of coherence effects. The dynamics of the DY process is controlled by the coherence length,

$$l_c = \frac{2E_q\,\alpha(1-\alpha)}{(1-\alpha)\,M^2 + \alpha^2\,m_q^2 + p_T^2} = \frac{1}{m_N\,x_2}\frac{(1-\alpha)\,M^2}{(1-\alpha)\,M^2 + m_q^2\,\alpha^2 + p_T^2}\ , \tag{4}$$

where $E_q = x_q s/2m_N$ and $m_q$ is the energy and mass of the projectile quark. The fraction of the proton momentum $x_q$ carried by the quark is related to $x_1$ as $\alpha x_q = x_1$.

The coherence length is related to the longitudinal momentum transfer, $q_L = 1/l_c$, which controls the interference between amplitudes of the hard reaction occurring on different nucleons. The

condition for the onset of shadowing in a hard reaction is sufficiently **long coherence length** (LCL) in comparison with the nuclear radius, $l_c \gtrsim R_A$, Here the special advantage of the color dipole approach allows to incorporate nuclear shadowing effects via a simple eikonalization of $\sigma_{\bar{q}q}(x,r)$ [17], i.e. replacing $\sigma_{\bar{q}q}(x,r)$ in Eq. (2) by $\sigma^A_{\bar{q}q}(x,r)$:

$$\sigma^A_{\bar{q}q} = 2\int d^2b \left\{1 - \left[1 - \frac{1}{2\,A}\,\sigma_{\bar{q}q}\,T_A(b)\right]^A\right\}. \tag{5}$$

The corresponding predictions for nuclear broadening in DY reaction based on the theory [12] for LCL limit were presented in [18].

In the **short coherence length** (SCL) regime the coherence length is shorter than the mean internucleon spacing, $l_c \lesssim 1 \div 2\,\mathrm{fm}$. In this limit there is no shadowing due to very short duration of the $\gamma^* + q$ fluctuation. The corresponding theory for description of the quark transverse momentum broadening can be found in [19, 20].

In this regime the transverse momentum distribution for an incident proton can be obtained integrating over $\alpha$ similarly as in Eq. (3):

$$\frac{d\sigma(pA \to \gamma^* X)}{d\,x_F\,d^2p_T\,dM^2} = \frac{\alpha_{em}}{3\,\pi\,M^2}\frac{x_1}{x_1+x_2}\int_{x_1}^1 \frac{d\alpha}{\alpha^2}\sum_q Z_q^2\left\{f_q(\frac{x_1}{\alpha},Q^2) + f_{\bar{q}}(\frac{x_1}{\alpha},Q^2)\right\}\sigma^{qA}(\alpha,p_T)\,, \tag{6}$$

where $\sigma^{qA}(\alpha,p_T)$ represents the cross section for an incident quark to produce a photon on a nucleus $A$ with transverse momentum $p_T$. This cross section can be expressed convolving the probability function $W^{qA}(\vec{k}_T,x_q)$ with the cross section $\sigma^{qN}(\alpha,k_T)$ (see Eq. (2)),

$$\sigma^{qA}(\alpha,p_T) = \int d^2k_T W^{qA}(\vec{k}_T,x_q)\sigma^{qN}(\alpha,\vec{l}_T)\,, \tag{7}$$

where $\vec{l}_T = \vec{p}_T - \alpha\vec{k}_T$.

Probability distribution in Eq. (7) that a quark will acquire transverse momentum $\vec{k}_T$ on the nucleus, $W^{qA}(\vec{k}_T,x_q)$, is obtained by the averaging procedure over the nuclear density $\rho_A(b,z)$:

$$W^{qA}(\vec{k}_T,x_q) = \frac{1}{A}\int d^2b dz \rho_A(b,z)\,W^q_A(\vec{k}_T,x_q,\vec{b},z)\,, \tag{8}$$

where $W^q_A(\vec{k}_T,x_q,\vec{b},z) = dn_q/d^2k_T$ means now the partial probability distribution that a valence quark arriving at the position $(\vec{b},z)$ in the nucleus $A$ will have acquired transverse momentum $\vec{k}_T$. It can be written in term of the quark density matrix, $\Omega_q(\vec{r}_1,\vec{r}_2) = (b_0^2/\pi)\,\exp(-b_0^2(r_1^2+r_2^2)/2)$,

$$W^q_A(\vec{k}_T,x_q,\vec{b},z) = \frac{1}{(2\pi)^2}\int d^2r_1 d^2r_2\, e^{i\,\vec{k}_T\cdot(\vec{r}_1-\vec{r}_2)}\Omega_q(\vec{r}_1,\vec{r}_2)\,e^{-\frac{1}{2}\,\sigma_{\bar{q}q}(x_q,\vec{r}_1-\vec{r}_2)\,T_A(\frac{\vec{r}_1+\vec{r}_2}{2}+\vec{b},z)}\,, \tag{9}$$

where $b_0^2 = \frac{2}{3\,\langle r^2_{ch}\rangle}$ with $\langle r^2_{ch}\rangle = 0.79 \pm 0.03\,\mathrm{fm}^2$ representing the mean-square charge radius of the proton. $T_A(b,z)$ in Eq. (9) is the partial nuclear thickness function, $T_A(b,z) = \int_{-\infty}^z dz'\,\rho_A(b,z')$.

Nuclear effects in $p+A$ collisions are usually investigated via the so called nuclear modification factor, defined as $R_A(p_T,x_F,M) = \frac{d\sigma(pA\to\gamma^* X)}{d\,x_F\,d^2p_T\,dM^2}/A\,\frac{d\sigma(pN\to\gamma^* X)}{d\,x_F\,d^2p_T\,dM^2}$, where the numerator is calculated in SCL and LCL regimes as described above. Corrections for the finite coherence length was realized by linear interpolation using nuclear longitudinal formfactor [21] (for more sophisticate Green function method see [12, 22]).

Note that at RHIC energy and at forward rapidities the eikonal formula for LCL regime, Eqs. (3) and (5), is not exact since higher Fock components containing gluons lead to additional corrections, called gluon shadowing (GS). The corresponding suppression factor $R_G$ was derived in [21, 18] and included in calculations replacing in Eq. (5) $\sigma_{\bar{q}q}$ by $R_G\,\sigma_{\bar{q}q}$. GS leads to reduction of the Cronin effect [23] at medium-high $p_T$ and to additional suppression (see Fig. 3).

In the fixed target FNAL energy range, for elimination of the coherence effects one can study production of dileptons at large $M$ (see Eq. (4)) as has been realized by the E772 Collaboration [5]. Another possibility is to study the DY process at large $x_1 \to 1$, when also $\alpha \to 1$, and $l_c \to 0$ in this limit (see Eq. (4)).

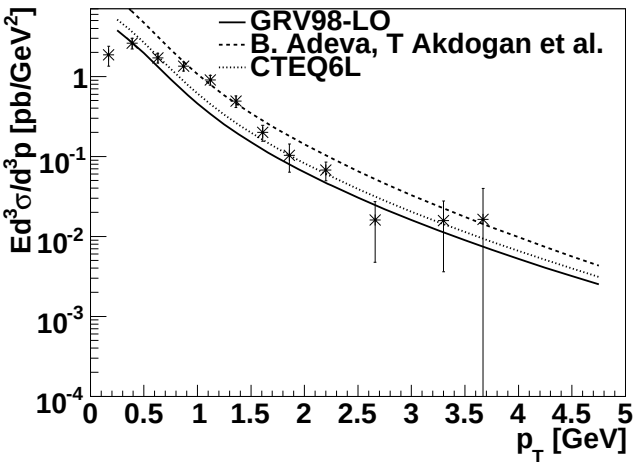


**Figure 1.** Differential cross section of dileptons in $p+p$ collisions at $x_F = 0.63$ and $M = 4.8\,\mathrm{GeV}$ vs. E866 data [24].

**4. Nuclear suppression at forward rapidities: model vs. data**

We start with the DY process in $p+p$ collisions. Besides calculations based on Eq. (3) using GRV98 PDFs [16] (see the solid line in Fig. 1) we present by the dashed and dotted line also predictions using proton structure functions from [25] and CTEQ6L parametrization of PDFs from [26], respectively. Fig. 1 shows a reasonable agreement of the model with data from the E866/NuSea Collaboration [24]. This encourages us to apply the color dipole approach to nuclear targets as well.

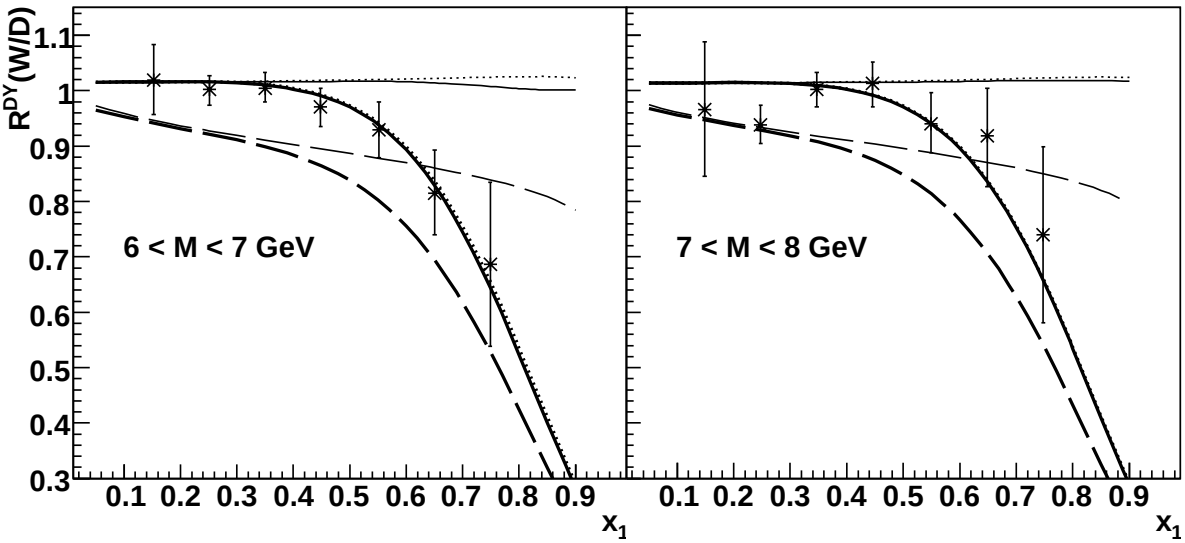


**Figure 2.** Ratio $R^{DY}(W/D)$ of Drell-Yan cross sections on W and D vs. E772 data for $6 < M < 7\,\mathrm{GeV}$ (Left) and $7 < M < 8\,\mathrm{GeV}$ (Right). Predictions correspond to SCL (dotted curves), LCL (dashed curves) regimes and their interpolation (solid curves). Thick and thin curves are calculated with and without effects of effective energy loss, respectively.

The E772 Collaboration [5] found a significant suppression of DY pairs at large $x_1$ (see Fig. 2). Large invariant masses of the photon allows to minimize shadowing effects (see a small differences between dotted and solid lines in Fig. 2). If effects of energy conservation are not included one can not describe a strong suppression at large $x_1$. In the opposite case a reasonable agreement of our model with data is achieved.

One can approach the kinematic limit increasing $p_T$ at fixed $x_F$. Therefore we present also predictions for $p_T$ dependence of the nuclear modification factor $R_{d+Au}$ at RHIC energy and at several fixed values of $x_F$. Similarly as in [9] instead of usual Cronin enhancement, a suppression is found (see Fig. 3). The onset of isotopic effects (IE) in $d + Au$ collisions at large $p_T$ gives the values $R^{IE}_{d+Au} \sim 0.73 \div 0.79$ depending on $x_F$. In $p + Au$ collisions the corresponding ratio $R_{p+Au} \to 1$ from above and no nuclear effects are assumed at large $p_T$ expecting so QCD factorization. However, we predict a strong onset of effective energy loss effects at large $x_F$ (see Fig. 3) quantifying itself as a large deviation of suppression from the above values $R^{IE}_{d+Au}$. The predicted huge rise of suppression with $x_F$ in Fig. 3 reflects much smaller survival probability $S(x_F)$ at larger $x_F$ and can be tested in the future by the new data from RHIC. Note that effects of GS depicted in Fig. 3 by the thick lines lead to additional suppression which rises with $x_F$.

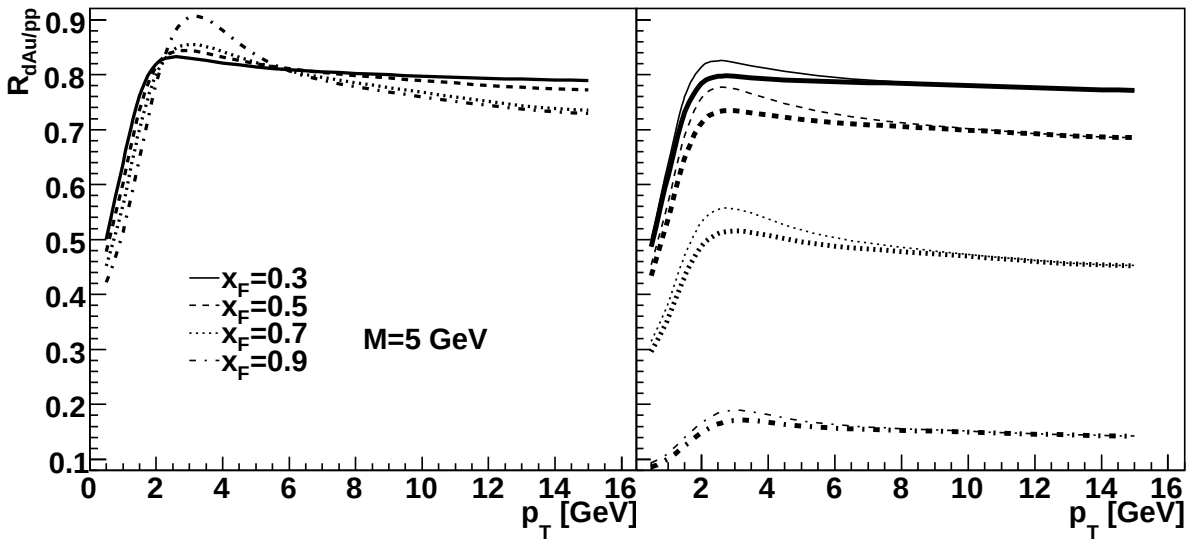


**Figure 3.** (Left) Predictions for the ratio $R_{d+Au}(p_T)$ at $\sqrt{s} = 200\,\mathrm{GeV}$ for several fixed values of $x_F$ without effects of effective energy loss. (Right) The same as (Left) but with effects of effective energy loss (thin lines). Thick lines additionally include gluon shadowing effects.

Finally we present in Fig. 4 for the first time predictions for $x_1$ dependence of the nucleus-to-nucleon ratio in the kinematic range corresponding to a new E906 experiment planned at Fermilab. We shoud not expect any shadowing effects since initial energy is small, $E_{lab} = 120\,\mathrm{GeV}$ and a strong nuclear suppression at large $x_1$ is caused predominantly by the energy conservation constraints.

**5. Summary**

We demonstrate that besides an onset of coherence a nuclear suppression at forward rapidities (large $x_1$, $x_F$) can be induced also by energy conservation effects in multiple parton rescatterings interpreted alternatively as a parton effective energy loss proportional to initial energy. Universality of this treatment is in its applicability to any reaction studied at any energy also in the kinematic regions where coherence phenomena (shadowing, CGC) can not be manifested. First we apply this approach to the DY process and explain well a significant suppression at large $x_1$ in accordance with the E772 data. The FNAL energy range and large invariant masses of the photon allow to minimize the effects of coherence, what does not leave much room for other mechanisms, such as CGC. Then we predict a significant suppression also for $d + Au$ collisions at RHIC in the forward region (see Fig. 3). At small $p_T$ we show an importance of GS effects and their rise with $x_F$. Finally we present for the first time predictions for strong nuclear effects expected in a new E906 experiment planned at FNAL. Much smaller beam energy than in E772 experiment allows to exclude safely interpretations based on coherence phenomena.

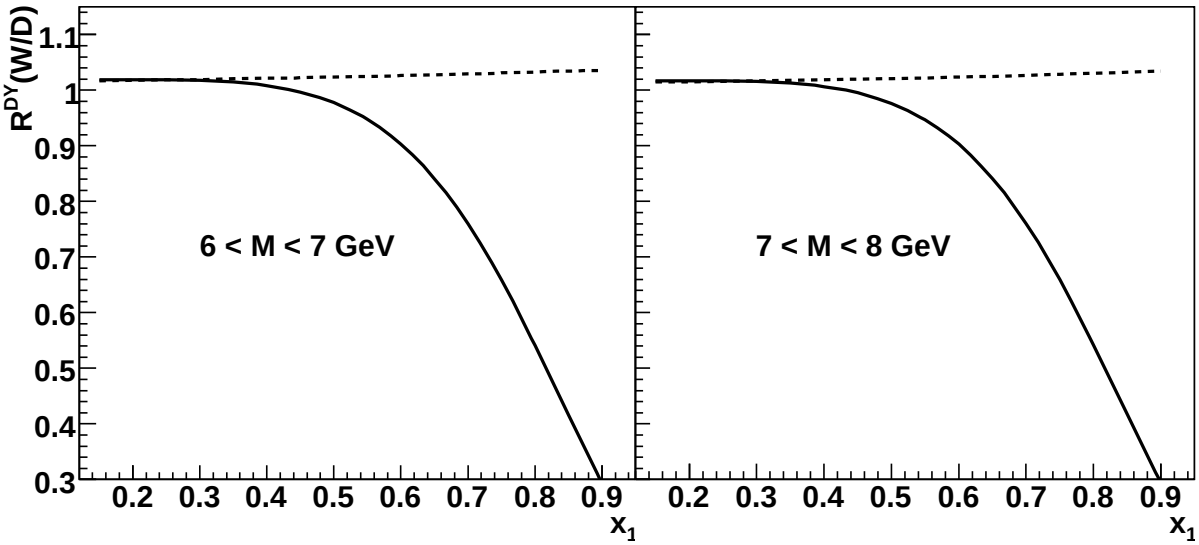


**Figure 4.** (Left) Predictions for the ratio $R^{DY}(W/D)$ of Drell-Yan cross sections on W and D for $6 < M < 7\,\mathrm{GeV}$ (Left) and $7 < M < 8\,\mathrm{GeV}$ (Right) realized for the kinematic range of the planned E906 experiment at Fermilab. Solid and dashed curves are calculated with and without effects of effective energy loss, respectively.


## Acknowledgments

This work was supported in part by the Slovak Funding Agency, Grant 2/0092/10 and by Grants VZ MŠMT 6840770039 and LC 07048 (Ministry of Education of the Czech Republic).


## References


[1] Barton D S, et al. 1983 *Phys. Rev.* D **27** 2580; Geist W M 1991 *Nucl. Phys.* A **525** 149c; Beretvas A, et al. 1986 *ibid.* **34** 53; Binkley M, et al. 1976 *Phys. Rev. Lett.* **37** 571; Bailey R, et al. 1984 *Z. Phys.* C **22** 125; Skubic P, et al. 1978 *Phys. Rev.* D **18** 3115

[2] *NA49 Collaboration*, Boimska B 2004 *Ph.D. Dissertation* (Warsaw 2004) **CERN-THESIS-2004-035**

[3] *NA3 Collaboration*, Badier J, et al. 1983 *Z. Phys.* C **20** 101

[4] *NA38 Collaboration*, Abreu M C, et al. 1999 *Phys. Lett.* B **449** 128

[5] *E772 Collaboration*, Alde D M, at al. 1990 *Phys. Rev. Lett.* **64** 2479

[6] *E866 Collaboration*, Leitch M J, et al. 2000 *Phys. Rev.Lett.* **84** 3256

[7] *BRAHMS Collaboration*, Arsene I, et al. 2004 *Phys. Rev. Lett.* **93** 242303; Hongyan Yang, et al. 2007 *J. Phys.* G **34** S619

[8] *STAR Collaboration*, Adams J, et al. 2006 *Phys. Rev. Lett.* **97** 152302

[9] Kopeliovich B Z, et al. 2005 *Phys. Rev.* **C72** 054606; Nemchik J, et al. 2008 *Phys. Rev.* C **78** 025213

[10] Abramovsky A V, Gribov V N and Kancheli O V 1973 *Yad. Fiz.* **18** 595

[11] Kopeliovich B Z and Nemchik J 2010 *paper in preparation*

[12] Kopeliovich B Z, Schäfer A and Tarasov A V 1999 *Phys. Rev.* C **59** 1609

[13] Kowalski H, Motyka L and Watt G 2006 *Phys. Rev.* D **74** 074016

[14] Kopeliovich B Z, Schäfer A and Tarasov A V 2000 *Phys. Rev.* D **62** 054022

[15] Kopeliovich B Z, Raufeisen J and Tarasov A V 2001 *Phys. Lett.* B **503** 91

[16] Gluck M, Reya E and Vogt A 1998 *Eur. Phys. J.* C **5** 461

[17] Zamolodchikov A B, Kopeliovich B Z and Lapidus L I 1981 *Sov. Phys. JETP Lett.* **33** 595

[18] Kopeliovich B Z, et al. 2003 *Phys. Rev.* C **67** 014903

[19] Johnson M B, Kopeliovich B Z and Tarasov A V 2001 *Phys. Rev.* C **63** 035203

[20] Johnson M B, Kopeliovich B Z and Schmidt I 2007 *Phys. Rev.* C **75** 064905

[21] Kopeliovich B Z, Nemchik J, Schäfer A and Tarasov A V 2002 *Phys. Rev.* C **65** 035201

[22] Nemchik J 2003 *Phys. Rev.* C **68** 035206

[23] Kopeliovich B Z, Nemchik J, Schäfer A and Tarasov A V 2002 *Phys. Rev. Lett.* **88** 232303

[24] *E886/NuSea Collaboration*, Webb J C, at al. 2003 *preprint* **arXiv:hep-ex/0302019**; Webb J C 2002 **FERMILAB -THESIS-2002-56** (*Preprint* **hep-ex-0301031**)

[25] *SMC Collaboration*, Adeva B, et al. 1998 *Phys. Rev.* D **58** 112001

[26] Pumplin J, Stump D R, Huston J, Lai H L, Nadolsky P and Tung W K 2002 *JHEP* **0207** 012

# QCD factorization at forward rapidities

**J. Čepila[1], J. Nemchik[1,2] and M Šumbera[3]**

[1] Czech Technical University in Prague, FNSPE, Břehová 7, 11519 Prague, Czech Republic
[2] Institute of Experimental Physics SAS, Watsonova 47, 04001 Košice, Slovakia
[3] Nuclear Physics Institute AS CR, 25068 Řež/Prague, Czech Republic

E-mail: jan.cepila@fjfi.cvut.cz ; nemchik@saske.sk ; sumbera@ujf.cas.cz

**Abstract.** We analyze several reactions on nuclear targets at forward rapidities and different energies. Forward kinematic region at high energies allows to access smallest Bjorken $x$. Nuclear effects are then usually interpreted as a result of the coherence effects associated with shadowing or the Color Glass Condensate. QCD factorization of soft and hard interactions requires the nucleus to be an universal filter for different Fock components of the projectile hadron. We demonstrate, however, that this is not the case in the vicinity of the kinematic limit, $x \to 1$, where sharing of energy between the projectile constituents becomes an issue. The rise of suppression with $x$ is confirmed by the E772 and E886 data on the Drell-Yan and heavy quarkonium production. We show that this effect can be treated alternatively as an effective energy loss proportional to initial energy. This leads to a nuclear suppression at any energy, and predicts Feynman $x_F$ scaling of the suppression. We demonstarte how the kinematic limit influences the high-$p_T$ particle production at mid-rapidity where the Cronin enhancement at medium-high $p_T$ switches to a suppression at larger $p_T$ violating thus QCD factorization. Such an expectation seems to be confirmed by RHIC data for pion and direct photon production. We show that this effect as an additional large-$p_T$ suppression significantly revises calculations for jet quenching in heavy ion collisons at RHIC.

## 1. Introduction

If a particle with mass $m$ and transverse momentum $p_T$ is produced in a hard reaction then the corresponding values of Bjorken variable in the beam and the target are $x_{1,2} = \sqrt{m^2+p_T^2}\, e^{\pm y}/\sqrt{s}$. Thus, at forward rapidities the target $x_2$ is $e^y$- times smaller than at midrapidities, $y = 0$. This allows to study coherent phenomena (shadowing, Color Glass Condensate (CGC)), which are expected to suppress particle yields.

Forward rapidity region, $y > 0$, was studied already in the fixed target experiments [1] investigating a production of different species of hadrons in $p + A$ collisions, in charge pion [2] and charmonium production [3, 4] at SPS, in the Drell-Yan process and charmonium production at Fermilab [5, 6] and later on at larger RHIC energies in production of high-$p_T$ particles in $d + Au$ collisions [7, 8]. This region is expected to be studied also at LHC by the ALICE Collaboration [9].

Interpretation of large-$y$ suppression at RHIC via coherent phenomena should be realized with a great caution since there is no consensus so far about the strength of gluon shadowing and CGC. The BRAHMS data [7] at $y = 3.2$ to be explained are just fitted [10]. Moreover, the recent global leading order (LO) analysis [11] including besides DIS also this BRAHMS data leads to grossly exaggerated gluon shadowing which conflicts with unitarity bound [12].

Besides, an energetic universality of a significant suppression at large $y$ is manifested so far for any reaction. Namely, all fixed target experiments have too low energy for the onset of coherence effects since $x_2$ is not small. The rise of suppression with $y$ (with Feynman $x_F$) shows

the same pattern as observed at RHIC. Such an energy independent feature common for all known reactions allows to favor another mechanism [13] which describes observed suppression via corrections for energy conservation in initial state parton rescatterings and could be also alternatively interpreted as a parton effective energy loss proportional to initial energy leading so to $x_F$ scaling of nuclear effects.

Interpretation of suppression can be also realized via decomposition of the projectile hadron over different Fock states. In comparison with a proton case, a nucleus has a higher resolution due to multiple interactions and so can resolve higher Fock components containing more constituents. Corresponding parton distributions fall off steeper at $x \to 1$.

In the vicinity of the kinematic limit any hard reaction can be treated as a large rapidity gap (LRG) process where no particle is produced within rapidity interval $\Delta y = -\ln(1-x)$. The suppression factor as a survival probability for LRG was found [13] to be approximately,

$$S(x) \approx 1 - x. \tag{1}$$

Each of multiple interactions of projectile partons produces an extra $S(x)$ and the weight factors are given by the AGK cutting rules [14]. Then in terms of the nuclear thickness function $T_A(\vec{b})$ and the effective cross section $\sigma_{eff} = 20\,\mathrm{mb}$ [13] the cross sections of hard reaction on a nuclear target $A$ at impact parameter $\vec{b}$ and on a nucleon $N$ are related as,

$$\frac{d\sigma_A}{dx\,d\,^2b} = \frac{d\sigma_N}{dx}\frac{1}{\sigma_{eff}} e^{-\sigma_{eff}T_A(\vec{b})} \sum_{n=1}^{A} \frac{n}{n!} \left[\sigma_{eff}\, T_A(\vec{b})\right]^n S(x)^{n-1} = \frac{d\sigma_N}{dx} T_A(\vec{b}) e^{-[1-S(x)]\sigma_{eff}T_A(\vec{b})}\,. \tag{2}$$

Consequently, the effective projectile parton distribution correlates with the nuclear target breaking thus expected QCD factorization [13].

In this paper using a mechanism from [13, 15] and including also coherent phenomena (shadowing) at small $x_2$ we analyze several reactions at forward rapidities and different energies.

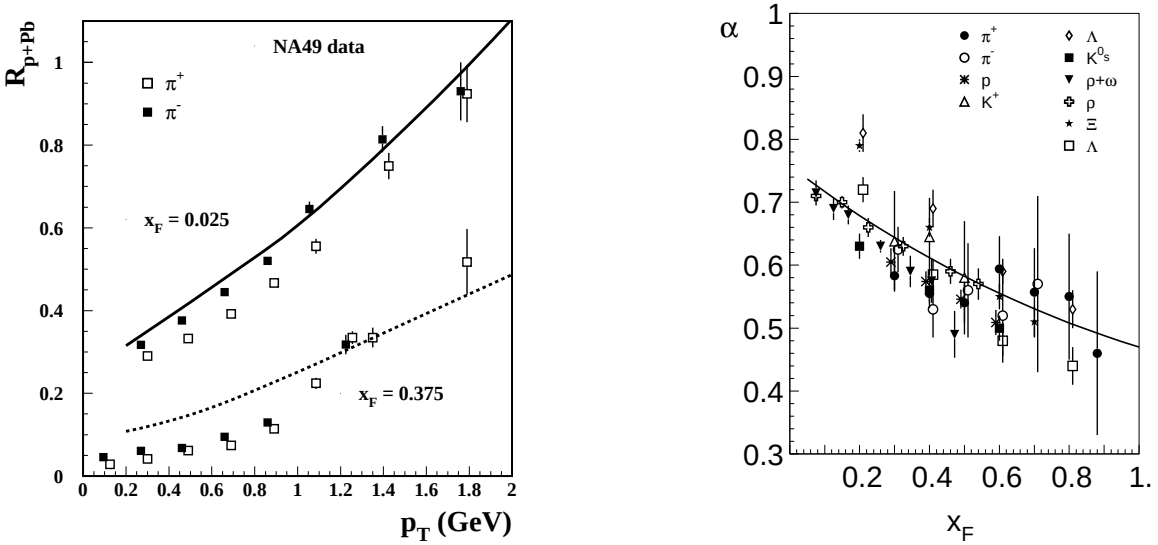


**Figure 1.** (Left) Ratio, $R_{p+Pb}(p_T)$, for $\pi^{\pm}$ production rates in $p+Pb$ and $p+p$ collisions as function of $p_T$ at $E_{lab} = 158\,\mathrm{GeV}$ and two fixed $x_F = 0.025$ and 0.375 [16] vs. NA49 data [2]. (Right) The exponent describing the A-dependence ($\propto A^{\alpha}$) of the ratio for the production of different hadrons in $p+A$ relative to $p+p$ collisions as function of $x_F$ [13] vs. data [1].

## 2. Nuclear suppression at small energies

Figs. 1 and 2 (see also Fig. 4) clearly exhibit the same pattern as that seen at RHIC [7, 8] - a significant rise of suppression with $x_F$ ($x_1$) at SPS, $E_{lab} = 158\,GeV$, and FNAL energy,

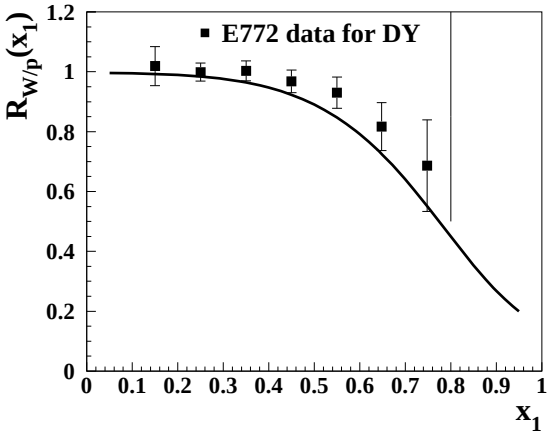


**Figure 2.** Ratio $R^{DY}(W/D)$ of Drell-Yan cross sections on W and D vs. E772 data [5] at $E_{lab} = 800\,\mathrm{GeV}$ for $6 < M < 7\,\mathrm{GeV}$.

$E_{lab} = 800\,\mathrm{GeV}$. All those fixed target experiments have too low energy for the onset of coherent effects in gluon radiation since the target $x_2$ is not small and consequently the coherence length $l_c = P/(x_2 m_N)$, where $P \sim 0.1$ [17], is shorter than the mean inter-nucleon spacing.

The mechanism of nuclear suppression can be interpreted as a energy dissipation of the projectile hadron and its debris when propagating through the nucleus. As a result, the probability of production of a particle carrying the substantial fraction $x_F$ of the initial momentum decreases compared to a free proton target [13, 15].

Model predictions [13, 16] including corrections Eq. (1) for energy deficit in initial state parton multiple interactions lead to a reasonable agreement with low energy data.

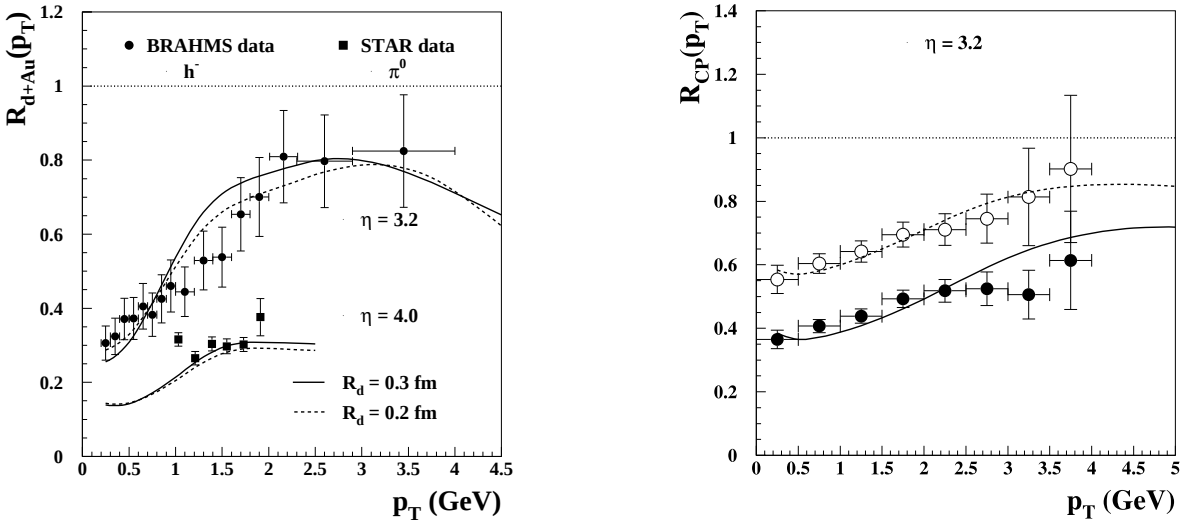


**Figure 3.** (Left) Ratio of $h^-$ and $\pi^0$ production rates in $d + Au$ and $p + p$ collisions as function of $p_T$ at pseudorapidity $\eta = 3.2$ and $\eta = 4$ vs. data from the BRAHMS [7] and STAR Collaborations [8], respectively. (Right) Ratio of negative particle production in central $(0 - 20\%)$ and semi-central $(30 - 50\%)$ to peripheral $(60 - 80\%)$ $d + Au$ collisions, shown by closed and open points respectively. Corresponding calculations [13] are depicted by solid and dashed curves.

### 3. Nuclear suppression of hadrons at RHIC

In 2004 the BRAHMS Collaboration [7] reported a significant suppression of $h^-$ at $\eta = 3.2$. Much stronger nuclear effects were found later on by the STAR Collaboration [8] for $\pi^0$ production at $\eta = 4$. All these data are consistent with model calculations [13] (see Fig. 3) including besides coherent phenomena also corrections for energy deficit Eq. (1). The onset of coherent effects alone cannot successfully describe a rise of nuclear effects with $y$. Namely corrections for energy

conservation reflecting much smaller survival probability $S(x)$ of a LRG at larger $x$ allows to describe data as is shown in Fig. 3.

## 4. Charmonium suppression at SPS and FNAL

Fig. 4 clearly demonstrates a strong suppression of charmonium production at large $x_F$ in the SPS (Left) and fixed target FNAL (Right) energy range where no shadowing effects are expected. This suppression represents another manifestation of the energy sharing problem in multiple initial state interactions Eq. (1) near the kinematic limit.

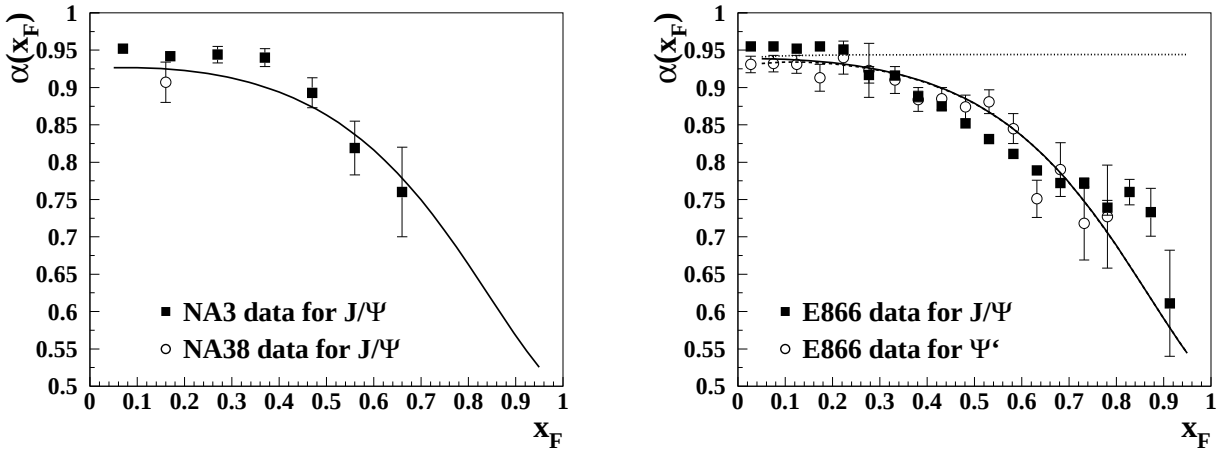


**Figure 4.** (Left) The exponent describing the A-dependence ($\propto A^{\alpha}$) of the nucleus-to-nucleon ratio for the charmonium production as a function of $x_F$ vs. NA3 data [3] at $E_{lab} = 158\,\mathrm{GeV}$. (Right) The exponent describing the A-dependence ($\propto A^{\alpha}$) of the nucleus-to-nucleon ratio for the charmonium production as a function of $x_F$ vs. E866 data [6] at $E_{lab} = 800\,\mathrm{GeV}$.

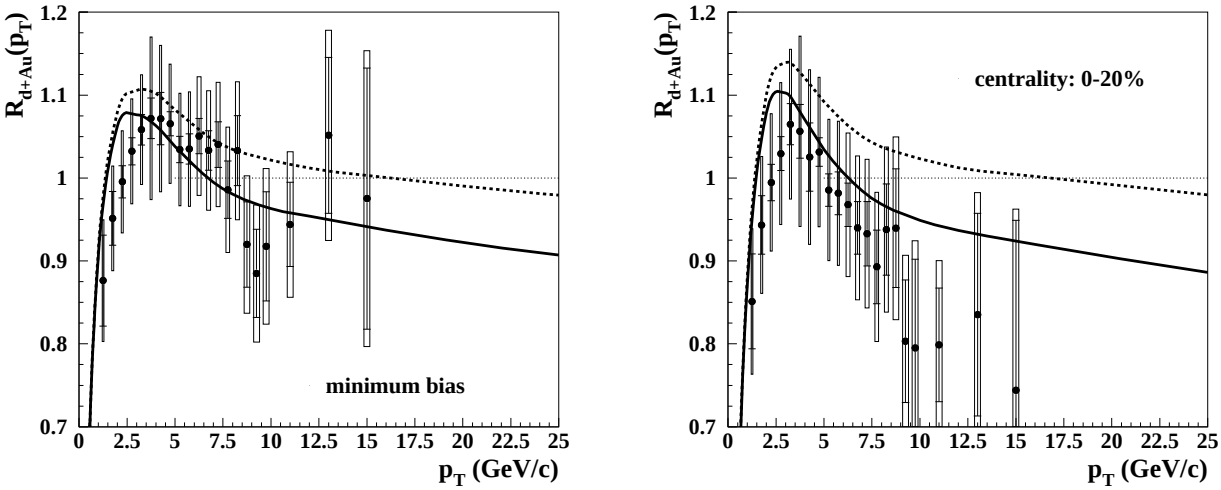


**Figure 5.** Nuclear attenuation factor for $\pi^0$ produced in $d + Au$ collisions at $\sqrt{s} = 200\,\mathrm{GeV}$ corresponding to minimum bias (Left) and centrality 0-20% (Right), respectively. Solid and dashed lines represent calculations [16] with and without corrections Eq. (1) for energy conservation, respectively. The data are from the PHENIX Collaboration [19].

## 5. Nuclear suppression at large $x_T$, central rapidity

Besides large $x_F$ one can approach the kinematic limit increasing $x_T = 2p_T/\sqrt{s}$. In this case again the energy conservation constraints Eq. (1) cause a nuclear suppression.

The $d$+$A$ to $p$+$p$ ratio was predicted correctly including also the Cronin effect at medium-high $p_T$ [18]. Assuming QCD factorization one expects that this ratio should approach one at large $p_T$ (with small corrections for isotopic effects). However, corrections for energy conservation Eq. (1) leads to a considerable suppression [16], which seems to be confirmed by data (see Fig. 5).

## 6. Direct photons at central rapidity

Assuming heavy ion collisions, production of prompt photons in a hard reaction should not be accompanied with any final state interaction, either energy loss, or absorption. Therefore, besides the Cronin enhancement at medium-high $p_T$ and small isotopic corrections at larger $p_T$ we should not expect any nuclear effects.

Unexpectedly, data from the PHENIX experiment [20] exhibit a significant suppression in $Au + Au$ collisions at large $p_T$ as is demonstrated in Fig. 6. No explanation for this behavior has been proposed so far. Central production of prompt photons with large $p_T$ at RHIC cannot be accompanied by coherent phenomena and is again a subject to the energy sharing problem.

In Fig. 6 the PHENIX data are compared also with model predictions [16] for the ratio $R_{Au+Au}$ as a function of $p_T$. If the factor Eq. (1) suppressing multiple interactions is excluded model calculations depicted by the dashed lines give a value $R_{Au+Au} \to 0.8$ in accord with onset of isotopic effects and cannot describe a suppression at large $p_T$ observed especially at $\sqrt{s} = 200\,\mathrm{GeV}$. Inclusion of corrections for energy conservation Eq. (1) leads to strong nuclear effects at large $p_T$ as is demonstrated by solid lines.

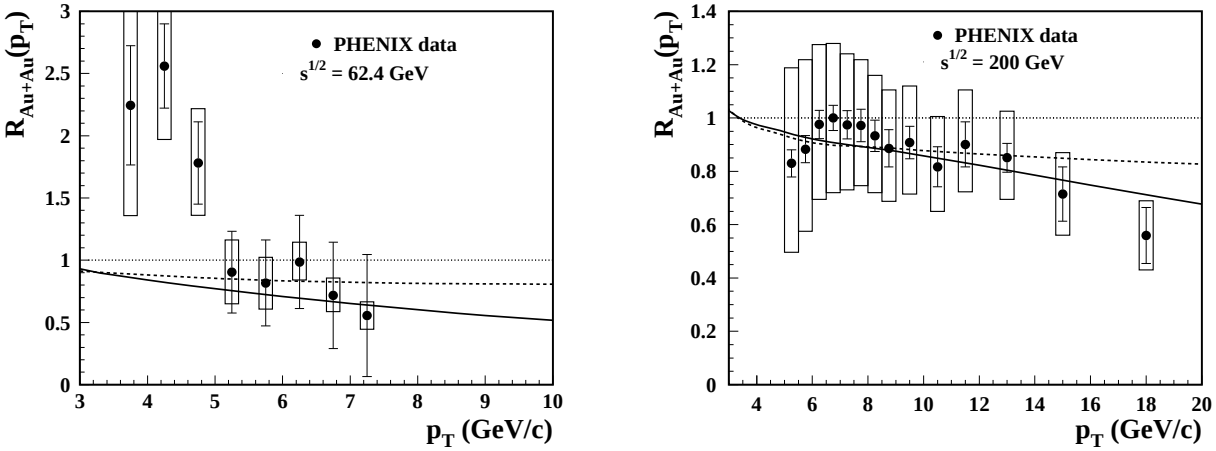


**Figure 6.** Nuclear modification factor for direct photon production in $Au + Au$ collisions at a centrality range $0 - 10\%$ and at $\sqrt{s} = 62\,\mathrm{GeV}$ (Left) and $\sqrt{s} = 200\,\mathrm{GeV}$ (Right) vs. PHENIX data [20]. Solid and dashed curves correspond to calculations [16] done with and without the corrections for energy deficit, the factor Eq. (1) suppressing multiple interactions, respectively.

## 7. Jet quenching in heavy ion collision

Large-$p_T$ hadrons produced in heavy ion collisions demonstrate a strong suppression, which surprisingly does not vanish at high $p_T$, but seems to be constant giving thus a rise to breakdown of QCD factorization. Corrections for energy conservation Eq. (1) should cause a considerable additional suppression which is stronger at larger $p_T$ compensating so an expected rise of $R_{AA}$ (see Fig. 7).

## 8. Summary

- Interpretation of a strong nuclear suppression in the forward rapidity region allowing to access smallest Bjorken $x$ should be presented with caution. Assuming that only gluon saturation induces the suppression observed at RHIC, one arrives at an astonishingly small amount of gluons in nuclei, which breaks down a bottom unitarity bound.
- Treating the nucleus to be an universal filter for different Fock components of the projectile hadron, one comes to factorization of soft and hard interactions. However, this is not the case at large either $x_F$ or $x_T$ where sharing of energy between the constituents becomes an issue and higher Fock components are resolved better.
- This effect can be treated as an effective energy loss proportional to initial energy.

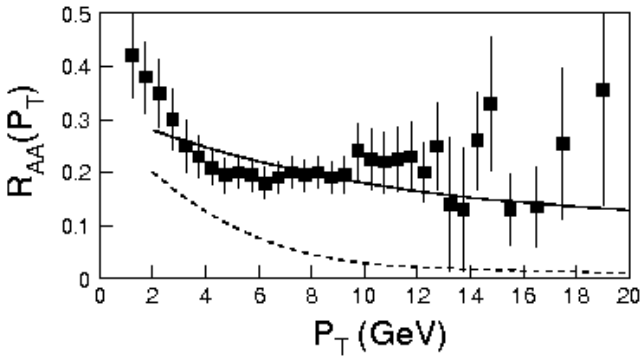


**Figure 7.** Pion suppression in $Au + Au$ central collisions as a function of $p_T$ at $\sqrt{s} = 200\,\mathrm{GeV}$ (solid line) and $\sqrt{s} = 5500\,\mathrm{GeV}$ (dashed line) vs. PHENIX data. Fig. taken from [21].

- Energy loss proportional to energy leads to a nuclear suppression at any energy, and predicts Feynman $x_F$ scaling of the suppression. This provides also an explanation for the longstanding puzzle of $J/\Psi$ suppression scaling in $x_F$.
- Besides large $x_F \to 1$ the kinematic limit can be approached also in transverse momentum increasing $x_T$. Similar effects of energy conservation are expected to be manifested. As a result, the Cronin enhancement of particle production at medium-high $p_T$ switches to a suppression at larger $p_T$. Such an unexpected effect demonstrating a violation of the QCD factorization seems to be confirmed by data for pion production in d+Au collisions at RHIC, and even for direct photons.
- Additional suppression coming from the effective energy loss effects represents significant corrections to all calculations for jet quenching.

**Acknowledgments**

This work was supported in part by the Slovak Funding Agency, Grant 2/0092/10 and by Grants VZ MŠMT 6840770039 and LC 07048 (Ministry of Education of the Czech Republic).

**References**

[1] Barton D S, et al. 1983 *Phys. Rev.* D **27** 2580; Geist W M 1991 *Nucl. Phys.* A **525** 149c; Beretvas A, et al. 1986 *ibid.* **34** 53; Binkley M, et al. 1976 *Phys. Rev. Lett.* **37** 571; Bailey R, et al. 1984 *Z. Phys.* C **22** 125; Skubic P, et al. 1978 *Phys. Rev.* D **18** 3115
[2] *NA49 Collaboration*, Boimska B 2004 *Ph.D. Dissertation* (Warsaw 2004) **CERN-THESIS-2004-035**
[3] *NA3 Collaboration*, Badier J, et al. 1983 *Z. Phys.* C **20** 101
[4] *NA38 Collaboration*, Abreu M C, et al. 1999 *Phys. Lett.* B **449** 128
[5] *E772 Collaboration*, Alde D M, at al. 1990 *Phys. Rev. Lett.* **64** 2479
[6] *E866 Collaboration*, Leitch M J, et al. 2000 *Phys. Rev.Lett.* **84** 3256
[7] *BRAHMS Collaboration*, Arsene I, et al. 2004 *Phys. Rev. Lett.* **93** 242303; Hongyan Yang, et al. 2007 *J. Phys.* G **34** S619
[8] *STAR Collaboration*, Adams J, et al. 2006 *Phys. Rev. Lett.* **97** 152302
[9] *ALICE Collaboration*, Alessandro G, et al. 2006 *J. Phys.* G **32** 1295
[10] Kharzeev D, Kovchegov Y V and Tuchin K 2004 *Phys. Lett.* B **599** 23
[11] *EPS08*, Eskola K, Paukkunen H and Salgado C 2008 *JHEP* **0807** 102
[12] Kopeliovich B Z, et al. 2009 *Phys. Rev.* C **79** 064906
[13] Kopeliovich B Z, et al. 2005 *Phys. Rev.* **C72** 054606; Nemchik J, et al. 2008 *Phys. Rev.* C **78** 025213
[14] Abramovsky A V, Gribov V N and Kancheli O V 1973 *Yad. Fiz.* **18** 595
[15] Nemchik J and Šumbera M 2009 *Nucl. Phys.* A **830** 611c
[16] Kopeliovich B Z and Nemchik J 2010 *arXiv:***1009.1162** [hep-ph]
[17] Kopeliovich B Z, Raufeisen J and Tarasov A V 2000 *Phys. Rev.* C **62** 035204
[18] Kopeliovich B Z, Nemchik J, Schäfer A and Tarasov A V 2002 *Phys. Rev. Lett.* **88** 232303
[19] *PHENIX Collaboration*, Adler S S, et al. 2007 *Phys. Rev. Lett.* **98** 172302
[20] *PHENIX Collaboration*, Isobe T, et al. 2007 *J. Phys.* G **34** S1015
*PHENIX Collaboration*, Sakaguchi T, et al 2008 *Nucl. Phys.* A **805** 355
[21] Kopeliovich B Z, Potashnikova I K and Schmidt I 2007 *arXiv:***0707.4302**; 2008 *J. Phys.* G **35** 054001

# Direct Photon Production in Proton-Nucleus and Nucleus-Nucleus Collisions

J. Cepila [a] J. Nemchik [a,b]

[a] *Czech Technical University in Prague, FNSPE, Břehová 7, 11519 Prague, Czech Republic*
[b] *Institute of Experimental Physics SAS, Watsonova 47, 04001 Košice, Slovakia*

**Abstract**

Prompt photons produced in a hard reaction are not accompanied with any final state interaction, either energy loss or absorption. Therefore, besides the Cronin enhancement at medium transverse momenta $p_T$ and small isotopic corrections at larger $p_T$, one should not expect any nuclear effects. However, data from PHENIX experiment exhibits a significant large-$p_T$ suppression in central $d+Au$ and $Au+Au$ collisions that cannot be accompanied by coherent phenomena. We demonstrate that such an unexpected result is subject to the energy sharing problem near the kinematic limit and is universally induced by multiple initial state interactions. We describe production of photons in the color dipole approach and find a good agreement with available data in $p+p$ collisions. Besides explanation of large-$p_T$ nuclear suppression at RHIC we present for the first time predictions for expected nuclear effects also in the LHC energy range at different rapidities. We include and analyze also a contribution of gluon shadowing as a leading twist shadowing correction modifying nuclear effects at small and medium $p_T$.

*Key words:* direct photons, nuclear suppression, gluon shadowing
*PACS:* 13.85.Qk, 24.85.+p, 25.75.-q, 25.75.Cj

## 1. Introduction

If a particle with mass $M$ and transverse momentum $p_T$ is produced in a hard reaction then the corresponding values of Bjorken variable in the beam and the target are $x_{1,2} = \sqrt{M^2+p_T^2}\, e^{\pm y}/\sqrt{s}$. Thus, forward rapidity region $y>0$ allows to study already at RHIC coherence phenomena (shadowing), which are expected to suppress particle yields.

Observed suppression at large $y$ at RHIC [1] should be interpreted carefully. Similar suppression is observed for any reaction studied so far at any energy. Namely, all fixed target experiments have too low energy for the onset of coherence effects. The rise of suppression with $y$ shows the same pattern as observed at RHIC.

This universality of suppression favors another mechanism which was proposed in [2] and is based on energy conservation effects in initial state parton rescatterings. As a result the effective projectile parton distribution correlates with the nuclear target [2,3] and can be expressed in term of the suppression factor, $S(x) \sim 1-x$ [2],

$$f_{q/N}^{(A)}\big(x,Q^2,\vec{b}\big) = C\, f_{q/N}\big(x,Q^2\big)\, exp\Big[-[1-S(x)]\,\sigma_{eff} T_A(\vec{b})\Big], \qquad (1)$$

*Email addresses:* jan.cepila@fjfi.cvut.cz, nemchik@saske.sk (J. Nemchik).

where $T_A(\vec{b})$ is the nuclear thickness function defined at impact parameter $\vec{b}$, $\sigma_{eff} = 20\,\mathrm{mb}$ [2] and the normalization factor $C$ is fixed by the Gottfried sum rule.

In this paper we study a production of direct photons on nuclear targets. Photons produced in a hard reaction have no final state interactions and so no nuclear effects are expected at large $p_T$. However, we show that large-$p_T$ photons are universally suppressed by energy deficit in multiple interactions Eq. (1) since the kinematic limit can be approached increasing $p_T$ at fixed $y$. We study also a rise of this suppression with $y$ in the RHIC and LHC kinematic regions.

## 2. The color dipole approach

The process of direct photon production in the target rest frame can be treated as radiation of a real photon by a projectile quark. The $p_T$ distribution of photon bremsstrahlung in quark-nucleon interactions reads [4]:

$$\frac{d\sigma(qN \to \gamma\, X)}{d(ln\,\alpha)\,d^2p_T} = \frac{1}{(2\pi)^2}\sum_{in,f}\int d^2r_1\,d^2r_2\,e^{i\vec{p}_T\cdot(\vec{r}_1-\vec{r}_2)}\Phi^{*\ T}_{\gamma q}(\alpha,\vec{r}_1)\Phi^T_{\gamma q}(\alpha,\vec{r}_2)\,\Sigma(\alpha,r_1,r_2) \quad (2)$$

where $\Sigma(\alpha,r_1,r_2) = \big\{\sigma_{\bar{q}q}(\alpha r_1)+\sigma_{\bar{q}q}(\alpha r_2)-\sigma_{\bar{q}q}(\alpha|\vec{r}_1-\vec{r}_2|)\big\}/2$, $\alpha = p^+_\gamma/p^+_q$ and the light-cone (LC) wave functions of the projectile $q+\gamma$ fluctuation $\Phi_{\gamma q}(\alpha,\vec{r})$ are presented in [4]. Feynman variable is given as $x_F = x_1 - x_2$ and in the target rest frame $x_1 = p^+_\gamma/p^+_p$. For the dipole cross section $\sigma_{\bar{q}q}(\alpha r)$ in Eq. (2) we used GBW [5] parametrization. The hadron cross section is given convolving the parton cross section, Eq. (2), with the corresponding parton distribution functions (PDFs) $f_q$ and $f_{\bar{q}}$ [4],

$$\frac{d\sigma(pp \to \gamma X)}{dx_F\,d^2p_T} = \frac{x_1}{x_1+x_2}\int\limits_{x_1}^{1}\frac{d\alpha}{\alpha^2}\sum_q Z_q^2\Big\{f_q\big(\frac{x_1}{\alpha},Q^2\big)+f_{\bar{q}}\big(\frac{x_1}{\alpha},Q^2\big)\Big\}\frac{d\sigma(qN\to\gamma X)}{d(ln\,\alpha)\,d^2p_T}, \quad (3)$$

where $Z_q$ is the fractional quark charge, PDFs $f_q$ and $f_{\bar{q}}$ are used with the lowest order parametrization from [6] at the scale $Q^2 = p^2_T$.

Assuming production of direct photons on nuclear targets the onset of coherence effets is controlled by the coherence length, $l_c = 2E_q\,\alpha(1-\alpha)/(\alpha^2\,m_q^2 + p_T^2)$, where $E_q = x_q s/2m_N$ and $m_q$ is the energy and mass of the projectile quark. The fraction of the proton momentum $x_q$ carried by the quark is related to $x_1$ as $\alpha x_q = x_1$.

The condition for the onset of shadowing is a long coherence length (LCL), $l_c \gtrsim R_A$, where $R_A$ is the nuclear radius. Then the color dipole approach allows to incorporate shadowing effects via a simple eikonalization of $\sigma_{\bar{q}q}(x,r)$ [7], i.e. replacing $\sigma_{\bar{q}q}(x,r)$ in Eq. (2) by $\sigma^A_{\bar{q}q}(x,r) = 2\int d^2b\,\big\{1-\big[1-\frac{1}{2\,A}\,\sigma_{\bar{q}q}(x,r)\,T_A(b)\big]^A\big\}$. This LCL limit can be safely used in calculations of nuclear effects in the RHIC and LHC energy regions especially at forward rapidities. Here higher Fock components containing gluons lead to additional corrections, called gluon shadowing (GS). The corresponding suppression factor $R_G$ [8] was included in calculations replacing $\sigma_{\bar{q}q}$ by $R_G\,\sigma_{\bar{q}q}$ in the above expression for $\sigma^A_{\bar{q}q}(x,r)$.

## 3. Predictions for nuclear effects

We start with production of direct photons in $p+p$ collisions. The left panel of Fig. 1 shows model calculations based on Eq. (3) using GRV98 PDFs [6] and demonstrates so a reasonable agreement with data from PHENIX experiment [9]. Another test of the model is a comparison with PHENIX data [10] obtained in $d+Au$ collisions as is depicted in the

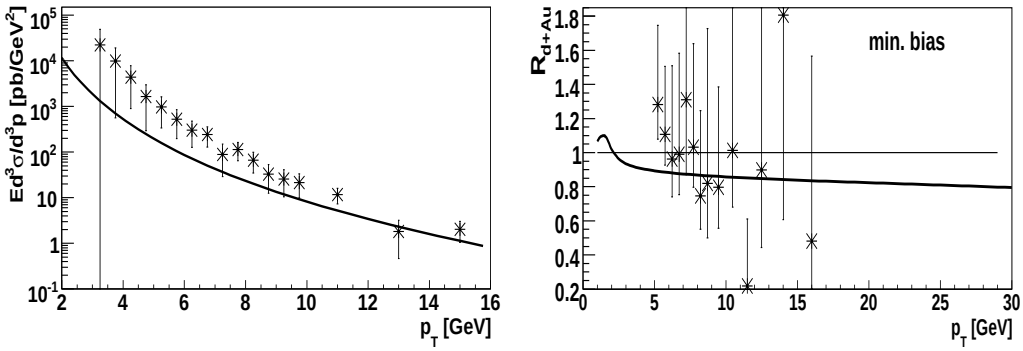


Fig. 1. (Left) Invariant cross section for direct photon production in $p+p$ collisions at $y=0$ as a function of $p_T$ vs. data from PHENIX experiment [9]. (Right) Ratio of the cross sections in $d+Au$ to $p+p$ collisions $R_{d+Au}(p_T)$ at $\sqrt{s_{NN}}=200\,\mathrm{GeV}$ vs. preliminary data from PHENIX experiment [10].

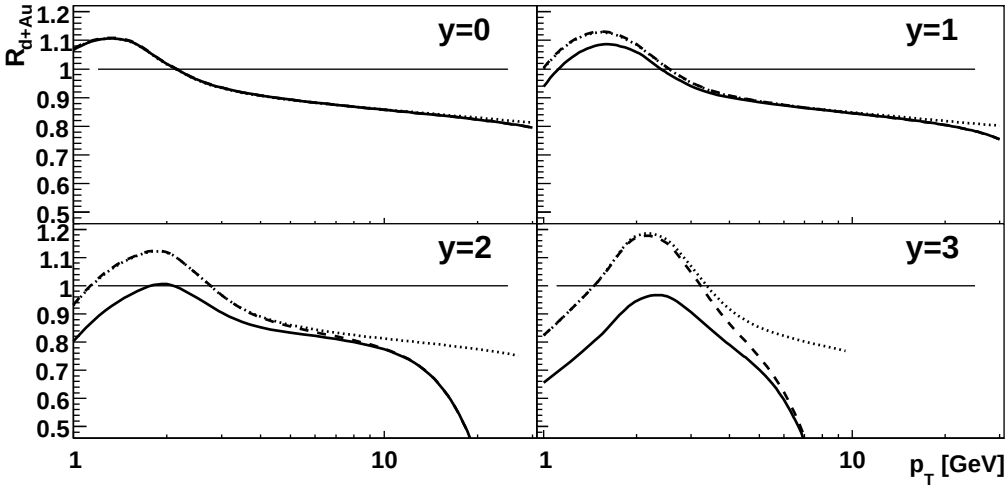


Fig. 2. Ratio of the cross sections in $d+Au$ to $p+p$ collisions $R_{d+Au}(p_T)$ at $\sqrt{s_{NN}}=200\,\mathrm{GeV}$ and at different fixed values of $y=0$, 1, 2 and 3. Dotted lines represent calculations without corrections for energy conservation and GS. Dashed lines additionally include corrections for energy deficit Eq. (1) and solid lines also GS.

right panel of Fig. 1. Besides isotopic effects giving a value $R_{d+Au}\sim 0.83$ at large $p_T$, we predict also an additional suppression coming from corrections for energy conservation Eq. (1).

Since one can approach the kinematic limit increasing $p_T$ we present predictions for nuclear effects at several fixed $y$ as $p_T$ dependence of the nuclear modification factor $R_{d+Au}$ at RHIC energy depicted in Fig. 2 and $R_{p+Pb}$ at LHC energy depicted in Fig. 3. All these Figs. clearly demonstrate a dominance of GS at small and medium $p_T$ and energy conservation effects Eq. (1) at large $p_T$. Both effects rise rapidly with $y$. Note that unexpected large-$p_T$ suppression violating so QCD factorization can be tested in the future by the new data from RHIC and LHC experiments especially at forward rapidities.

The same mechanism allows to explain also large-$p_T$ suppression of photons produced in $Au+Au$ collisions at the energies $\sqrt{s_{NN}}$ =200 and 62 GeV in accordance with data from PHENIX experiment [11]. Corresponding results can be found in [3]. Large error bars of the data do not allow to provide a definite confirmation for the predicted suppression.

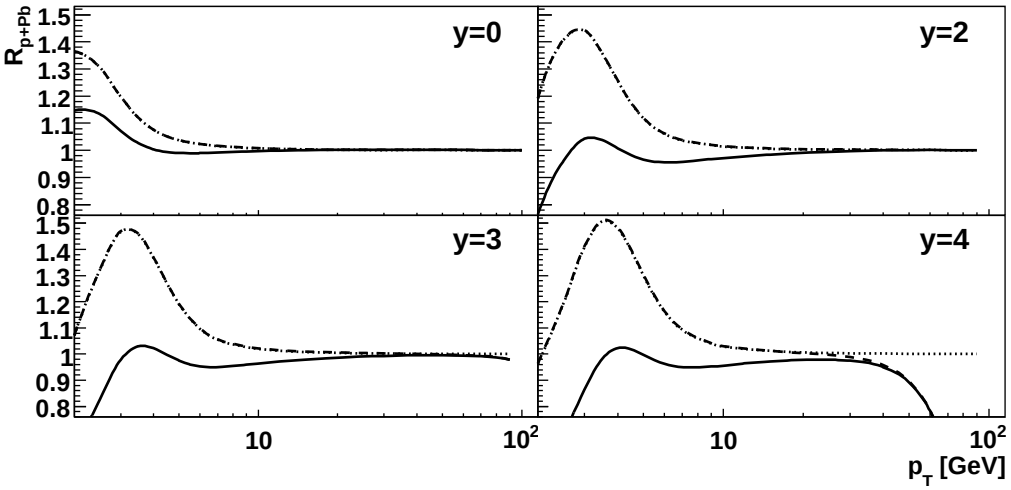


Fig. 3. The same as Fig. 2 but for the ratio $R_{p+Pb}(p_T)$ at $\sqrt{s_{NN}} = 5.5\,\mathrm{TeV}$ and at fixed $y$ =0, 2, 3 & 4.

## 4. Summary

Using the color dipole approach we study production of direct photons in collisions on nuclear targets. We demonstrate that at fixed rapidities effects of coherence (GS) dominate at small and medium $p_T$ whereas corrections for energy conservation Eq. (1) are important at larger $p_T$. Both effects cause a suppression and rise rapidly with rapidity.

First we test this approach in the RHIC kinematic region demonstrating a good agreement with PHENIX data in $p+p$ and $d+Au$ collisons at mid rapidities (see Fig. 1).

Then we present predictions for $p_T$ behavior of nuclear effects at different fixed rapidities in the RHIC and LHC kinematic regions. Since photons have no final state interactions, no suppression is expected at large $p_T$. However, we specify for the first time the kinematic regions at RHIC and LHC where one can expect and study in the future a rather strong $p_T$-suppression, which is caused by energy sharing problem Eq. (1).

The same mechanism explains well also a strong suppression at large $p_T$ observed in $Au+Au$ collisions at RHIC in accordance with data from PHENIX experiment.


## Acknowledgements

This work was supported by the Slovak Funding Agency, Grant 2/0092/10 and by Grants VZ MŠMT 6840770039 and LC 07048 (Ministry of Education of the Czech Rep.).


## References


[1] I. Arsene et al., [BRAHMS Collaboration], *Phys. Rev. Lett.* **93**, 242303 (2004); Hongyan Yang et al., *J. Phys.* G**34**, S619 (2007).

[2] B.Z. Kopeliovich et al., *Phys. Rev.* C**72**, 054606 (2005); J. Nemchik et al., *Phys. Rev.* C**78**, 025213 (2008).

[3] B.Z. Kopeliovich and J. Nemchik, *J. Phys.* G**38**, 043101 (2011); arXiv:**1009.1162**[hep-ph].

[4] B.Z. Kopeliovich, A. Schäfer and A.V. Tarasov, *Phys. Rev.* C**59**, 1609 (1999).

[5] H. Kowalski, L. Motyka and G. Watt, *Phys. Rev.* D**74**, 074016 (2006).

[6] M. Gluck, E. Reya and A. Vogt, [GRV98], *Eur. Phys. J.* C**5**, 461 (1998).

[7] A.B. Zamolodchikov, B.Z. Kopeliovich and L.I. Lapidus, *Sov. Phys. JETP Lett.* **33**, 595 (1981).

[8] B.Z. Kopeliovich, J. Nemchik, A. Schäfer and A. Tarasov, *Phys. Rev.* C**65**, 035201 (2002).

[9] S.S. Adler et al., [PHENIX Collaboration], *Phys. Rev. Lett.* **98**, 012002 (2007).

[10] D. Peressounko et al., [PHENIX Collaboration], *Nucl. Phys.* A**783**, 577 (2007).

[11] T. Isobe et al., [PHENIX Collaboration], *J. Phys.* G**34**, S1015 (2007); T. Sakaguchi et al., [PHENIX Collaboration], *Nucl. Phys.* A**805**, 355 (2008).

# Calculation of Direct photon production in nuclear collisions

**J Cepila**

E-mail: jan.cepila@fjfi.cvut.cz

**Abstract.** Prompt photons produced in a hard reaction are not expected to be accompanied by any final state interaction, either energy loss or absorption and one should not expect any nuclear effects at high $p_T$. However, data from the PHENIX experiment indicates large-$p_T$ suppression in d+Au and central Au+Au collisions that cannot be accompanied by coherent phenomena. We propose a mechanism based on the energy sharing problem at large $p_T$ near the kinematic limit that is induced by multiple initial state interactions and that improves the agreement of calculations with PHENIX data. We calculate inclusive direct photon production cross sections in p+p collisions at RHIC and LHC energies using the color dipole approach without any additional parameter. Our predictions are in good agreement with the available data. Within the same framework, we calculate direct photon production rates in d+A and A+A collisions at RHIC energy. We also provide predictions for the same process in p+A collisions at LHC energy. Since the kinematic region where the expected suppression manifests can be achieved also at forward rapidity, we present a comparison of forward rapidity to midrapidity behaviour. We also include and analyze the contribution of gluon shadowing as a leading twist shadowing correction that modifies nuclear effects especially at small $p_T$.

## 1. Introduction

It is known for a long time that the cross section of the particle production in proton-nucleus collisions is not equal to A times the cross section of the particle production in proton-proton collisions, where A is the mass number of a nucleus. The ratio of these two cross sections is called nuclear modification factor and the deviation of this quantity from unity is a measure of nuclear effects. The suppression of the production rate in the region of high Feynman $x_F$ was first observed in BRAHMS experiment at RHIC collider[1] for the charged hadron production, but later was rediscovered in NA49 experiment at SPS[2] for the pion production and even in E772 experiment at FNAL[3] for the dilepton production. Coherence phenomena(shadowing) are expected to be responsible for the suppression, but one has to interpret it carefully. If a particle with mass $M$ and transverse momentum $p_T$ is produced in a hard reaction with pseudo-rapidity $\eta$ then the corresponding values of Bjorken variable in the beam and the target are

$$x_{1,2} = \frac{\sqrt{M^2 + p_T^2}}{\sqrt{s}} e^{\pm\eta} \qquad x_F = x_1 - x_2$$

and the region, where coherence phenomena are expected to be strongest, corresponds to forward pseudo-rapidity for energies accessible at RHIC. As a result coherence effects exhibit the $x_2$ scaling, but as shown in [4] this scaling is known to be broken. The fact, that the suppression has been also observed at any reaction studied so far at any energy suggest that the effect which suppresses particle yields has to be energy independent and as shown in [4] or [5] has to scale with $x_F$. Such mechanism was formulated in [5, 6] as energy conservation restrictions in the multiple parton rescattering inside the nuclear medium.

In this paper a production of direct photons on nuclear targets is studied. Photons produced in a hard reaction have no final state interactions and so no nuclear effects are expected at high-$p_T$. However, we show that high-$p_T$ photons are universally suppressed by energy deficit in multiple interactions. We study also a rise of this suppression with $\eta$ in RHIC and LHC kinematic regions.

## 2. Energy conservation restrictions in multiple interactions within the color dipole approach calculation

For the calculation of direct photon production cross section, the light-cone color dipole approach is used. The production mechanism is formulated in the rest frame of the target, where the photon emission is treated as bremsstrahlung radiation of a real photon by a projectile quark. On a partonic level, the quark from the incident hadron can fluctuate into the coherent state $|q\gamma>$ of a quark and a photon with the transverse separation $\rho$ where the quark and the photon carries a fraction of the incident momenta $p_q$ of the magnitude of $(1-\alpha)p_q$ and $\alpha p_q$ respectively. The coherence of the fluctuation is disrupted after the coherence length by the interaction with the color field of the target nucleon. The cross section on a partonic level can be calculated[7] as a convolution of the perturbativelly calculated light-cone wave function $\Psi_{\gamma q}(\alpha, \rho)$[8] that describes the probability to produce the fluctuation of the transverse separation $\rho$ and the completely nonperturbative dipole cross section $\sigma^N_{q\bar{q}}(\rho, x)$ of the interaction between the fluctuation and the color field of the nucleon which are obtained from fits to HERA data on the deep inelastic scattering

$$\frac{d\sigma(qN \to \gamma X)}{dln\alpha d^2p_T} = \frac{1}{(2\pi)^2} \sum_{in,f} \int d^2\rho_1 d^2\rho_2 e^{-i\vec{p}_T(\vec{\rho}_1 - \vec{\rho}_2)} \Psi^{*T}_{\gamma q}(\alpha, \rho_1) \Psi^T_{\gamma q}(\alpha, \rho_2) \Sigma(\alpha, \rho_1, \rho_2)$$

$$\Sigma(\alpha, \rho_1, \rho_2) = \frac{1}{2}(\sigma^N_{\bar{q}q}(\alpha\rho_1) + \sigma^N_{\bar{q}q}(\alpha\rho_2) - \sigma^N_{\bar{q}q}(\alpha|\vec{\rho}_1 - \vec{\rho}_2|)),$$

where $\alpha = p^+_\gamma / p^+_q$. In our calculation the GBW approximation to the dipole cross section was used[9]. Consequently, the cross section for the proton - proton collisions on the hadronic level is

$$\frac{d\sigma(pp\to\gamma X)}{d^2p_T}=\frac{x_1}{x_1+x_2}\int_{x_1}^1\frac{d\alpha}{\alpha^2}\sum_q Z_q^2\left(f_q\left(\frac{x_1}{\alpha},Q^2\right)+f_{\bar{q}}\left(\frac{x_1}{\alpha},Q^2\right)\right)\frac{d\sigma(qN\to\gamma X)}{dln\alpha d^2p_T},$$

where $Z_q$ is the fractional quark charge and the structure function is composed of parton distribution functions $f_{q,\bar{q}}$ from the GRV98 parametrization[10] at the lowest order at the scale $Q^2=p_T^2$.

For the calculation of the cross section on the nuclear target, one has to discuss the coherence length of the fluctuation. It can be expressed as

$$l_c=\frac{2E_q\alpha(1-\alpha)}{\alpha^2m_q^2+p_T^2}\qquad E_q=\frac{x_1s}{2m_N\alpha},$$

where $m_q$ and $m_N$ is the mass of the projectile quark and nucleon respectively. The limit of the long coherence length(LCL) corresponds to the situation where the coherence length is longer than the nuclear radius $R_A$. The fluctuation arises long before the quark enters the nucleus and is subject to maximal quark shadowing. Since the transverse size of the fluctuation is "frozen" through the propagation inside the nucleus, different transverse configurations form eigenstates of the interaction in the impact parameter space and the cross section can be eikonalized using the Glauber approximation[11]

$$\sigma_{q\bar{q}}^N(\rho,x)\to\sigma_{q\bar{q}}^A(\rho,x)=2\int d^2b\left(1-\left(1-\frac{1}{2A}\sigma_{q\bar{q}}^N(\rho,x)T_A(b)\right)^A\right),$$

where $T_A(b)$ is the nuclear thickness function. This LCL limit can be safely used in calculations of nuclear effects in RHIC and LHC energy domains especially at forward rapidities. Here higher Fock components containing gluons lead to additional corrections called gluon shadowing (GS). The corresponding suppression factor $R_G$ [12] was included in calculations replacing $\sigma_{q\bar{q}}$ by $R_G\sigma_{q\bar{q}}$.

The suppression mechanism can be understood via the survival probability of the large rapidity gap in multiple interactions inside the nucleus. One can see any hard process in the limit $x_1\to 1$ as the large rapidity gap process. The produced particle takes most of the momenta leaving only the small rapidity interval $\Delta y=-ln(1-x_1)$ for the others. The probability to radiate no gluons in the interval $\Delta y$ is suppressed by Sudakov form factor derived in [13] as $S(x_1)\sim 1-x_1$. The suppression at $x_1\to 1$ can be formulated such that each of the multiple interactions of projectile partons with the nucleus produces an extra factor $S(x_1)$. Corresponding weight factors are related to the Glauber coefficients via Abramovski-Gribov-Kancheli cutting rules [14]. Resuming over the number of scatterings leads to effective parton distribution function[5, 15]

$$f_{q/N}^A(x_1,Q^2)=Cf_{q/N}(x_1,Q^2)e^{-(1-S(x_1))\sigma_{eff}T_A(b)}$$

that correlates with the target and predicts the breakdown of the QCD factorization. The normalization factor $C$ is fixed by Gottfried sum rules and the effective cross section is calculated in [13].

## 3. Predictions for nuclear effects

First, the cross sections of direct photons in p + p collisions at midrapidity is shown for RHIC and LHC energy. Since there are no relevant data available from LHC yet, the reasonable agreement with data is presented only on PHENIX experiment data(see Fig. 1).

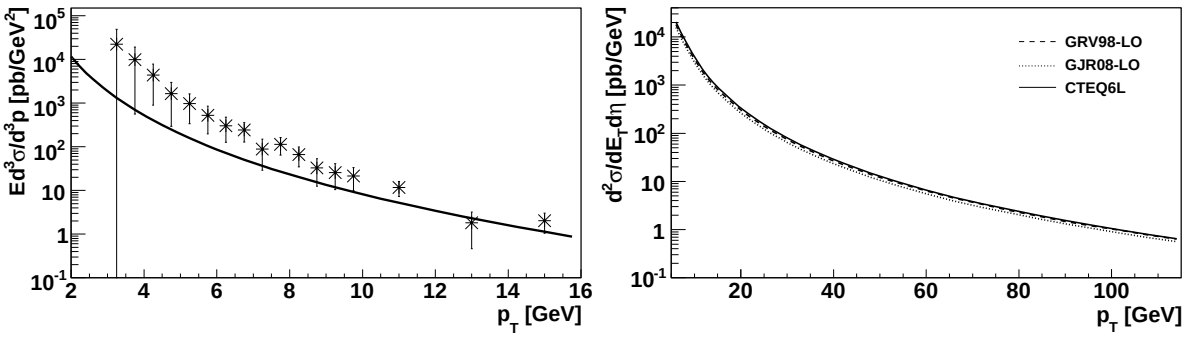


**Figure 1.** Invariant cross section for direct photon production in p + p collisions at y = 0 at energy of (left) RHIC vs. data from PHENIX experiment[16] (right) LHC for different PDF parametrizations[10, 17, 18]

Since one can approach the kinematic limit by increasing $p_T$, predictions for nuclear effects at several fixed y for the nuclear modification factor $R_{d+Au}$ at RHIC energy and $R_{p+Pb}$ at LHC energy is presented.

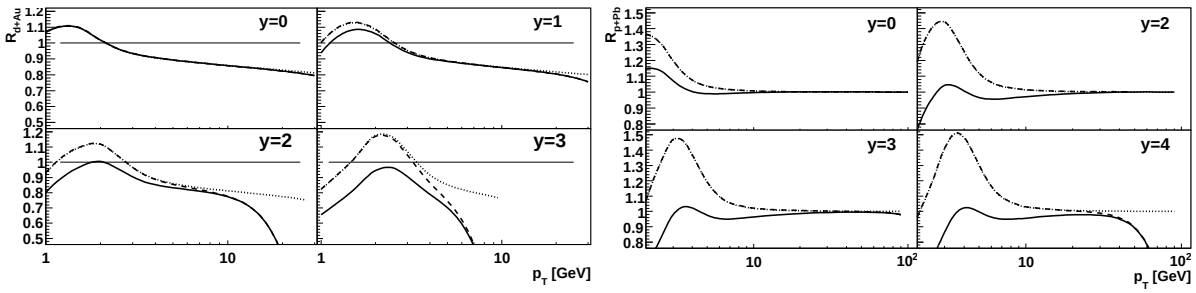


**Figure 2.** Ratio of the cross sections in (left) d + Au to p + p collisions at $\sqrt{s}$ = 200 GeV (right) p + Pb to p + p collisions at $\sqrt{s}$ = 5,5 TeV and at different values of rapidity. Dotted lines represent calculations without corrections for energy conservation and GS. Dashed lines additionally include corrections for energy deficit and solid lines also GS.

All these figures clearly demonstrate dominance of GS at small and medium $p_T$ and energy conservation effects at high $p_T$. Both effects rise rapidly with y. Note that unexpected high $p_T$ suppression violating QCD factorization can be tested in the future by new data from RHIC and LHC experiments especially at forward rapidities.

## 4. Summary

Using the color dipole approach the study of production of direct photons in collisions on nucleon and nuclear targets is presented. The unified approach to large $x_1$ nuclear

suppression based on energy conservation effects in multiple parton rescattering is discussed. This effect clearly dominates the high $p_T$ region of the production rate mainly at forward rapidity(up to small izotopic corrections in d + Au). Also coherence effects(GS) are demonstrated to be dominant at small and medium $p_T$. Both effects cause a suppression and rise rapidly with rapidity. First this approach is tested in RHIC kinematic region demonstrating a good agreement with PHENIX data in p + p at midrapidity and also predictions in the LHC kinematic region is presented. Then predictions for $p_T$ behavior of nuclear effects at different fixed rapidities are presented in RHIC and LHC kinematic regions. Quite strong suppression is observed at high $p_T$ in all kinematic regions and it can be tested by future data from LHC and RHIC experiments.

**Acknowledgments**
This work was supported by grant MSMT LC07048 (Czech Ministry of Education)

## References

[1] BRAHMS, Phys. Rev. Lett. 91, 072305 (2003)
[2] B. Boimska, CERN-THESIS-2004-035
[3] E772 Collaboration, Phys. Rev. Lett. 64, 2479 (1990)
[4] PHENIX Collaboration, Phys. Rev. C77, 0214912 (2008)
[5] B.Z.Kopeliovich et al. Phys. Rev. C72,054606 (2005)
[6] J.Nemchik et al.,Phys. Rev. C78, 025213 (2008)
[7] B.Z. Kopeliovich, A. Schafer and A.V. Tarasov, Phys. Rev. C59, 1609 (1999)
[8] S.J.Brodsky, A.Hebecker, E.Quack, Phys. Rev. D55, 2584 (1997)
[9] K.J.Golec-Biernat and M.Wusthoff, Phys. Rev. D60, 114023 (1999)
[10] M.Gluck, E.Reya, A.Vogt, Z. Phys. C67, 433 (1995)
[11] A.B. Zamolodchikov, B.Z. Kopeliovich and L.I. Lapidus, Sov. Phys. JETP Lett. 33, 595 (1981)
[12] B.Z. Kopeliovich, J. Nemchik, A. Sch fer and A. Tarasov, Phys. Rev. C65, 035201 (2002)
[13] B.Z.Kopeliovich, J.Nemchik, I.K.Potashnikova, M.B.Johnson and I.Schmidt, Nucl. Phys. Proc. Suppl. 146, 171 (2005)
[14] V.A.Abramovsky, V.N.Gribov and O.V.Kancheli, Yad. Fiz. 18, 595 (1973) [Sov. J. Nucl. Phys. 18, 308 (1974)]
[15] J. Nemchik et al., Phys. Rev. C78, 025213 (2008)
[16] S.S. Adler et al., [PHENIX Collaboration], Phys. Rev. Lett. 98, 012002 (2007)
[17] M. Gluck, P. Jimenez-Delgado and E. Reya, Eur. Phys. J. C 53 (2008) 355
[18] J. Pumplin, D. R. Stump, J. Huston, H. L. Lai, P. Nadolsky, W. K. Tung, JHEP 0207:012(2002)

EPJ Web of Conferences will be set by the publisher
DOI: will be set by the publisher


# Direct photons at large $p_T$: from RHIC to LHC

J. Cepila[1, a] and J. Nemchik[1,2, b]

[1] *Czech Technical University in Prague, FNSPE, Brehova 7, 11519 Prague, Czech Republic*
[2] *Institute of Experimental Physics SAS, Watsonova 47, 04001 Kosice, Slovakia*

**Abstract.** Using the color dipole formalism we study production of direct photons in proton-nucleus and nucleus-nucleus collisions at energies corresponding to RHIC and LHC experiments. Prompt photons produced in a hard reaction are not accompanied with any final state interaction, either energy loss or absorption. Therefore, in the RHIC energy range besides small isotopic corrections one should not expect any nuclear effects at large $p_T$. However, data from the PHENIX experiment indicates a significant large-$p_T$ suppression in $d+Au$ and central $Au+Au$ collisions that cannot be accompanied by coherent phenomena. We demonstrate that such an unexpected result is subject to the energy sharing problem universally induced by multiple initial state interactions (ISI) at large $p_T$ and/or at forward rapidities. In the LHC kinematic region ISI corrections are irrelevant at mid rapidities but cause rather strong suppression at forward rapidities. We present for the first time predictions for expected nuclear effects at large $p_T$ in $p + Pb$ and $Pb + Pb$ collisions at different rapidities. We include and analyze also a contribution of coherent effects associated with gluon shadowing modifying nuclear effects predominantly at small and medium-high $p_T$.

## 1 Introduction

Direct photons can serve as a valuable tool to study properties of nuclear collisions, since they are not accompanied by any final state interaction, either energy loss, or absorption. Therefore, no nuclear effects are expected, besides the Cronin enhancement and small isotopic corrections.

Nuclear effects are usually studied through the nucleus-to-nucleon ratio, the so called nuclear modification factor, $R_A(p_T) = \sigma_{p+A\to\gamma+X}(p_T)/A\,\sigma_{p+p\to\gamma+X}(p_T)$ for $p + A$ collisions and $R_{A+B}(p_T) = \sigma_{A+B\to\gamma+X}(p_T)/AB\,\sigma_{p+p\to\gamma+X}(p_T)$ for $A+B$ collisions, where $A$ and $B$ are corresponding mass numbers.

The Cronin enhancement of particle production, when the ratio $R_A(p_T) > 1$ at medium-high $p_T$, was studied in [1] within the color dipole formalism. Predicted magnitude and the shape of this effect was confirmed later by the PHENIX data [2] at RHIC and recently by the ALICE experiment [3] at LHC. However, none from other models presented in [4] was able to describe successfully the last ALICE data [3].

At large $p_T$ the PHENIX data [2, 5, 6] clearly indicate a significant suppression at midrapidity ($\eta = 0$), $R_{dAu}(p_T) < 1$, $R_{AuAu}(p_T) < 1$, that can not be interpreted, besides isotopic corrections, by a weak onset of coherent phenomena (shadowing, Color Glass Condensate (CGC)). Moreover, the BRAHMS and STAR data [7] exhibit much stronger suppression at forward rapidities allowing to reach much smaller target Bjorken $x = p_T e^{-\eta}/\sqrt{s}$, where $\sqrt{s}$ is c.m. energy, and investigate so a stronger onset of coherent phenomena. However, interpretations of large-$\eta$ suppression at RHIC and

a. e-mail: jan.cepila@fjfi.cvut.cz
b. e-mail: nemchik@saske.sk

LHC via assumption that CGC is the dominant source of suppression leads to severe problems with understanding of a wider samples of data at smaller energies (see examples in [8]) where no coherence effects are possible.

Besides coherence effects another mechanism, which is not related to coherence and is valid at any energy, was proposed in [8] and applied for description of various processes in $p(d) + A$ interactions [9] and in heavy ion collisions [10]. This mechanism is responsible for a significant suppresion at $\xi \to 1$, where $\xi = \sqrt{x_F^2 + x_T^2}$ with Feynman $x_F$ and variable $x_T = 2p_T/\sqrt{s}$. Dissipation of energy due to initial state interactions (ISI) [8] leads to breakdown of the QCD factorization at large $\xi$ and to a modification of the proton structure function $F_2^p$ in Eq. (3) replacing the parton distribution function (PDF) by the nuclear modified one, $f_{q(\bar{q})/N}(x, Q^2) \Rightarrow f^{(A)}_{q(\bar{q})/N}(x, Q^2, b)$, where

$$f^{(A)}_{q(\bar{q})/N}(x, Q^2, b) = C_N f_{q(\bar{q})/N}(x, Q^2) \frac{e^{-\xi \sigma_{eff} T_A(b)} - e^{-\sigma_{eff} T_A(b)}}{(1-\xi)\left(1 - e^{-\sigma_{eff} T_A(b)}\right)} \qquad \text{with} \qquad \sigma_{eff} = 20\, mb\,, \tag{1}$$

where $T_A(b)$ is the nuclear thickness function at a given impact parameter $b$ and the normalization factor $C_N$ is fixed by the Gottfried sum rule.

## 2 Direct photons via color dipole formalism

In the color dipole formalism the process of direct photon production is treated in the target rest frame [11] as radiation of a real photon by a projectile quark. The corresponding $p_T$ distribution of the photon bremmstrahlung in quark-nucleon interactions can be expressed in terms of the light-cone (LC) wave functions of the projectile $q+\gamma$ fluctuation $\Psi_{\gamma q}(\alpha, \vec{\rho})$ and the dipole cross section $\sigma^N_{q\bar{q}}(\alpha\rho, x)$ [11]:

$$\frac{d\sigma(qN \to \gamma X)}{d\ln\alpha d^2 p_T} = \frac{1}{(2\pi)^2} \int \sum_{in,f} d^2\rho_1\, d^2\rho_2\, e^{i\vec{p}_T\cdot(\vec{\rho}_1 - \vec{\rho}_2)}\, \Psi^*_{\gamma q}(\alpha, \vec{\rho}_1)\, \Psi_{\gamma q}(\alpha, \vec{\rho}_2)\, \Sigma(\alpha, \rho_1, \rho_2, x_2) \tag{2}$$

where $\Sigma(\alpha, \rho_1, \rho_2, x) = \{\sigma^N_{\bar{q}q}(\alpha\rho_1, x) + \sigma^N_{\bar{q}q}(\alpha\rho_2, x) - \sigma^N_{\bar{q}q}(\alpha(\vec{\rho}_1 - \vec{\rho}_2, x))\}/2$, $\alpha = p^+_\gamma/p^+_q$ is a fraction of quark LC momenta taken by the photon and Bjorken variables $x_1$ and $x_2$ are linked with the Feynman variable as $x_F = x_1 - x_2$ with $x_1 = p^+_\gamma/p^+_p$ in the target rest frame. For the dipole cross-section $\sigma^N_{q\bar{q}}(\alpha\rho, x)$ in Eq. (2) we used the parametrization from [12]. The hadronic cross-section reads [11],

$$\frac{d\sigma(pp \to \gamma X)}{dx_1 d^2 p_T} = \frac{1}{x_1 + x_2} \int_{x_1}^1 \frac{d\alpha}{\alpha} F_2^p\left(\frac{x_1}{\alpha}, Q^2\right) \frac{d\sigma(qN \to \gamma X)}{d\ln\alpha d^2 p_T}, \tag{3}$$

where $F_2^p(x, Q^2) = \sum\limits_q Z_q^2 (x f_{q/N}(x, Q^2) + x f_{\bar{q}/N}(x, Q^2))$ is the proton structure function at the scale $Q^2 = p_T^2$, $Z_q$ is a fractional quark charge and $f_{q/N}$ resp. $f_{\bar{q}/N}$ are parton distribution functions with GRV98 parametrization from [13].

The dynamics of direct photon production on nuclear targets is controlled by the mean coherence length, $l_c = \left\langle \frac{2E_q\alpha(1-\alpha)}{\alpha^2 m_q^2 + p_T^2} \right\rangle_\alpha$, where $E_q = x_q s/2m_N$ and $m_q$ is the energy and mass of the projectile quark and the fraction of the proton momentum $x_q$ carried by the quark is related to $x_1$ as $x_q = x_1/\alpha$. The condition for the onset of shadowing is that the coherence length exceeds the nuclear radius $R_A$, $l_c \gtrsim R_A$. This long coherence length (LCL) limit can be safely used in calculations for the RHIC and LHC energy regions especially at forward rapidities and allows to incorporate shadowing effects via eikonalization of $\sigma^N_{\bar{q}q}(\rho, x)$ [14], i.e. replacing in Eq. (2)

$$\sigma^N_{\bar{q}q} \Rightarrow \sigma^A_{\bar{q}q} = 2\int d^2 s\, \sigma^A_{\bar{q}q}(\vec{s}) \qquad \sigma^A_{\bar{q}q}(\vec{s}) = \left(1 - \left(1 - \frac{1}{2A}\sigma^N_{\bar{q}q} T_A(\vec{s})\right)^A\right) \qquad \text{for } p + A \text{ collisions}\,, \tag{4}$$

$$\sigma^{N}_{\bar{q}q} \Rightarrow \sigma^{AB}_{\bar{q}q} = \int d^2b\, d^2s\, \left\{\sigma^{B}_{\bar{q}q}(\vec{s})\, T_A(\vec{b}-\vec{s}) + \sigma^{A}_{\bar{q}q}(\vec{b}-\vec{s})\, T_B(\vec{s})\right\} \qquad \text{for heavy ion collisions}\,. \quad (5)$$

In the LCL limit higher Fock components containing gluons become imporartant and lead to additional corrections, called gluon shadowing (GS). The corresponding attenuation factor $R_G$ [15] can be incorporated using substitution $T_A(\vec{s}) \Rightarrow T_A(\vec{s})\, R_G(x_2, Q^2, A, \vec{s})$ in Eq. (4) for $p+A$ interactions and substitutions $T_B(\vec{s}) \Rightarrow T_B(\vec{s})\, R_G(x_2, Q^2, B, \vec{s})$ and $T_A(\vec{b}-\vec{s}) \Rightarrow T_A(\vec{b}-\vec{s})\, R_G(x_1, Q^2, A, \vec{b}-\vec{s})$ in Eq. (5) for heavy ion collisions.

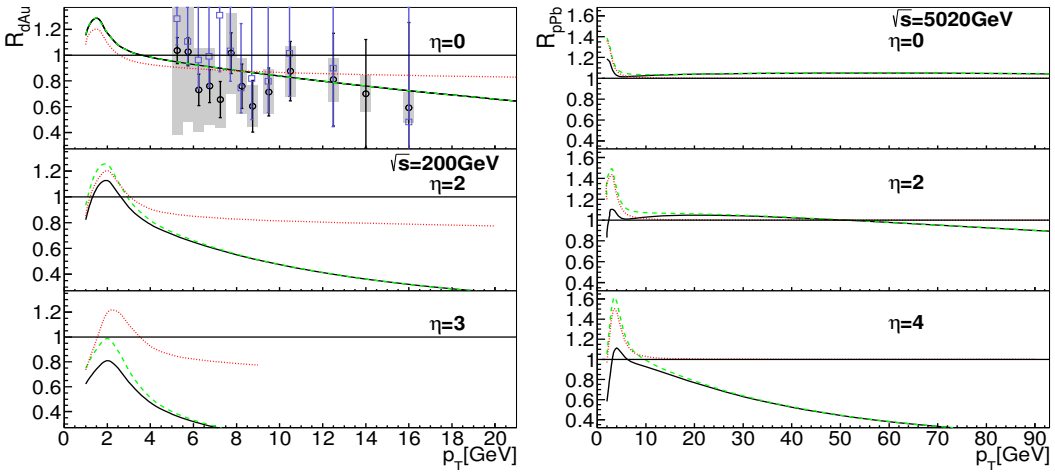


**Figure 1.** Ratio of direct photon production cross-sections $R_{d+Au}(p_T)$ at $\sqrt{s} = 200$ GeV (left boxes) and $R_{p+Pb}(p_T)$ at $\sqrt{s} = 5020$ GeV (right boxes) at different values of $\eta$. The data are from [16] - open blue squares and from [17] - open black circles. Dotted red lines include only the Cronin enhancement and eventual isotopic corrections, while dashed green lines include addidionally ISI corrections, Eq. (1) and solid black lines represent full calculations including both effects ISI and gluon shadowing [15].

Figs. 1 and 2 show predictions for nuclear effects at several fixed $\eta$ in $p(d) + A$ interactions and in heavy ion collisions at RHIC and LHC. Besides $p + Pb$ interactions at LHC, we predict a weak onset of isotopic effects giving values $R_{dAu}$, $R_{AuAu}$, $R_{PbPb} \sim 0.8 - 0.83$ at large $p_T$. At $\eta = 0$ ISI effects, Eq. (1), are not very strong at RHIC but are fully irrelevant at LHC. However they cause a significant large-$p_T$ suppression at forward rapidities that can be clearly distinguished from isotopic effects. Figs. 1 and 2 demonstrate also that coherent effects (shadowing) [15] dominate at small and medium-high $p_T$ while ISI effects are important at large $p_T$. Coherent effects cause also an additional suppression and rise rapidly with rapidity. Both Figs. show also a good agreement of predictions with available data [5, 6, 16, 17].

## 3 Summary

We study production of direct photons in $p(d)+A$ interactions and in heavy ion collisions at RHIC and LHC using the color dipole formalism. Performing predictions for $p_T$-behavior of nuclear effects at different rapidities, besides Cronin enhancement at medium-high $p_T$ and isotopic corrections, we include in calculations also effects of coherence (gluon shadowing) [15] and ISI effects, Eq. (1). Since photons are not subject to final state interactions, no large-$p_T$ suppression is expected. However, we predict a significant suppression due to corrections for energy conservation constraints in initial state parton rescatterings, Eq. (1). We demonstrate that the nuclear suppression at small and medium $p_T$ is dominated by coherence effects. Both effects grow strongly with rapidity. Predicted large-$p_T$ suppression is in contrast with the QCD factorization and can be tested in the future by experiments at RHIC and LHC.

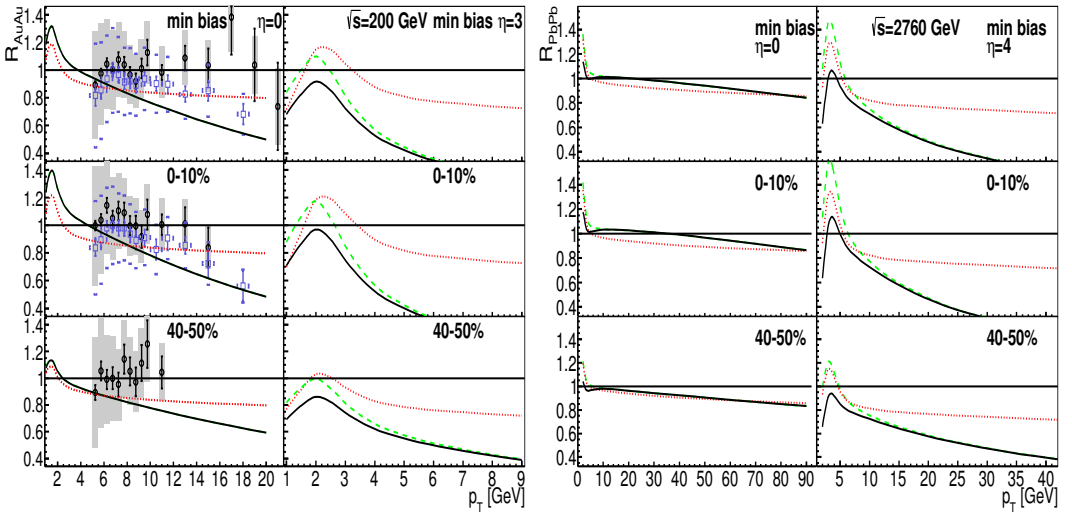


**Figure 2.** Ratio of direct photon production cross-sections $R_{Au+Au}(p_T)$ at $\sqrt{s}$ = 200 GeV (left boxes) and $R_{Pb+Pb}(p_T)$ at $\sqrt{s}$ = 2760 GeV (right boxes) at two values of rapidity and at different centralities. The data are from [5] - open blue squares and from [6] - open black circles. Specification of curves is the same as in Fig. 1.

## Acknowledgements

This work has been supported by the grant 13-02841S of the Czech Science Foundation (GAČR), by the Grant VZ MŠMT 6840770039, by the Slovak Research and Development Agency APVV-0050-11 and by the Slovak Funding Agency 2/0092/10.

## References

[1] B.Z. Kopeliovich, et al., Phys. Rev. Lett. **88**, 232303 (2002).
[2] S.S. Adler, et al. (PHENIX Collaboration), Phys. Rev. Lett. **98**, 172302 (2007).
[3] B. Abelev, et al. (ALICE Collaboration), Phys. Rev. Lett. **110**, 082302 (2013).
[4] J. Albacete, N. Armesto, et al., Int. J. Mod. Phys. E**22**, 1330007 (2013)
[5] T. Isobe, et al. (PHENIX Collaboration), J. Phys. G**34**, S1015 (2007); T. Sakaguchi, et al. (PHENIX Collaboration), Nucl. Phys. A**805**, 355 (2008).
[6] S. Afanasiev, et al. [PHENIX Collaboration], Phys. Rev. Lett. **109**, 152302 (2012).
[7] I. Arsene, et al. (BRAHMS Collaboration), Phys. Rev. Lett. **93**, 242303 (2004); J. Adams, et al. (STAR Collaboration), Phys. Rev. Lett. **97**, 152302 (2006).
[8] B. Z. Kopeliovich et al., Phys. Rev. C**72**, 054606 (2005); B. Z. Kopeliovich and J. Nemchik, J. Phys. G**38**, 043101 (2011).
[9] J. Nemchik, et al., Phys. Rev. C**78**, 025213 (2008); Nucl. Phys. A**830**, 611c (2009).
[10] B.Z. Kopeliovich and J. Nemchik, Phys. Rev. C**86**, 054904 (2012).
[11] B.Z. Kopeliovich, A.V. Tarasov and A. Schafer, Phys. Rev. C**59**, 1609 (1999).
[12] H. Kowalski, L. Motyka and G. Watt, Phys. Rev. D**74**, 074016 (2006).
[13] M. Gluck, E. Reya and A. Vogt, Eur. Phys. J. C**5**, 461 (1998).
[14] B.Z. Kopeliovich, L.I. Lapidus and A.B. Zamolodchikov, JETP Lett. **33**, 595 (1981).
[15] B.Z. Kopeliovich, J. Nemchik, A. Schafer and A.V. Tarasov, Phys. Rev. C**65**, 035201 (2002).
[16] D. Peressounko, et al. [PHENIX Collaboration], Nucl. Phys. A**783**, 577 (2007).
[17] A. Adare, et al. [PHENIX Collaboration], Phys. Rev. C**87**, 054907 (2013).